THE UNIVERSITY of ADELAIDE

THE UNIVERSITY OF ADELAIDE
FACULTY OF SCIENCE
SCHOOL OF BIOLOGICAL SCIENCES
THE ENVIRONMENT INSTITUTE

UNIVERSITY OF COPENHAGEN
FACULTY OF SCIENCE
CENTER FOR MACROECOLOGY,
EVOLUTION AND CLIMATE

PhD Thesis

Elisabetta Canteri

Guiding biodiversity conservation by integrating ecological models, genes, and fossils

Academic advisors: Associate Professor Damien A. Fordham, Professor David Nogués-Bravo

May 2022

TITLE	Guiding biodiversity conservation by integrating ecological models, genes, and fossils
SUBTITLE	Integrating ecological models, genes, and fossils to quantify patterns and processes behind species responses to global change
AUTHOR	Elisabetta Canteri
DEPARTMENTS	The School of Biological Sciences and the Environment Institute**,** The University of Adelaide, Australia Centre for Macroecology, Evolution and Climate**,** GLOBE Institute, University of Copenhagen, Denmark
ACADEMIC ADVISORS	**Associate Professor Damien A. Fordham** School of Biological Sciences and the Environment Institute, Faculty of Science, The University of Adelaide, Australia **Professor David Nogués-Bravo** Center for Macroecology, Evolution and Climate, GLOBE Institute, University of Copenhagen, Denmark
SUBMITTED TO	The Graduate Centre, The University of Adelaide, Australia PhD School of The Faculty of Science, University of Copenhagen, Denmark
FRONT COVER	Layout by Elisabetta Canteri. Photos and icons were purchased from Shutterstock and downloaded from Unsplash and the Noun Project. Credits: Pascal Beyer, Geronimo Giqueaux, Mattia Lombardini, IronSV, David Khai, Atif Arshad, and Hadi.

Table of Contents

Abstract

Anthropogenic activities are threatening biodiversity worldwide, with impacts on every biome on Earth. A better understanding of how species will respond to different magnitudes and rates of anthropogenic-induced climatic change and other global change drivers is therefore needed to predict extinction risk and avert future species loss. In this PhD dissertation, I combine contemporary occurrence records and genetic sequences, paleo-archives, and process-explicit models to improve our understanding of biodiversity change and extinction risk, and to test whether inferences from the past can provide more informed predictions of future climate change impacts. In **Chapter II**, I analysed thousands of mitochondrial DNA sequences across ~1000 bird species to identify whether a relationship exists between conservation status and intra-specific genetic diversity. Results show that threatened birds have lower levels of genetic diversity compared to non-threatened ones, indicating that current assessment criteria already indirectly prioritize the conservation of species with low genetic diversity. Nevertheless, a small proportion of non-threatened species carries low genetic diversity, making them more vulnerable to future environmental changes than their conservation status indicates. In **Chapter III** and **Chapter IV**, I used hundreds of thousands of models, that explicitly simulate demographic and dispersal processes responding to different degrees of habitat change and human hunting pressures, to reconstruct the distributions of the muskox and the reindeer over the last 21,000 years. These models, validated using inferences of past demographic change from fossils and ancient DNA, were able to determine the ecological processes that favoured the survival of the two species until present day and to disentangle the roles of climate and humans in driving their range and population dynamics. Results show that high dispersal ability, small Allee effect and broader climatic requirements are important processes for correctly replicating demographic and biogeographic patterns of both species. They also show that while muskox range dynamics were mostly driven by climatic changes, with small contributions of human hunting, reindeer populations were highly regulated by a synergy of human and climatic pressures, with regional differences. In **Chapter IV**, validated projections of the past were also used to inform future predictions of reindeer extinction risk. Results show that, although population and range size are expected to decline, the estimated magnitudes of reduction have already been experienced by the species during times of abrupt warming events. Researching past biodiversity dynamics can therefore unlock valuable knowledge on future species responses to climate change and help improve management decisions aiming to safeguard biological diversity under global change.

Declaration

I certify that this work contains no material which has been accepted for the award of any other degree or diploma in my name in any university or other tertiary institution and, to the best of my knowledge and belief, contains no material previously published or written by another person, except where due reference has been made in the text. In addition, I certify that no part of this work will, in the future, be used in a submission in my name for any other degree or diploma in any university or other tertiary institution without the prior approval of the University of Adelaide and where applicable, any partner institution responsible for the joint award of this degree. The author acknowledges that copyright of published works contained within this thesis resides with the copyright holder(s) of those works.

I give permission for the digital version of my thesis to be made available on the web, via the University's digital research repository, the Library Search and also through web search engines, unless permission has been granted by the University to restrict access for a period of time.

Date: 14 May 2022

Elisabetta Canteri

Summary

Anthropogenic activities are threatening biodiversity worldwide, with impacts on every biome on Earth. A better understanding of how species will respond to different magnitudes and rates of anthropogenic-induced climatic change and other global change drivers is therefore needed to predict extinction risk and avert future species loss. In this PhD thesis, I explore biodiversity responses to global change drivers across different levels of biotic organization, from genetic to biogeographic responses, to gain a better understanding of biotic change and extinction risk. In **Chapter II**, thousands of mitochondrial DNA sequences across ~1000 bird species were analysed to identify whether a relationship exists between conservation status and intra-specific genetic diversity. Results show that threatened birds have lower levels of genetic diversity compared to non-threatened ones, indicating that current assessment criteria already indirectly prioritize the conservation of species with low genetic diversity. Nevertheless, a small proportion of non-threatened species harbours low genetic diversity, making them more vulnerable to future environmental changes than their conservation status indicates. Still, in this context, extinction risk is assessed by only considering the latest stages of the extinction process, when populations reach critically small sizes. However, population and range declines can start many millennia before the final extinction event. Correlative approaches have normally been used to describe and predict species range dynamics, but they do not include the demographic and dispersal processes that determine species distributions and survival through time. Therefore, a better understanding of how these processes interact with extinction drivers through time and space is needed to better estimate past and future biotic change and predict extinction risk. This can be achieved by using process-explicit models, integrated with fossil and modern occurrence records, ancient DNA, and paleoclimate reconstructions, which improve the calibration, prediction, and evaluation of ecological models. In **Chapter III** and **Chapter IV**, I used hundreds of thousands of models, that explicitly simulate demographic and dispersal processes responding to different degrees of habitat change and human hunting pressures, to reconstruct the distributions of the muskox and the reindeer over the last 21,000 years. The aim was to determine the ecological processes that favoured their survival until present day and to disentangle the roles of climate and humans in driving the range dynamics of the two species. Models were validated using inferences of past demographic change from fossils and ancient DNA. Results show that high dispersal ability, small Allee effect and strong constraints in the climatic requirements are important processes for correctly replicating demographic and biogeographic patterns for both species. They also show that while muskox range dynamics were mostly driven by climatic changes, with small

contributions of human hunting, reindeer populations were highly regulated by a synergy of human and climatic pressures, with regional differences. In **Chapter IV**, validated projections of the past were also used to inform future predictions of reindeer extinction risk. Results show that, although population and range size are expected to decline, the estimated magnitudes of reduction have already been experienced by the species during times of abrupt warming events. Researching past biodiversity dynamics can therefore unlock valuable knowledge on future species responses to climate change and help improve management decisions aiming to safeguard biological diversity under global change.

Resumé

Menneskeskabte aktiviteter truer biodiversiteten på verdensplan med indvirkning på alle biomer på Jorden. En bedre forståelse af, hvordan arter vil reagere på forskellige påvirkninger af menneskeskabte klimaændringer og andre globale påvirkninger er derfor nødvendig for at forudsige udryddelsesrisiko og afværge fremtidige artstab. I denne ph.d.-afhandling udforskes biodiversitets reaktioner på globale divere på tværs af forskellige niveauer af biotisk organisation, fra genetiske til biogeografiske reaktioner, for at få en bedre forståelse af biotiske ændringer og risiko for udryddelse. I **Chapter II** analyseres tusinder af mitokondrielle DNA-sekvenser på tværs af ~1000 fuglearter for at identificere, om der eksisterer en sammenhæng mellem bevaringsstatus og intra-specifik genetisk diversitet. Resultater viser, at truede fugle har lavere niveauer af genetisk diversitet sammenlignet med ikke-truede fugle, hvilket indikerer, at de nuværende vurderingskriterier allerede indirekte prioriterer bevaring af arter med lav genetisk diversitet. Ikke desto mindre har en lille del af ikke-truede arter lav genetisk diversitet, hvilket gør dem mere sårbare over for fremtidige miljøændringer, end deres bevaringsstatus indikerer. Alligevel vurderes udryddelsesrisiko i denne sammenhæng ved kun at overveje de seneste stadier af udryddelsesprocessen, når populationer når kritisk små størrelser. Dog kan befolknings- og udbredelsesfald starte mange årtusinder før den endelige udryddelsesbegivenhed. Korrelative tilgange er normalt blevet brugt til at beskrive og forudsige arternes rækkeviddedynamik, men de inkluderer ikke de demografiske og spredningsprocesser, der bestemmer arternes udbredelse og overlevelse gennem tiden. Derfor er der behov for en bedre forståelse af, hvordan disse processer interagerer med udryddelsesdrivere gennem tid og rum for bedre at kunne vurdere tidligere og fremtidige biotiske forandringer og forudsige udryddelsesrisiko. Dette kan opnås ved at bruge procesbaserede modeller, integreret med fossile og moderne hændelsesregistre, ældgammelt DNA og palæoklima-rekonstruktioner, som forbedrer kalibrering, forudsigelse og evaluering af økologiske modeller. I **Chapter III** og **Chapter IV** er der brugt hundredtusindvis af modeller, der eksplicit simulerer demografiske og spredningsprocesser, der reagerer på forskellige grader af habitatændringer og menneskeligt jagttryk, til at rekonstruere fordelingen af moskusoksen og rensdyret over de sidste 21.000 år. Målet var at bestemme de økologiske processer, der begunstigede deres overlevelse indtil i dag, og at adskille klimaets og menneskers roller i at drive rækkevidden af de to arter. Modellerne blev valideret ved hjælp af slutninger om tidligere demografiske ændringer fra fossiler og gammelt DNA. Resultater viser, at høj spredningsevne, lille Allee-effekt og stærke begrænsninger i de klimatiske krav er vigtige processer for korrekt at replikere demografiske og biogeografiske mønstre for begge arter. De viser også, at

mens moskusokseområdets dynamik for det meste var drevet af klimatiske ændringer, med små bidrag fra menneskelig jagt, var rensdyrpopulationer stærkt reguleret af en synergi af menneskelige og klimatiske pres med regionale forskelle. I **Chapter IV** bliver validerede fremskrivninger af fortiden også brugt til at informere om fremtidige forudsigelser om risiko for udryddelse af rensdyr. Resultater viser, at selvom populationen og udbredelsesstørrelsen forventes at falde, er de estimerede størrelser af reduktion allerede blevet oplevet af arten i tider med pludselige opvarmningsbegivenheder. At forske i tidligere biodiversitetsdynamikker kan derfor frigøre værdifuld viden om fremtidige arters reaktioner på klimaændringer og hjælpe med at forbedre forvaltningsbeslutninger, der sigter mod at beskytte biologisk mangfoldighed under globale forandringer.

Acknowledgments

Finishing this thesis is for me a great achievement. These past three years have been challenging, including moving to a new country in the midst of a pandemic, and I could not have done it without the love and support of many people.

I would like to thank my supervisors, Damien and David, for believing in me even before I started believing in myself. For guiding me, supporting me, and always helping me feel excited about my work. I would like to thank Stu, because without your help I probably would not have a thesis right now, and Sean, for being my emotional support, always cheering me up when I needed it the most. Thanks to Julia for being my PhD companion and for sharing with me the frustration of being enrolled in a joint programme between two universities. Thanks to all the other people in the lab for the support.

Thanks to all my co-authors for the comments, suggestions and ideas that greatly contributed to the research presented in this thesis.

I would like to thank Miriam, Katie, Tom, Brock, Adam, Charlotte, Eilish, Colette, Nicole, for being my Aussie family, you made this Australian experience so incredible. Special thanks go to Brock, for feeding me during the last weeks of my PhD, and Miri, for being my office mate, my roommate, but most of all my friend. There are so many others to thank, including Daniel, Alana, Tyler. I hope to see you all in Europe soon!

Thanks to all my friends back in Europe and big thanks to Julie for translating the summary in Danish for me. I look forward to catching up with you again. A special thanks to Martino, my home away from home, and my parents, for being my number one fans.

List of Manuscripts

I. **Canteri, E.**, Fordham, D. A., Li, S., Hosner, P. A., Rahbek, C., & Nogués-Bravo, D. (2021). IUCN Red List protects avian genetic diversity. *Ecography*, *44*, 1808-1811. doi:10.1111/ecog.05895

II. **Canteri, E.**, Brown, S. C., Schmidt, N. M., Heller, R., Nogues-Bravo, D., & Fordham, D. A. (2022). Spatiotemporal influences of climate and humans on muskox range dynamics over multiple millennia. The Environment Institute and School of Biological Sciences. University of Adelaide. *Invited resubmission.*

III. **Canteri, E.**, Brown, S. C., Schmidt, N. M., Post E., Nogues-Bravo, D., & Fordham, D. A. (2022). Ecological resilience of reindeers to past and future climatic change. The Environment Institute and School of Biological Sciences. University of Adelaide. *Unsubmitted work written in manuscript style.*

Preface

This PhD dissertation is the result of a three-year joint PhD programme at the University of Adelaide and the University of Copenhagen. The work presented in this thesis was conducted at the Center for Macroecology, Evolution and Climate at the University of Copenhagen for the first year, and at the Environment Institute and School of Biological Sciences at the University of Adelaide for the last two years. The ideas presented in this thesis are based on extensive work done by my two academic advisors. Specifically, it is a development, among others, of Lorenzen et al. (2011), Nogues-Bravo et al. (2018), and Fordham et al. (2020), the latter being a publication to which I gave my contribution. The aim of this PhD dissertation is to gain a better understanding of biodiversity change and extinction risk. As there are multiple levels of biodiversity, biodiversity responses to extinction drivers differ depending on the level considered, from genes to ecosystems. The work presented in this PhD dissertation starts at the genetic level and then scales up to the population and species levels, where paleo-archives are integrated with a new generation of ecological models to understand past species responses to climatic changes and human hunting, and to help guide the conservation of species. This thesis is divided in five chapters. The first chapter is an introduction of the state-of-the-art concepts and approaches this thesis builds upon, starting from an overview of current trends in global biodiversity change across all levels of biodiversity, knowledge gaps preventing the accurate prediction of future biodiversity change that can be solved by looking at the past, the Late Quaternary and the Arctic as model systems, patterns and processes behind species distributions and extinction dynamics, and, finally, new modelling approaches and data that can be used to fill the knowledge gaps and improve future predictions of extinction risk. The following three chapters are research papers, the core of this thesis. The last chapter is a summary of results, integrated with a discussion in the context of the state-of-the-art. In this last chapter, a discussion of future directions is also included. Lastly, an appendix includes the online published version of **Chapter II**.

Chapter I: Introduction

Global Biodiversity Change

Anthropogenic activities are impacting biodiversity worldwide, resulting in biodiversity loss and profound alterations (Pereira et al., 2012). Biodiversity loss refers to species extinctions and loss of genetic diversity, while alterations to biodiversity are the consequence of changes in abundance, community structure and range shifts (Pereira et al., 2012). There are six major drivers of global biodiversity change: habitat change and degradation, overexploitation, pollution, invasive species, climate change, and co-extinctions. Habitat change, overexploitation and invasive species are currently the biggest drivers of biodiversity loss and alteration worldwide, as they directly affect population and range size and ecosystem function (Pereira et al., 2012). The loss of species and populations can result in a cascading effect of co-extinctions (Brook et al., 2008) and in loss of functional diversity, which induces shifts in species' behavioural and physiological responses (Young et al., 2016). Finally, climate change is expected to be an additional driver of biodiversity loss and alteration in the future, as it induces range shifts, and it increases the extinction risk for species that are unable to move, have narrow climatic niches, or are unable to phenotypically adapt (Pereira et al., 2012). These global change drivers are likely to work in synergy and hasten the dynamics of extinction (Brook et al., 2008). For example, climate change is expected to interact with the other global change drivers by reducing habitat quality, which is exacerbated by direct habitat loss, habitat fragmentation, and overexploitation, and by potentially increasing suitable conditions for invasive species (Brook et al., 2008).

Recent trends of change have been recorded worldwide, across all levels of biodiversity. Ecosystem extent and condition have suffered a 47% decline (IPBES, 2019). Due to land use alone, ~58% of terrestrial areas are biotically compromised, with the largest effects recorded in grasslands (Newbold et al., 2016). According to the IUCN Red List of Threatened Species, 979 species have gone extinct or extinct in the wild since 1500 (IUCN, 2021). Considering that species are still being discovered and described, with an estimated 5 to 9 million animal species, it has been calculated that we are likely losing ~11,000 to 58,000 species annually (Dirzo et al., 2014). We are currently losing species at rates between 8 and 100 times higher than background rates (Ceballos et al., 2015), with faster extinction rates than the ones involved in the Big 5 mass extinctions over geological times (Barnosky et al., 2011). Beyond global extinctions, local extirpation of populations has caused many species to currently occupy only a small portion of their historical range (Ceballos & Ehrlich, 2002;

Ripple et al., 2016). These reductions in population and range size result in losses of intraspecific genetic diversity, as a consequence of stronger effects of inbreeding (Keller, 2002), genetic drift (Reed & Frankham, 2003), and the accumulation of deleterious mutations (Lynch et al., 1995). Genetic diversity loss reduces the potential for adaptation and evolution of a species in response to environmental changes (Banks et al., 2013), and is thus important for the prediction of the viability of species and populations under future global change drivers. Still, genetic diversity tends to be overlooked when assessing the extinction risk of species, as assessments only rely on measures of decline in range and population sizes (e.g. IUCN, 2019). In **Chapter II** of this PhD dissertation, I explore the relationship between genetic diversity and conservation status in birds, to investigate whether genetic diversity can improve our understanding of extinction risk.

Future projections of global biodiversity change are highly uncertain, as variations in the projected intensity of anthropogenic activities result in multiple scenarios of climate and land-use change (IPCC, 2014; Pereira et al., 2010). Also, methodological issues and differences in models' structure can provide different results, making it difficult to agree on a specific future scenario (Pereira et al., 2010). Future species responses to global change drivers depend on the ability of species to tolerate and adapt to environmental change *in situ*, or to track and disperse to new environmentally suitable habitats (Nogues-Bravo et al., 2018). Species that will not be able to adapt or disperse may go extinct (Nogues-Bravo et al., 2018). However, there is still a significant gap in the role of different processes regulating biodiversity change, and accurately predicting future biodiversity change and extinction risk requires a deeper understanding of these processes. The impact of different rates and magnitudes of climate change on adaptation, evolution and range shifting remains obscure, as well as the interaction between these processes in determining extinction risk (Nogues-Bravo et al., 2018). Finally, the interaction between multiple global change drivers makes it harder to predict future extinctions. However, the integration of paleoecology, paleogenomics, and process-explicit models is quickly becoming the answer to fill these knowledge gaps (Nogues-Bravo et al., 2018). With fine spatial and temporal resolution of fossils and ancient genomes, abrupt climatic shifts and megafaunal extinctions, the Late Quaternary (last ~130,000 years) offers the perfect natural laboratory to explore the roles of adaptation and dispersal under climate change (Fordham et al., 2020; Nogues-Bravo et al., 2018).

The spatiotemporal context: cold areas of the Late Quaternary

The Late Quaternary, specifically the last 21,000 years, is the period chosen in **Chapter III** and **Chapter IV** to investigate species responses to global change drivers. During this period, approximately 40% of terrestrial ecosystems experienced past climatic shifts at magnitudes and rates similar to what is predicted for the future (Brown et al., 2020). Between ~130,000 and ~11,700 years ago, climate shifted abruptly multiple times. Just over the last ~ 21,000 years, it is possible to count six rapid warming or cooling events (Andersen et al., 2004; Grootes et al., 1993), in some cases with temperature increases up to 10 ˚C in just a few centuries and decades (Dansgaard et al., 1993). These climatic changes had profound impacts on species and ecosystems (Botta et al., 2019). Paleogenetic approaches and the fossil record suggest that climate change has promoted adaptation at different levels, like macroevolutionary divergences, adaptive evolution, and phenotypic adaptation, depending on the time scale considered (Nogues-Bravo et al., 2018). Climate change has also driven range shifts and population declines (Lorenzen et al., 2011; Ordonez & Williams, 2013), extinctions (Cooper et al., 2015), changes in functional diversity, phylogenetic diversity, and community composition (Eiserhardt et al., 2015; Ordonez & Svenning, 2017; Ordonez et al., 2016), and shifts in ecosystem function (Malhi et al., 2016; Zimov et al., 1995).

During the Late Quaternary, anatomically modern humans spread across the globe. Models simulate the spread and colonisation of humans across Europe, Asia, and Australasia by 40,000 years BP (Eriksson et al., 2012; Timmermann & Friedrich, 2016), and recent archaeological discoveries suggest that humans were already present in Mexico at the terminus of the Last Glacial Maximum (Ardelean et al., 2020). The rapid expansion of anatomically modern humans likely amplified the effects of climate and environmental change on biodiversity via direct effects of hunting (Barnosky & Lindsey, 2010; Koch & Barnosky, 2006), but also indirectly through habitat alteration, introduced predators and “hyperdiseases” (Koch & Barnosky, 2006).

Between 50,000 and 4,000 years before present, about 90 genera of mammals weighing ≥ 44 kg (megafauna) disappeared across continents (Brook & Barnosky, 2012; Stuart, 2015). Extinction was total for mammalian species > 1,000 kg, and > 50% for species weighting > 30 kg (Stuart, 2015). Given regional and continental variations in the velocity and severity of megafaunal extinctions during the Late Quaternary, the relative contributions of climate change and human hunting are still debated (Koch & Barnosky, 2006; Monjeau et al., 2017). Resolving the debate has led to use the Late Quaternary as a model for understanding extinctions and extinction dynamics (Fordham et al., 2021; Stuart et al., 2004; Stuart & Lister, 2012).

The Arctic is a robust model system for using the past to understand extinction dynamics and predict future biodiversity loss. Some Arctic regions have experienced rates of warming that are analogous to future forecasts (Fordham et al., 2020), and have a relatively high number of plant and animal fossils with good spatial and temporal coverage (Chevalier et al., 2020; Nogues-Bravo et al., 2018), a large volume of sequenced ancient DNA from a diverse range of species (Orlando & Cooper, 2014; Smith et al., 2003; Willerslev et al., 2003), and paleoclimate reconstructions with high-temporal resolutions (Steffensen et al., 2008).

The Arctic is also one of the regions that are expected to be more impacted by climate change. Indeed, Arctic regions are warming almost twice as fast as the rest of the world (Meredith et al., 2019; Screen & Simmonds, 2010), with mean annual temperatures forecast to increase by 3°C – 12°C (above 2010 conditions) by the end of the 21st century (Lee et al., 2021). The accelerating warming of the Arctic is already shifting plant phenology, with longer growing seasons and shorter flowering seasons (Post et al., 2019). Alterations of wind and precipitation patterns are more likely, with an increased frequency of rain-on-snow events that prevent access to food for herbivores (Berger et al., 2018). Population crashes in muskox (*Ovibos moschatus*) and reindeer (*Rangifer tarandus*) have also been recorded due to parasites and diseases, which are shifting their distributions in a northerly direction (Kafle et al., 2020; Vors & Boyce, 2009).

Muskox and reindeer are the only two remaining megaherbivore species in the polar regions, the survivors of the Late Quaternary extinctions. They play key roles in the tundra ecosystem. As generalist species, they eat a wide variety of plants (Kristensen et al., 2011; Schmidt et al., 2018), preventing wooded taxa to expand in distribution and thus facilitating the maintenance of the tundra ecosystem (Olofsson et al., 2009). Their grazing effects are among the main drivers of vegetation dynamics (Van Der Wal, 2006) and several studies have shown that herbivory might induce resistance and resilience of the tundra vegetation to climatic changes (Olofsson et al., 2009; Post, 2013; Post & Pedersen, 2008). The rapid warming of the Arctic is concerning, but the responses of species and the tundra ecosystem are complex. For example, the increased productivity of the arctic vegetation due to climate change may benefit the muskox, which relies on the spring green-up for breeding success (Post et al., 2019). Thus, being able to understand and predict these mixed responses is essential for effective conservation strategies and management decisions.

Chapters III and **IV** of this PhD dissertation are based in this spatiotemporal context, where the impacts of climatic change and human hunting on muskox and reindeer populations over the last 21,000 years are being investigated. Being survivors of the Late Quaternary extinctions, muskox and

reindeer are the perfect study species to identify the ecological processes and traits that facilitate resilience against global change drivers and to better predict their responses in a warming Arctic.

Conservation Biogeography

This PhD dissertation also takes roots in the field of conservation biogeography, which applies biogeographical theories and approaches, concerning the distribution of species, to the conservation of biodiversity (Whittaker et al., 2005). This includes theories regarding the patterns and processes that determine species geographical ranges and extinction pathways.

The size, shape, boundaries and internal structure of a species' range are the result of spatiotemporal responses of demographic and dispersal processes to changes in environmental conditions (Brown et al., 1996). There is high variation in the size of species ranges. Many species have small to moderate range sizes, and only few species have very large ones (Brown et al., 1996). Furthermore, closely related species tend to have similar range sizes compared to distantly related ones (Brown et al., 1996). This variability in range size is structured across space in a latitudinal gradient, with larger ranges at higher latitudes (Brown et al., 1996). Processes that determine the size of a species range include colonisation and extinction dynamics (source-sink dynamics), and ecological niche processes or environmental limitations (Brown et al., 1996). Regarding the shape of a species range, it has been noticed that the periphery-to-area ratio tends to remain constant (Brown et al., 1996). Plus, peripheral areas are more fragmented compared to the centre, where population abundances are higher and habitat conditions are assumed to be more favourable (Brown et al., 1996; Gaston, 2003). Biotic interactions seem to be the limiting factor of distributions at lower latitudes, compared to higher latitudes where environmental factors are the key players (Brown et al., 1996). Finally, range boundaries can be smooth or highly unstable (Brown et al., 1996; Holt & Keitt, 2005), but they are extremely dynamic, and constantly changing based on range shifts, expansions and contractions (Brown et al., 1996).

Few hypotheses have been proposed to describe how ranges contract. The demographic hypothesis is based on demographic characteristics of populations and suggests that the contraction of the range starts in the periphery and moves inwards towards the centre (Rob Channell & Mark V. Lomolino, 2000). The demographic hypothesis assumes that extinction probability increases with declines in population size, that populations are larger and less variable in the centre of the range, and that environmental change uniformly drives population declines across the entire range (Rob Channell & Mark V. Lomolino, 2000). The contagion hypothesis suggests that contraction starts in

one point along the edge of the range and then spreads like a contagion through the centre until reaching the other edge, with populations last impacted by the extinction driver persisting the longest (Lomolino & Channell, 1995). Finally, the refuge hypothesis assumes that the variation in the intensity of anthropogenic pressures within a species range will determine which populations go extinct first and which will persist in fragments (Ceballos & Ehrlich, 2002). Multiple studies have shown that species tend to persist in the periphery of their historical range (R. Channell & M. V. Lomolino, 2000; Lomolino & Channell, 1995, 1998) giving support to the contagion hypothesis. However, none of these hypotheses has been able to prevail in describing patterns of range contraction (Lucas et al., 2016), as multiple hypotheses can be applied to different species, and investigations that explicitly integrate the processes driving range dynamics are still lacking.

In summary, multiple processes and drivers are involved in extinction dynamics. Processes during the early stages of decline differ from the ones involved in the final stages of extinctions, and there are spatiotemporal variations in the extinction drivers and their interaction. Until recently, most of the research looking at extinction dynamics has focused on the latest stages of the extinction process, when populations under the effects of genetic and stochastic processes reach critically small sizes (Frankham, 2005; Simberloff, 1986). Less attention has been paid to early-stage population declines, without considering the initial stages of range contractions and the final extinction event as a continuum (Caughley, 1994). By taking advantage of process-explicit models, new studies are showing that extinction pathways can start many millennia before the final extinction event (Fordham et al., 2021), and are now able to disentangle the impacts of multiple extinction drivers across space and time (Fordham et al., 2021). In this thesis, the demographic and dispersal processes that shape species ranges, and their interaction with extinction drivers, are explicitly simulated to reconstruct the range and population dynamics of two cold-adapted species over multiple millennia (**Chapter III** and **Chapter IV**). Local extirpation and colonisation events are being simulated over large time scales, to gain a better understanding of range contractions, range shifting and extinction pathways.

Process-explicit models, paleoclimate reconstructions, genes, and fossils

The study of population and geographical range dynamics has been dominated by the use of correlative models. Ecological niche models (ENMs), also called species distribution models (SDM) or bioclimate envelope models (BEM), use the climatic and environmental conditions in sites of occurrence of a species to find correlates in space and time, resulting in maps of suitable habitats that

can potentially support a species (Franklin, 2010). ENMs were initially used for describing species-environment relationships, to test ecological or biogeographical hypotheses about species ranges (Austin, 1987; MacArthur, 1958; Whittaker, 1956). In the last few decades, ENMs have been widely used for prediction, to estimate occurrence in areas where data is lacking (Fois et al., 2018), or to forecast the future distribution of species under global change (Thomas et al., 2004), including the success of potential translocations or biological invasions (Guisan et al., 2013; Peterson, 2003), thus being implemented in conservation biology and climate change research (Franklin, 2010; Guisan & Zimmermann, 2000). ENMs have also been used for hindcasting species distributions under past climatic changes, to test biogeographic and evolutionary scenarios, and for quantifying past climate change impacts on current-day distributions (Svenning et al., 2011; Varela et al., 2011).

One of the greatest limitations of ENMs is that, as correlative models, they assume that the current distribution of a species is the best indicator of its climatic requirements (Pearson & Dawson, 2003), without considering biotic interactions, evolutionary change, dispersal, and the other population processes that play key roles in determining species distributions and dynamics through time (Elith & Leathwick, 2009; Lavergne et al., 2010; Pearson & Dawson, 2003; Wisz et al., 2013). Overcoming this limitation and improving ENMs prediction have led to the development of process-explicit models.

Process-explicit (or process-based) models can be defined as 'models that characterize changes in a system's state as explicit functions of the events that drive those state changes' (Connolly et al., 2017). They incorporate 'causality' (Connolly et al., 2017), as they translate the interaction between an organism and its environment into fitness and survival components (Kearney & Porter, 2009). Process-explicit models have their origin in Global Dynamics Vegetation Models (DGVMs), which simulate the biogeochemical cycles that determine the vegetation responses to environmental drivers (Prentice et al., 2007). This new process-explicit approach has proven to improve predictions when compared to ENMs projections, accounting only for variations in climate (Fordham, Bertelsmeier, et al., 2018; Hickler et al., 2004). Process-explicit models are increasingly being used to simulate the ecological processes and the global change drivers that shaped past spatiotemporal patterns of biodiversity (Fordham et al., 2020). These new approaches are improving knowledge of eco-evolutionary dynamics (Hagen et al., 2021), allowing to assess contested ecological and evolutionary theories (Rangel et al., 2018), and to better understand and manage biodiversity (Fordham et al., 2016).

Process-explicit models are more complex than statistical models, leading to multiple risks and limitations. For example, there is a higher risk of modelling errors and of confirmation bias, where researchers might be less inclined to interrogate models to reveal weaknesses or failures (Connolly et al., 2017). Additionally, process-explicit models often require more time, effort, resources, and data (Kearney & Porter, 2009). However, research at the intersection of paleoecology, paleoclimatology, paleogenetics, and macroecology is integrating process-explicit models with paleo-archives (e.g., fossil and pollen records, paleoclimate reconstructions, ancient DNA), to improve model calibration, prediction, and evaluation (Nogues-Bravo et al., 2018).

The fossil record has been previously used to establish historical baseline conditions for ecological restoration (Fordham et al., 2016; Jackson & Hobbs, 2009). However, it can provide also key information that integrated with process-explicit models can improve future projections of range and population dynamics (Fordham et al., 2016). As fossils represent snapshots in time and space where a species was present, they can be used to build multi-temporal niches, representing the full range of environmental conditions that a species has occupied through time and better approximating the fundamental niche of the species (Nogués-Bravo, 2009). Not only do they represent 'presence' data, but they also give information on patterns like population change, colonisation and extinction events that can be used for evaluating whether models are correctly parameterized to replicate those patterns (Fordham et al., 2016; Fordham et al., 2020). Despite multiple temporal and spatial biases in the fossil record, linked to the modes of fossilization, preservation, and analysis of fossils (Barnosky & Lindsey, 2010; Behrensmeyer et al., 2000; Moreno-Amat et al., 2017; Rodríguez-Rey et al., 2015), and to geological processes that may cause fossil displacement (Behrensmeyer et al., 2000), the quality and reliability of fossils and their age are becoming more precise thanks to new protocols and advanced statistical techniques (Barnosky & Lindsey, 2010; Fordham et al., 2020; Rodríguez-Rey et al., 2015; Stuart et al., 2004).

Paleoclimate reconstructions are commonly used to test ecological theories and to determine the impacts of climate change on past and current species diversity (Cooper et al., 2015; Jackson & Blois, 2015; Williams et al., 2013). Paleoclimate reconstructions have commonly been available at low-temporal resolutions, represented by climate snapshots separated by multiple millennia, thus assuming that climate changed across millennia at a linear pace (Fordham, Saltre, et al., 2018). However, records from terrestrial, marine and ice cores show that climate shifts in the past were abrupt, with fluctuations happening within centuries or decades (Mayewski et al., 2004; Steffensen et al., 2008). Therefore, paleoclimate reconstructions at high-temporal and spatial resolutions are

needed to better understand ecological and evolutionary responses to climatic changes (Fordham, Saltre, et al., 2018). Atmosphere-ocean general circulation (AOGCM) models use information on the physical components of the climate system (like atmosphere, ocean, land and sea ice), to simulate past or future global-scale climate scenarios (Flato et al., 2013). For example, the Hadley Centre Climate Model version 3 (HadCM3) (Gordon et al., 2000) and the Community Climate System Model version 3 (CCSM3) (Collins et al., 2006) can produce realistic simulations of climate at monthly time steps for the last 50,000 years (Braconnot et al., 2012), and new software tools like PaleoView (Fordham et al., 2017), facilitate the access of paleoclimate reconstructions at customized temporal scales since the Last Glacial Maximum (Fordham, Saltre, et al., 2018; Fordham et al., 2017).

Finally, genetic information has multiple applications in ecological models. Historical and ancient DNA (aDNA) extracted from museum specimens and fossils can reveal climate-induced range shifts and population dynamics, inferred from estimates of effective population size (N_e) coupled with paleoclimate simulations (Lorenzen et al., 2011). DNA extracted from historical specimens can also provide insights into adaptive and evolutionary responses, which can be accounted in future forecasts of species distributions and extinction risk (Fordham et al., 2014). Sedimentary and environmental DNA can be used to assess spatiotemporal variations in species occurrence and community compositions (Fordham et al., 2014; Wang et al., 2021), and contemporary DNA can be used to infer dispersal and metapopulation dynamics from estimates of gene flow and genetic structure across populations (Fordham et al., 2014; Yannic et al., 2020). All this information can directly be integrated into ecological models in either the calibration or validation phase (Fordham et al., 2014), providing opportunities to strengthen predictions of future global biodiversity change and species extinction risk.

In this PhD dissertation, the correlative approaches widely used to describe range and extinction dynamics are being advanced by integrating process-explicit models with fossils, paleoclimate reconstructions and aDNA (**Chapter III** and **Chapter IV**).

Grand objectives and specific aims

Given the concerning trends of current and expected biodiversity change, accurately predicting future biodiversity declines, alterations and species susceptibility to extinction is becoming a pressing task in conservation. Doing so requires dissecting the processes that shape biodiversity patterns, and modelling frameworks that robustly validate the observed patterns over space and time. In this PhD dissertation, I combine contemporary occurrence records and genetic sequences, paleo-archives, and

process-explicit models to improve our understanding of extinction dynamics and extinction risk, and to test whether inferences from the past can provide more informed predictions of future climate change impacts. Specifically, I use mitochondrial DNA sequences of birds to assess whether a relationship exists between intraspecific genetic diversity and extinction risk (**Chapter II**). I then move away from the latest stages of the extinction process and use long-term ecological proxies to gain a deeper understanding of extinction risk, by reconstructing the range dynamics of muskox and reindeer over the last 21,000 years (**Chapter III** and **Chapter IV**). Doing so allows us to determine the ecological traits that facilitated the survival of these two species during the Quaternary/Holocene transition, and to disentangle the spatiotemporal effects of climate change and human hunting on population abundances. The techniques involved in **Chapter III** and **Chapter IV** include the use of fossils and paleoclimate reconstructions to build multi-temporal niches of the species, integrated in process-explicit models that explicitly simulate the demographic, population and dispersal processes that shape the geographic distribution of species in response to climatic changes and human harvest. Inferences of demographic changes from fossils and aDNA are used to validate the models, which are in turn used to build informed projections of population and range dynamics under future climate change (**Chapter IV**). Ultimately, this novel approach could provide useful for testing ecological theories behind range contractions and extinction pathways, and, ultimately, for building effective conservation strategies that aim to prevent future species loss.

Chapter II: IUCN Red List protects avian genetic diversity

Statement of Authorship

Title of Paper	IUCN Red List protects avian genetic diversity
Publication Status	☑ Published ☐ Accepted for Publication ☐ Submitted for Publication ☐ Unpublished and Unsubmitted work written in manuscript style
Publication Details	Title: IUCN Red List protects avian genetic diversity Author(s): Elisabetta Canteri, Damien A. Fordham, Sen Li, Peter A. Hosner, Carsten Rahbek, David Nogués-Bravo Journal: Ecography Vol./page: 44/1-4 DOI: 10.1111/ecog.05895

Principal Author

Name of Principal Author (Candidate)	Elisabetta Canteri		
Contribution to the Paper	The candidate conceived the idea, together with their advisors. The candidate cleaned the data, ran the analyses, produced the results, and led the writing of the manuscript, with contribution from all the co-authors.		
Overall percentage (%)	50%		
Signature		Date	26 January 2022

Co-Author Contributions

By signing the Statement of Authorship, each author certifies that:

i. the candidate's stated contribution to the publication is accurate (as detailed above);

ii. permission is granted for the candidate in include the publication in the thesis; and

iii. the sum of all co-author contributions is equal to 100% less the candidate's stated contribution.

Name of Co-Author	Damien A. Fordham		
Contribution to the Paper	Contributed with the conceptualization of the research idea, with supervision, writing of the manuscript and funding acquisition.		
Signature		Date	02/05/2022

Name of Co-Author	Sen Li		
Contribution to the Paper	Contributed with data collection, with writing of part of the code to run the analyses and with writing the manuscript.		
Signature		Date	28/03/2022

Name of Co-Author	Peter A. Hosner		
Contribution to the Paper	Contributed with cleaning and analysing the data, and with writing the manuscript.		
Signature		Date	26 January 2021

Name of Co-Author	Carsten Rahbek		
Contribution to the Paper	Contributed with funding acquisition and writing of the manuscript.		
Signature		Date	03/05/2022

Name of Co-Author	David Nogués-Bravo		
Contribution to the Paper	Contributed with the conceptualization of the research idea, with supervision, writing of the manuscript and funding acquisition.		
Signature		Date	02/05/2022

Title Page

Title

IUCN Red List protects avian genetic diversity

Elisabetta Canteri[1,2]*, Damien A. Fordham[1,2], Sen Li[3], Peter A. Hosner[2,4], Carsten Rahbek[2,5], and David Nogués-Bravo[2]

[1]The Environment Institute and School of Biological Sciences, University of Adelaide, South Australia 5005, Australia.
[2]Center for Macroecology, Evolution and Climate, GLOBE Institute, Faculty of Health and Medical Sciences, University of Copenhagen, Universitetsparken 15, 2100 Copenhagen, Denmark.
[3]Section for Evolutionary Genomics, GLOBE Institute, Faculty of Health and Medical Sciences, University of Copenhagen, Øster Farimagsgade 5, 1353 Copenhagen, Denmark.
[4]Natural History Museum of Denmark, University of Copenhagen, Copenhagen, Denmark.
[5]Department of Life Sciences, Imperial College London, Ascot SL5 7PY, UK.
Corresponding authors: Elisabetta Canteri (elisabetta.canteri@adelaide.edu.au), David Nogués-Bravo (dnogues@sund.ku.dk)

Acknowledgments

We thank Jonathan Kennedy for technical support and guidance. We thank Tim Melling for allowing us to use his photo of the Sooty Tit.

Funding

This research was funded by the Australian Research Council (FT140101192, DP180102392), the Danish National Research Foundation and the DFF (Danmarks Frie Forskningsfond).

Brevia

Low genetic diversity may be associated with an increase in species' extinction risk (Spielman et al. 2004, Frankham 2005). Still, global conservation assessments do not consider relevant genetic-based estimates for evaluating species threat status. Rather, they rely primarily on changes in population abundance and range size, with the inherent assumption that intra-specific genetic variability is tightly correlated with population size and range area (Frankham 1996). If this assumption was universally true, species considered to be at high risk, because of small range sizes and/or low abundances, should have lower levels of genetic diversity than low-risk species and *vice-versa*. However, contradictory evidence, for birds and mammals (Reed 2010), suggests that omitting genetic diversity from threat classification criteria could potentially lead to under- or over-estimating the actual extinction risk of species.

Here, we investigate whether bird species considered at risk of extinction, by widely used threat assessment criteria (IUCN 2021), have less intra-specific nucleotide diversity than non-threatened bird species (Supporting information). To accomplish this aim, we established differences in intra-specific nucleotide diversity for threatened (Vulnerable – VU, Endangered – EN and Critically Endangered – CR) vs non- threatened bird species (Least Concern – LC and Near Threatened – NT) by compiling 28,403 publicly available avian mitochondrial DNA (mtDNA) sequences from GenBank. We calculated cytochrome-b (*cyt-b*) nucleotide diversity for 1,036 species (approximately 10% of all bird species), with an average number of sequences per species being 27 ± 44 (Supporting information). The average sequence length (base-pairs) across species was 887 ± 201. Using phylANOVAs, to control for phylogenetic signal (Freckleton et al. 2002), corrected for varying sample sizes between groups, we show that threatened species have significantly lower *cyt-b* nucleotide diversity ($p < 0.05$, in 953 out of the 1000 phylANOVA repetitions; mean $p = 0.010 \pm 0.025$) than non-threatened species (Fig. 1a; Supporting information), with medium to large effect size in 97.2% of repetitions ($\omega 2 > 0.06$). The mean effect size was 0.16 ± 0.05 (Supporting information).

Our results reveal that current threat assessment criteria indirectly prioritize species with low levels of *cyt-b* nucleotide diversity, which can be at greater risk of extinction by virtue of low genetic diversity (Frankham 2005) (Fig. 1c). For example, the African houbara (*Chlamydotis undulata*, VU) is among the birds with the lowest *cyt-b* nucleotide diversity in our data set (≤10th percentile: GD ≤ 0.0015; Fig. 1d), and its persistence is affected by inbreeding and/or genetic drift (Korrida et al. 2012). Moreover, the millerbird (*Acrocephalus familiaris*, CR) and the inaccessible finch (*Nesospiza*

acunhae, VU) are both range-restricted small-island endemics with limited *cyt-b* nucleotide diversity (≤ 10th percentile; Supporting information), making them particularly vulnerable to rapid environmental changes from introduced predators and extreme climatic events (Vincenzi et al. 2017). Although mtDNA has been shown, under some circumstances, to be of limited use for inferring population size (Bazin et al. 2006, Nabholz et al. 2009), the low levels of nucleotide diversity in threatened species of birds suggest a correlation, direct or indirect, between *cyt-b* nucleotide diversity and small population or range size. For species that have not experienced large range contractions and population declines in recent times (non-threatened species), we found that *cyt-b* nucleotide diversity was generally high (≥ 90th percentile: GD ≥ 0.0302). Higher levels of genetic diversity might, through the process of local adaptation, aid species' resilience to rapid environmental changes (DeWoody et al. 2021) and reverse or slow species' decline (Fig. 1c). However, in some instances, non-threatened species can harbour low genetic diversity, most probably due to recent or past bottlenecks (Weber et al. 2000).

Four per cent of all non-threatened birds analysed had low levels of *cyt-b* nucleotide diversity (≤ 10th percentile; Fig. 1b). For example, the sooty tit (*Aegithalos fuliginosus*, LC; Fig. 1d) is the non-threatened species with the lowest *cyt-b* nucleotide diversity in our data set (Supporting information). Despite having a restricted range, the sooty tit is considered as 'Least Concern', due to a population that is suspected to be stable (IUCN 2021). Low nucleotide diversity for the sooty tit signals that extinction risk for the species might be higher than its IUCN threat status indicates, encouraging further assessments of its conservation status using census and genomic techniques. Low genetic diversity in non-threatened species can result from recent or past dramatic demographic events, after which levels of intra-specific genetic diversity remain temporally low, while the overall population size increases (Weber et al. 2000). For these species, whole-genome studies will help reveal the role of genetic diversity in long-term species survival.

While our results could be contingent on the length of sequences, sample size, and geographic and taxonomic biases associated with genetic sequences in public repositories such as GenBank, we found no correlation between nucleotide diversity and average sequence length or number of sequences (Supporting information). Furthermore, we found a low phylogenetic signal ($\lambda = 0.56$, $p < 0.001$), and the phylANOVAs confirm the independence of the data in relation to the evolutionary history of the species (Supporting information). Indeed, there is a significant difference between the F-statistics calculated on the actual data and the F-statistics calculated with simulated data (null hypothesis; Supporting information). Lastly, our results do not reflect geographic biases in our

dataset, which covers ~57% of all avian families and all zoogeographic realms (Supporting information). Despite existing challenges with using mitochondrial data and single genetic markers (Carling and Brumfield 2007), including the real possibility that genetic diversity calculated using mtDNA might not reflect genome-wide diversity or the diversity of specific functionally relevant parts of the genome, the relationship between conservation status and genetic diversity, explored in this paper, concords with long-standing expectations from the literature (DeWoody et al. 2021), including findings from meta-analyses across smaller subsets of taxa (Spielman et al. 2004, Willoughby et al. 2015) using nuclear DNA (allozymes, microsatellites, minisatellites), and other mtDNA genes (Petit-Marty et al. 2021).

Species-level conservation criteria capture low levels of intra-specific nucleotide variability in species of greatest concern. Nonetheless, low levels of nucleotide diversity are present in a small proportion of non-threatened birds, causing them, in theory, to be more vulnerable to rapidly changing environmental conditions than their conservation status, alone, indicates (Frankham 2005). As genomic techniques get cheaper, the inclusion of whole-genome data in relevant measures of genetic diversity is a likely near-term prospect for conservation. Future research should aim to integrate large-scale field-work campaigns with strategic sequencing of contemporary and historical specimens from biological collections, in order to unravel eco-evolutionary determinants of increased extinction risk.

References

Bazin, E. et al. 2006. Population size does not influence mitochondrial genetic diversity in animals. – Science 312: 570–572.

Canteri, E. et al. 2021. Data from: IUCN Red List protects avian genetic diversity. – Dryad Digital Repository, <https://doi.org/10.5061/dryad.pzgmsbcn6>.

Carling, M. D. and Brumfield, R. T. 2007. Gene sampling strategies for multi-locus population estimates of genetic diversity (θ). – PLoS One 2: e160.

DeWoody, J. A. et al. 2021. The long-standing significance of genetic diversity in conservation. – Mol. Ecol. 30: 4147–4154.

Frankham, R. 1996. Relationship of genetic variation to population size in wildlife. – Conserv. Biol. 10: 1500–1508.

Frankham, R. 2005. Genetics and extinction. – Biol. Conserv. 126: 131–140.

Freckleton, R. et al. 2002. Phylogenetic analysis and comparative data: a test and review of evidence. – Am. Nat. 160: 712–726.

IUCN 2021. The IUCN Red List of threatened species. Ver. 2021-1. – <www.iucnredlist.org>.

Korrida, A. et al. 2012. Patterns of genetic diversity and population structure of the threatened houbara and macqueen's bustards as revealed by microsatellite markers. – Genet. Mol. Res. 11: 3207–3221.

Nabholz, B. et al. 2009. The erratic mitochondrial clock: variations of mutation rate, not population size, affect mtDNA diversity across birds and mammals. – BMC Evol. Biol. 9: 1–13.

Petit-Marty, N. et al. 2021. Use of the nucleotide diversity in COI mitochondrial gene as an early diagnostic of conservation status of animal species. – Conserv. Lett. 14: e12756.

Reed, D. H. 2010. Albatrosses, eagles and newts, Oh My!: exceptions to the prevailing paradigm concerning genetic diversity and population viability? – Anim. Conserv. 13: 448–457.

Spielman, D. et al. 2004. Most species are not driven to extinction before genetic factors impact them. – Proc. Natl Acad. Sci. USA 101: 15261–15264.

Vincenzi, S. et al. 2017. Genetic and life-history consequences of extreme climate events. – Proc. R. Soc. B 284: 2016–2118.

Weber, D. S. et al. 2000. An empirical genetic assessment of the severity of the northern elephant seal population bottleneck. – Curr. Biol. 10: 1287–1290.

Willoughby, J. R. et al. 2015. The reduction of genetic diversity in threatened vertebrates and new recommendations regarding IUCN conservation rankings. – Biol. Conserv. 191: 495–503.

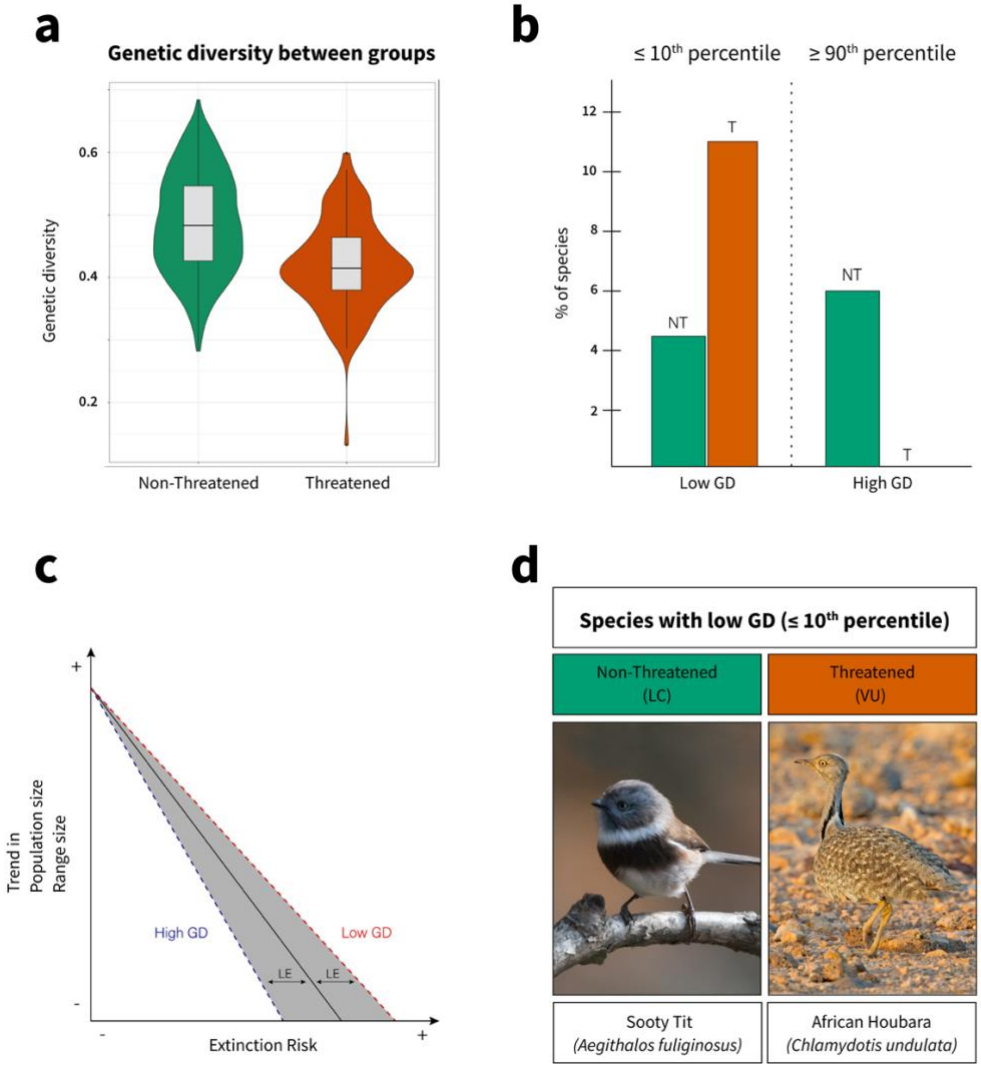

Figure 1. Genetic diversity in threatened and non-threatened bird species. (a) Threatened species have significantly lower intra-specific *cyt-b* nucleotide diversity than non-threatened species. (b) Percentage of threatened (T) and non-threatened (NT) species with the lowest (≤ 10th percentile) and highest (≥ 90th percentile) values of *cyt-b* nucleotide diversity. (c) Conceptual figure showing a species experiencing declines (negative trend) in range size and/or population abundance through time, enhancing its extinction risk. Due to low or high genetic diversity (GD; low or high GD), the same species might be of greater (red dashed line) or lesser (blue dashed line) extinction risk, respectively, potentially producing a mismatch between the evaluated extinction risk (black solid line) and the actual extinction risk (latent extinction risk, LE). (d) Examples of a non-threatened (sooty tit: *Aegithalos fuliginosus*; photo credits: Tim Melling) and a threatened bird species (African houbara: *Chlamydotis undulata*) with some of the lowest levels of *cyt-b* nucleotide diversity (≤ 10th percentile).

Supporting Information

Summary

We tested for significant differences in the intra-specific genetic diversity of *Threatened* versus *Non-threatened* species, by compiling a dataset of genetic sequences of birds, doing species-specific alignments, and calculating genetic diversity. Because closely related species share evolutionary history and, therefore, might show similar values of genetic diversity, we identified the phylogenetic signal (Pagel's $\lambda = 0.56$, $P < 0.001$; see "Analyses" section below) and accounted for it directly in our analysis of genetic diversity. We did this using phylANOVAs (Revell 2019). To account for differences in group sizes (threatened versus non-threatened) we re-sampled the data without replacement. Lastly, we explored the geographic coverage of species in the dataset, using zoogeographical realms, and identified the species with the lowest and highest values of genetic diversity.

Dataset compilation

We retrieved all the mitochondrial DNA (*mtDNA*) sequences for birds available in GenBank (181,290 sequences) (Benson et al. 2003), using "mitochondrion" as the search query and by filtering by taxonomic group (class: *Aves*). We chose the cytochrome-b (*cytb*) locus of the *mtDNA* because it maximized the number of sequences and species covered. We compiled a dataset consisting of 45,348 *cytb* sequences of bird species and their associated metadata, retrieved from GenBank the 5th of April 2018. Sequence information includes: *Accession Number*, *Species Name*, *Locus Name* and *Sequence Length* (number of base pairs).

Species names in GenBank are provided either at the species level or at the subspecies level. No specific taxonomy is followed in GenBank, and the species names are not updated according to recent taxonomic changes. Because there is not one universal taxonomy for Aves, we merged three different taxonomies, following the steps below.

1) To calculate the phylogenetic signal (and account for phylogenetic autocorrelation in our analysis), we aligned the GenBank names with the taxonomy of the Hackett Tree sourced from (Jetz et al. 2012), which is the most comprehensive phylogeny of birds at the species level. We matched the GenBank names, at the species level, to the BirdLife International Checklist v3 (2010) (BirdLife International 2010), which is the main taxonomy used by (Jetz et al. 2012). If a name failed the matching process, we looked manually in Avibase (Lepage

et al. 2014) to verify its presence as a synonym in the Checklist. If no equivalent name was available, we discarded the species and its sequences from the analyses. All the new species names were then matched to the nomenclature provided by (Jetz et al. 2012), to verify their presence in the phylogeny.

2) We did the same process to standardize the original GenBank names, at the species level, to the IOC v2.2 taxonomy (Gill et al. 2009), to identify the zoogeographic realms inhabited by the bird species (Holt et al. 2013).

3) We used the latest taxonomy at the time, the HBW-BirdLife Checklist v2 (2017) (HBW and BirdLife International 2017), to assign the different IUCN Red List categories to the new species names (aligned with the Hackett Tree taxonomy). Categories include: *Extinct* (EX), *Extinct in the Wild* (EW), *Critically Endangered Possibly Extinct* (CR(PE)), *Critically Endangered Possibly Extinct in the Wild* (CR(PEW)), *Critically Endangered* (CR), *Endangered* (EN), *Vulnerable* (VU), *Near Threatened* (NT), *Least Concern* (LC) and *Data Deficient* (DD, i.e. species for which the data is too scarce to make an assessment). A category was assigned only if the new species names had a positive match in the checklist, either under the "*Species*" column or the "*Synonyms*" column. Sometimes, the species names were not recognized anymore by the latest taxonomy, and therefore they were assigned to the category "NR" (i.e., *Not Recognized*). We then grouped species into *Threatened* and *Non-Threatened*, whereby *Threatened* species were CR(PE), CR(PEW), CR, EN and VU; while *Non-Threatened* were NT and LC species (IUCN 2012).

Hybrid, extinct, domesticated species, and species with uncertain nomenclature were excluded from the alignments and the calculation of genetic diversity. Hybrids were easily recognised as they are reported in GenBank as a combination of the parent species, e.g., *"Saxicola rubetra x Phoenicurus phoenicurus"*. Species with uncertain nomenclature are usually reported only by the genus name, e.g., *"Adelomyia sp. JAMG"*. Domesticated species were identified both by checking the World Watch List (FAO 2000) of the Food and Agriculture Organisation of the United Nations (FAO) and other sources. Because different species of parrots and birds of prey are used as pets by humans, we thoroughly checked the source literature to verify whether the individuals sequenced were either taken from captive individuals or from wild populations. When no information about the location was provided, we followed a conservative approach and excluded the sequences.

After doing species-specific alignments and calculating genetic diversity (described in the sections below), we further checked for taxonomic splits and found 184 species with possible taxonomic uncertainty. For each of these 184 species, we reviewed the source literature to identify which sequences belonged to the species name under consideration or to new taxonomic splits included in the phylogeny. If the sequences belonged to species not included in the phylogeny, we corrected the alignments by removing the sequences.

To perform additional checks on the correctness of sequences and taxonomy, we built a phylogenetic tree for each "Genus" in our dataset and checked that all sequences belonged to the correct species. We used Geneious v9.1.8 (Kearse et al. 2012) to align the sequences belonging to the species in the same "Genus", and we built phylogenetic trees using the PhyML plugin (Guindon et al. 2010), with a HKY85 substitution model and default parameters. Based on the phylogenetic tree, we corrected the sequences that were wrongly assigned and, for species showing clade divergence, we removed sequences belonging to separate clades. The final dataset consisted of genetic diversity values for 1,036 species, with 934 *Non-threatened* and 102 *Threatened* species. The final dataset consists of mean 27 sequences per species, median 11 sequences and a standard deviation of 44.

The final selection of species covers approximately 10% of all bird species, representing ~57% of all avian families, and all biogeographical realms. We estimated the geographical representation by checking the zoogeographic realms (Holt et al. 2013) our species inhabit. The dataset provided by Holt et al. 2013 includes a list of species names for each realm. Therefore, for each realm, we matched the species in our dataset to the list of species names and calculated the percentage of species represented by our dataset, compared to the total number of species inhabiting the realm. Some species might belong to multiple zoogeographic realms because breeding and wintering ranges may not be confined to the same realm. Our final dataset covers the 5.5% of the total number of species present in the Afrotropical realm, the 9.0% in the Australian, the 12.6% in the Madagascan, the 18.8% in the Nearctic, the 8.9% in the Neotropical, the 6.5% in the Oceanian, the 12.1% in the Oriental, the 28.7% in the Palearctic, the 9.1% in the Panamanian, the 24.3% in the Saharo-Arabian and the 22.3% in the Sino-Japanese realm.

Species-specific alignments

Because the sequences downloaded from GenBank might contain more than one locus, we isolated the regions of the sequences that belong to *cytb*, by mapping all the sequences to a well-known species' complete genome (*Gallus gallus gallus*: AP003322) in Geneious v9.1.8 (Kearse et al. 2012).

The regions of the sequences that successfully assembled to the reference were then extracted. Some sequences were either wrongly mapped by the algorithm or failed the assemblage test. One explanation for the failure could be that some species have a re-organization in the position of the loci along the *mtDNA* and therefore they could not match with the reference during the assemblage. They were therefore mapped again using a reference species which is known to have the gene order differing from the standard order in birds (*Phylloscopus inornatus* KF742677.1 and DQ792800) (Qing et al. 2015), to maximize the extraction of *cytb* regions. 44,675 sequences successfully assembled to the reference sequences, while 673 sequences were discarded because unsuccessfully mapped to the references. At the end of the process, the length of the sequences can vary greatly within the same locus, ranging from complete *cytb* sequences (1,143 base pairs, *bp*) to less than 100 base pairs (*bp*).

We did species-specific alignments by using default settings of MUSCLE and a gap open penalty of -1000, to avoid an excessive creation of gaps (Edgar 2004). Each species-specific alignment was then manually checked for errors (e.g., insertions, deletions, untrue gaps), using Geneious v9.1.8. Because the MUSCLE algorithm forces the sequences to overlap, some alignments contained gaps. Gaps can be either incorrectly generated during the alignment process (untrue gaps) or they can result from the presence of non-overlapping sequences (i.e., sequences that belong to different areas of the gene). In the latter case, the sequences were re-mapped to a reference genome (*Gallus gallus gallus*: AP003322), to identify their specific position within the locus and to verify that the sequences were non-overlapping or overlapping only in few base pairs. After detecting the correct position of the sequences, we manually removed the gaps and moved the sequences to non-overlapping positions or their respective positions. Sometimes, few gaps were necessary to keep the correctness of the alignments, as some sequences missed the transcription of some nucleotide bases when uploaded to GenBank. While checking the alignments one by one, the reading frame was translated to verify that all sequences were free of stop codons, therefore representing true *mtDNA* sequences and not pseudogenes (or numts). Some alignments contained identical sequences identified with different accession numbers. In GenBank, the "NC_" prefix is used to define complete genomes (Pruitt et al. 2002). Because we extracted the *cytb* locus from all the sequences, the sequences with "NC_" as a prefix were identical to other sequences belonging to the same individuals. The sequences with the prefix "NC_" were therefore removed from the alignments to avoid duplicates.

Calculation of genetic diversity

Genetic diversity (GD) can be calculated using different metrics (Hughes et al. 2008). The most common for *mtDNA* is haplotype diversity (*h*), which identifies unique haplotypes in the population (Nei 1987). Metrics that consider haplotypes require sequences to be of the same length. Because the data uploaded to GenBank does not fulfil this requirement, we used nucleotide diversity (π) as a measure of genetic diversity. Nucleotide diversity (π) can be calculated as the average number of different nucleotides per site for pairs of sequences (Nei et al. 1979, Goodall-Copestake et al. 2012). However, this definition assumes sequences to be of the same length. Because the sequences in the species-specific alignments differ in the total number of base pairs (*bp)*, we account for the difference in length in each pairwise comparison, to obtain an unbiased measure of π. We followed part of the methodology described in (Miraldo et al. 2016), which is mathematically shown in Equation 1:

$$\widehat{\Pi} = \frac{1}{\binom{n}{2}} \sum_{i=1}^{n-1} \sum_{j=i+1}^{n} \frac{k_{ij}}{m_{ij}}$$

Equation 1

where $\binom{n}{2}$ is the number of pairwise comparisons and k_{ij} is the number of variable sites between sequence *i* and sequence *j*. The k_{ij} of each pairwise comparison is divided by the length of the overlapped sequences (m_{ij}). To avoid under-estimates of π, only sequences that overlap in at least 50% of the longer sequence are used to calculate nucleotide diversity. Likewise, very short sequences ($\leq$ 60 *bp*, ~5% of the total length of the *cytb* gene) were discarded from the alignments before calculating genetic diversity (Accession numbers: AY141960.1, AY141961.1, AY141962.1, AY141963.1, AY141964.1, AY141965.1, AY141966.1, AY141967.1, AY141968.1, AY141969.1, KC875857.1). These calculations were done in Matlab R2018b (MATLAB 2018). After obtaining intra-specific genetic diversity values for each species, we removed species with zero values, because they are likely to be an artefact of the methodology we employed to calculate genetic diversity. Zero values can result from sequences being too short to show variability or because sequences get eliminated by the 50% overlap criteria. Finally, we kept only species with > 5 sequences, because estimations based on < 5 may lead to unreliable estimates of genetic diversity (Miraldo et al. 2016).

Analyses

We used analysis of variance to determine differences in intra-specific genetic diversity between *Threatened* and *Non-threatened* species. We used Pagel's lambda (λ) (Pagel 1999) to compute the

phylogenetic signal, using the '*phytools'* R package (Revell 2019). A value of $\lambda < 1$ means that the trait is less similar among species compared to what is expected given their relatedness, while a value of $\lambda > 1$ has the opposite explanation (Pagel 1999). We obtained $\lambda = 0.5559083$, with $P < 0.001$ from the likelihood ratio test. Although the signal is relatively low, we used phylogenetic ANOVAs (phylANOVA) to account for any phylogenetic autocorrelation. Because our genetic diversity values do not meet the assumption of normality, required by the ANOVA, the GD values were transformed using a power transformation:

$$GD_{pt} = \hat{\Pi} * 0.15$$

Equation 2

where 0.15 is the lambda value defined by Tukey's Ladder of Power, using the '*rcompanion'* R package (Mangiafico 2016).

We did 1,000 phylANOVAs (package *'phytools'* in R) using re-sampling (number of species = 50) to ensure equal sample size for the two groups. The phylANOVA first computes the F-statistic using a normal one-way ANOVA based on the given data. Then, it generates new data by simulating a generic trait along the tree and calculates the F-statistic using a one-way ANOVA on the generated data. It performs this last step for 1,000 times (default). Lastly, it compares the F-value from the given data to the F-values from the generated data and outputs a p-value, together with the ANOVA table on the given data. Because the phylANOVA function does not return the F-values from the simulated data, we modified the function to output the F-values of both the given and the simulated data, so we could view their distributions. The distributions of the F-values and of the p-values from the 1,000 repetitions are shown in **Figure S1**. Our results are contingent on the fragmented and scarce availability of avian genetic sequences (mean 27 sequences per species; median 11, standard deviation 44), which may not represent all the populations within species. In order to estimate the effect size in our models, we calculated omega-squared (ω^2) for each of the phylANOVA repetitions. Omega-squared is a less biased measure of the strength of association between variables and represents the proportion of the total population variance that is explained by the group of interest (Hays 1963, Okada 2013). Omega-squared is defined in Equation 3 (Hays 1963) as:

$$\omega^2 = \frac{SS_b - df_b MS_w}{(SS_b + SS_w) + MS_w}$$

Equation 3

Where SS_b is the sum of squares between groups, df_b is the degrees of freedom between groups, MS_w is the mean of squares within groups, and SS_w is the sum of squares within groups. Because omega-squared is less influenced by the sample size, it is preferred to other effect size metrics used in one-way ANOVA (Okada 2013, Lakens 2013). Omega-squared takes values ± 1, and effect size is considered small if ω^2 = 0.01, medium if ω^2 = 0.06 and large ω^2 = 0.14 (Cohen 1988, Lakens 2013). 97.2% of the phylANOVA repetitions have a medium or large effect (ω^2 > 0.06). The distribution of ω^2 values from the 1,000 repetitions can be found in **Figure S1**. In the main text, we report mean and standard deviation of the distribution of p-values and omega-squared values from the 1,000 repetitions.

To identify *Non-threatened* and *Threatened* bird species with particularly low and high values of genetic diversity, we split the genetic diversity values in percentiles and identified the species falling in the lowest and the highest percentile based on three thresholds: 1) lowest 5th and highest 95th percentile; 2) lowest 10th and highest 90th percentile; 3) lowest 20th and highest 80th percentile. We filtered for species that have >10 sequences, to account for possible variance in the estimations of genetic diversity (Miraldo et al. 2016). 7 (6.9%) *Threatened* species and 21 (2.2%) *Non-threatened* species fall in the lowest 5th percentile, while 0 (0%) *Threatened* and 26 (2.8%) *Non-threatened* species fall in the highest 95th percentile. 11 (10.8%) *Threatened* and 43 (4.6%) *Non-threatened* species fall in the lowest 10th percentile, while 0 (0%) *Threatened* and 57 (6.1%) *Non-threatened* species fall in the highest 90th percentile. 20 (19.6%) *Threatened* and 87 (9.3%) *Non-threatened* species fall in the lowest 20th percentile, while 1 (1%) *Threatened* and 111 (11.9%) *Non-threatened* species fall in the highest 80th percentile. Because the pattern is similar even if using different thresholds, we decided to show the species falling in the lowest 10th (non-transformed GD = 0.0015) and highest 90th percentile (transformed GD = 0.378). The list of species is shown in **Table S1**.

Genetic diversity can be affected by the number of sequences for each species and the sequences length. In the first case, a sample size too low might not give a well representation of the species, and in the latter case, it can be difficult to find variability if sequences are too short. Therefore, we performed simple sensitivity analyses to identify potential biases. We performed a correlation test using the Kendall's rank correlation coefficient (Kendall 1938) to measure the relationship between genetic diversity and the number of sequences for each species. Because each species is represented by an alignment of multiple sequences, sequence length was calculated as the average length of sequences for each species. We tested the relationship between genetic diversity and average

sequence length using the Kendall's rank correlation coefficient. The results of these analyses are shown in **Figure S2**.

All the data and code used for the analyses are publicly available on DataDryad at: https://doi.org/10.5061/dryad.pzgmsbcn6

References

FAO 2000. World Watch List for domestic animal diversity (FAO, Ed.). - Food and Agriculture Organization of the United Nations (FAO).

Benson, D. A. et al. 2003. GenBank. - Nucleic Acids Res. 31: 23–27.

BirdLife International 2010. The BirdLife checklist of the birds of the world, with conservation status and taxonomic sources. Version 3.

Cohen, J. 1988. Statistical power analysis for the behavioural sciences. - Laurence Erlbaum Associates.

Edgar, R. C. 2004. MUSCLE: multiple sequence alignment with high accuracy and high throughput. - Nucleic Acids Res. 32: 1792–7.

Gill, F. et al. 2009. IOC World Bird List (v2.2). - IOC

Goodall-Copestake, W. P. et al. 2012. On the comparison of population-level estimates of haplotype and nucleotide diversity: A case study using the gene cox1 in animals. - Heredity. 109: 50–56.

Guindon, S., et al. 2010. New algorithms and methods to estimate maximum-likelihood phylogenies: assessing the performance of PhyML 3.0. - Syst Biol 59: 307-21.

Hays, W. L. Statistics for psychologists 1963 New York Holt. - Rinehart & Winston

HBW and BirdLife International 2017. Handbook of the Birds of the World and BirdLife International digital checklist of the birds of the world. Version 2.

Holt, B. G. et al. 2013. An Update of Wallace's Zoogeographic Regions of the World. - Science. 339: 74–78.

Hughes, A. R. et al. 2008. Ecological consequences of genetic diversity. - Ecol. Lett. 11: 609–623.

IUCN 2012. IUCN Red List categories and criteria, version 3.1, second edition. - IUCN.

Jetz, W. et al. 2012. The global diversity of birds in space and time. - Nature 491: 444–448.

Kearse, M. et al. 2012. Geneious Basic: An integrated and extendable desktop software platform for the organization and analysis of sequence data. - Bioinformatics 28: 1647–1649.

Kendall, M. G. 1938. A New Measure of Rank Correlation. - Biometrika 30: 81.

Lakens, D. 2013. Calculating and reporting effect sizes to facilitate cumulative science: a practical primer for t-tests and ANOVAs. - Front Psychol 4: 863.

Lepage, D. et al. 2014. Avibase - A database system for managing and organizing taxonomic concepts. - Zookeys: 117–135.

Mangiafico, S.S. 2016. Summary and Analysis of Extension Program Evaluation in R, version 1.18.1. rcompanion.org/handbook/.

MATLAB 2018. version 9.5.0.944444 (R2018b). Natick, Massachusetts: The MathWorks Inc.

Miraldo, A. et al. 2016. An Anthropocene map of genetic diversity. - Science. 353: 1532–1535.

Nei, M. 1987. Molecular evolutionary genetics. - Columbia University Press.

Nei, M. et al. 1979. Mathematical model for studying genetic variation in terms of restriction endonucleases. - Proc. Natl. Acad. Sci. U. S. A. 76: 5269–73.

Okada, K. 2013. Is Omega Squared Less Biased? a Comparison of Three Major Effect Size Indices in One-Way Anova. - Behaviormetrika 40: 129-147.

Pagel, M. 1999. Inferring the historical patterns of biological evolution. - Nature 401: 877–884.

Pruitt, K. et al. 2002. The Reference Sequence (RefSeq) Database. - In: McEntyre, J. and Ostell, J. (eds), Dictionary of Bioinformatics and Computational Biology. 2nd ed.n. Bethesda (MD): National Center for Biotechnology Information (US).

Qing, H. et al. 2015. Complete mitochondrial genome of Yellow-browed warbler Phylloscopus inornatus inornatus (Passeriformes: Sylviidae). - Mitochondrial DNA 26: 939–940.

Revell, L. J. 2019. Package 'phytools': Phylogenetic Tools for Comparative Biology (and Other Things).: 1–195.

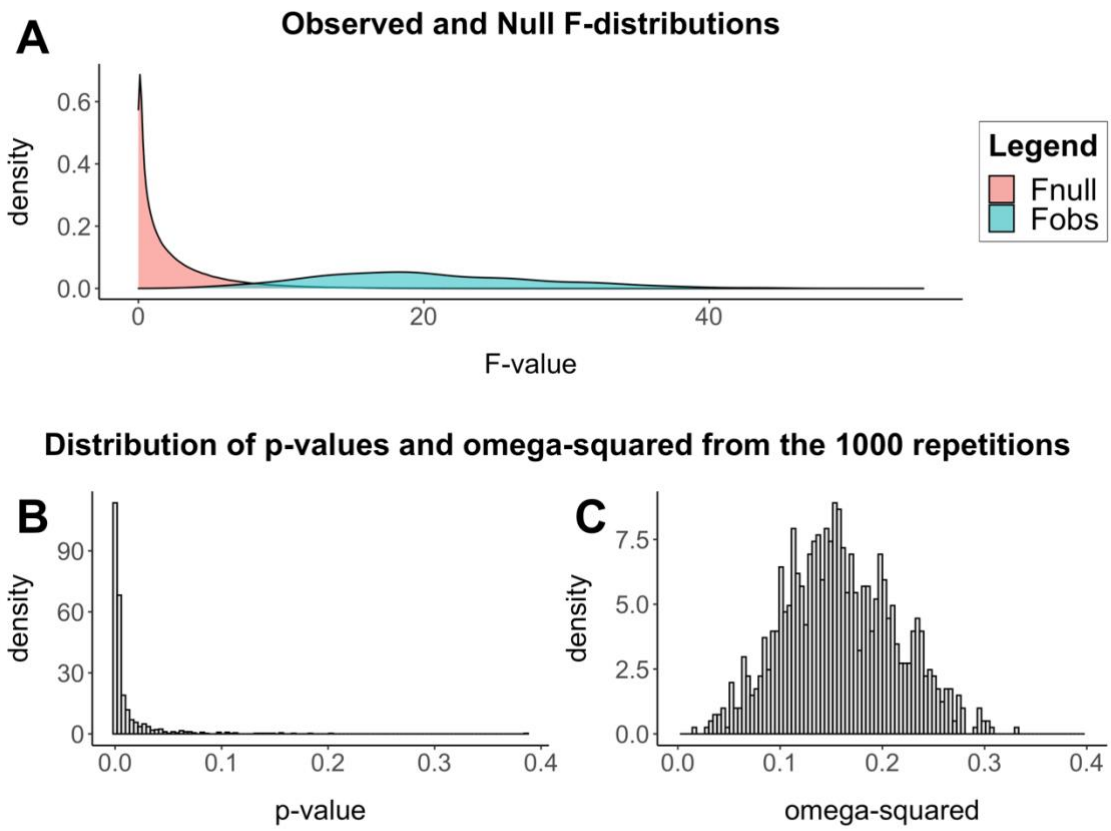

Figure S1. **Results from the 1,000 phylANOVA repetitions. A**) The distribution of the F-values calculated on the actual data (blue) and the distribution of the F-values calculated on the simulated data (pink) during the 1,000 phylANOVA repetitions. The ANOVAs performed with the simulated data represent the null hypotheses. The two distributions overlap only in a small area, which represents the area where the null hypotheses cannot be rejected. The p-value in phylANOVA is given by the proportion of F-values, calculated on the actual data (blue), that are greater or equal to the F-values calculated on the simulated data (pink). Given that the overlap between distributions is small, the majority of the phylANOVA models are statistically significant. **B**) Histogram showing the distribution of p-values from the 1,000 phylANOVA repetitions. The repetitions with p-values > 0.05 reflect the overlap in the F-values distributions (**A**). **C**) Histogram showing the distribution of the omega-squared (ω^2) values from the 1,000 repetitions. Omega-squared measures the proportion of total variation in the population associated to the factor of interest.

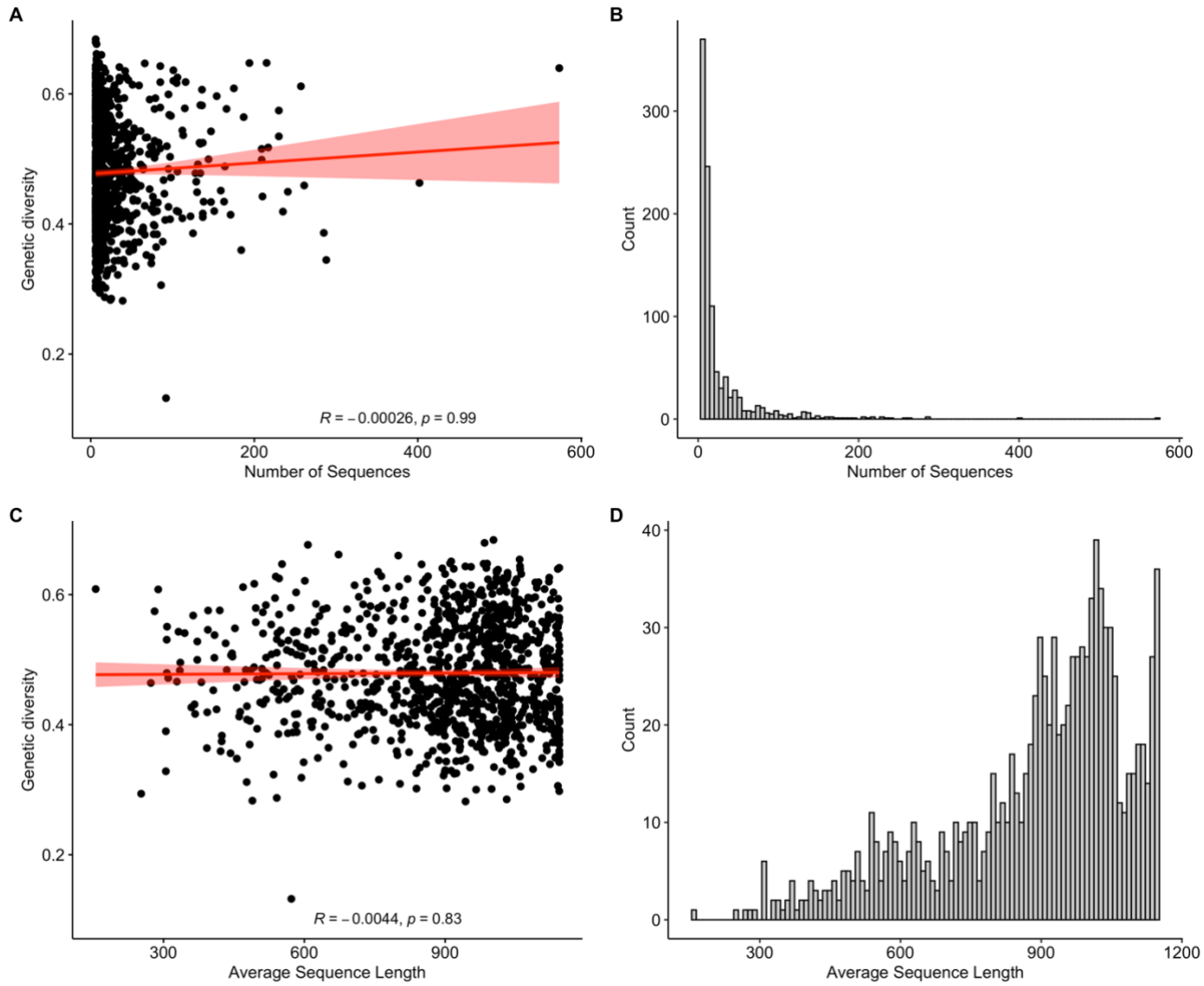

Figure S2. Sensitivity analyses. Sequence number and sequence length correlation to genetic diversity. (**A**) Correlation between genetic diversity and number of sequences for the 1,036 species included in the analyses. The correlation coefficient is Kendall's rank coefficient. (**B**) Distribution of the number of sequences among the 1,036 species included in the analyses. The minimum number of sequences is 6, and the maximum is 573. (**C**) Correlation between genetic diversity and the average sequence length for each species. The correlation coefficient is Kendall's rank coefficient. (**D**) Distribution of the average sequence length for each species. The minimum length is 64 base-pairs (bp) and the maximum is the full cytochrome-b gene (1143 bp).

Table S1. List of species with the lowest (≤ 10th percentile) and highest (≥ 90th percentile) genetic diversity (GD) values in the dataset. The species are sorted from the lowest to the highest genetic diversity values within the percentile.

Low GD (≤ 10th percentile)		High GD (≥ 90th percentile)	
Threatened	Non-Threatened	Threatened	Non-Threatened
Platalea minor	*Aegithalos fuliginosus*		*Basileuterus hypoleucus*
Nesospiza acunhae	*Zonotrichia leucophrys*		*Eopsaltria australis*
Chlamydotis undulata	*Dendragapus fuliginosus*		*Malacocincla malaccensis*
Anodorhynchus hyacinthinus	*Chen canagica*		*Sylvietta rufescens*
Charadrius obscurus	*Larus occidentalis*		*Rhipidura javanica*
Puffinus yelkouan	*Phoebetria palpebrata*		*Hylophilus ochraceiceps*
Acrocephalus familiaris	*Halobaena caerulea*		*Nectarinia jugularis*
Goura cristata	*Milvus milvus*		*Lepidothrix coronata*
Pterodroma madeira	*Zosterops xanthochroa*		*Phoenicurus ochruros*
Pterodroma solandri	*Dendroplex kienerii*		*Bleda eximius*
Pterodroma magentae	*Fringilla teydea*		*Malacoptila rufa*
	Anser anser		*Phylloscopus trochiloides*
	Anas strepera		*Cardinalis cardinalis*
	Plectrophenax hyperboreus		*Taraba major*
	Anas platyrhynchos		*Aulacorhynchus derbianus*

	Icterus abeillei		*Chloropsis cochinchinensis*
	Ficedula albicilla		*Copsychus saularis*
	Larus heermanni		*Capito auratus*
	Gavia immer		*Forpus xanthopterygius*
	Zosterops japonicus		*Chiroxiphia caudata*
	Paroaria coronata		*Tachymarptis melba*
	Catharus fuscescens		*Colluricincla megarhyncha*
	Newtonia archboldi		*Ithaginis cruentus*
	Parus rufescens		*Aegotheles bennettii*
	Rhegmatorhina berlepschi		*Dendrocincla fuliginosa*
	Aythya fuligula		*Francolinus coqui*
	Xiphorhynchus obsoletus		*Sclerurus mexicanus*
	Lonchura spectabilis		*Sclerurus rufigularis*
	Plectrophenax nivalis		*Bleda notatus*
	Pachyptila salvini		*Saltator coerulescens*
	Puffinus pacificus		*Scytalopus speluncae*
	Parus atricapillus		*Basileuterus culicivorus*
	Anairetes reguloides		*Bernieria zosterops*
	Leucosticte tephrocotis		*Alethe poliocephala*
	Lagopus muta		*Pycnonotus goiavier*
	Parus cyanus		*Microcerculus marginatus*
	Zonotrichia atricapilla		*Tyto alba*

	Lonchura melaena		*Pomatorhinus schisticeps*
	Aegolius acadicus		*Phaeothlypis fulvicauda*
	Calidris ptilocnemis		*Aphelocoma unicolor*
	Sitta pygmaea		*Hylophylax naevius*
	Bambusicola thoracicus		*Premnoplex brunnescens*
	Garrulax delesserti		*Trogon rufus*
			Henicorhina leucosticta
			Athene noctua
			Colonia colonus
			Collocalia esculenta
			Habia rubica
			Chlorospingus ophthalmicus
			Glyphorynchus spirurus
			Adelomyia melanogenys
			Bleda syndactylus
			Arremon aurantiirostris
			Aulacorhynchus prasinus
			Schiffornis turdina
			Xenops minutus
			Megascops guatemalae

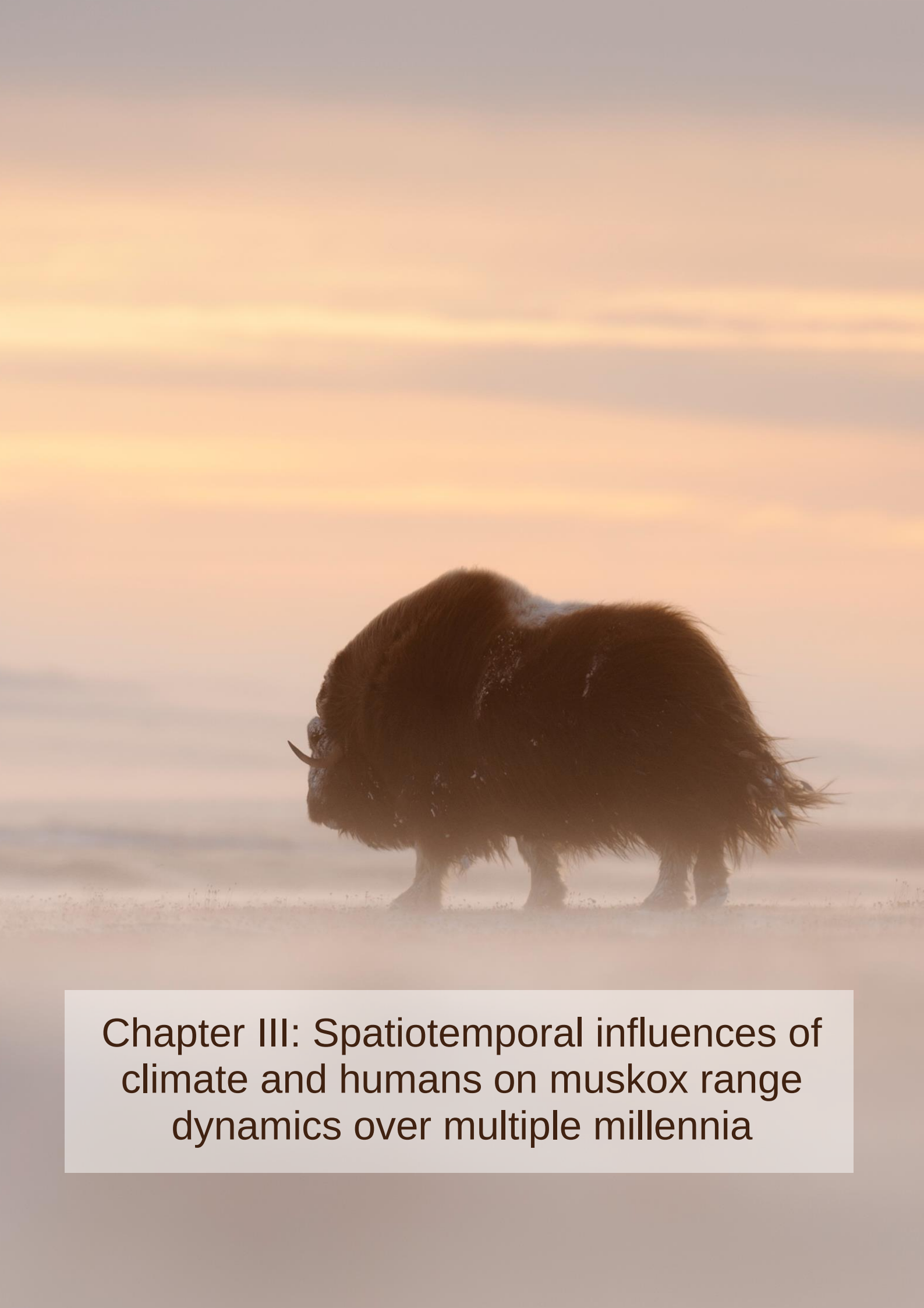

Chapter III: Spatiotemporal influences of climate and humans on muskox range dynamics over multiple millennia

Photo by Lars Holst Hansen

Statement of Authorship

Title of Paper	Spatiotemporal influences of climate and humans on muskox range dynamics over multiple millennia
Publication Status	☐ Published ☐ Accepted for Publication ☑ Submitted for Publication ☐ Unpublished and Unsubmitted work written in manuscript style
Publication Details	Title: Spatiotemporal influences of climate and humans on muskox range dynamics over multiple millennia Author(s): Elisabetta Canteri, Stuart C. Brown, Niels Martin Schmidt, Rasmus Heller, David Nogués-Bravo, Damien A. Fordham Journal: Global Change Biology

Principal Author

Name of Principal Author (Candidate)	Elisabetta Canteri		
Contribution to the Paper	The candidate conceived the idea, together with their advisors. The candidate collected and processed the data, ran the analyses, produced the results, and led the writing of the manuscript, with contribution from all the co-authors.		
Overall percentage (%)	60%		
Signature		Date	28 March 2022

Co-Author Contributions

By signing the Statement of Authorship, each author certifies that:

iv. the candidate's stated contribution to the publication is accurate (as detailed above);

v. permission is granted for the candidate in include the publication in the thesis; and

vi. the sum of all co-author contributions is equal to 100% less the candidate's stated contribution.

Name of Co-Author	Stuart C. Brown		
Contribution to the Paper	Helped running the analyses and contributed with results interpretation and the writing of the manuscript.		
Signature		Date	28 April 2022

Name of Co-Author	Niels Martin Schmidt		
Contribution to the Paper	Contributed with expert knowledge of the species under study, results interpretation, and with the writing of the manuscript.		
Signature		Date	2022-03-28

Name of Co-Author	Rasmus Heller		
Contribution to the Paper	Contributed with expert knowledge of the species under study, results interpretation, and with the writing of the manuscript.		
Signature		Date	29 March 2022

Name of Co-Author	David Nogués-Bravo		
Contribution to the Paper	Contributed with the conceptualization of the research idea, with supervision, writing of the manuscript and funding acquisition.		
Signature		Date	02/05/2022

Name of Co-Author	Damien A. Fordham		
Contribution to the Paper	Contributed with the conceptualization of the research idea, with supervision, writing of the manuscript and funding acquisition.		
Signature		Date	02/05/2022

Title

Spatiotemporal influences of climate and humans on muskox range dynamics over multiple millennia

Running Title

21,000 years of muskox range dynamics

Elisabetta Canteri[1,2], Stuart C. Brown[1,3], Niels Martin Schmidt[4], Rasmus Heller[5], David Nogues-Bravo[2] and Damien A. Fordham[1,2].

[1] The Environment Institute and School of Biological Sciences, University of Adelaide, Adelaide, Australia
[2] Centre for Macroecology, Evolution and Climate, GLOBE Institute, Faculty of Health and Medical Sciences, University of Copenhagen, Copenhagen, Denmark
[3] Section for Evolutionary Genomics, GLOBE Institute, University of Copenhagen, Copenhagen, Denmark
[4] Department of Ecoscience, Aarhus University, Roskilde, Denmark
[5] Bioinformatics Centre, Department of Biology, University of Copenhagen, Copenhagen, Denmark

Abstract

Processes leading to range contractions and population declines of Arctic megafauna during the late Pleistocene and early-Holocene are uncertain, with intense debate on the roles of human hunting, climatic change, and their synergy. Obstacles to a resolution, have included an over reliance on correlative rather than process-explicit approaches for inferring drivers of distributional and demographic change. Using process-explicit macroecological models that integrate modern and fossil occurrence records, ancient DNA, spatiotemporal reconstructions of past climatic change, species-specific population ecology and the growth and spread of anatomically modern humans, we disentangle the ecological mechanisms and threats that were integral in the decline and extinction of the muskox (*Ovibos moschatus*) in Eurasia, and in its expansion in North America. We show that accurately reconstructing inferences of past demographic changes for muskox over the last 21,000 years requires high dispersal abilities, large maximum densities, and a small Allee effect. Climatic change was the primary driver of muskox distribution shifts and demographic changes across its previously extensive (circumpolar) range, with populations responding negatively to rapid warming events. Regional analyses reveal that the range collapse and extinction of the muskox in Europe (~ 13 thousand years ago) was caused by hunting by humans operating in synergy with climatic warming. In Canada and Greenland, climatic change and human activities combined to drive recent population sizes. The impact of past climatic change on the range and extinction dynamics of muskox during the Pleistocene-Holocene transition signals a vulnerability of this species to future increased warming. By disentangling the ecological processes that shaped the distribution of the muskox through space and time, we show that process-explicit models have important applications for the future conservation and management of this iconic species in a warming Arctic.

Introduction

The Arctic is warming almost twice as fast as the rest of the world (Meredith et al., 2019; Screen & Simmonds, 2010), with mean annual temperatures forecast to increase by 3°C – 12°C (above 2010 conditions) by the end of the 21st century (Lee et al., 2021). This warming is causing biodiversity change, which is disrupting the structure and function of ecological systems (Post et al., 2019). However, climatic conditions in the Arctic have rarely been stable, with temperatures fluctuating enormously during glacial-interglacial cycles (Dansgaard et al., 1993), resulting in large biotic changes. These climate-driven biotic changes include declines in species distributions, population sizes and genetic diversity (Hansen et al., 2018; Lorenzen et al., 2011), regional and range-wide extinctions (Cooper et al., 2015; Stuart, 2015), shifts in community assembly (Wang et al., 2021), and ecosystem function (Zimov et al., 1995).

During the Late Quaternary, vast areas of Earth's terrestrial ecosystems experienced warming events that are similar in magnitude and pace to conditions predicted for the end of the 21st century (Brown et al., 2020). Establishing biotic responses to these past warming events can improve projections of future biodiversity, through a better understanding of how different spatiotemporal scales of climatic change affect biodiversity (Fordham et al., 2020). However, this often requires integrating ecological and evolutionary models with fossil and molecular inferences of biotic change (Fordham et al., 2014; Nogues-Bravo et al., 2018). Although this has generally been done correlatively (Svenning et al., 2011), process-explicit models are increasingly being used to simulate the ecological processes and the global change drivers that shaped spatiotemporal patterns of biodiversity (Fordham et al., 2020). These new approaches in macroecology (Connolly et al., 2017) are improving knowledge of eco-evolutionary dynamics (Hagen et al., 2021), allowing contested ecological and evolutionary theories to be assessed (Rangel et al., 2018), and biodiversity to be better understood and managed (Fordham et al., 2016).

The geographic distributions of Arctic species are highly dynamic (Beumer et al., 2019), with ranges forecast to shift in future decades (van Beest et al., 2021), due to demographic processes (population growth and dispersal) responding to spatiotemporal variations in abiotic and biotic conditions (Brown et al., 1996), affecting source-sink dynamics (Gaston, 2003). Thus, making robust projections of past and future range shifts for Arctic species requires spatially explicit population models (SEPMs) that simulate metapopulation and dispersal dynamics under climate and environmental change (Anderson et al., 2009). SEPMs that directly reconstruct spatiotemporal variations in demographic change not only establish dynamic responses of species to climatic change

and anthropogenic activities, but can also disentangle the spatiotemporal impacts of each of these drivers (Fordham, Brown, et al., 2021). This is particularly so, if spatiotemporal patterns inferred from the paleo-record and or historical observations are used to assess whether a model is adequate in its parameterisation and structure to simulate the underlying mechanisms (Fordham et al., 2016; Nogues-Bravo et al., 2018).

New approaches for reconstructing species' responses to multiple millennia of global change use inferences of demographic and distributional change from fossils and ancient DNA (aDNA) as independent, objective targets to identify whether models have the structural complexity and parameterisation needed to simulate species' range shifts and extinction risk (Fordham, Brown, et al., 2021). Under this pattern-oriented approach (Grimm et al., 2005), competing models are evaluated based on their ability to reconstruct biogeographical patterns inferred from paleo-archives, such as time and location of extirpation and colonization events, and changes in relative abundance (Fordham, Haythorne, et al., 2021). This approach, which integrates the disciplines of (macro)ecology, paleoecology, climatology, and genomics, is revealing the chains of causality that lead to species' range collapse and extinction over decades to millennia (Fordham, Brown, et al., 2021).

The Artic is an ideal system for using the past to inform contemporary conservation management and policy, because some Arctic regions experienced rates of warming that are analogous to future forecasts (Fordham et al., 2020). It also has a relatively high number of plant and animal fossils with good spatial and temporal coverage (Chevalier et al., 2020; Nogues-Bravo et al., 2018), a large volume of sequenced ancient DNA from a diverse range of species (Orlando & Cooper, 2014; Smith et al., 2003; Willerslev et al., 2003), and paleoclimate reconstructions with high-temporal resolutions (Steffensen et al., 2008). Consequently, the causes of late Quaternary extinctions of Arctic megafauna have been well studied (Cooper et al., 2015; Lister & Stuart, 2008; Lorenzen et al., 2011), including, most recently, with process-explicit models and pattern-oriented methods (Fordham, Brown, et al., 2021). However, the range dynamics of Arctic species that survived the climatically unstable Pleistocene/Holocene transition are less well understood. Here we use process-explicit macroecological models to reveal the range dynamics of the muskox (*Ovibos moschatus*) — a cold-adapted Arctic herbivore that regulates the structure and function of the tundra ecosystem (Post, 2013; Post & Pedersen, 2008) — over the last 21,000 years, and to potentially predict its responses to climatic change.

The muskox is naturally distributed in Northern Canada, Canadian Islands, and North and East Greenland, with translocated populations in Russia, Alaska (US), and Western Greenland (Cuyler et al., 2020). During the late Pleistocene, the muskox had a Holarctic distribution, stretching from Europe to North America (Markova et al., 2015). Its Eurasian range contracted during the last deglaciation, with the last surviving population going extinct ~ 2.6 ka BP (thousand years before present) in Taymir (Russia) (Campos et al., 2010; Markova et al., 2015). Conversely, when the range of the muskox was collapsing in Eurasia, North American populations were expanding their range on their route to colonising Greenland (Hansen et al., 2018). Previously, warming has been advocated as the primary driver of muskox extirpation in Eurasia, with little or no contribution of human activities such as harvesting (Campos et al., 2010; Lorenzen et al., 2011). However, the ecological processes of range collapse of muskox in Eurasia and range expansion in North America remain a mystery, having never been reconstructed at high spatiotemporal resolutions using validated process-explicit macroecological models.

We built one-hundred thousand plausible SEPMs that continuously reconstructed the range and population dynamics of the muskox since 21 ka BP under different levels of climate-driven resource availability and human exploitation. We used fossil evidence of past changes in the distribution and demography of muskox and pattern-oriented methods to validate these simulations. Models that could reconcile inferences of demographic change from fossils were used to determine the chains of causality responsible for the contemporary distribution of muskox, and to disentangle the ecological processes and drivers responsible for its extinction in Eurasia and range expansion in North America. We show that accurately reconstructing past demographic changes for muskox over the last 21,000 years from fossils and aDNA requires high dispersal abilities, large maximum densities, and a small Allee effect. Climatic change was the primary driver of the structure and dynamics of the geographic range of muskox, with exploitation by humans and its interaction with climatic changes being important in some regions.

Materials and Methods

We built process-explicit macroecological models of muskox that simulate interactions between metapopulation dynamics, climate variability, and hunting by humans (Figure 1). We used these models to continuously reconstruct 21,000 years of range contraction and expansion across Eurasia and North America. We refined the parameter space of our simulations of spatiotemporal abundance with pattern-oriented methods (Grimm & Railsback, 2012), using inferences of range shifts,

extirpation and colonisation events estimated from hundreds of fossils. The R code for the models can be found in Appendix 2 and the approach is described in detail in the Supplementary Methods. Appendix 1, Appendix 2, and Appendix 3 in support of this manuscript can be downloaded from this link: https://protect-au.mimecast.com/s/2JGoCoV140cK15mDi11ZQD?domain=datadryad.org

Ecological niche

To reconstruct the ecological niche of the muskox through space and time, we intersected radiocarbon dated and georeferenced fossils, and modern observations of muskox, with gridded climatic data: paleoclimate reconstructions and interpolated current day climate observation.

Fossils from the Late Pleistocene and Holocene were compiled from publicly available databases and published literature (see Supplementary Methods). The quality and reliability of all radiocarbon dates were assessed (Barnosky & Lindsey, 2010) and only fossils with an age quality score > 10 were used. The radiocarbon ages of these fossils were calibrated using OxCal and the IntCal20 calibration curve (Bronk Ramsey, 2009; Reimer et al., 2020). This resulted in 135 reliable fossil ages with geolocations and calibrated ages younger than 21 ka BP: the limit of our high-temporal resolution paleoclimatic data (Figure S1; Appendix 1). Fossil data was supplemented with modern occurrence observations for muskox in North America for the period 1700 AD – 2019 AD (Figure S1; Appendix 1). These records were retrieved from GBIF (GBIF.org, 2019).

Occurrence records from observations and fossils were intersected spatiotemporally with seven climatic variables: average minimum daily temperature in January, average maximum daily temperature in January, average maximum daily temperature in July, precipitation seasonality, annual precipitation, temperature seasonality, and evapotranspiration in spring and summer. Paleoclimate data came from the TraCE-21 ka simulation (Liu et al., 2009) accessed through PaleoView (Fordham et al., 2017) and is described in detail in Fordham et al. (2017). Because TraCE-21 data is not available after 1989 AD, we harmonised recent climate observations from CRU TS v4 (Harris et al., 2020) with the TraCE-21 simulation using the change factor method (Beyer et al., 2020). All climate data was resampled to a 1° × 1° resolution. Climate variables were tested for collinearity. Three variables with $|r| < 0.7$ (Dormann et al., 2013) were retained for modelling the ecological niche of the muskox: average minimum daily temperature in January, annual precipitation, and total evapotranspiration in spring and summer (Figure S2). These three climatic variables have been used previously to model the range dynamics of large vertebrates in Eurasia (Lorenzen et al., 2011;

Nogues-Bravo et al., 2010; Yannic et al., 2020; Yannic et al., 2014). These climatic variables are important distal predictors for arctic grazers, as they influence plant community composition and primary productivity, and thus forage availability and quality, which ultimately affect vital demographic rates and muskox population dynamics (Asbjornsen et al., 2005; Desforges et al., 2021). While important proximal predictors, such as snow depth and snow conditions (Asbjornsen et al., 2005; Desforges et al., 2021) were considered, they are difficult to simulate at a Holarctic scale (Foster et al., 1996), particularly over paleo time scales.

The climate-occurrence data was used to build a 3-dimensional hypervolume of climate suitability through time (Figure S3), generating a biologically relevant representation of the climatic conditions over which the muskox occurred at fossil and modern occurrence sites (Nogués-Bravo, 2009). We built a gaussian hypervolume of climate suitability using the 'hypervolume' R package (Blonder et al., 2014). We tuned the kernel density estimation (KDE) bandwidth using cross-validation (Blonder et al., 2014). We used the 'hypervolume' package because it does not require absence data, and because it generates projections that are less sensitive to extrapolation (Blonder et al., 2018).

The resulting hypervolume, which approximates the fundamental niche of the muskox (Nogués-Bravo, 2009), was exhaustively subsampled to generate thousands of potential realized niches (Fordham, Brown, et al., 2021). Subsampling of the niche was done using Outlier Mean Index (OMI) analysis (Dolédec et al., 2000), using plausible bounds of climatic specialisation and niche breadth (Fordham, Brown, et al., 2021). For each niche subsample (n = 2500), we generated spatial projections of climate suitability from 21 ka BP to 1500 AD at 8-years generational time steps. This allowed the realized niche of the muskox to be identified using process-explicit macroecological modelling (described below). Methods used to model the ecological niche of the muskox are described in detail in the Supplementary Methods.

Human relative abundance

Relative abundance and expansion of humans in Eurasia and North America was modelled using a Climate Informed Spatial Genetics Model (CISGeM) (Eriksson et al., 2012). Pattern-oriented modelling has shown that CISGeM can accurately reconstruct arrival times of anatomically modern humans and current-day distributions of effective population sizes (N_e) (Eriksson et al., 2012; Raghavan et al., 2015). This is done in CISGeM by modelling local N_e as a function of genetic history, local demography, paleoclimate, sea level and net primary productivity over the last 125k years (Eriksson et al., 2012; Raghavan et al., 2015).

Arrival time, occupancy, and density (here N_e) of humans were forced in CISGeM by spatiotemporal estimates of climate, sea level changes and ice sheet dynamics over the past 125 k years, operating at 25-year time steps. To do this, climate data from the HadCM3 global circulation model prior to the last glacial maximum was harmonized with TraCE-21 data (Fordham, Brown, et al., 2021). To account for parameter uncertainty in spatiotemporal projections of N_e, we used published upper and lower confidence bounds for CISGeM parameters (Eriksson et al. 2012) to generate ~ 4000 different plausible models of human migration (each with a unique combination of parameters), using Latin hypercube sampling (McKay et al. 1979). We rejected model simulations that were unable to successfully replicate arrival times in North America. We then calculated the multi-model mean and standard deviation for each grid-cell at each time step in the model from 21 ka BP and used this information to generate 100,000 potential human migration and population growth scenarios (Fordham, Brown, et al., 2021). All N_e values were scaled between 0 and 1 (using the 95th percentile of the values from the multi-model mean) and used as a measure of relative abundance of humans in the process-explicit macroecological model (Fordham, Haythorne, et al., 2021). CISGeM and its application are described in detail in the Supplementary Methods.

Climate-human-muskox interactions

The range dynamics of the muskox were simulated using a spatially explicit population modelling (SEPM) framework (Fordham, Haythorne, et al., 2021). Demographic processes (population growth, dispersal, source-sink dynamics and Allee effect etc.) were simulated as dynamically responding to changing climatic conditions, human harvesting, and their interactions, from 21k BP until 1500 AD. We did this using lattice-based stochastic demographic models, operating at a generational time step of 8 years (Hansen et al., 2018). These process-explicit models have been shown to be successful at projecting the range dynamics of species (Fordham et al., 2018; Fordham, Haythorne, et al., 2021), including extinct megafauna (Fordham, Brown, et al., 2021). SEPMs were built using the 'poems' and 'paleopop' R packages (Haythorne, Fordham, et al., 2021; Haythorne, Pilowsky, et al., 2021).

Driver-state relationships simulated the effects of climatic change and hunting by humans on key ecological processes of extinction: lability of the ecological niche, dispersal, population growth, and Allee effect. Dispersal was simulated using a distance-based function that limited movement to resource-depleted areas, and blocked movement across grid cells covered by sea or glacial ice (Haythorne, Fordham, et al., 2021). Carrying capacities and initial abundances were generated as a function of habitat suitability (i.e., availability of resources) (Fordham et al., 2018), and proportion

of glacial ice present in a grid-cell. We modelled density dependent growth using a logistic function (Ricker, 1954). Harvesting was modelled as a function of prey density, human density, exploitation rate, and prey availability (Alroy, 2001; Fordham, Brown, et al., 2021). An Allee effect was used to simulate rapid extinction at small population size (Fordham et al., 2013).

Models were parameterised using best estimates for demographic processes (population growth rate and variance, dispersal, Allee effect), environmental attributes (niche breadth and climatic specialisation), and threats (human abundance and exploitation rate). Values for these processes were varied across biologically plausible ranges (Table S1), using Latin Hypercube sampling of uniform probability distributions (Fordham, Haythorne, et al., 2021). This resulted in 100,000 conceivable model parametrizations, each with different demographic processes and rates of climate change and exploitation by humans. Each model was run for a single replicate (Prowse et al., 2016). The process-explicit model is described in detail in the Supplementary Methods.

Pattern-oriented modelling

We used pattern-oriented modelling (POM) to validate model simulations and optimize model parameters (Grimm et al., 2005). The capacity of models to replicate inferences of occupancy, extirpation and colonisation events from the fossil record were tested using Approximate Bayesian Computation (ABC) analysis (Csilléry et al., 2010). We did this using a multivariate validation target, consisting of occupancy at fossil sites (age ± 1 SD), arrival time in Greenland, timing of regional extirpation in Eurasia, and distance from extinction location in Eurasia. Estimates for these targets are in Table S2.

We used POM and ABC to identify and select the top 1% of model simulations (n = 1000) that most closely replicate the validation targets. We did this using the rejection method (Csilléry et al., 2012). We calculated the parameter distributions of selected models (i.e., posterior distribution) and compared them with their prior ranges (van der Vaart et al., 2015). We mapped muskox abundance in space and time using an ensemble average of the selected simulations (weighted by the Euclidean distance from the targets) and calculated timing of extirpation and change in total and regional population size. The regions were Europe, with the Ural Mountains defining the eastern boundary; Asia, between the Urals and the Lena River; Beringia, between the Lena River and Alaska; and North America, encompassing northern Canada and Greenland (Fordham, Brown, et al., 2021) (Table S2). All multi-model average reconstructions of spatiotemporal abundance accounted for probability of occurrence and Allee effect (Fordham, Brown, et al., 2021). The POM methods are described in detail in the Supplementary Methods.

We compared changes in relative total population size (effective population size) from aDNA with change in relative total population size from the 'best' models selected using POM validation procedures. The methods and data used to calculate effective population size are described in the Supplementary Methods. This secondary test, using independent targets, tested whether the 'best' models, did indeed adequately capture the ecological processes of range dynamics and their driver state relationships (Grimm & Railsback, 2012). The correlation between the simulated trends in total abundance for the selected models and abundance trends inferred from aDNA was calculated. We also compared magnitudes of change in relative population size for the last deglaciation (19 ka BP – 11 ka BP) and Holocene (11 ka BP – 1500 AD) across both groups. To do this we calculated the magnitude of change in abundance between 19 ka BP and 11 ka BP, for the deglaciation, and between 11ka BP and 1500 AD, for the Holocene, for each of the selected models and for an equivalent number of uniformly sampled points within the 95% CI of the N_e trend at those specific time points. We then did a Welch's t-test to determine if there were significant differences in magnitude of change for each period between the aDNA and our simulations.

Statistical analysis

We used machine learning techniques to identify and distinguish the effects of climate and humans on the extinction risk of the muskox during the deglaciation period (19 ka BP – 11 ka BP; (Clark et al., 2012)). For the selected simulations, we calculated five spatiotemporal descriptors for climatic change and five spatiotemporal descriptors for human harvesting (these are described in detail here: Appendix 3) at the regional level. We calculated Expected Minimum Abundance (EMA) during the last deglaciation for Asia, Beringia, and North America, which is a measure of risk of population decline and extinction (McCarthy & Thompson, 2001). We used time to extinction in Europe instead of EMA, because the muskox went extinct before the end of the last deglaciation in Europe (Table S2). We used a similar approach to assess the roles of climate and human harvesting during the Holocene (11 ka BP – 1500 AD) on population abundance of muskox in North America and East Beringia (Alaska, US) in 1500 AD (i.e., the end of the simulation).

Random forest classification trees, implemented with the 'ranger' package in R (Wright & Ziegler, 2017), were used to identify spatiotemporal effects of climate and human drivers on EMA and time to extinction. We constructed 1,000 trees and tuned the number of variables and minimum node size at each split via 10 x 10-fold cross validation, to maximize model accuracy. Variable

importance scores were calculated using unscaled permutation importance (Strobl et al., 2007) and converted to % contribution of the variance explained.

Results

To reconstruct inferences of past demographic changes from fossils, SEPMs for muskox required large maximum densities, high dispersal abilities, small Allee effects and niches that approximate the fundamental niche of the species (Figure 2). Based on the multi-model ensemble average, the muskox is projected to have declined in population size and contracted their range in a north easterly direction in Eurasia during the last deglaciation (Figure 3 and Figure 4); and to have expanded its populations in North America (north of 50˚ latitude) during the Holocene, colonising Greenland (Movie S1).

The 'best' models, according to POM methods implemented using ABC, correctly projected spatiotemporal occurrence in up to 96% of fossil sites (94 ± 11) and predicted the timing of extirpation (especially the extinction time in Europe; Figure 4) and the distance from the last fossil in Eurasia (Figure S5) with good accuracy (RMSE: 324 ± 83; distance from extinction location: 1161 ± 241 km). However, they did predict a mean arrival time in Greenland that is ~2 k years earlier than expected from the current fossil record (Figure S5).

Validation using genetic inferences of change in total population size showed that projections of total population size for the best SEPMs matched changes in population size inferred from ancient DNA reasonably closely ($\bar{r} = 0.64 \pm 0.07$). Both reconstructions show a steep decline in total population size at the beginning of the deglaciation period, stabilisation, and then an increase during the Holocene (Figure S6). The means of the slopes for magnitude of change in relative population size between selected simulations (mean slope = -0.0000188) and those inferred from N_e (mean slope = -0.0000193) were not significantly different for the last deglaciation ($t(1955.6) = 0.99$, $p = 0.32$). However, they were significantly different in the Holocene ($t(1334.3) = -25.53$, $p < 0.001$), with our selected simulations (mean slope = 0.0000203) showing an earlier increase in relative population abundance compared to the estimates from N_e (mean slope = 0.0000385) as shown in Figure S6.

Demographic and ecological processes

Models needed to have large maximum densities, high dispersal abilities (a high proportion of dispersing individuals, with a long dispersal tail), and a small Allee effect to simulate the validation targets (Figure 2). The ecological niches of muskox needed to have large volumes and low specialisation, with selected niches closely approximating the fundamental niche of the muskox. The

posterior distribution of some parameters more closely matched their prior distribution (Figure 2), suggesting a lesser role in the structure and dynamics of the geographic range of the muskox. These non-identifiable parameters included some demographic parameters (environmental stochasticity and maximum growth rate) and parameters linked to harvesting by humans [exploitation rate (Harvest Max) and prey functional response (Harvest z)].

Structure and dynamics of the geographic range

Our simulations accurately reconstruct the past distribution, extirpation, and abundance of the muskox across the last 21 k years. The multi-model average estimate of timing of extirpation (Figure 3a) simulated a range collapse in Eurasia in a north-eastward direction, experiencing severe and wide-scale population declines following large magnitude and rapid warming ~ at 14.7 ka BP (Figure 4). Populations in central Europe went extinct before 17 ka BP, persisting in north-eastern Europe until ~13 ka BP, which is in strong agreement with the fossil record (Figure S5). Population abundance of muskox declined sharply following the 14.7 ka BP warming event. The simulations suggest that a secondary warming phase, immediately following the 14.7 event, caused the extinction of muskox in Europe (Figure 4).

In North America, populations that persisted during the last glacial maximum south of the Laurentide ice sheet, are projected to have moved in a northerly direction from 17 ka BP in response to melting of the ice sheet (Movie S1), going extinct south of the ice sheet at approximately 13 ka BP (Figure 3). From 14.5 ka BP, populations in Alaska migrated towards the Canadian Arctic Archipelago and Greenland (Movie S1), colonising much of North America north of 65° in latitude. North America north of 55° in latitude is projected to have been colonised by 6 ka BP (Movie S1). The simulated distribution of muskox in North America in 1500 AD (Figure 3b; the end of the simulation) aligns closely with the current endemic distribution of muskox (Figure 3c), with the southern boundary of the simulated distribution matching the southern boundary of today's non-translocated range.

In Asia and Beringia, the distribution of the muskox is projected to have contracted in a northerly direction, with animals being isolated in fragments by 13 ka BP, and with populations persisting at low densities in Siberia and Beringia until 1500 AD (Figure 3b). Our models project persistence in Asia at 1500 AD, which does not align with fossil evidence of regional extinction at ~ 2.6 ka BP. However, the areas where these populations are projected to have persisted in low numbers are the same areas where muskox have been recently translocated (Figure 3c; Cuyler et al., 2020).

The total population size of muskox is projected to have declined during the deglaciation period (19 ka BP – 11 ka BP), and then increased during the Holocene (Figure 4) owing to range expansion in North America. The largest declines in regional population size occurred during or immediately following the 14.7 warming event, where regional temperatures warmed at rates of up to 3˚C per century (Figure 4). In North America, the population size of muskox also declined with an abrupt increase in temperature at around ~7 ka BP.

Climate-human-muskox interactions

Climatic changes explain 62%, 74%, and 45% of the variance in expected minimum abundance (EMA) during the deglaciation period in Asia, Beringia, and North America, respectively (Figure 5). The impact of exploitation by humans on EMA in these three regions was minimal prior to the Holocene, with human hunting activities explaining only 0.4%, 1.4%, and 2.3% of the variance (Figure 5). Large contractions in climate suitability and a faster pace of loss in suitable climatic conditions resulted in lower EMA in Asia (Figure S8). In Beringia and North America, a northern movement of climate suitability positively influenced EMA, while the magnitude of change in this climate suitability had a negative effect (Figures S9 – S10).

In Europe, the effects of climate and humans were similar, explaining 13% and 10% of the variance in time to extinction, respectively. Timing of extinction occurred sooner in simulations where climate suitability in Europe declined quicker in a westerly direction, and where humans expanded slowly in a northerly direction following the last glacial maximum (Figure S7), causing relatively high levels of hunting in Europe.

In Eastern Beringia (Alaska, US), climate change is simulated to have had the largest influence on abundance during the Holocene. Climatic change explained 17% of the variance in muskox population size in 1500 AD in Eastern Beringia, with human hunting explaining < 1% of variance. Abundance in Eastern Beringia was negatively influenced by the extent of change in core climatic conditions in a north-east direction, a slower pace of increased climatically suitability, and larger amount of habitat fragmentation (Figure S11). While in North America (excluding Alaska), humans and climate are projected to have been equally important drivers of abundance during the Holocene (Figure 6). Climatic changes during the Holocene explained 7.8% of the variance in muskox population size, while indices of human activities explained 8.2%. Population size at 1500 AD was negatively influenced by human expansion (magnitude and pace) during the Holocene, and by a southern movement in climate suitability during this period (Figure S12). A lower explained variance for Holocene models is expected because the climate-human-muskox interactions occurring

during the Holocene are affected by climate and human processes happening before the Holocene (Figure 5), which are not directly considered in this analysis.

Discussion

Spatially explicit population models (SEPMs) that continuously simulate climate-human-muskox interactions show that the population structure and range dynamics of muskox have been shaped by deglacial climatic change, with rapid warming events causing population crashes and range contractions. Conversely, more stable climatic conditions during the Holocene enabled the populations of muskox in North America to grow and expand. Hunting by humans, operating in synergy with climatic change, affected muskox in some regions, contributing to its extirpation in Europe approximately 12,000 years ago, and its contemporary population structure in North America. We show that reconciling past inferences of demographic changes from the fossil record and aDNA requires specific demographic and niche constraints, and regional variations in rates of climatic change, human exploitation, and their interaction.

Differences between the posterior and prior distributions of SEPM parameters indicate that long-distance dispersal and metapopulation processes, and their interactions with climatic change and human activities, are important ecological mechanisms driving the structure and dynamics of the geographic range of the muskox. The role of human activities in driving muskox population dynamics has previously been rejected, due to low numbers of muskox remains at archaeological sites (Lent, 1999). This has been interpreted as indicating small level of range overlap between muskox and Palaeolithic humans (Lorenzen et al., 2011). However, we show that the ranges of Palaeolithic humans and muskox are likely to have overlapped in Eurasia for long periods of time during the most recent deglacial period (Movie S2), with human harvesting having a pronounced effect on population abundances in areas more densely populated by humans, such as Europe (Movie S2). These impacts on muskox populations by humans are likely to have been both direct and indirect, with humans regularly occupying pathways between resource-rich zones, potentially hindering important metapopulation processes (Cooper et al., 2015).

We show that simulating inferences of demographic change from fossils and aDNA requires a north-easterly contraction of the Eurasian range of the muskox during the late Pleistocene, and an expansion of its range and abundance in North America during the Holocene. Population sizes of muskox declined abruptly in response to the Dansgaard-Oeschger warming event (~14.7 ka BP),

when temperatures increased by as much as 10 ˚C in less than 50 years (Dansgaard et al., 1993), signalling a vulnerability of muskox to abrupt climatic warming. This and other abrupt warming events of the Pleistocene (Botta et al., 2019) caused severe range contractions and population crashes for other megafaunal species, including the Cave lion (Stuart & Lister, 2011), woolly rhinoceros (Lord et al., 2020; Stuart & Lister, 2012), and woolly mammoth (Fordham, Brown, et al., 2021; Stuart & Lister, 2012).

These rapid warming events are likely to have affected snow conditions, and more specifically snow accumulation, negatively impacting the breeding success and survival of the muskox (Desforges et al., 2021). They are also likely to have altered wind and precipitation patterns, intensifying the frequency of rain-on-snow events, which today prevent Arctic ungulates from accessing food, increasing mortality (Berger et al., 2018). Following the termination of the Pleistocene, population sizes of muskox increased, resulting in simulated population sizes at 1500 AD that were similar to those at the height of the last glacial maximum (Figure 4e). While population growth and range expansion were a feature of muskox range dynamics in North America during the Holocene, owing to more gradual rates of warming compared to the Pleistocene, populations did crash at ~7 ka BP, in response to temperatures being as warm or warmer than today (Kaufman, 2004; Wanner et al., 2008).

Our simulations of range contraction for muskox in Eurasia during the Pleistocene align with existing vegetation reconstructions and vegetation models, showing that the shrub and steppe tundra biomes, preferred by the muskox, became fragmented and were gradually replaced by temperate and boreal forests, as a result of warmer and wetter climatic conditions (Allen et al., 2020; Binney et al., 2017). Furthermore, our models correctly simulate the expansion of muskox in North America from Alaska to the northern part of Canada, Canadian Islands and into Greenland. This pattern is supported by genetic data, which shows signs of multiple founder effects during the colonization of the Canadian Arctic Archipelago and Greenland (Hansen et al., 2018); and fossil data, suggesting that the species entered Greenland from Ellesmere Island via the Nares Trait (Bennike, 1999). In North America, a moisture gradient shift in the tundra biome towards wetter conditions, following the retreat of the Laurentide ice sheet starting at 14 ka BP, favoured mesic specialists like muskox and reindeers, while dryland specialists like horse, bison and mammoth went extinct (Mann et al., 2013).

Tundra is the preferred habitat of muskox (Beumer et al., 2019; Schmidt et al., 2016), where it consumes a wide variety of plants (Kristensen et al., 2011; Schmidt et al., 2018). In Europe, climate-driven transformation of tundra to forest vegetation began at the onset of the deglaciation period,

being complete by 13 ka BP (Binney et al., 2017). While the timing of this transformation in vegetation coincides with our projections of population declines in Europe, and its later extinction from the region, we show that humans are likely to have played an additional and important role in the extirpation of muskox in Europe. Measures of human activities had nearly as strong an influence on the simulated timing of extirpation in Europe as did measures of climate change. Thus, a synergy between human hunting and climate-induced vegetational changes, likely hastened the extinction of muskox in Europe during the late-Pleistocene.

A comparison of the effects of climate and humans during the Holocene on muskox abundance in North America also shows that human activities, as well as climatic change, shaped the structure and size of muskox populations. Muskox remains are more frequently associated with Holocene-age human artefacts in North America, potentially indicating a more specialized muskox-hunting culture in this region following the Holocene (Lent, 1999), which our results corroborate. Furthermore, it is hypothesized that humans reached Greenland by following the muskox, using the so called "Muskox Way" (Lent, 1999), suggesting that muskox played an important role in the establishment of humans in Arctic North America and, subsequently, in Paleo-Inuit culture.

While our process-explicit models do well at reconstructing inferences of range shifts and demographic change from fossils, they were unable to simulate the extinction of muskox in Eurasia at ~2.6 ka BP (Campos et al., 2010; Markova et al., 2015). Rather they simulate persistence of muskox in areas of Siberia (its last refuge in Eurasia) where they have been recently translocated and where populations are currently increasing (Cuyler et al., 2020). Although it is likely that the muskox went extinct in Eurasia after 2.6 ka BP (Wang et al., 2021), it is unlikely that they would have been in Eurasia during the 16th century as projected by our model. Possible reasons for simulating prolonged persistence in Siberia include an absence of inter-specific interactions in the model, other than muskox-human interactions. Bears and wolves, which are primary predators of muskox (Heard, 1992; Reynolds et al., 2002), could have amplified the effect of Holocene warming on muskox persistence in Eurasia. Moreover, our SEPM for muskox does not account for land-use change during the Holocene, where pastoralism and agriculture began as early as 4 ka BP in Siberia (Stephens et al., 2019). It also does not account for potential diseases. Infectious diseases and pathogens have caused populations of muskox to decline by up to 85% in Alaska and Canada (Cuyler et al., 2020), with the range dynamics of common pathogens being sensitive to climatic warming (Kafle et al., 2020).

We project a time of arrival in Greenland that on average is approximately 2,000 years earlier than the time estimated from the fossil record (~5 ka BP). This could be because our models are coarse, resulting in overly high connectivity between the Canadian Arctic Archipelago and Greenland, preventing isolation between populations, as determined by their genetic structure (Hansen et al., 2018). However, there is also a real possibility that muskox did colonise Greenland earlier than previously thought and that older fossils are still yet to be discovered. Extirpation and extinction events of megafaunal species are commonly revised as younger fossils and environmental DNA are discovered, often causing persistence to be extended by several millennia (Haile et al., 2009; Murchie et al., 2021; Wang et al., 2021). Because the fossil record indicates when a species was abundant (Bradshaw et al., 2012), it is possible that Greenland was colonised at 7 ka BP (as predicted by our models), but abundances remained low until ~5 ka BP, when the first muskox fossils appear in the fossil record. Indeed, ice free areas of Greenland were occupied by reindeers at ~9 ka BP, long before the estimated arrival date for muskox (Meldgaard, 1986).

While our model was able to simulate important demographic changes, it was not able to account for the effect of demographic factors operating at finer spatial scales. These include, but are not limited to, narrow intervening bodies of open water in the Canadian Arctic Archipelago, which are likely to have had an effect on dispersal limitation. Such factors could impact important aspects of muskox biology, as indicated by high genetic differentiation observed between populations in the Canadian mainland, Canadian Arctic Archipelago, and Greenland (Hansen et al. 2018).

Using SEPMs, integrated with inferences from fossils and aDNA, we were able to unravel the ecological mechanisms and drivers responsible for the range collapse of muskox in Eurasia during the late Pleistocene and its expansion in North America during the Holocene. We show that while the structure and dynamics of the geographic range of muskox has been shaped by climate at the circumpolar scale, hunting by humans, operating in synergy with climate change, affected the range and extinction dynamics of muskox in particular regions, at particular times. We also show that muskox populations crashed in response to rapid warming and ancient warm periods. Given that these Arctic warming events are directly comparable to 21st century projections (Fordham et al., 2020), our results suggest a high vulnerability of muskox to future climate warming. More generally, our process-explicit models, optimised and validated on inferences of past demographic change from fossils and aDNA, provide a new validated modelling framework for conserving muskox and other Arctic grazing megafauna under future climatic and environmental change, including pinpointing new sites for translocations.

References

Allen, J. R. M., Forrest, M., Hickler, T., Singarayer, J. S., Valdes, P. J., & Huntley, B. (2020). Global vegetation patterns of the past 140,000 years. *J Biogeogr*, *47*(10), 2073-2090. https://doi.org/10.1111/jbi.13930

Alroy, J. (2001). A multispecies overkill simulation of the end-Pleistocene megafaunal mass extinction. *Science*, *292*(5523), 1893-1896. https://doi.org/10.1126/science.1059342

Anderson, B. J., Akcakaya, H. R., Araujo, M. B., Fordham, D. A., Martinez-Meyer, E., Thuiller, W., & Brook, B. W. (2009). Dynamics of range margins for metapopulations under climate change. *Proc R Soc B*, *276*(1661), 1415-1420. https://doi.org/10.1098/rspb.2008.1681

Asbjornsen, E. J., Saether, B. E., Linnell, J. D. C., Engen, S., Andersen, R., & Bretten, T. (2005). Predicting the growth of a small introduced muskox population using population prediction intervals. *J Anim Ecol*, *74*(4), 612-618. https://doi.org/10.1111/j.1365-2656.2005.00946.x

Barnosky, A. D., & Lindsey, E. L. (2010). Timing of Quaternary megafaunal extinction in South America in relation to human arrival and climate change. *Quat Int*, *217*(1-2), 10-29. https://doi.org/10.1016/j.quaint.2009.11.017

Bennike, O. (1999). Colonisation of Greenland by plants and animals after the last ice age: a review. *Polar Rec*, *35*(195), 323-336. https://doi.org/10.1017/s0032247400015679

Berger, J., Hartway, C., Gruzdev, A., & Johnson, M. (2018). Climate Degradation and Extreme Icing Events Constrain Life in Cold-Adapted Mammals. *Sci Rep*, *8*(1), 1156. https://doi.org/10.1038/s41598-018-19416-9

Beumer, L. T., van Beest, F. M., Stelvig, M., & Schmidt, N. M. (2019). Spatiotemporal dynamics in habitat suitability of a large Arctic herbivore: Environmental heterogeneity is key to a sedentary lifestyle. *Glob Ecol Conserv*, *18*, e00647. https://doi.org/10.1016/j.gecco.2019.e00647

Beyer, R., Krapp, M., & Manica, A. (2020). An empirical evaluation of bias correction methods for palaeoclimate simulations. *Clim. Past*, *16*(4), 1493-1508. https://doi.org/10.5194/cp-16-1493-2020

Binney, H., Edwards, M., Macias-Fauria, M., Lozhkin, A., Anderson, P., Kaplan, J. O., Andreev, A., Bezrukova, E., Blyakharchuk, T., Jankovska, V., Khazina, I., Krivonogov, S., Kremenetski, K., Nield, J., Novenko, E., Ryabogina, N., Solovieva, N., Willis, K., & Zernitskaya, V. (2017). Vegetation of Eurasia from the last glacial maximum to present:

Key biogeographic patterns. *Quat Sci Rev*, *157*, 80-97. https://doi.org/10.1016/j.quascirev.2016.11.022

Blonder, B., Lamanna, C., Violle, C., & Enquist, B. J. (2014). The n-dimensional hypervolume. *Glob Ecol Biogeogr*, *23*(5), 595-609. https://doi.org/10.1111/geb.12146

Blonder, B., Morrow, C. B., Maitner, B., Harris, D. J., Lamanna, C., Violle, C., Enquist, B. J., Kerkhoff, A. J., & McMahon, S. (2017). New approaches for delineating n-dimensional hypervolumes. *Methods Ecol Evol*, *9*(2), 305-319. https://doi.org/10.1111/2041-210x.12865

Botta, F., Dahl-Jensen, D., Rahbek, C., Svensson, A., & Nogues-Bravo, D. (2019). Abrupt Change in Climate and Biotic Systems. *Curr Biol*, *29*(19), R1045-R1054. https://doi.org/10.1016/j.cub.2019.08.066

Bradshaw, C. J. A., Cooper, A., Turney, C. S. M., & Brook, B. W. (2012). Robust estimates of extinction time in the geological record. *Quat Sci Rev*, *33*, 14-19. https://doi.org/10.1016/j.quascirev.2011.11.021

Bronk Ramsey, C. (2009). Bayesian analysis of radiocarbon dates. *Radiocarbon*, *51*(1), 337-360. https://doi.org/10.1017/s0033822200033865

Brown, J. H., Stevens, G. C., & Kaufman, D. M. (1996). THE GEOGRAPHIC RANGE: Size, Shape, Boundaries, and Internal Structure. *Annu Rev Ecol Syst*, *27*(1), 597-623. https://doi.org/10.1146/annurev.ecolsys.27.1.597

Brown, S. C., Wigley, T. M. L., Otto-Bliesner, B. L., Rahbek, C., & Fordham, D. A. (2020). Persistent Quaternary climate refugia are hospices for biodiversity in the Anthropocene. *Nat Clim Chang*, *10*(3), 244-248. https://doi.org/10.1038/s41558-019-0682-7

Campos, P. F., Willerslev, E., Sher, A., Orlando, L., Axelsson, E., Tikhonov, A., Aaris-Sorensen, K., Greenwood, A. D., Kahlke, R. D., Kosintsev, P., Krakhmalnaya, T., Kuznetsova, T., Lemey, P., MacPhee, R., Norris, C. A., Shepherd, K., Suchard, M. A., Zazula, G. D., Shapiro, B., & Gilbert, M. T. (2010). Ancient DNA analyses exclude humans as the driving force behind late Pleistocene musk ox (*Ovibos moschatus*) population dynamics. *Proc Natl Acad Sci U S A*, *107*(12), 5675-5680. https://doi.org/10.1073/pnas.0907189107

Chevalier, M., Davis, B. A. S., Heiri, O., Seppä, H., Chase, B. M., Gajewski, K., Lacourse, T., Telford, R. J., Finsinger, W., Guiot, J., Kühl, N., Maezumi, S. Y., Tipton, J. R., Carter, V. A., Brussel, T., Phelps, L. N., Dawson, A., Zanon, M., Vallé, F., . . . Kupriyanov, D. (2020). Pollen-based climate reconstruction techniques for late Quaternary studies. *Earth Sci Rev*, *210*, 103384. https://doi.org/10.1016/j.earscirev.2020.103384

Clark, P. U., Shakun, J. D., Baker, P. A., Bartlein, P. J., Brewer, S., Brook, E., Carlson, A. E., Cheng, H., Kaufman, D. S., Liu, Z., Marchitto, T. M., Mix, A. C., Morrill, C., Otto-Bliesner, B. L., Pahnke, K., Russell, J. M., Whitlock, C., Adkins, J. F., Blois, J. L., . . . Williams, J. W. (2012). Global climate evolution during the last deglaciation. *Proc Natl Acad Sci U S A*, *109*(19), E1134-1142. https://doi.org/10.1073/pnas.1116619109

Connolly, S. R., Keith, S. A., Colwell, R. K., & Rahbek, C. (2017). Process, Mechanism, and Modeling in Macroecology. *Trends Ecol Evol*, *32*(11), 835-844. https://doi.org/10.1016/j.tree.2017.08.011

Cooper, A., Turney, C., Hughen, K. A., Brook, B. W., McDonald, H. G., & Bradshaw, C. J. (2015). Abrupt warming events drove Late Pleistocene Holarctic megafaunal turnover. *Science*, *349*(6248), 602-606. https://doi.org/10.1126/science.aac4315

Csilléry, K., Blum, M. G., Gaggiotti, O. E., & Francois, O. (2010). Approximate Bayesian Computation (ABC) in practice. *Trends Ecol Evol*, *25*(7), 410-418. https://doi.org/10.1016/j.tree.2010.04.001

Csilléry, K., François, O., & Blum, M. G. B. (2012). abc: an R package for approximate Bayesian computation (ABC). *Methods Ecol Evol*, *3*(3), 475-479. https://doi.org/10.1111/j.2041-210X.2011.00179.x

Cuyler, C., Rowell, J., Adamczewski, J., Anderson, M., Blake, J., Bretten, T., Brodeur, V., Campbell, M., Checkley, S. L., Cluff, H. D., Côté, S. D., Davison, T., Dumond, M., Ford, B., Gruzdev, A., Gunn, A., Jones, P., Kutz, S., Leclerc, L. M., . . . Ytrehus, B. (2020). Muskox status, recent variation, and uncertain future. *Ambio*, *49*, 805-819. https://doi.org/10.1007/s13280-019-01205-x

Dansgaard, W., Johnsen, S. J., Clausen, H. B., Dahl-Jensen, D., Gundestrup, N. S., Hammer, C. U., Hvidberg, C. S., Steffensen, J. P., Sveinbjörnsdottir, A. E., Jouzel, J., & Bond, G. (1993). Evidence for general instability of past climate from a 250-kyr ice-core record. *Nature*, *364*(6434), 218-220. https://doi.org/10.1038/364218a0

Desforges, J. P., Marques, G. M., Beumer, L. T., Chimienti, M., Hansen, L. H., Pedersen, S. H., Schmidt, N. M., & van Beest, F. M. (2021). Environment and physiology shape Arctic ungulate population dynamics. *Glob Chang Biol*, *27*(9), 1755-1771. https://doi.org/10.1111/gcb.15484

Dolédec, S., Chessel, D., & Gimaret-Carpentier, C. (2000). Niche Separation in Community Analysis: A New Method. *Ecology*, *81*(10), 2914-2927. https://doi.org/10.1890/0012-9658(2000)081[2914:Nsicaa]2.0.Co;2

Dormann, C. F., Elith, J., Bacher, S., Buchmann, C., Carl, G., Carré, G., Marquéz, J. R. G., Gruber, B., Lafourcade, B., Leitão, P. J., Münkemüller, T., McClean, C., Osborne, P. E., Reineking, B., Schröder, B., Skidmore, A. K., Zurell, D., & Lautenbach, S. (2013). Collinearity: a review of methods to deal with it and a simulation study evaluating their performance. *Ecography*, *36*(1), 27-46. https://doi.org/10.1111/j.1600-0587.2012.07348.x

Eriksson, A., Betti, L., Friend, A. D., Lycett, S. J., Singarayer, J. S., von Cramon-Taubadel, N., Valdes, P. J., Balloux, F., & Manica, A. (2012). Late Pleistocene climate change and the global expansion of anatomically modern humans. *Proc Natl Acad Sci U S A*, *109*(40), 16089-16094. https://doi.org/10.1073/pnas.1209494109

Fordham, D. A., Akçakaya, H. R., Alroy, J., Saltré, F., Wigley, T. M. L., & Brook, B. W. (2016). Predicting and mitigating future biodiversity loss using long-term ecological proxies. *Nat Clim Chang*, *6*(10), 909-916. https://doi.org/10.1038/nclimate3086

Fordham, D. A., Akçakaya, H. R., Brook, B. W., Rodríguez, A., Alves, P. C., Civantos, E., Triviño, M., Watts, M. J., & Araújo, M. B. (2013). Adapted conservation measures are required to save the Iberian lynx in a changing climate. *Nat Clim Chang*, *3*(10), 899-903. https://doi.org/10.1038/nclimate1954

Fordham, D. A., Bertelsmeier, C., Brook, B. W., Early, R., Neto, D., Brown, S. C., Ollier, S., & Araujo, M. B. (2018). How complex should models be? Comparing correlative and mechanistic range dynamics models. *Glob Chang Biol*, *24*(3), 1357-1370. https://doi.org/10.1111/gcb.13935

Fordham, D. A., Brook, B. W., Moritz, C., & Nogues-Bravo, D. (2014). Better forecasts of range dynamics using genetic data. *Trends Ecol Evol*, *29*(8), 436-443. https://doi.org/10.1016/j.tree.2014.05.007

Fordham, D. A., Brown, S. C., Akcakaya, H. R., Brook, B. W., Haythorne, S., Manica, A., Shoemaker, K. T., Austin, J. J., Blonder, B., Pilowsky, J., Rahbek, C., & Nogues-Bravo, D. (2021). Process-explicit models reveal pathway to extinction for woolly mammoth using pattern-oriented validation. *Ecol Lett*, *25*(1), 125-137. https://doi.org/10.1111/ele.13911

Fordham, D. A., Haythorne, S., Brown, S. C., Buettel, J. C., & Brook, B. W. (2021). poems: R package for simulating species' range dynamics using pattern-oriented validation. *Methods Ecol Evol*, *12*(12), 2364-2371. https://doi.org/10.1111/2041-210x.13720

Fordham, D. A., Jackson, S. T., Brown, S. C., Huntley, B., Brook, B. W., Dahl-Jensen, D., Gilbert, M. T. P., Otto-Bliesner, B. L., Svensson, A., Theodoridis, S., Wilmshurst, J. M., Buettel, J. C., Canteri, E., McDowell, M., Orlando, L., Pilowsky, J., Rahbek, C., & Nogues-Bravo, D. (2020). Using paleo-archives to safeguard biodiversity under climate change. *Science*, *369*(6507), 10-10. https://doi.org/10.1126/science.abc5654

Fordham, D. A., Saltre, F., Haythorne, S., Wigley, T. M. L., Otto-Bliesner, B. L., Chan, K. C., & Brook, B. W. (2017). PaleoView: a tool for generating continuous climate projections spanning the last 21 000 years at regional and global scales. *Ecography*, *40*(11), 1348-1358. https://doi.org/10.1111/ecog.03031

Foster, J., Liston, G., Koster, R., Essery, R., Behr, H., Dumenil, L., Verseghy, D., Thompson, S., Pollard, D., & Cohen, J. (1996). Snow cover and snow mass intercomparisons of general circulation models and remotely sensed datasets. *J Clim*, *9*(2), 409-426. https://doi.org/10.1175/1520-0442(1996)009<0409:scasmi>2.0.co;2

Gaston, K. J. (2003). *The Structure and Dynamics of Geographic Ranges*. Oxford University Press. https://books.google.com.au/books?id=zBqpX1ajLFMC

GBIF.org (2019). *GBIF Occurrence Download.* The Global Biodiversity Information Facility. Accessed 08 April 2019. https://doi.org/10.15468/DL.QW3LPI

Grimm, V., & Railsback, S. F. (2012). Pattern-oriented modelling: a 'multi-scope' for predictive systems ecology. *Philos Trans R Soc Lond B Biol Sci, 367*(1586), 298-310. https://doi.org/10.1098/rstb.2011.0180

Grimm, V., Revilla, E., Berger, U., Jeltsch, F., Mooij, W. M., Railsback, S. F., Thulke, H. H., Weiner, J., Wiegand, T., & DeAngelis, D. L. (2005). Pattern-oriented modeling of agent-based complex systems: lessons from ecology. *Science*, *310*(5750), 987-991. https://doi.org/10.1126/science.1116681

Hagen, O., Fluck, B., Fopp, F., Cabral, J. S., Hartig, F., Pontarp, M., Rangel, T. F., & Pellissier, L. (2021). gen3sis: A general engine for eco-evolutionary simulations of the processes that shape Earth's biodiversity. *PLoS Biol*, *19*(7), e3001340. https://doi.org/10.1371/journal.pbio.3001340

Haile, J., Froese, D. G., Macphee, R. D., Roberts, R. G., Arnold, L. J., Reyes, A. V., Rasmussen, M., Nielsen, R., Brook, B. W., Robinson, S., Demuro, M., Gilbert, M. T., Munch, K., Austin, J. J., Cooper, A., Barnes, I., Moller, P., & Willerslev, E. (2009). Ancient DNA reveals late survival of mammoth and horse in interior Alaska. *Proc Natl Acad Sci U S A*, *106*(52), 22352-22357. https://doi.org/10.1073/pnas.0912510106

Hansen, C. C. R., Hvilsom, C., Schmidt, N. M., Aastrup, P., Van Coeverden de Groot, P. J., Siegismund, H. R., & Heller, R. (2018). The muskox lost a substantial part of Its genetic diversity on its long road to Greenland. *Curr Biol*, *28*(24), 4022-4028 e4025. https://doi.org/10.1016/j.cub.2018.10.054

Harris, I., Osborn, T. J., Jones, P., & Lister, D. (2020). Version 4 of the CRU TS monthly high-resolution gridded multivariate climate dataset. *Sci Data*, *7*(1), 109. https://doi.org/10.1038/s41597-020-0453-3

Haythorne, S., Fordham, D., Brown, S., Buettel, J., & Brook, B. (2021). *poems: Pattern-Oriented Ensemble Modeling System.* In (Version 1.0.1) [R package]. R. https://CRAN.R-project.org/package=poems

Haythorne, S., Pilowsky, J., Brown, S., & Fordham, D. (2021). *paleopop: Pattern-Oriented Modeling Framework for Coupled Niche-Population Paleo-Climatic Models.* In (Version 2.1.2) [R package]. R. https://CRAN.R-project.org/package=paleopop

Heard, D. C. (1992). The effect of wolf predation and snow cover on musk-ox group size. *Am Nat*, *139*(1), 190-204. http://www.jstor.org.proxy.library.adelaide.edu.au/stable/2462592

Kafle, P., Peller, P., Massolo, A., Hoberg, E., Leclerc, L. M., Tomaselli, M., & Kutz, S. (2020). Range expansion of muskox lungworms track rapid arctic warming: implications for geographic colonization under climate forcing. *Sci Rep*, *10*(1), 17323. https://doi.org/10.1038/s41598-020-74358-5

Kaufman, D. (2004). Holocene thermal maximum in the western Arctic (0–180°W). *Quat Sci Rev*, *23*(5-6), 529-560. https://doi.org/10.1016/j.quascirev.2003.09.007

Kristensen, D. K., Kristensen, E., Forchhammer, M. C., Michelsen, A., & Schmidt, N. M. (2011). Arctic herbivore diet can be inferred from stable carbon and nitrogen isotopes in C3 plants, faeces, and wool. *Can J Zool*, *89*(10), 892-899. https://doi.org/10.1139/z11-073

Lee, J.-Y., Marotzke, J., Bala, G., Cao, L., Corti, S., Dunne, J. P., Engelbrecht, F., Fischer, E., Fyfe, J. C., Jones, C., Maycock, A., Mutemi, J., Ndiaye, O., Panickal, S., & Zhou, T. (2021). Future global climate: scenario-based projections and near-term information. In V. Masson-

Delmotte, P. Zhai, A. Pirani, S. L. Connors, C. Péan, S. Berger, N. Caud, Y. Chen, L. Goldfarb, M. I. Gomis, M. Huang, K. Leitzell, E. Lonnoy, J. B. R. Matthews, T. K. Maycock, T. Waterfield, O. Yelekçi, R. Yu, & B. Zhou (Eds.), *Climate Change 2021: The Physical Science Basis. Contribution of Working Group I to the Sixth Assessment Report of the Intergovernmental Panel on Climate Change*. Cambridge University Press.

Lent, P. C. (1999). *Muskoxen and their hunters: A history* (Vol. 5). University of Oklahoma Press.

Lister, A. M., & Stuart, A. J. (2008). The impact of climate change on large mammal distribution and extinction: Evidence from the last glacial/interglacial transition. *Collect C R Geosci*, *340*(9-10), 615-620. https://doi.org/10.1016/j.crte.2008.04.001

Liu, A. Z., Otto-Bliesner, A. B. L., He, A. F., Brady, A. E. C., Tomas, A. R., Clark, A. P. U., Carlson, A. A. E., Lynch-Stieglitz, A. J., Curry, A. W., Brook, A. E., Erickson, A. D., Jacob, A. R., Kutzbach, A. J., & Cheng, A. J. (2009). Transient simulation of last deglaciation with a new mechanism for Bølling-Allerød warming. *Science*, *325*(5938), 310-314. https://doi.org/10.1126/science.1171041

Lord, E., Dussex, N., Kierczak, M., Diez-Del-Molino, D., Ryder, O. A., Stanton, D. W. G., Gilbert, M. T. P., Sanchez-Barreiro, F., Zhang, G., Sinding, M. S., Lorenzen, E. D., Willerslev, E., Protopopov, A., Shidlovskiy, F., Fedorov, S., Bocherens, H., Nathan, S., Goossens, B., van der Plicht, J., . . . Dalen, L. (2020). Pre-extinction demographic stability and genomic signatures of adaptation in the Woolly Rhinoceros. *Curr Biol*, *30*(19), 3871-3879 e3877. https://doi.org/10.1016/j.cub.2020.07.046

Lorenzen, E. D., Nogues-Bravo, D., Orlando, L., Weinstock, J., Binladen, J., Marske, K. A., Ugan, A., Borregaard, M. K., Gilbert, M. T., Nielsen, R., Ho, S. Y., Goebel, T., Graf, K. E., Byers, D., Stenderup, J. T., Rasmussen, M., Campos, P. F., Leonard, J. A., Koepfli, K. P., . . . Willerslev, E. (2011). Species-specific responses of Late Quaternary megafauna to climate and humans. *Nature*, *479*(7373), 359-364. https://doi.org/10.1038/nature10574

Mann, D. H., Groves, P., Kunz, M. L., Reanier, R. E., & Gaglioti, B. V. (2013). Ice-age megafauna in Arctic Alaska: extinction, invasion, survival. *Quat Sci Rev*, *70*, 91-108. https://doi.org/10.1016/j.quascirev.2013.03.015

Markova, A. K., Puzachenko, A. Y., van Kolfschoten, T., Kosintsev, P. A., Kuznetsova, T. V., Tikhonov, A. N., Bachura, O. P., Ponomarev, D. V., van der Plicht, J., & Kuitems, M. (2015). Changes in the Eurasian distribution of the musk ox (Ovibos moschatus) and the

extinct bison (Bison priscus) during the last 50 ka BP. *Quat Int*, *378*, 99-110. https://doi.org/10.1016/j.quaint.2015.01.020

McCarthy, M. A., & Thompson, C. (2001). Expected minimum population size as a measure of threat. *Anim Conserv*, *4*(4), 351-355. https://doi.org/10.1017/s136794300100141x

Meldgaard, M. (1986). *The Greenland Caribou - Zoogeography, Taxonomy and Population Dynamics* (Bioscience, Ed. Vol. 20). The Commission for Scientific Research in Greenland.

Meredith, M., Sommerkorn, M., Cassotta, S., Derksen, C., Ekaykin, A., Hollowed, A., Kofinas, G., Mackintosh, A., Melbourne-Thomas, J., Muelbert, M. M. C., Ottersen, G., Pritchard, H., & Schuur, E. A. G. (2019). Polar Regions. In H.-O. Pörtner, D. C. Roberts, V. Masson-Delmotte, P. Zhai, M. Tignor, E. Poloczanska, & N. Weyer (Eds.), *IPCC Special Report on the Ocean and Cryosphere in a Changing Climate*. Intergovernmental Panel on Climate Change.

Murchie, T. J., Monteath, A. J., Mahony, M. E., Long, G. S., Cocker, S., Sadoway, T., Karpinski, E., Zazula, G., MacPhee, R. D. E., Froese, D., & Poinar, H. N. (2021). Collapse of the mammoth-steppe in central Yukon as revealed by ancient environmental DNA. *Nat Commun*, *12*(1), 7120. https://doi.org/10.1038/s41467-021-27439-6

Nogués-Bravo, D. (2009). Predicting the past distribution of species climatic niches. *Glob Ecol Biogeogr*, *18*(5), 521-531. https://doi.org/10.1111/j.1466-8238.2009.00476.x

Nogues-Bravo, D., Ohlemuller, R., Batra, P., & Araujo, M. B. (2010). Climate predictors of late quaternary extinctions. *Evolution*, *64*(8), 2442-2449. https://doi.org/10.1111/j.1558-5646.2010.01009.x

Nogues-Bravo, D., Rodriguez-Sanchez, F., Orsini, L., de Boer, E., Jansson, R., Morlon, H., Fordham, D. A., & Jackson, S. T. (2018). Cracking the Code of Biodiversity Responses to Past Climate Change. *Trends Ecol Evol*, *33*(10), 765-776. https://doi.org/10.1016/j.tree.2018.07.005

Orlando, L., & Cooper, A. (2014). Using Ancient DNA to Understand Evolutionary and Ecological Processes. *Annu Rev Ecol Evol Syst*, *45*(1), 573-598. https://doi.org/10.1146/annurev-ecolsys-120213-091712

Post, E. (2013). Erosion of community diversity and stability by herbivore removal under warming. *Proc R Soc B*, *280*(1757), 20122722. https://doi.org/10.1098/rspb.2012.2722

Post, E., Alley, R. B., Christensen, T. R., Macias-Fauria, M., Forbes, B. C., Gooseff, M. N., Iler, A., Kerby, J. T., Laidre, K. L., Mann, M. E., Olofsson, J., Stroeve, J. C., Ulmer, F., Virginia, R.

A., & Wang, M. (2019). The polar regions in a 2 degrees C warmer world. *Sci Adv*, *5*(12), eaaw9883. https://doi.org/10.1126/sciadv.aaw9883

Post, E., & Pedersen, C. (2008). Opposing plant community responses to warming with and without herbivores. *Proc Natl Acad Sci U S A*, *105*(34), 12353-12358. https://doi.org/10.1073/pnas.0802421105

Prowse, T. A. A., Bradshaw, C. J. A., Delean, S., Cassey, P., Lacy, R. C., Wells, K., Aiello-Lammens, M. E., Akçakaya, H. R., & Brook, B. W. (2016). An efficient protocol for the global sensitivity analysis of stochastic ecological models. *Ecosphere*, *7*(3), e01238. https://doi.org/10.1002/ecs2.1238

Raghavan, M., Steinrücken, M., Harris, K., Schiffels, S., Rasmussen, S., Degiorgio, M., Albrechtsen, A., Valdiosera, C., Ávila-Arcos, M. C., Malaspinas, A.-S., Eriksson, A., Moltke, I., Metspalu, M., Homburger, J. R., Wall, J., Cornejo, O. E., Moreno-Mayar, J. V., Korneliussen, T. S., Pierre, T., . . . Willerslev, E. (2015). Genomic evidence for the Pleistocene and recent population history of Native Americans. *Science*, *349*(6250), aab3884-aab3884. https://doi.org/10.1126/science.aab3884

Rangel, T. F., Edwards, N. R., Holden, P. B., Diniz-Filho, J. A. F., Gosling, W. D., Coelho, M. T. P., Cassemiro, F. A. S., Rahbek, C., & Colwell, R. K. (2018). Modeling the ecology and evolution of biodiversity: Biogeographical cradles, museums, and graves. *Science*, *361*(6399). https://doi.org/10.1126/science.aar5452

Reimer, P. J., Austin, W. E. N., Bard, E., Bayliss, A., Blackwell, P. G., Bronk Ramsey, C., Butzin, M., Cheng, H., Edwards, R. L., Friedrich, M., Grootes, P. M., Guilderson, T. P., Hajdas, I., Heaton, T. J., Hogg, A. G., Hughen, K. A., Kromer, B., Manning, S. W., Muscheler, R., . . . Talamo, S. (2020). The IntCal20 Northern Hemisphere radiocarbon age calibration curve (0–55 cal kBP). *Radiocarbon*, *62*(4), 725-757. https://doi.org/10.1017/rdc.2020.41

Reynolds, P. E., Reynolds, H. V., & Shideler, R. T. (2002). Predation and multiple kills of muskoxen by grizzly bears. *Ursus*, *13*, 79-84. https://www.jstor.org/stable/3873189

Ricker, W. E. (1954). Stock and recruitment. *J Fish Res Board Can*, *11*(5), 559-623.

Schmidt, N. M., Mosbacher, J. B., Vesterinen, E. J., Roslin, T., & Michelsen, A. (2018). Limited dietary overlap amongst resident Arctic herbivores in winter: complementary insights from complementary methods. *Oecologia*, *187*(3), 689-699. https://doi.org/10.1007/s00442-018-4147-x

Schmidt, N. M., van Beest, F. M., Mosbacher, J. B., Stelvig, M., Hansen, L. H., Nabe-Nielsen, J., & Grondahl, C. (2016). Ungulate movement in an extreme seasonal environment: year-round movement patterns of high-arctic muskoxen. *Wildlife Biol*, *22*(6), 253-267. https://doi.org/10.2981/wlb.00219

Screen, J. A., & Simmonds, I. (2010). The central role of diminishing sea ice in recent Arctic temperature amplification. *Nature*, *464*(7293), 1334-1337. https://doi.org/10.1038/nature09051

Smith, C. I., Chamberlain, A. T., Riley, M. S., Stringer, C., & Collins, M. J. (2003). The thermal history of human fossils and the likelihood of successful DNA amplification. *J Hum Evol*, *45*(3), 203-217. https://doi.org/10.1016/s0047-2484(03)00106-4

Steffensen, J. P., Andersen, K. K., Bigler, M., Clausen, H. B., Dahl-Jensen, D., Fischer, H., Goto-Azuma, K., Hansson, M., Johnsen, S. J., Jouzel, J., Masson-Delmotte, V., Popp, T., Rasmussen, S. O., Rothlisberger, R., Ruth, U., Stauffer, B., Siggaard-Andersen, M.-L., Sveinbjornsdottir, A. E., Svensson, A., & White, J. W. C. (2008). High-resolution Greenland ice core data show abrupt climate change happens in few years. *Science*, *321*(5889), 680-684. https://doi.org/10.1126/science.1157707

Stephens, L., Fuller, D., Boivin, N., Rick, T., Gauthier, N., Kay, A., Marwick, B., Armstrong, C. G., Barton, C. M., Denham, T., Douglass, K., Driver, J., Janz, L., Roberts, P., Rogers, J. D., Thakar, H., Altaweel, M., Johnson, A. L., Sampietro Vattuone, M. M., . . . Ellis, E. (2019). Archaeological assessment reveals Earth's early transformation through land use. *Science*, *365*(6456), 897-902. https://doi.org/10.1126/science.aax1192

Strobl, C., Boulesteix, A. L., Zeileis, A., & Hothorn, T. (2007). Bias in random forest variable importance measures: illustrations, sources and a solution. *BMC Bioinform*, *8*(1), 25. https://doi.org/10.1186/1471-2105-8-25

Stuart, A. J. (2015). Late Quaternary megafaunal extinctions on the continents: a short review. *Geol J*, *50*(3), 338-363. https://doi.org/10.1002/gj.2633

Stuart, A. J., & Lister, A. M. (2011). Extinction chronology of the cave lion Panthera spelaea. *Quat Sci Rev*, *30*(17-18), 2329-2340. https://doi.org/10.1016/j.quascirev.2010.04.023

Stuart, A. J., & Lister, A. M. (2012). Extinction chronology of the woolly rhinoceros Coelodonta antiquitatis in the context of late Quaternary megafaunal extinctions in northern Eurasia. *Quat Sci Rev*, *51*, 1-17. https://doi.org/10.1016/j.quascirev.2012.06.007

Svenning, J.-C., Fløjgaard, C., Marske, K. A., Nógues-Bravo, D., & Normand, S. (2011). Applications of species distribution modeling to paleobiology. *Quat Sci Rev*, *30*(21-22), 2930-2947. https://doi.org/10.1016/j.quascirev.2011.06.012

van Beest, F. M., Beumer, L. T., Andersen, A. S., Hansson, S. V., Schmidt, N. M., & Zhang, Z. (2021). Rapid shifts in Arctic tundra species' distributions and inter-specific range overlap under future climate change. *Divers Distrib*, *27*(9), 1706-1718. https://doi.org/10.1111/ddi.13362

van der Vaart, E., Beaumont, M. A., Johnston, A. S. A., & Sibly, R. M. (2015). Calibration and evaluation of individual-based models using Approximate Bayesian Computation. *Ecol Modell*, *312*, 182-190. https://doi.org/10.1016/j.ecolmodel.2015.05.020

Wang, Y., Pedersen, M. W., Alsos, I. G., De Sanctis, B., Racimo, F., Prohaska, A., Coissac, E., Owens, H. L., Merkel, M. K. F., Fernandez-Guerra, A., Rouillard, A., Lammers, Y., Alberti, A., Denoeud, F., Money, D., Ruter, A. H., Mccoll, H., Larsen, N. K., Cherezova, A. A., . . . Willerslev, E. (2021). Late Quaternary dynamics of Arctic biota from ancient environmental genomics. *Nature*. https://doi.org/10.1038/s41586-021-04016-x

Wanner, H., Beer, J., Bütikofer, J., Crowley, T. J., Cubasch, U., Flückiger, J., Goosse, H., Grosjean, M., Joos, F., Kaplan, J. O., Küttel, M., Müller, S. A., Prentice, I. C., Solomina, O., Stocker, T. F., Tarasov, P., Wagner, M., & Widmann, M. (2008). Mid- to Late Holocene climate change: an overview. *Quat Sci Rev*, *27*(19-20), 1791-1828. https://doi.org/10.1016/j.quascirev.2008.06.013

Willerslev, E., Hansen, A. J., Binladen, J., Brand, T. B., Gilbert, M. T. P., Shapiro, B., Bunce, M., Wiuf, C., Gilichinsky, D. A., & Cooper, A. (2003). Diverse plant and animal genetic records from Holocene and Pleistocene sediments. *Science*, *300*(5620), 791-795. https://doi.org/10.1126/science.1084114

Wright, M. N., & Ziegler, A. (2017). ranger: A fast implementation of random forests for high dimensional data in C++ and R. *J Stat Softw*, *77*(1), 1-17. https://doi.org/10.18637/jss.v077.i01

Yannic, G., Hagen, O., Leugger, F., Karger, D. N., & Pellissier, L. (2020). Harnessing paleo-environmental modeling and genetic data to predict intraspecific genetic structure. *Evol Appl*, *13*(6), 1526-1542. https://doi.org/10.1111/eva.12986

Yannic, G., Pellissier, L., Ortego, J., Lecomte, N., Couturier, S., Cuyler, C., Dussault, C., Hundertmark, K. J., Irvine, R. J., Jenkins, D. A., Kolpashikov, L., Mager, K., Musiani, M., Parker, K. L., Roed, K. H., Sipko, T., Porisson, S. G., Weckworth, B. V., Guisan, A., . . . Cote, S. D. (2014). Genetic diversity in caribou linked to past and future climate change. *Nat Clim Chang*, *4*(2), 132-137. https://doi.org/10.1038/Nclimate2074

Zimov, S. A., Chuprynin, V. I., Oreshko, A. P., Chapin, F. S., Reynolds, J. F., & Chapin, M. C. (1995). Steppe-Tundra Transition: A Herbivore-Driven Biome Shift at the End of the Pleistocene. *Am Nat*, *146*(5), 765-794. https://doi.org/10.1086/285824

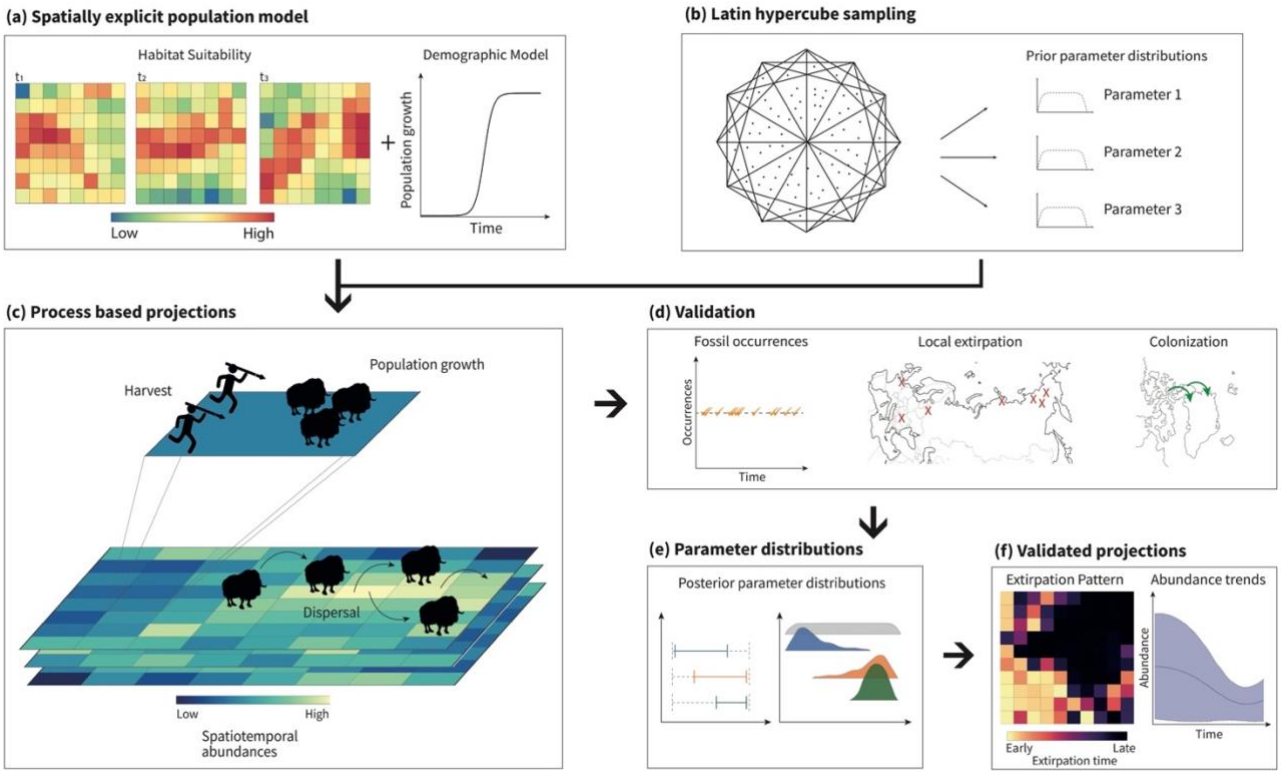

Figure 1. Modelling the range dynamics of muskox using spatially explicit population models.

Spatially explicit population models (SEPMs) account for spatiotemporal change in habitat suitability and demography (a). Uncertainty in climate-human-muskox interactions is modelled by generating thousands of models with unique combinations of parameter values sampled from wide but plausible ranges, using Latin Hypercube sampling (b). Each model simulates changes in spatiotemporal abundance in response to climatic change and hunting by humans (c). Model projections are validated using Approximate Bayesian Computation and pattern-oriented methods, which compare observed or inferred patterns (targets) to simulated patterns (d). Prior and posterior distributions can be visualized to identify important model parameters (e). A subset of 'best' models can be used to generate validated projections of abundance and extinction dynamics (f).

(a)

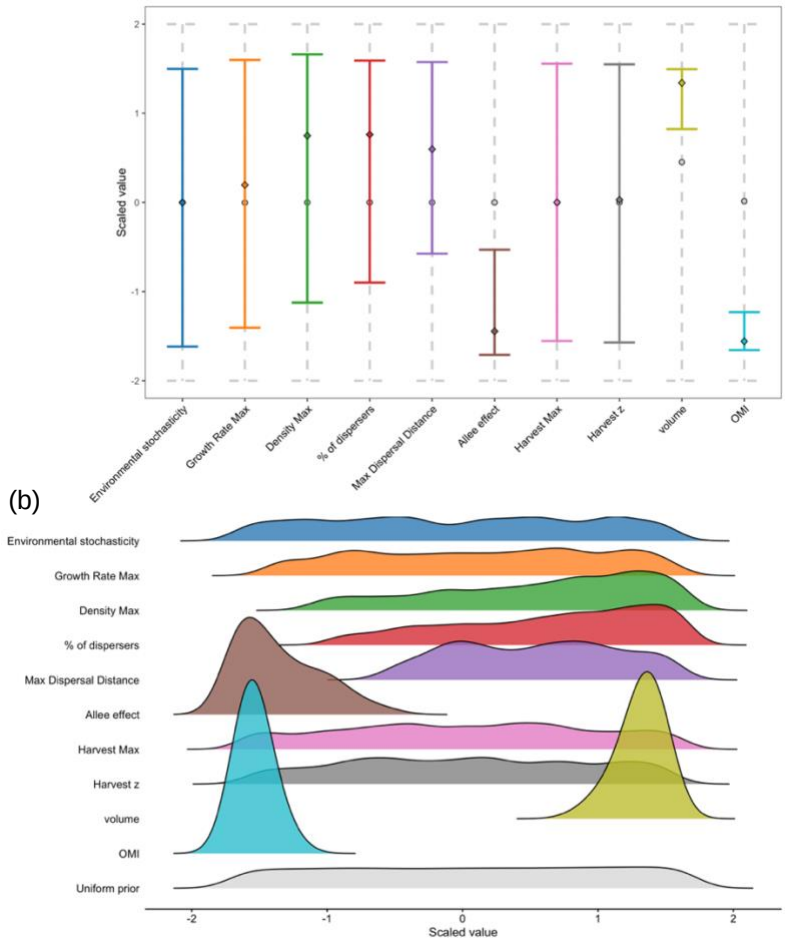

Figure 2. Prior and posterior distributions for modelled parameters

a) shows scaled parameter ranges for prior (broken line) and posterior (coloured line) parameters in the muskox SEPM. Circles and diamonds represent the mean of the prior and posterior distributions, respectively. Raw values for prior and posterior parameter ranges are provided in Table S1. b) shows the density of the posterior distribution compared to a uniformly distributed prior. Variable demographic parameters in the muskox SEPM are: variation in population growth rate (Environmental stochasticity); maximum population growth rate (Growth Rate Max); proportion of individuals dispersing at each time step (% of dispersers); maximum dispersal distance (Max Dispersal Distance); Alle effect; and maximum abundance (Density Max). Variable harvest parameters are: percentage of the population that is harvested (Harvest Max); extent to which harvest follows a Type II to Type III functional response (Harvest z). Variable parameters describing ecological niche requirements are: distance between the climatic conditions of the occupied and potential fundamental niche (OMI), and breadth of climatic conditions the species can occupy (volume).

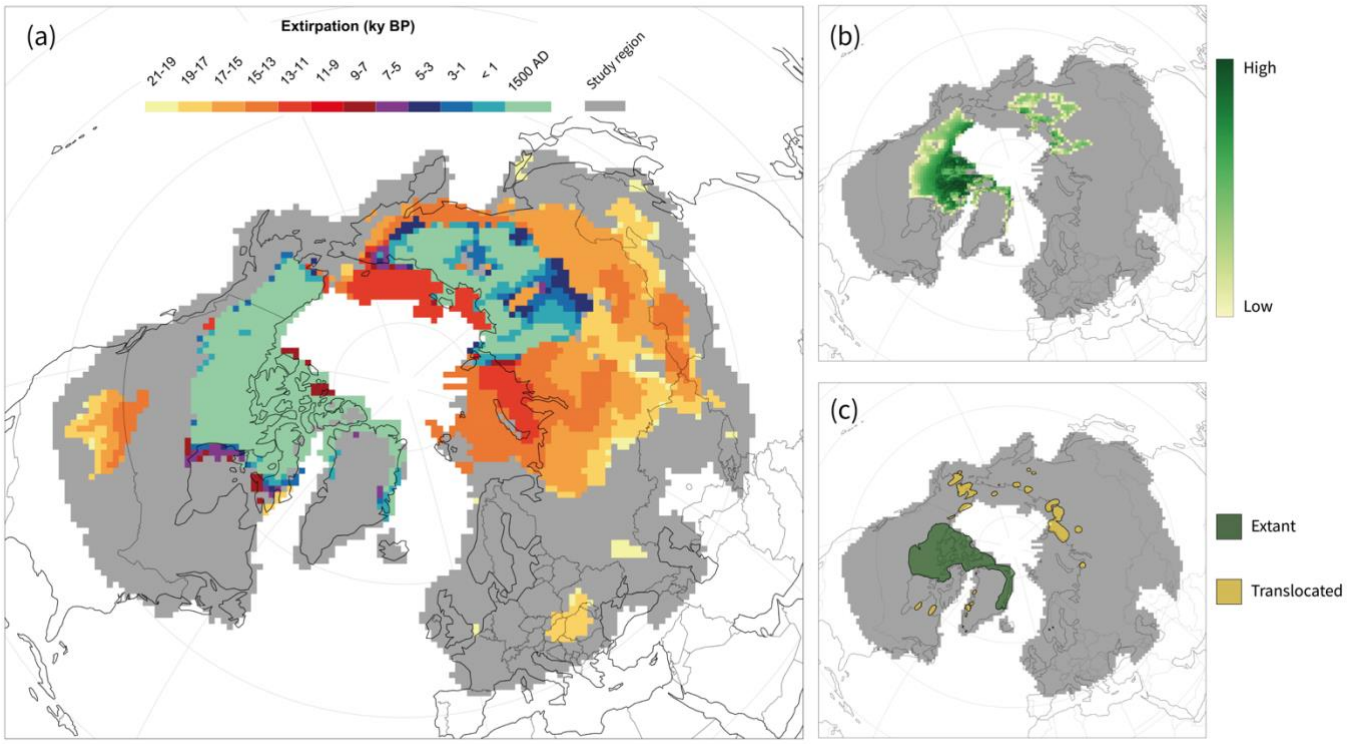

Figure 3. Change in the distribution of muskox over the last 21,000 years.

Projected time of extirpation of muskox (a). Areas simulated to be occupied in 1500 AD, with their relative densities (b). Panel (c) shows the current natural distribution of muskox (extant), and where muskox have been recently translocated for conservation purposes (Cuyler et al., 2020).

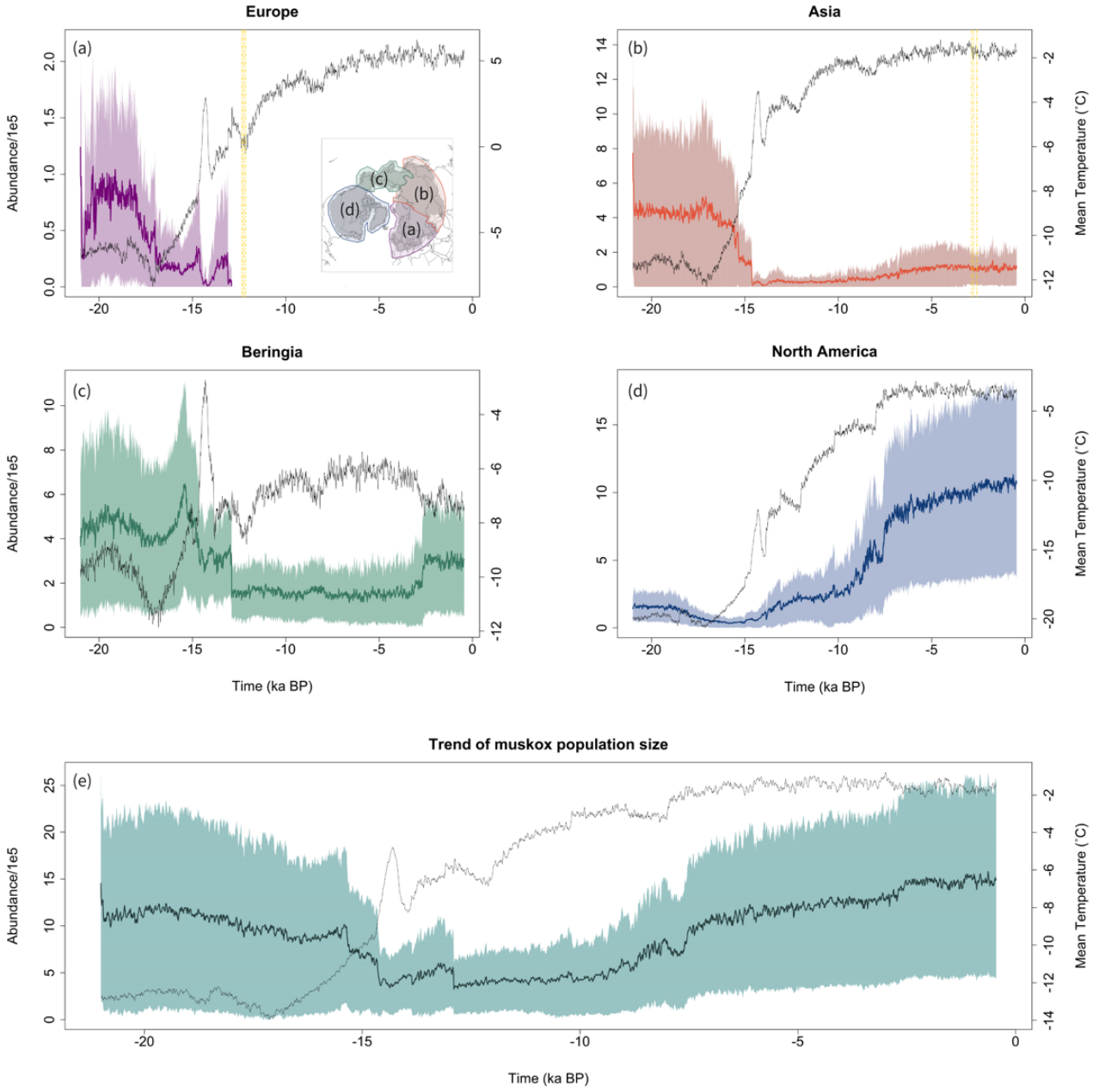

Figure 4. Temporal changes in population size.

Total population size (mean abundance ± 1 SD; left y axis) (coloured lines) and mean annual temperature (thin black line; right y axis) since 21 ka BP simulated for Europe (a), Asia (b), Beringia (c), North America (d) and for its once entire Holarctic range (e). The geographical division of sub-regions is shown in the inset of panel (a). The yellow vertical lines represent time of extinction based on the fossil record.

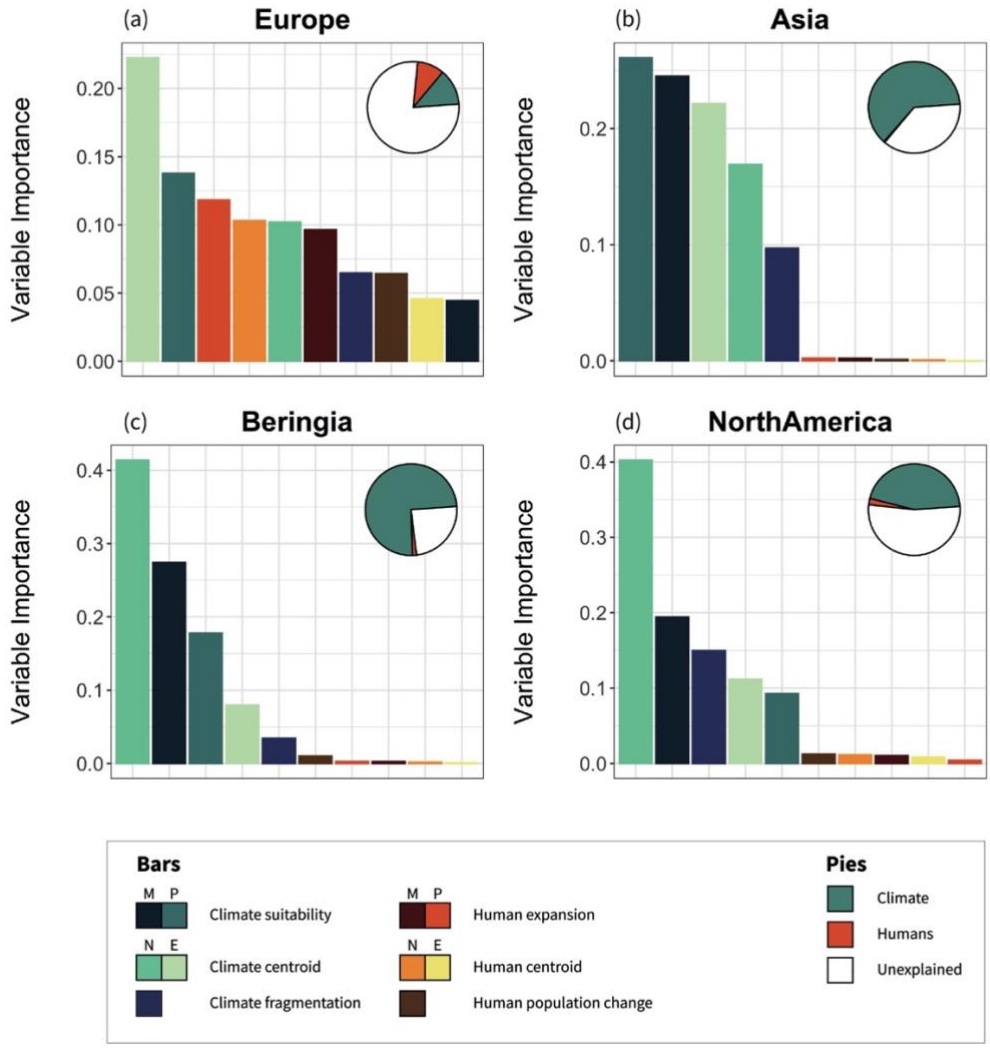

Figure 5. Effects of climate and humans on muskox abundance at the termination of the last deglaciation.

Drivers of time to extinction in Europe (a), and of expected minimum abundance (EMA) at 11 ka BP in Asia (b), Beringia (c), and North America (d). Bars represent individual contributions of measures of climatic change and human activities on explained variance in EMA or time to extinction. Variables are divided into magnitude (M) and pace (P) of change in climate suitability and human expansion, movement north (N) and east (E) of core climate suitability (climate centroid) and human abundance (human centroid), amount of fragmentation in climatically suitable areas (climate fragmentation), and growth in the human population (Human population change). All variables are explained in detail in Appendix 3. Pie charts show the variance explained (%) by climate (blue) and humans (red). White areas in the pie charts represent unexplained variance.

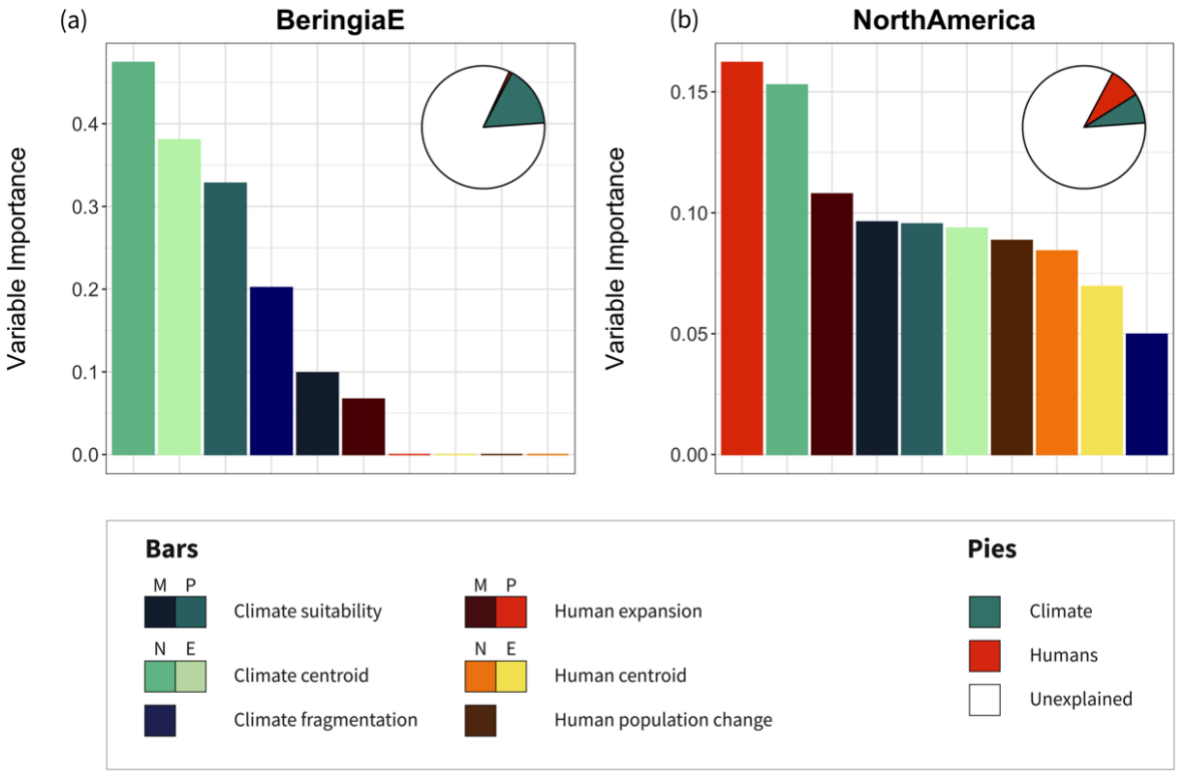

Figure 6. Effects of climate and humans on muskox final abundance.

Drivers of final abundance in Eastern Beringia (Alaska, US) (a) and North America (b) during the Holocene. Bars represent individual contributions of measures of climatic change and human activities on explained variance in population size at 1500 AD. Pie charts show the variance explained (%) by climate (blue) and humans (red). White areas in the pie charts represent unexplained variance. See Figure 5 for further details.

Supplementary Methods

Data

Fossil records and modern occurrences

We compiled dated georeferenced fossil records and modern observations of muskoxen (*Ovibos moschatus*). This database was used to model the ecological niche of the muskox over the last 21,000 years and to estimate the timing of regional extirpation events.

Fossil records provide geolocations of individual animals that roamed in Eurasia and North America during the Late Pleistocene and Holocene. All records were obtained from the literature and publicly available databases, including Stage3, Neotoma, CARD, PIDBA (Anderson et al., 2010; Martindale et al., 2016; van Andel, 2002; Williams et al., 2018). For each fossil record, we obtained information about its location, age, dating method, and association with human remains. We calibrated all radiocarbon dates using the OxCal and the IntCal20 calibration curve (Bronk Ramsey, 2009; Reimer et al., 2020). For fossils with no associated radiocarbon dating error (n = 70), we assumed an error equal to the mean error of fossils in a time bin of ± 10,000 years around the date.

The quality of dates for all fossils was assessed using the criteria defined by Barnosky & Lindsey (2010). We discarded all records identified as unreliable (i.e., score ≤ 10) according to the criteria (n = 41). Records with calibrated dates older than 21,000 years BP were also excluded (n = 193), as were records without location data (n = 10). This filtering resulted in 135 fossil records (Appendix 1; Figure S1).

Modern records of muskox (n = 4,683) were retrieved from GBIF (GBIF.org, 2019). We removed records with missing or incorrect coordinates (e.g., latitude and longitude = 0), missing date information, and records from re-introduction or translocation areas, fossils, and zoo specimens. The remaining records come from museum specimens, and human (citizen science projects) or machine (camera-traps) observations. We filtered out unreliable records, by constraining records to the known range limits of the species. We retained observations from a translocated population in Kangerlussuaq (West Greenland) after consulting species' experts, as this population expanded rapidly after the translocation event, indicating an area with extremely suitable conditions for the species. This filtering resulted in 248 modern records of muskox (Appendix 1; Figure S1).

Paleoclimate data

We used PaleoView (Fordham et al., 2017) to generate gridded paleoclimate reconstructions for the Northern Hemisphere for the period 21,000 BP to 0 BP. Climatic variables were chosen by considering the potential direct and indirect effects on population dynamics of the species. Temperature in boreal spring-summer and mean annual precipitation are important distal predictors for grazing arctic species because they drive primary productivity, and subsequently food availability and quality, which in turn indirectly determines the breeding success and the viability of offspring (Asbjornsen et al., 2005). Evapotranspiration in spring and summer affects the productivity of vegetation (Rosenzweig, 1968), hence providing a good proxy of food availability and survival and reproduction for arctic ungulates during the following autumn and winter (Desforges et al., 2021).

We generated continuous 30-year average projections of average minimum daily temperature in January, average maximum daily temperature in January and July, temperature seasonality, total annual precipitation, and precipitation seasonality at generational time steps (8 years; see below) for the last 21,000 years (Figure S2). We also generated monthly, seasonal, and annual reference evapotranspiration (ET) using mean minimum temperature, mean maximum temperature, monthly precipitation (all extracted from PaleoView) and solar radiation estimated from latitude, using a modified Hargreaves equation (Equation 5 in Droogers & Allen, 2002). Combinations of mean annual temperature, mean temperature of the warmest month, mean temperature of the coldest month, mean winter temperature, mean summer temperature, annual precipitation, precipitation seasonality and ET have been previously used to model range dynamics of large vertebrates in Eurasia (Lorenzen et al., 2011; Nogues-Bravo et al., 2010; Yannic et al., 2020; Yannic et al., 2014).

The spatial resolution of the paleoclimatic data was resampled from 2.5 x 2.5˚ to 1 x 1˚ resolution, using bilinear interpolation. All fossil records were paired to paleoclimate projections by intersecting climatic values in each specific georeferenced fossil location for the period ± 1SD around the age of the fossil (Fordham, Brown, et al., 2021). Values for precipitation and ET were then rounded to 2 decimal places, with temperature rounded to one decimal place. Fossil records that had identical climate values in space and time were then merged to keep unique records only. For example, in a location (grid-cell) with records: fossil A = 10,800 – 7,500 cal BP; fossil B = 11,500 – 10,000 cal BP; fossil C = 11,200 – 9,400 cal BP, the resulting set of climatic conditions will belong only to fossil A (10,800 – 7,500) and fossil B up to the starting age of fossil A (11,500 – 10,800).

Modern climate data

As PaleoView projections do not go beyond 1989 AD (Fordham et al., 2017), we used the CRU TS v. 4.03 (Harris et al., 2020) to pair the modern climate with the modern occurrences of the species. The CRU climate data contains temperature and precipitation data from 1901 to 2018 at a 0.5 x 0.5° resolution. We resampled the resolution to a 1 x 1˚ grid cell resolution using bilinear interpolation. To align the CRU data with PaleoView, we used a change factor bias correction (Beyer et al., 2020), allowing us to align the modern climate data to PaleoView at 1974 AD. This resulted in continuous projections of our climate variables from 21,000 BP to 2018 AD.

We paired the historical (GBIF) records with the climate data by assuming that the individuals were present on the same location for one generation. We extracted all the climatic values associated to half a generation before and after the year of the observation, in a specific location. As an example, a muskox record dated 2001 will be associated to climatic values that span the interval 1998-2004, with a generation length of 8 years. We excluded records that did not have matching years. As for the paleoclimate, we removed duplicated sets of values.

Muskox niche

We used the climatic values associated with fossil and modern occurrence records to derive a multi-temporal n-dimensional hypervolume of the climatic niche requirements of the muskox, representing the climatic space where the species can persist and thrive (Blonder et al., 2014; Nogués-Bravo, 2009). We did this using the 'hypervolume' package in R (Blonder et al., 2014).

Before building the niche models we tested for collinearity among climatic variables, applying a threshold $|r| > 0.7$ (Dormann et al., 2013). We used the three least correlated variables ($|r| < 0.7$) to generate the niche hypervolume: 1) average minimum daily temperature in January; 2) annual precipitation; 3) total ET in boreal spring and summer. We built gaussian hypervolumes, tuning the kernel density estimation (KDE) bandwidth using cross-validation (Blonder et al., 2014). The final multi-temporal hypervolume contained 3,551 points (set of climatic conditions; Figure S3) and approximates the fundamental niche of the muskox (Nogués-Bravo, 2009).

We exhaustively subsampled the full multi-temporal niche hypervolume by cutting 'boxes' with different widths (from 0.5 to 1, every 0.05), and moving them throughout the 3-dimensional space. These subsamples are representative of the potential realised niche used by the muskox and allowed the actual realized niche of the muskox to be identified in a later step using process-explicit macroecological modelling (see below). This subsampling process generated 4,496 unique niche

subsamples. We calculated marginality (OMI) of each unique niche subsample using the ade4 R package (Thioulouse et al., 2018), based on the method described in Dolédec et al. (2000). The breadth of each niche subsample was calculated based on the volume of the resulting 3-dimensional hypervolume. To do this, each subsample hypervolume was generated, using the KDE bandwidth of the full niche hypervolume. To relate each subsample to the full niche, the data was scaled and centred based on the mean and SD of the full niche. We used measures of marginality and volume to select 2,500 potential realised niches for muskox, ensuring that the distributions of marginality and breadth for the 4,496 niche samples were maintained.

We used the 2,500 models of the potential realised niche of the muskox to project climate suitability through space and time (every 8 years), using the 'hypervolume_project' function in the hypervolume R package (Blonder et al., 2014), for the period 21,000BP to 1500 AD.

Projections using this kernel density approach at its default settings, produce similar results to the standard maximum entropy method (Blonder et al., 2018). Ecological niche models of climate suitability were then reprojected using bilinear interpolation to a Lambert Azimuthal Equal Area projection centred on -15° east and 57° north, with a resolution of 100 km x 100 km.

Human density

We modelled the peopling of Eurasia and North America by Paleolithic humans using the Climate Informed Spatial Genetic Model (CISGEM), where genetic history and local demography is informed by paleoclimatic and paleo-vegetation reconstructions of net primary productivity (NPP) (Eriksson et al., 2012), which has been shown to be a primary determinant of global hunter-gatherer population densities (Tallavaara et al., 2018). The model has previously been shown to reconstruct arrival times of anatomically modern humans and current-day distributions of global and regional genetic diversity (Eriksson et al., 2012; Raghavan et al., 2015). It simulates local effective population sizes (N_e) as a function of genetic history, local demography as well as primary productivity (Eriksson et al., 2012; Raghavan et al., 2015). Like other numerical models of early human migration (Timmermann & Friedrich, 2016), arrival, occupancy, and density (here N_e) are forced by spatiotemporal estimates of climate and sea level changes over the past 125 thousand years.

In CISGEM, the world is represented by a hexagonal grid, each cell approximately 100 km wide. The potential number of people who can live in each cell (carrying capacity) is determined by reconstructions of NPP done by coupling the HadCM3 paleoclimate model to the Miami vegetation model (Lieth, 1975). Every 25 years (approximately the generation time of humans), the carrying capacity is updated to allow for changes in climate, as well as sea level and ice sheet extent. At each

generation, any cell that is inhabited will grow with a rate *r* (until it reaches the local carrying capacity), sending out migrants to other inhabited cells at rate *m*, or colonists to previously uninhabited cells at rate *c*. The relationship between carrying capacity and NPP, as well as the values of other demographic parameters, were fitted using pattern-oriented methods (Grimm et al., 2005) using an Approximate Bayesian Computation framework (Csilléry et al., 2010). Targets for model calibration were pairwise genetic differentiation among a large panel of modern-day human populations. In other words, the demography was calibrated to produce realistic genetic differentiation patterns across the globe. Eriksson et al. (2012) provide a detailed description of CISGEM parameters and procedures.

Based on the ABC fit provided by Eriksson et al. (2012), we took the best 4,000 parameter combinations and reconstructed population sizes through time. Effective population size in 21,000 BP was initialised (for each parameter combination) with values based on the HadCM3 climate model. A burn-in period of approximately 80 generations (where climatic conditions were held constant at 21,000 BP conditions) was used to ensure equilibrium effective population size at the beginning of the simulation. We filtered for runs in which humans colonize North America and Greenland, and we calculated average $N_e \pm$ SD. The final average and SD in human populations was projected to match the climate suitability projections. Finally human densities based on N_e were scaled between 0 and 1, using the 95^{th} percentile of the ensemble mean as threshold.

Process-explicit models

Ecological niche models of climate suitability and CISGEM estimates of human population size were coupled with stochastic demographic models to simulate extinction and colonization dynamics and other metapopulation processes at the landscape level (Figure 1). The resulting process-explicit macroecological model was coded in R using the 'poems' and 'paleopop' packages (Haythorne, Fordham, et al., 2021; Haythorne, Pilowsky, et al., 2021). The models were run at generational time steps (8 years) from 21,000 BP to 1,500 AD.

Generation Length

We used a generation length of 8 years following Hansen et al. (2018), based on long-term life-history observations of the species. The value agrees with the generation length calculated using the method used by IUCN Red List guidelines (IUCN, 2019):

$$GL = \sum x l_x m_x / \sum l_x m_x$$

where the summations are from age (x) 0 to the last age of reproduction; mx is (proportional to) the fecundity at age x; and lx is survivorship up to age x (i.e., lx = S0 · S1 ⋯ Sx-1 where S is annual survival rate, and l0 =1 by definition).

Upper abundance

The upper abundance (carrying capacity) of each cell was based on climate suitability (VanDerWal et al., 2009). To convert climate suitability to upper abundance, we assumed that the maximum area of suitable habitat in any given cell was ≤ 2,500 km^2 not 10,000 km^2. This approach appropriately addresses the mismatch between the spatial scale of the model and how the muskox is likely to have used the landscape (Fordham et al., 2013; Fordham, Brown, et al., 2021). For muskox, we set upper abundance at 1.42 individuals/km^2 and allowed it to vary, across models, at a rate between 0.04 and 2.8 animals/km^2 (Table S1). The estimates are based on maximum densities of muskox in highly suitable areas in the Canadian Islands and Greenland (Cuyler et al., 2020).

Population growth

We used time series data on population abundance to calculate finite rates of population increase and their variance, and maximum population growth rate (Brook & Bradshaw, 2006). Specifically, we fitted linear models to time series data from Russia (n = 2), Alaska (n = 2), Canada (n = 1), Greenland (n = 3) and Norway (n = 1) (Cuyler et al., 2020) (Figure S4), using the 'fit_easylinear' function of the growthrates package in R (Petzoldt, 2020). To better understand model fit and its sensitivity to the number of data points in the time series, we repeatedly fitted models to 3, 4, 5, 6 and 7 data points for each time-series. We then selected, for each time series, the estimate of maximum growth rate resulting from the model with the highest R^2. This provided a maximum annual growth rate estimate (Rmax; lambda) of 1.31 for muskox in Taimyr (Russia), based on a model fit with 4 continuous data points. The parameter range for Rmax was 1.06 to 1.31. The lower range of the estimates comes from the Cape Thompson (Alaska) time series, with model fit to 3 data points. We scaled Rmax to the generation level by taking the exponent (1.31^8) and treated this as an upper estimate of Rmax in the model, with a parameter range of maximum R0 = 1.54 – 8.82.

We used time series data (1998 – 2006) for a population of muskox in Greenland, that is stable, to calculate the standard deviation (SD) in population growth rate (Cuyler et al., 2020). We calculated SD in population growth at a generational time step by repeatedly running an annual model

for 500 years and then calculating the standard deviation of population growth at a generational level once the population had reached carrying capacity (Fordham, Brown, et al., 2021). Doing this resulted in an estimate of SD_{R0} of 0.30, which we treated as an upper estimate based on model simulations. The upper and lower bounds for SD_{R0} were set at 0 to 0.3. (Table S1).

Density dependence was modelled in the process-explicit simulations using a Ricker-logistic function (Ricker, 1954). A Ricker-logistic function was chosen because it assumes an almost exponential growth rate when populations abundances are small and predicts a decrease in population growth rate when populations approach carrying capacity, reflecting competition for resources at carrying capacity.

Dispersal

Information on muskox dispersal is very limited, and we therefore used information on observed range expansion for a muskox population (Reynolds, 1998) and movement of muskox lungworms (Kafle et al., 2020) to arrive at an estimate of 500 km as being the upper limit for maximal dispersal per generation (Table S1). We modelled a mean dispersal rate of 15% of the population moving per generation at an average maximum distance of 250 km. We set upper and lower bounds on these estimates of 5 – 25% and 0 – 500 km, respectively.

Dispersal was modelled using the following equation:

$$m_{ij} = \begin{cases} a^{\left(\frac{-D_{ij}}{b}\right)}, & D < D_{max} \\ 0, & D \geq D_{max} \end{cases} \quad (2)$$

Where movement (m) between cell *i* and *j* is a function of the parameters *a*, *b*, and *Dmax*; and *Dij* is the distance between the two populations. The parameter *a* is 0.5 × the total proportion of dispersers that leave a cell at each time step and *b* and *Dmax* are modelled as one of 9 combinations depending on the estimate of D [Appendix 3 (Table 2) in Fordham, Brown, et al. (2021)]. This approach prevents large dispersal rates to closely neighbouring cells (i.e., the drainage effect) by pre-calculating a fixed proportion of individuals that should move to a given cell based on *a*, *Dmax* and *Dij*.

Dispersal was limited depending on the habitat suitability within source and target cells, and on the proportion of ice present in target cells. Dispersal was completely blocked to cells covered by the sea and reduced to cells containing glacial ice. We did this using a friction map and distance-equivalence multipliers, calculated using a cost-surface generator (Fordham, Haythorne, et al., 2021).

For example, if two patches of highly suitable habitat are separated by a strait, following the land towards the second patch is less costly than directly crossing the strait.

Allee effect

We set a local quasi-extinction threshold (Fordham et al., 2013) which made cell abundance zero if abundance fell below the Allee threshold. Due to lack of information on Alle effect for muskox, we followed the methodology used for the woolly mammoth in Fordham, Brown, et al. (2021). The range of values for the Allee effect were 0 (i.e., no Allee effect) to 500 individuals per grid cell (Table S1).

Environmental correlation

This was a fixed parameter in our models that was set to b = 850 km (Pearson et al., 2014), where b is the decay constant of an exponential decline model. This parameter accounts for similarity in environmental fluctuations for populations located close together versus further apart.

Human hunting

Human hunting of muskox was modelled as a function of the timing of arrival and relative density (using N_e as a proxy for abundance) of humans at a given cell. Using Latin Hypercube sampling (see below) we generated 10,000 plausible reconstructions of human population abundance, by sampling within ± 1 SD of N_e using a lognormal distribution (Fordham, Brown, et al., 2021). Because information on exploitation of muskox by anatomically modern humans is lacking, we let the maximum exploitation rate vary between 0% and 25% of the population abundance, under a Type II to a Type III functional response (Fordham, Brown, et al., 2021). Harvesting is modelled as a function of density of prey population (current muskox population size, divided by maximum muskox population size), maximal exploitation rate (F), prey density at which exploitation is half-maximal (G), and a measure of departure from maximal exploitation (z). The equations used to model harvest can be found in (Fordham, Brown, et al., 2021). In our models, the parameter z is a variable parameter, which takes values between 1 and 2 (Alroy, 2001). A value of z = 1 results in a Type II functional response, where exploitation is modulated only by prey density and human satiation, implying complete naivety of prey. At z > 1.5 hunting success takes on an increasingly sigmoidal Type III functional response, under which prey become harder to hunt at low densities. This might result from prey adaptation (evolved or learned behaviour), prey switching by hunters, or prey being in refugia (Brook & Bowman, 2004; Brook & Johnson, 2006). Parameter G was set constant to 0.4 (Alroy,

2001; Brook & Johnson, 2006), and F varied from 0 to 0.25. The harvesting pressure was set globally – i.e., there were no regional differences in harvesting pressure.

Latin Hypercube Sampling and model simulations

We generated process-explicit macroecological models using combinations of values for demographic parameters and environmental attributes that varied across plausible ranges (Fordham, Haythorne, et al., 2021). Sampling of these values was done using Latin Hypercube sampling from uniform distributions, providing a robust coverage of the multi-dimensional parameter space (Fordham et al., 2016). We produced 100,000 conceivable models with different combinations of parameters values, each of which we ran as a single replicate (Prowse et al., 2016).

Models were initialised at carrying capacity in all areas except Greenland, where abundance was set to zero in any cells with carrying capacity greater than zero. We did this because although ice-free areas were present in Greenland during the Last Glacial Maximum, these were unlikely to have sustained vegetation and animals (Bennike, 1999).

Pattern-oriented modelling

We used pattern-oriented modelling (POM) techniques (Grimm et al., 2005) to evaluate the adequacy of the process-explicit macroecological models to simulate mechanistic responses to climate change and human exploitation, and to reconstruct known range dynamics and the current distribution of the muskox. Model simulations of changes in abundance through time and space were assessed using a multivariate target based on inferences from the fossil record and historical observations.

Observed and modelled summary statistics

We extracted summary statistics for each simulation and calculated the deviation from the simulated and inferred pattern. We did this for:

- Occupancy pattern: agreement between simulated and inferred occupancy. Occupancy at a fossil site was correctly simulated if there was positive abundance in that grid cell (or the 8 surrounding cells) during the calibrated age ± 1SD. We summed the number of records where there was agreement between simulated and inferred occupancy.
- Local extirpation pattern: based on the fossil record, we calculated times of extirpation across three sub-regions: Europe (with the Ural Mountains defining the eastern boundary), Asia (between the Urals and the Lena River), West Beringia (eastern Siberia) (Fordham, Brown,

et al., 2021) (Table S2). We used the 'GRIWM' method (Bradshaw et al., 2012) to calculate regional extinction time, which accounts for the Signor-Lipps effect (Signor et al., 1982). The resulting extinction times were: 12,254 BP (95% CI: 12,345 BP – 12,160 BP) for Europe, 2,738 BP (95% CI: 2,856 BP – 2,569 BP) for Asia and 3,157 BP (95% CI: 3,437 BP – 2633 BP) for Beringia. We calculated the Root Mean Square Error (RMSE) of the difference between the simulated and inferred regional extinction times, from the fossil records, and from each simulation (Fordham, Haythorne, et al., 2021).

- Distance from extinction location. The last remnant population of muskox in Eurasia was found in the Taimyr peninsula (Campos et al., 2010; Markova et al., 2015). Therefore, the distance from the extinction location for model simulations was calculated as the difference between the centre of Taimyr (Longitude = 94.3, Latitude = 72.9) and the location of the last simulated population. For persistent populations, we calculated a weighted centroid based on population abundance of the last populations persisting in Eurasia, and then calculated the distance to the centre of Taimyr.
- Arrival time in Greenland. We used 'GRIWM' to calculate an arrival time in Greenland of 5,607 BP (95% CI: from 5,752 BP to 5,461 BP) based on the fossil records. This estimate aligns with estimates published elsewhere (Lent, 1999). Simulated time of arrival was calculated as the first positive abundance in Greenland and the number of generations away from the inferred arrival window was noted. If the arrival time in our simulations fell within the mean ± 1SD arrival time based on the fossil records, the penalty was 0.

Approximate Bayesian Computation analysis

We used Approximate Bayesian Computation (ABC) (Csilléry et al., 2010) to validate our 100,000 process-explicit simulations using the 'abc' package in R (Csilléry et al., 2012). Specifically, we used ABC to fit the simulation models to data and estimate (i.e., refine) the posterior distribution of model parameters. There were 12 variable parameters in the process-explicit models, covering demographic, harvest, and niche parameters (Table S1). We scaled the data and used the 'rejection' method in the ABC, with a tolerance of 0.01. With the rejection method, Euclidian distances are calculated between each summary statistic and the target. Simulations were accepted if the sum of the distances fell below the threshold defined by a tolerance value of 0.01 (Csilléry et al., 2012). ABC modelling is therefore selecting simulations that can simultaneously replicate multiple key biogeographical patterns.

Effective population size

Trends in effective population size (N_e), as Bayesian Skyline plots, can be used as an independent validation of the change in total population size. The Bayesian Skyline plot of effective population size for muskox was calculated using a previously compiled dataset, containing 266 radiocarbon-dated fossils of muskox, out of which 138 have associated aDNA sequences, which are available in GenBank (Clark et al., 2016). Sequences were aligned in Geneious v1.9.8 (Kearse et al., 2012) using default settings of the MUSCLE algorithm (Edgar, 2004). Radiocarbon dates were calibrated using OxCal and the IntCal13 calibration curve (Reimer et al., 2016). We reconstructed the genealogy using BEAUti v.1.10.4 and BEAST v1.10.4 (Suchard et al., 2018). We used the average calibrated date of each fossil record as prior information for the tip-dates, and the standard deviation to derive uncertainty in the tip-dates. We used jModelTest v2.1.10 (Posada, 2008) to find the best substitution model and, based on Akaike's Information Criterion (AIC), we selected the TN93 + Gamma + Invariant Sites substitution model. We used a strict molecular clock, a Coalescent Bayesian Skyline Tree Prior, a constant Skyline Model and the UPGMA starting tree. The Markov Chain Monte Carlo run was set with a chain length of 10^8 and to log parameters every 10^4 simulations to avoid possible autocorrelation during the MCMC analysis. We then analysed the output using Tracer v1.7.1 (Rambaut et al., 2018). Our approach resembles the approach used by (Foote et al., 2013) to investigate changes in mammal N_e based on aDNA and contemporary sequences. The resulting estimate of N_e for the muskox mirrors estimates elsewhere (Campos et al., 2010; Figure S6).

To use inferences of demographic change from aDNA as an independent validation target, we compared simulated trends in total relative population size for selected models (from the ABC validation) and trend in relative effective population size inferred from aDNA, using the average correlation coefficient. We also compared magnitudes of change in relative population size for the last deglaciation (19 ka BP – 11 ka BP) and Holocene (11 ka BP – 1500 AD) across both groups. To do this we calculated the magnitude of change in abundance between 19 ka BP and 11 ka BP, for the deglaciation, and between 11ka BP and 1500 AD, for the Holocene, for each of the selected models and for an equivalent number of uniformly sampled points within the 95% CI of the N_e trend at those specific time points. We then did a Welch's t-test to determine if there were significant differences in magnitude of change for each period between the aDNA and our simulations.

Timing of extirpation and probability of occurrence

The top 1% of models, determined by ABC analysis to best replicate known biogeographical patterns, were used to generate an ensemble average of total population abundance (weighted by the inverse of the Euclidean distance of the model from the idealized targets), accounting for probability of occurrence (Fordham, Brown, et al., 2021). Based on the ensemble average of population abundance, we generated an extirpation map showing the timing of extirpation in each grid cell up to 1500 AD.

To generate spatiotemporal estimates of probability of occurrence, we produced a binary presence/absence map for each time step for each of the selected simulations. We then calculated an average probability of occurrence across the selected simulations. To determine a minimum threshold for occurrence, we calculated the probability of occurrence that maximized the area under the receiving operating curve for the fossil record based on predictions from a binomial GLM. We extracted the mean probability of occurrence for each fossil across time and for 10 randomly sampled background points (Merow et al., 2013) for the same temporal interval. Using 10 repeats of 10-fold cross validation, we built 100 binomial GLMs using different thresholds between 0 and 1 at 0.01 intervals. AUC was calculated for each of the models with the smallest threshold (0.06) being chosen that maximized AUC (AUC = 0.987). Probability of occurrences below the threshold were set to 0 and those above the threshold to 1. The binary map was then used as a multiplier to the ensemble weighted average of total population abundance. An Allee effect was applied based on the weighted average values of the selected simulations.

Drivers of extinction risk and final population abundance

We assessed the different roles that climate change and human harvesting could have had on the extinction risk of muskox during the deglaciation period (between 19 ka BP and 11 ka BP), by analysing the selected simulations using random forest classification trees, implemented with the 'ranger' package in R (Wright & Ziegler, 2017). To do this, we divided the study region into four sub-regions: Europe (with the Ural Mountains defining the eastern boundary), Asia (between the Urals and the Lena River), Beringia (including eastern Siberia and Alaska (US)), and North America (northern Canada and Greenland) and determined spatiotemporal differences in the impacts of climate and humans on Expected Minimum Abundance (EMA), which is a measure of extinction risk (McCarthy & Thompson, 2001). Expected minimum abundance was scaled by abundance at the start of the simulation (Fordham, Brown, et al., 2021). For each subregion and each selected simulation, we calculated a suite of metrics defining the magnitude, pace and movement of climate change and human expansion during the deglaciation period. These metrics are described in detail in Appendix

3, and are based on Fordham, Brown, et al. (2021). As the muskox goes extinct in Europe in our selected simulations before the end of the deglaciation, we used time to extinction instead of EMA for Europe.

We also assessed the relative roles of climate change and human harvesting on the final population abundances of muskox in Eastern Beringia and North America, where the species is extant. The muskox was reintroduced in Alaska after going extinct in the last century due to overhunting (Lent, 1998, 1999). Therefore, we considered Alaska as an endemic part of the range, given that the species was still present in the area at 1500 AD (end of our simulations). For each sub-region, metrics defining climate change and human expansion were calculated over the Holocene period (between 11 ka BP and 1500 AD). Final population abundance at 1500 AD were calculated using a 3-generation smoother to account for stochasticity.

Random forest classification trees, implemented with the 'ranger' package in R (Wright & Ziegler, 2017), were used to identify spatiotemporal effects of climate and human drivers on EMA and time to extinction. We constructed 1,000 trees and tuned the number of variables and minimum node size at each split via 10 x 10-fold cross validation, to maximize model accuracy. Variable importance scores were calculated using unscaled permutation importance (Strobl et al., 2007) and converted to % contribution of the variance explained.

References

Alroy, J. (2001). A multispecies overkill simulation of the end-Pleistocene megafaunal mass extinction. *Science*, *292*(5523), 1893-1896. https://doi.org/10.1126/science.1059342

Anderson, D. G., Miller, D. S., Yerka, S. J., Gillam, J. C., Johanson, E. N., Anderson, D. T., . . . Smallwood, A. M. (2010). PIDBA (Paleoindian Database of the Americas) 2010: current status and findings. *Archaeol East N Am*, *38*, 63-89.

Asbjornsen, E. J., Saether, B. E., Linnell, J. D. C., Engen, S., Andersen, R., & Bretten, T. (2005). Predicting the growth of a small introduced muskox population using population prediction intervals. *J Anim Ecol*, *74*(4), 612-618. https://doi.org/10.1111/j.1365-2656.2005.00946.x

Barnosky, A. D., & Lindsey, E. L. (2010). Timing of Quaternary megafaunal extinction in South America in relation to human arrival and climate change. *Quat Int*, *217*(1-2), 10-29. https://doi.org/10.1016/j.quaint.2009.11.017

Bennike, O. (1999). Colonisation of Greenland by plants and animals after the last ice age: a review. *Polar Rec*, *35*(195), 323-336. https://doi.org/10.1017/s0032247400015679

Beyer, R., Krapp, M., & Manica, A. (2020). An empirical evaluation of bias correction methods for palaeoclimate simulations. *Clim Past*, *16*(4), 1493-1508. https://doi.org/10.5194/cp-16-1493-2020

Blonder, B., Lamanna, C., Violle, C., & Enquist, B. J. (2014). The n-dimensional hypervolume. *Glob Ecol Biogeogr*, *23*(5), 595-609. https://doi.org/10.1111/geb.12146

Blonder, B., Morrow, C. B., Maitner, B., Harris, D. J., Lamanna, C., Violle, C., Enquist, B. J., Kerkhoff, A. J., & McMahon, S. (2017). New approaches for delineating n-dimensional hypervolumes. *Methods Ecol Evol*, *9*(2), 305-319. https://doi.org/10.1111/2041-210x.12865

Bradshaw, C. J. A., Cooper, A., Turney, C. S. M., & Brook, B. W. (2012). Robust estimates of extinction time in the geological record. *Quat Sci Rev*, *33*, 14-19. https://doi.org/10.1016/j.quascirev.2011.11.021

Bronk Ramsey, C. (2009). Bayesian analysis of radiocarbon dates. *Radiocarbon*, *51*(1), 337-360. https://doi.org/10.1017/s0033822200033865

Brook, B. W., & Bowman, D. M. J. S. (2004). The uncertain blitzkrieg of Pleistocene megafauna. *J Biogeogr*, *31*(4), 517-523. https://doi.org/10.1046/j.1365-2699.2003.01028.x

Brook, B. W., & Bradshaw, C. J. (2006). Strength of evidence for density dependence in abundance time series of 1198 species. *Ecology*, *87*(6), 1445-1451. https://doi.org/10.1890/0012-9658(2006)87[1445:soefdd]2.0.co;2

Brook, B. W., & Johnson, C. N. (2006). Selective hunting of juveniles as a cause of the imperceptible overkill of the Australian Pleistocene megafauna. *Alcheringa*, *30*(sup1), 39-48. https://doi.org/10.1080/03115510609506854

Campos, P. F., Willerslev, E., Sher, A., Orlando, L., Axelsson, E., Tikhonov, A., Aaris-Sorensen, K., Greenwood, A. D., Kahlke, R. D., Kosintsev, P., Krakhmalnaya, T., Kuznetsova, T., Lemey, P., MacPhee, R., Norris, C. A., Shepherd, K., Suchard, M. A., Zazula, G. D., Shapiro, B., & Gilbert, M. T. (2010). Ancient DNA analyses exclude humans as the driving force behind late Pleistocene musk ox (*Ovibos moschatus*) population dynamics. *Proc Natl Acad Sci U S A*, *107*(12), 5675-5680. https://doi.org/10.1073/pnas.0907189107

Clark, K., Karsch-Mizrachi, I., Lipman, D. J., Ostell, J., & Sayers, E. W. (2016). GenBank. *Nucleic Acids Res*, *44*(D1), D67-D72. https://doi.org/10.1093/nar/gkv1276

Csilléry, K., Blum, M. G., Gaggiotti, O. E., & Francois, O. (2010). Approximate Bayesian Computation (ABC) in practice. *Trends Ecol Evol*, *25*(7), 410-418. https://doi.org/10.1016/j.tree.2010.04.001

Csilléry, K., François, O., & Blum, M. G. B. (2012). abc: an R package for approximate Bayesian computation (ABC). *Methods Ecol Evol*, *3*(3), 475-479. https://doi.org/10.1111/j.2041-210X.2011.00179.x

Cuyler, C., Rowell, J., Adamczewski, J., Anderson, M., Blake, J., Bretten, T., Brodeur, V., Campbell, M., Checkley, S. L., Cluff, H. D., Côté, S. D., Davison, T., Dumond, M., Ford, B., Gruzdev, A., Gunn, A., Jones, P., Kutz, S., Leclerc, L. M., . . . Ytrehus, B. (2020). Muskox status, recent variation, and uncertain future. *Ambio*, *49*, 805-819. https://doi.org/10.1007/s13280-019-01205-x

Desforges, J. P., Marques, G. M., Beumer, L. T., Chimienti, M., Hansen, L. H., Pedersen, S. H., Schmidt, N. M., & van Beest, F. M. (2021). Environment and physiology shape Arctic ungulate population dynamics. *Glob Chang Biol*, *27*(9), 1755-1771. https://doi.org/10.1111/gcb.15484

Dolédec, S., Chessel, D., & Gimaret-Carpentier, C. (2000). Niche Separation in Community Analysis: A New Method. *Ecology*, *81*(10), 2914-2927. https://doi.org/10.1890/0012-9658(2000)081[2914:Nsicaa]2.0.Co;2

Dormann, C. F., Elith, J., Bacher, S., Buchmann, C., Carl, G., Carré, G., Marquéz, J. R. G., Gruber, B., Lafourcade, B., Leitão, P. J., Münkemüller, T., McClean, C., Osborne, P. E., Reineking, B., Schröder, B., Skidmore, A. K., Zurell, D., & Lautenbach, S. (2013). Collinearity: a review of methods to deal with it and a simulation study evaluating their performance. *Ecography*, *36*(1), 27-46. https://doi.org/10.1111/j.1600-0587.2012.07348.x

Droogers, P., & Allen, R. G. (2002). Estimating reference evapotranspiration under inaccurate data conditions. *Irrig Drain Syst*, *16*, 33–45.

Edgar, R. C. (2004). MUSCLE: multiple sequence alignment with high accuracy and high throughput. *Nucleic Acids Res*, *32*(5), 1792-1797. https://doi.org/10.1093/nar/gkh340

Eriksson, A., Betti, L., Friend, A. D., Lycett, S. J., Singarayer, J. S., von Cramon-Taubadel, N., Valdes, P. J., Balloux, F., & Manica, A. (2012). Late Pleistocene climate change and the global expansion of anatomically modern humans. *Proc Natl Acad Sci U S A*, *109*(40), 16089-16094. https://doi.org/10.1073/pnas.1209494109

Foote, A. D., Kaschner, K., Schultze, S. E., Garilao, C., Ho, S. Y., Post, K., Higham, T. F., Stokowska, C., van der Es, H., Embling, C. B., Gregersen, K., Johansson, F., Willerslev, E., & Gilbert, M. T. (2013). Ancient DNA reveals that bowhead whale lineages survived Late

Pleistocene climate change and habitat shifts. *Nat Commun*, *4*(1), 1677. https://doi.org/10.1038/ncomms2714

Fordham, D. A., Akçakaya, H. R., Brook, B. W., Rodríguez, A., Alves, P. C., Civantos, E., Triviño, M., Watts, M. J., & Araújo, M. B. (2013). Adapted conservation measures are required to save the Iberian lynx in a changing climate. *Nat Clim Chang*, *3*(10), 899-903. https://doi.org/10.1038/nclimate1954

Fordham, D. A., Brown, S. C., Akcakaya, H. R., Brook, B. W., Haythorne, S., Manica, A., Shoemaker, K. T., Austin, J. J., Blonder, B., Pilowsky, J., Rahbek, C., & Nogues-Bravo, D. (2021). Process-explicit models reveal pathway to extinction for woolly mammoth using pattern-oriented validation. *Ecol Lett*, *25*(1), 125-137. https://doi.org/10.1111/ele.13911

Fordham, D. A., Haythorne, S., & Brook, B. W. (2016). Sensitivity Analysis of Range Dynamics Models (SARDM): Quantifying the influence of parameter uncertainty on forecasts of extinction risk from global change. *Environ Model Softw*, *83*, 193-197. https://doi.org/10.1016/j.envsoft.2016.05.020

Fordham, D. A., Haythorne, S., Brown, S. C., Buettel, J. C., & Brook, B. W. (2021). poems: R package for simulating species' range dynamics using pattern-oriented validation. *Methods Ecol Evol*, *12*(12), 2364-2371. https://doi.org/10.1111/2041-210x.13720

Fordham, D. A., Saltre, F., Haythorne, S., Wigley, T. M. L., Otto-Bliesner, B. L., Chan, K. C., & Brook, B. W. (2017). PaleoView: a tool for generating continuous climate projections spanning the last 21 000 years at regional and global scales. *Ecography*, *40*(11), 1348-1358. https://doi.org/10.1111/ecog.03031

GBIF.org (2019). *GBIF Occurrence Download.* The Global Biodiversity Information Facility. Accessed 08 April 2019. https://doi.org/10.15468/DL.QW3LPI

Grimm, V., Revilla, E., Berger, U., Jeltsch, F., Mooij, W. M., Railsback, S. F., Thulke, H.-H., Weiner, J., Wiegand, T., & DeAngelis, D. L. (2005). Pattern-Oriented Modeling of Agent-Based Complex Systems: Lessons from Ecology. *Science*, *310*(5750), 987. https://doi.org/10.1126/science.1116681

Hansen, C. C. R., Hvilsom, C., Schmidt, N. M., Aastrup, P., Van Coeverden de Groot, P. J., Siegismund, H. R., & Heller, R. (2018). The muskox lost a substantial part of Its genetic diversity on its long road to Greenland. *Curr Biol*, *28*(24), 4022-4028 e4025. https://doi.org/10.1016/j.cub.2018.10.054

Harris, I., Osborn, T. J., Jones, P., & Lister, D. (2020). Version 4 of the CRU TS monthly high-resolution gridded multivariate climate dataset. *Sci Data*, *7*(1), 109. https://doi.org/10.1038/s41597-020-0453-3

Haythorne, S., Fordham, D., Brown, S., Buettel, J., & Brook, B. (2021). *poems: Pattern-Oriented Ensemble Modeling System.* In (Version 1.0.1) [R package]. R. https://CRAN.R-project.org/package=poems

Haythorne, S., Pilowsky, J., Brown, S., & Fordham, D. (2021). *paleopop: Pattern-Oriented Modeling Framework for Coupled Niche-Population Paleo-Climatic Models.* In (Version 2.1.2) [R package]. R. https://CRAN.R-project.org/package=paleopop

IUCN. (2019). *Guidelines for Using the IUCN Red List Categories and Criteria*. http://www.iucnredlist.org/documents/RedListGuidelines.pdf

Kafle, P., Peller, P., Massolo, A., Hoberg, E., Leclerc, L. M., Tomaselli, M., & Kutz, S. (2020). Range expansion of muskox lungworms track rapid arctic warming: implications for geographic colonization under climate forcing. *Sci Rep*, *10*(1), 17323. https://doi.org/10.1038/s41598-020-74358-5

Kearse, M., Moir, R., Wilson, A., Stones-Havas, S., Cheung, M., Sturrock, S., Buxton, S., Cooper, A., Markowitz, S., Duran, C., Thierer, T., Ashton, B., Meintjes, P., & Drummond, A. (2012). Geneious Basic: An integrated and extendable desktop software platform for the organization and analysis of sequence data. *Bioinformatics*, *28*(12), 1647-1649. https://doi.org/10.1093/bioinformatics/bts199

Lent, P. C. (1998). Alaska's indigenous muskoxen: a history. *Rangifer*, *18*(5), 133. https://doi.org/10.7557/2.18.3-4.1457

Lent, P. C. (1999). *Muskoxen and their hunters: A history* (Vol. 5). University of Oklahoma Press.

Lieth, H. (1975). Modeling the Primary Productivity of the World. In H. Lieth & R. H. Whittaker (Eds.), *Primary Productivity of the Biosphere* (pp. 237-263). Berlin, Heidelberg: Springer.

Lorenzen, E. D., Nogues-Bravo, D., Orlando, L., Weinstock, J., Binladen, J., Marske, K. A., Ugan, A., Borregaard, M. K., Gilbert, M. T., Nielsen, R., Ho, S. Y., Goebel, T., Graf, K. E., Byers, D., Stenderup, J. T., Rasmussen, M., Campos, P. F., Leonard, J. A., Koepfli, K. P., . . . Willerslev, E. (2011). Species-specific responses of Late Quaternary megafauna to climate and humans. *Nature*, *479*(7373), 359-364. https://doi.org/10.1038/nature10574

Markova, A. K., Puzachenko, A. Y., van Kolfschoten, T., Kosintsev, P. A., Kuznetsova, T. V., Tikhonov, A. N., Bachura, O. P., Ponomarev, D. V., van der Plicht, J., & Kuitems, M. (2015). Changes in the Eurasian distribution of the musk ox (Ovibos moschatus) and the extinct bison (Bison priscus) during the last 50 ka BP. *Quat Int*, *378*, 99-110. https://doi.org/10.1016/j.quaint.2015.01.020

Martindale, A., Morlan, R., Betts, R., Blake, M., Gajewski, K., Chaput, M., Mason, C. E., & Richards, P. V. (2016). *Canadian Archaeological Radiocarbon Database (CARD 2.1)*. Accessed October 04, 2019.

McCarthy, M. A., & Thompson, C. (2001). Expected minimum population size as a measure of threat. *Anim Conserv*, *4*(4), 351-355. https://doi.org/10.1017/s136794300100141x

Merow, C., Smith, M. J., & Silander, J. A. (2013). A practical guide to MaxEnt for modeling species' distributions: what it does, and why inputs and settings matter. *Ecography*, *36*(10), 1058-1069. https://doi.org/10.1111/j.1600-0587.2013.07872.x

Nogués-Bravo, D. (2009). Predicting the past distribution of species climatic niches. *Glob Ecol Biogeogr*, *18*(5), 521-531. https://doi.org/10.1111/j.1466-8238.2009.00476.x

Nogues-Bravo, D., Ohlemuller, R., Batra, P., & Araujo, M. B. (2010). Climate predictors of late quaternary extinctions. *Evolution*, *64*(8), 2442-2449. https://doi.org/10.1111/j.1558-5646.2010.01009.x

Pacifici, M., Santini, L., Di Marco, M., Baisero, D., Francucci, L., Marasini, G. G., Visconti, P., & Rondinini, C. (2013). Generation length for mammals. *Nat Conserv*, *5*, 87-94. https://doi.org/10.3897/natureconservation.5.5734

Pearson, R. G., Stanton, J. C., Shoemaker, K. T., Aiello-Lammens, M. E., Ersts, P. J., Horning, N., Fordham, D. A., Raxworthy, C. J., Ryu, H. Y., McNees, J., & Akçakaya, H. R. (2014). Life history and spatial traits predict extinction risk due to climate change. *Nat Clim Chang*, *4*(3), 217-221. https://doi.org/10.1038/nclimate2113

Petzoldt, T. (2020). *Estimation of Growth Rates with Package growthrates*. In [R package]. R. https://cran.r-project.org/web/packages/growthrates/vignettes/Introduction.html

Posada, D. (2008). jModelTest: phylogenetic model averaging. *Mol Biol Evol*, *25*(7), 1253-1256. https://doi.org/10.1093/molbev/msn083

Prowse, T. A. A., Bradshaw, C. J. A., Delean, S., Cassey, P., Lacy, R. C., Wells, K., Aiello-Lammens, M. E., Akçakaya, H. R., & Brook, B. W. (2016). An efficient protocol for the

global sensitivity analysis of stochastic ecological models. *Ecosphere*, *7*(3), e01238. https://doi.org/10.1002/ecs2.1238

Raghavan, M., Steinrücken, M., Harris, K., Schiffels, S., Rasmussen, S., DeGiorgio, M., Albrechtsen, A., Valdiosera, C., Ávila-Arcos, M. C., Malaspinas, A.-S., Eriksson, A., Moltke, I., Metspalu, M., Homburger, J. R., Wall, J., Cornejo, O. E., Moreno-Mayar, J. V., Korneliussen, T. S., Pierre, T., . . . Willerslev, E. (2015). Genomic evidence for the Pleistocene and recent population history of Native Americans. *Science*, *349*(6250), aab3884. https://doi.org/10.1126/science.aab3884

Rambaut, A., Drummond, A. J., Xie, D., Baele, G., & Suchard, M. A. (2018). Posterior Summarization in Bayesian Phylogenetics Using Tracer 1.7. *Syst Biol*, *67*(5), 901-904. https://doi.org/10.1093/sysbio/syy032

Reimer, P. J., Austin, W. E. N., Bard, E., Bayliss, A., Blackwell, P. G., Bronk Ramsey, C., Butzin, M., Cheng, H., Edwards, R. L., Friedrich, M., Grootes, P. M., Guilderson, T. P., Hajdas, I., Heaton, T. J., Hogg, A. G., Hughen, K. A., Kromer, B., Manning, S. W., Muscheler, R., . . . Talamo, S. (2020). The IntCal20 Northern Hemisphere Radiocarbon Age Calibration Curve (0–55 cal kBP). *Radiocarbon*, *62*(4), 725-757. https://doi.org/10.1017/rdc.2020.41

Reimer, P. J., Bard, E., Bayliss, A., Beck, J. W., Blackwell, P. G., Ramsey, C. B., Buck, C. E., Cheng, H., Edwards, R. L., Friedrich, M., Grootes, P. M., Guilderson, T. P., Haflidason, H., Hajdas, I., Hatté, C., Heaton, T. J., Hoffmann, D. L., Hogg, A. G., Hughen, K. A., . . . van der Plicht, J. (2016). IntCal13 and Marine13 Radiocarbon Age Calibration Curves 0–50,000 Years cal BP. *Radiocarbon*, *55*(4), 1869-1887. https://doi.org/10.2458/azu_js_rc.55.16947

Reynolds, P. E. (1998). Dynamics and Range Expansion of a Reestablished Muskox Population. *J Wildl Manage*, *62*(2), 734-744. https://doi.org/10.2307/3802350

Ricker, W. E. (1954). Stock and recruitment. *J Fish Res Board Can*, *11*(5), 559-623.

Rosenzweig, M. L. (1968). Net Primary Productivity of Terrestrial Communities: Prediction from Climatological Data. *Am Nat*, *102*(923), 67-74. https://doi.org/10.1086/282523

Signor, P. W., & Lipps, J. H. (1982). Sampling bias, gradual extinction patterns and catastrophes in the fossil record. In *Geological Implications of Impacts of Large Asteroids and Comets on the Earth* (Vol. 190, pp. 291-296): Geological Society of America. https://doi.org/10.1130/SPE190-p291

Strobl, C., Boulesteix, A. L., Zeileis, A., & Hothorn, T. (2007). Bias in random forest variable importance measures: illustrations, sources and a solution. *BMC Bioinform*, *8*(1), 25. https://doi.org/10.1186/1471-2105-8-25

Suchard, M. A., Lemey, P., Baele, G., Ayres, D. L., Drummond, A. J., & Rambaut, A. (2018). Bayesian phylogenetic and phylodynamic data integration using BEAST 1.10. *Virus Evol*, *4*(1), vey016. https://doi.org/10.1093/ve/vey016

Tallavaara, M., Eronen, J. T., & Luoto, M. (2018). Productivity, biodiversity, and pathogens influence the global hunter-gatherer population density. *Proc Natl Acad Sci U S A*, *115*(6), 1232-1237. https://doi.org/10.1073/pnas.1715638115

Thioulouse, J., Dray, S., Dufour, A.-B., Siberchicot, A., Jombart, T., & Pavoine, S. (2018). *Multivariate Analysis of Ecological Data with ade4* (1st ed.). New York, NY: Springer.

Timmermann, A., & Friedrich, T. (2016). Late Pleistocene climate drivers of early human migration. *Nature*, *538*(7623), 92-95. https://doi.org/10.1038/nature19365

van Andel, T. H. (2002). The Climate and Landscape of the Middle Part of the Weichselian Glaciation in Europe: The Stage 3 Project. *Quat Res*, *57*(1), 2-8. https://doi.org/10.1006/qres.2001.2294

VanDerWal, J., Shoo, L. P., Johnson, C. N., & Williams, S. E. (2009). Abundance and the environmental niche: environmental suitability estimated from niche models predicts the upper limit of local abundance. *Am Nat*, *174*(2), 282-291. https://doi.org/10.1086/600087

Williams, J. W., Grimm, E. C., Blois, J. L., Charles, D. F., Davis, E. B., Goring, S. J., Graham, R. W., Smith, A. J., Anderson, M., Arroyo-Cabrales, J., Ashworth, A. C., Betancourt, J. L., Bills, B. W., Booth, R. K., Buckland, P. I., Curry, B. B., Giesecke, T., Jackson, S. T., Latorre, C., . . . Takahara, H. (2018). The Neotoma Paleoecology Database, a multiproxy, international, community-curated data resource. *Quat Res*, *89*(1), 156-177. https://doi.org/10.1017/qua.2017.105

Wright, M. N., & Ziegler, A. (2017). ranger: A fast implementation of random forests for high dimensional data in C++ and R. *J Stat Softw*, *77*(1), 1-17. https://doi.org/10.18637/jss.v077.i01

Yannic, G., Hagen, O., Leugger, F., Karger, D. N., & Pellissier, L. (2020). Harnessing paleo-environmental modeling and genetic data to predict intraspecific genetic structure. *Evol Appl*, *13*(6), 1526-1542. https://doi.org/10.1111/eva.12986

Yannic, G., Pellissier, L., Ortego, J., Lecomte, N., Couturier, S., Cuyler, C., Dussault, C., Hundertmark, K. J., Irvine, R. J., Jenkins, D. A., Kolpashikov, L., Mager, K., Musiani, M., Parker, K. L., Roed, K. H., Sipko, T., Porisson, S. G., Weckworth, B. V., Guisan, A., . . . Cote, S. D. (2014). Genetic diversity in caribou linked to past and future climate change. *Nat Clim Chang*, *4*(2), 132-137. https://doi.org/10.1038/Nclimate2074

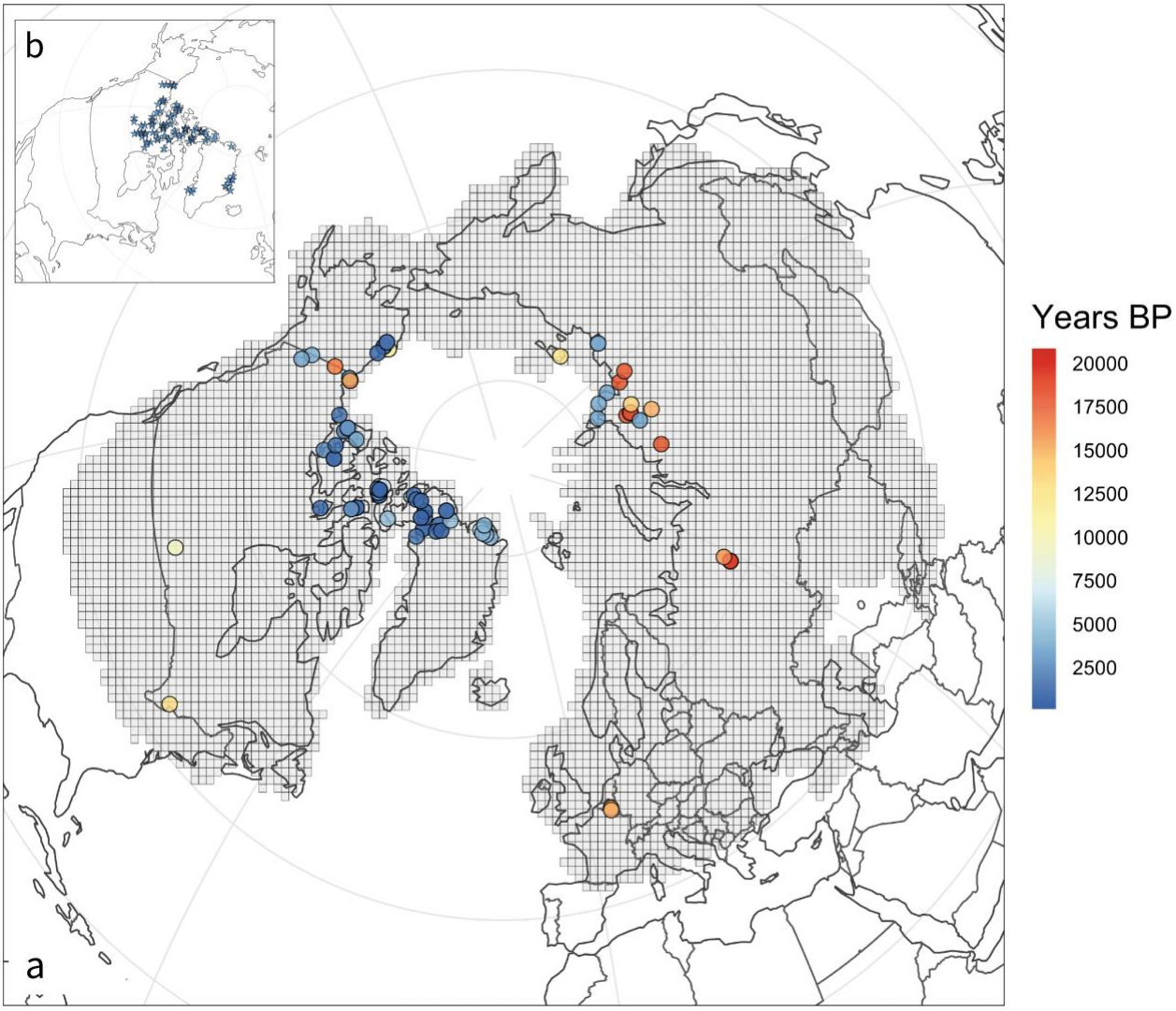

Figure S1. Distribution of fossil records and modern occurrences of muskox over the study region.

a) The distribution of fossil records over the study region, with red circles representing older fossils and blue circles representing more recent records. b) The distribution of modern occurrences obtained from GBIF (GBIF.org, 2019), representing sightings of individuals occurring only in areas where the muskox is endemic, except for a translocated population in Kangerlussuaq (West Greenland).

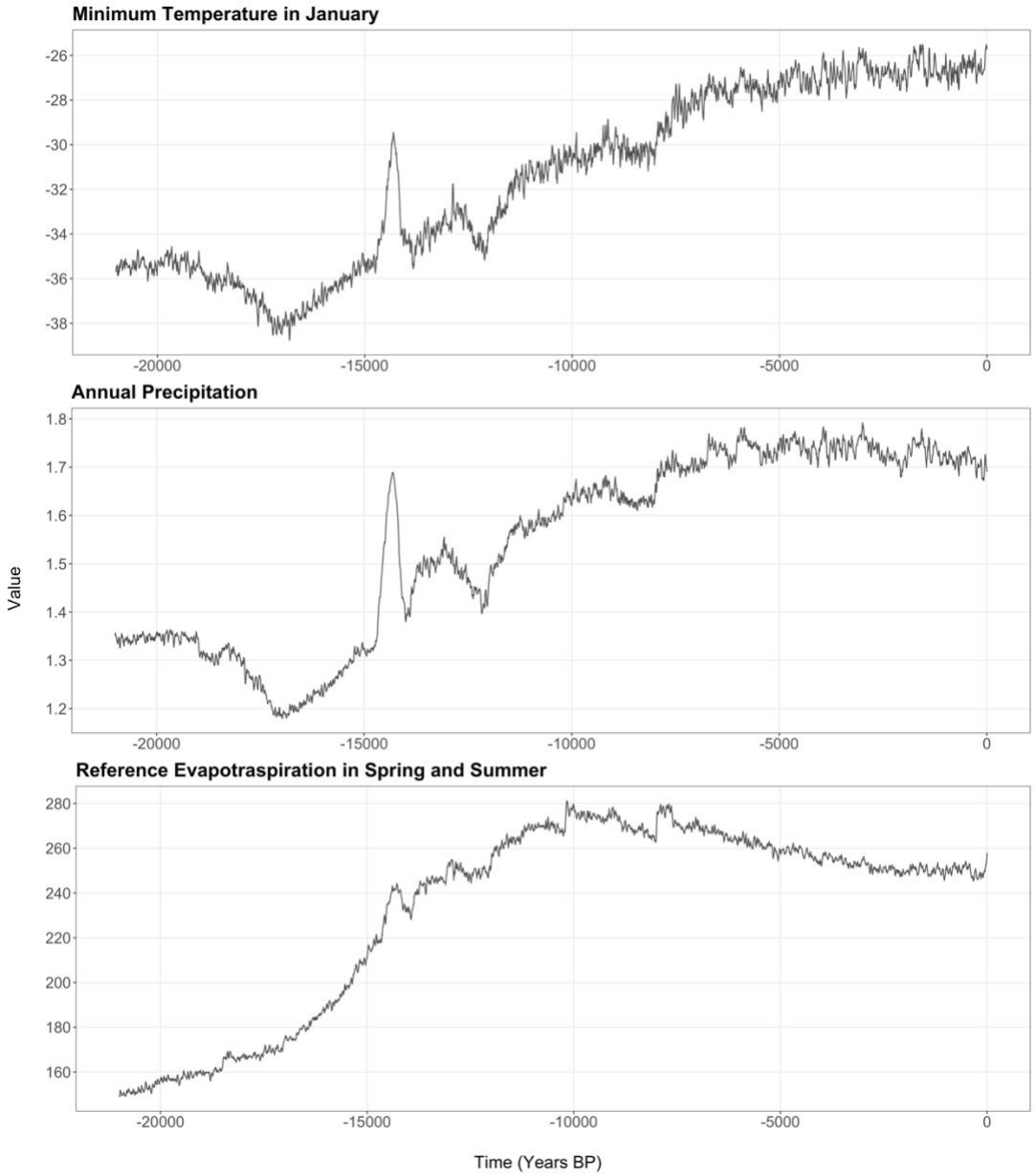

Figure S2. Climate trends for selected variables over the study region.

The plots show climatic trends for the three variables used to build the climatic niche of the muskox. Paleoclimate variables were generated using PaleoView with an interval step of 8 years and an interval size of 30 years, for the period 21,000 BP to 0 BP. These variables were selected because they indirectly affect the breeding success and survival of arctic herbivores. The deglaciation period, through to the Holocene, shows multiple abrupt climate oscillations, across all variables.

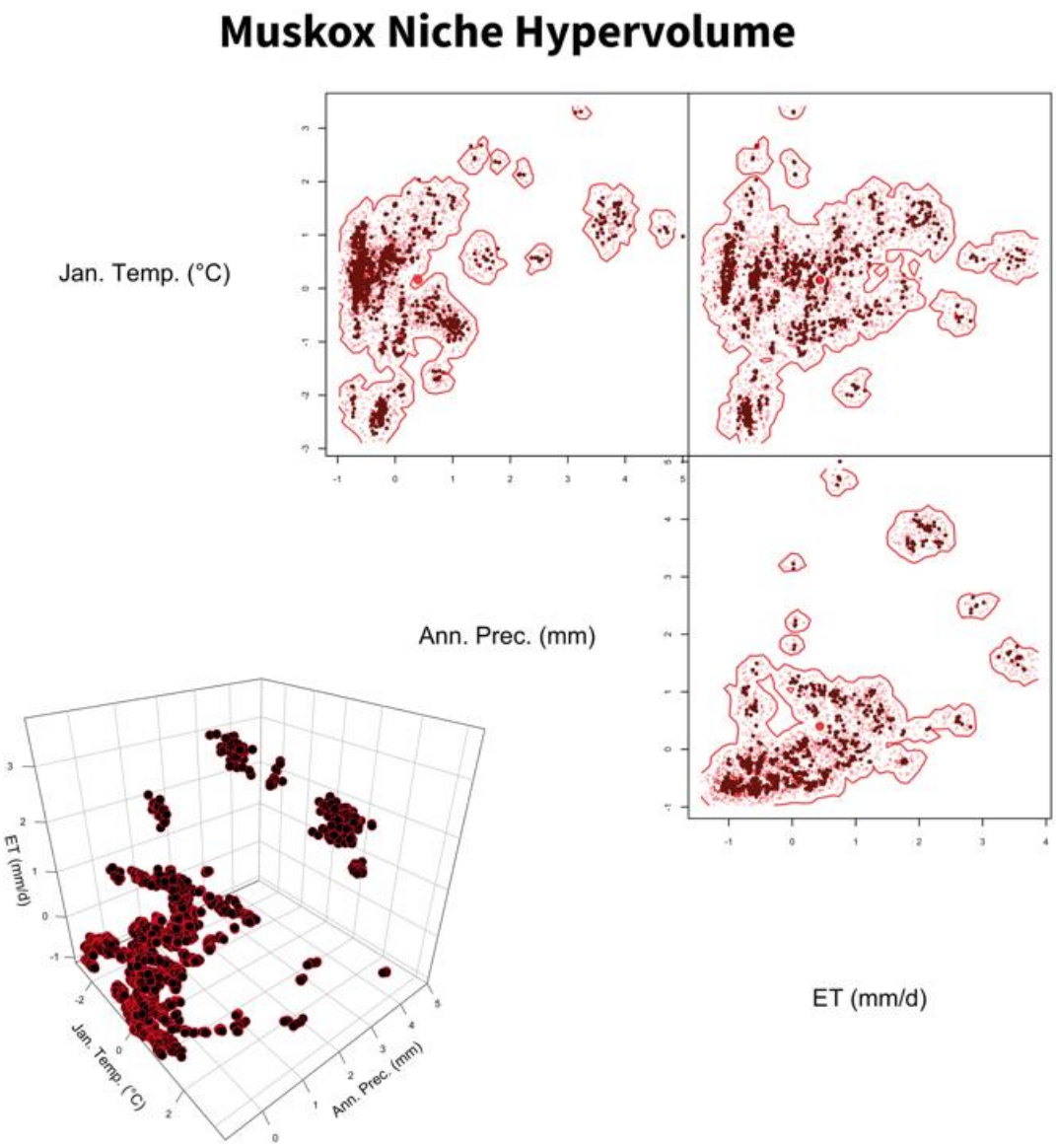

Figure S3. Muskox Niche Hypervolume.

Here is represented the multi-temporal niche hypervolume of the muskox in 2-dimensions and 3-dimensions. The hypervolume was built based on 3 climate variables: average minimum daily temperature in January, annual precipitation and reference evapotranspiration in spring and summer. These variables were chosen because they indirectly affect the survival of the species and because they were the least correlated variables. The hypervolume gives a representation of the climatic space where the species can persist and thrive.

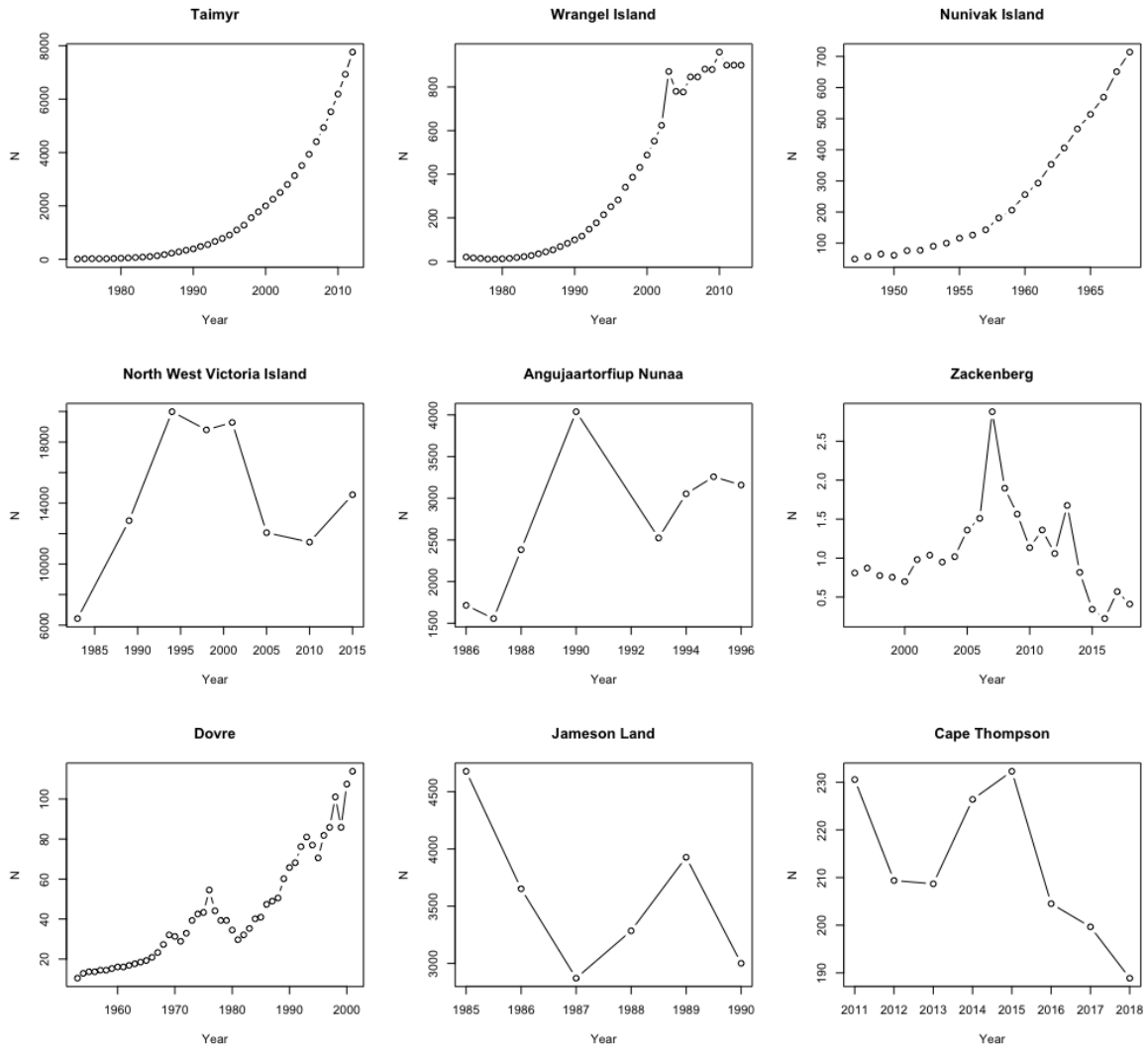

Figure S4. Time-series data of muskox populations.

The plots show the time-series data on population abundance used to calculate finite rates of population increase and their variance, and maximum population growth rate. The time-series data come for populations from Russia (Taimyr, Wrangel Island), Alaska (Nunivak Island, Cape Thompson), Canada (North West Victoria Island), Greenland (Angujaartorfiup Nunaa, Zackenberg, Jameson land) and Norway (Dovre) (Cuyler et al., 2020). We repeatedly fitted linear models to 3,4,5,6 and 7 data points of the time-series. We then selected, for each time series, the estimate of maximum growth rate resulting from the model with the highest r^2. This gave the range of annual maximum growth rate for muskox, which we scaled to generation length by taking the exponent. We used the Zackenberg time-series data for the interval 1998 – 2006, that is stable, to calculate the standard deviation (SD) in population growth rate (Cuyler et al., 2020).

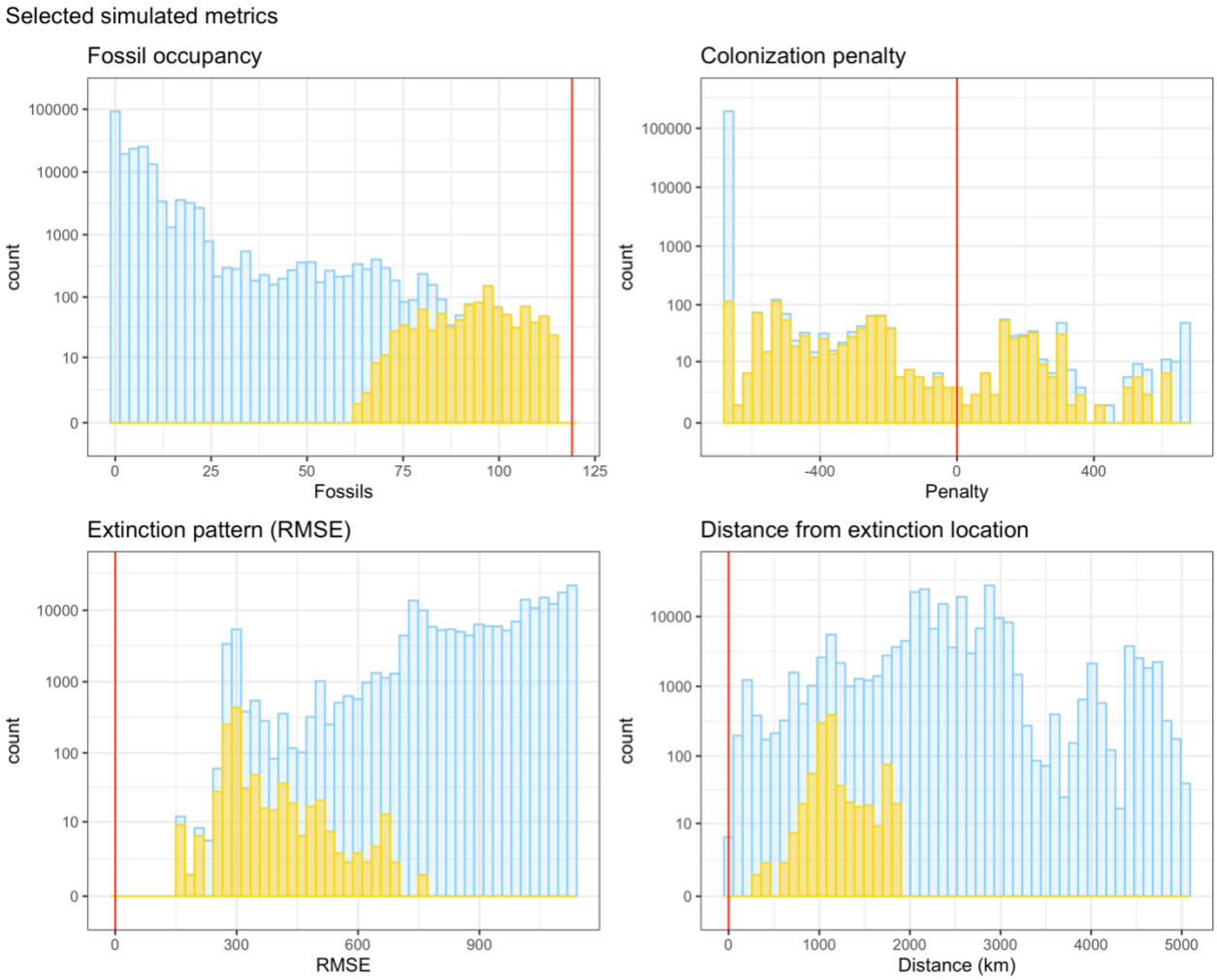

Figure S5. Model validation.

The histograms show the differences between simulated summary metrics and observed targets for fossil occupancy, penalty in time of colonization of Greenland, root mean square error (RMSE) of the difference in time of extirpation across three regions in Eurasia, and distance from extinction location. The blue bars represent the summary metrics from all the 100,000 simulations, while the yellow bars represent the metrics for the best 1% models, selected through pattern-oriented modelling and Approximate Bayesian Computation analysis. The red vertical lines represent the observed target value. The y-axes are on the log-scale. Targets are described in detail in Table S2.

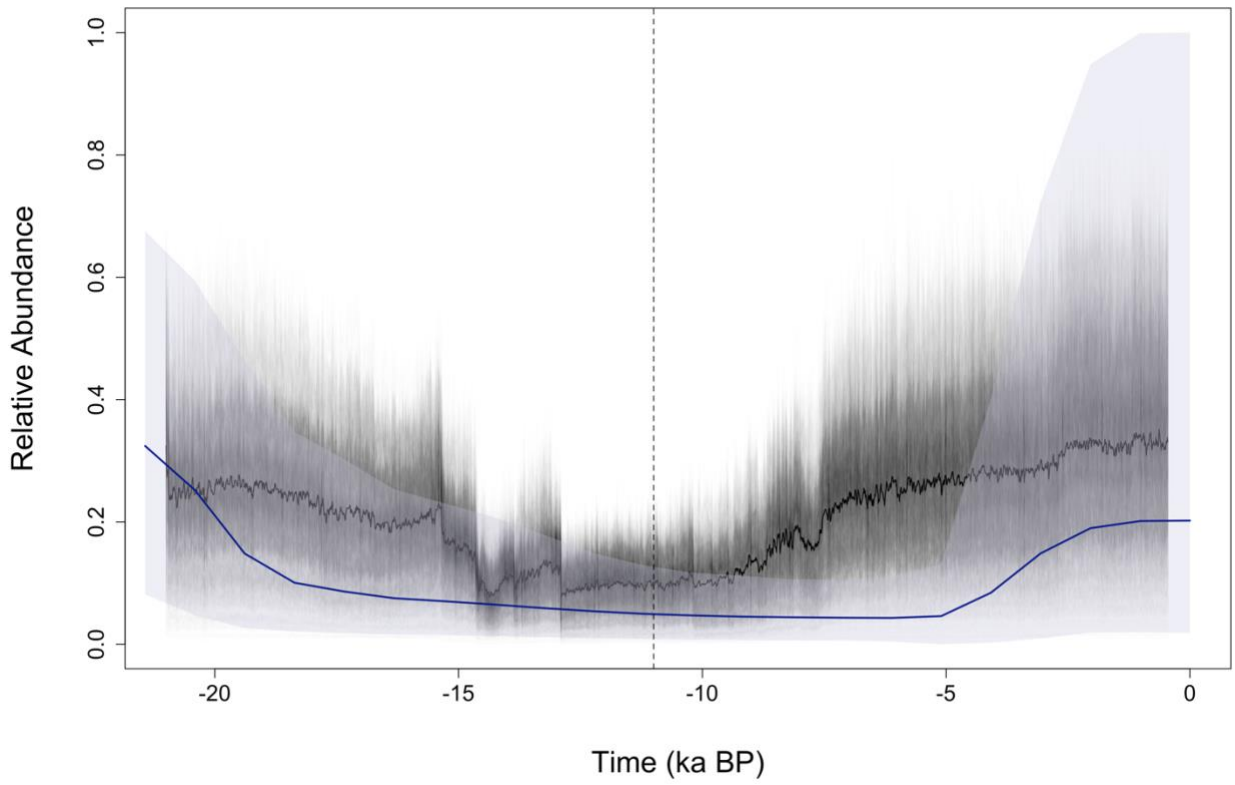

Figure S6. Effective population size (N_e) and simulated total population sizes.

Black lines show the total population size for each of the selected models, with the thick black line showing the total population size from the multi-model average. The blue banding represents the 95% CI around the mean (blue line) in effective population size (N_e). All values on the y-axis have been scaled between 0 and 1. The dashed vertical line represents the separation between the deglaciation period (19 ka BP – 11 ka BP) and the Holocene period (11 ka BP – 0 BP).

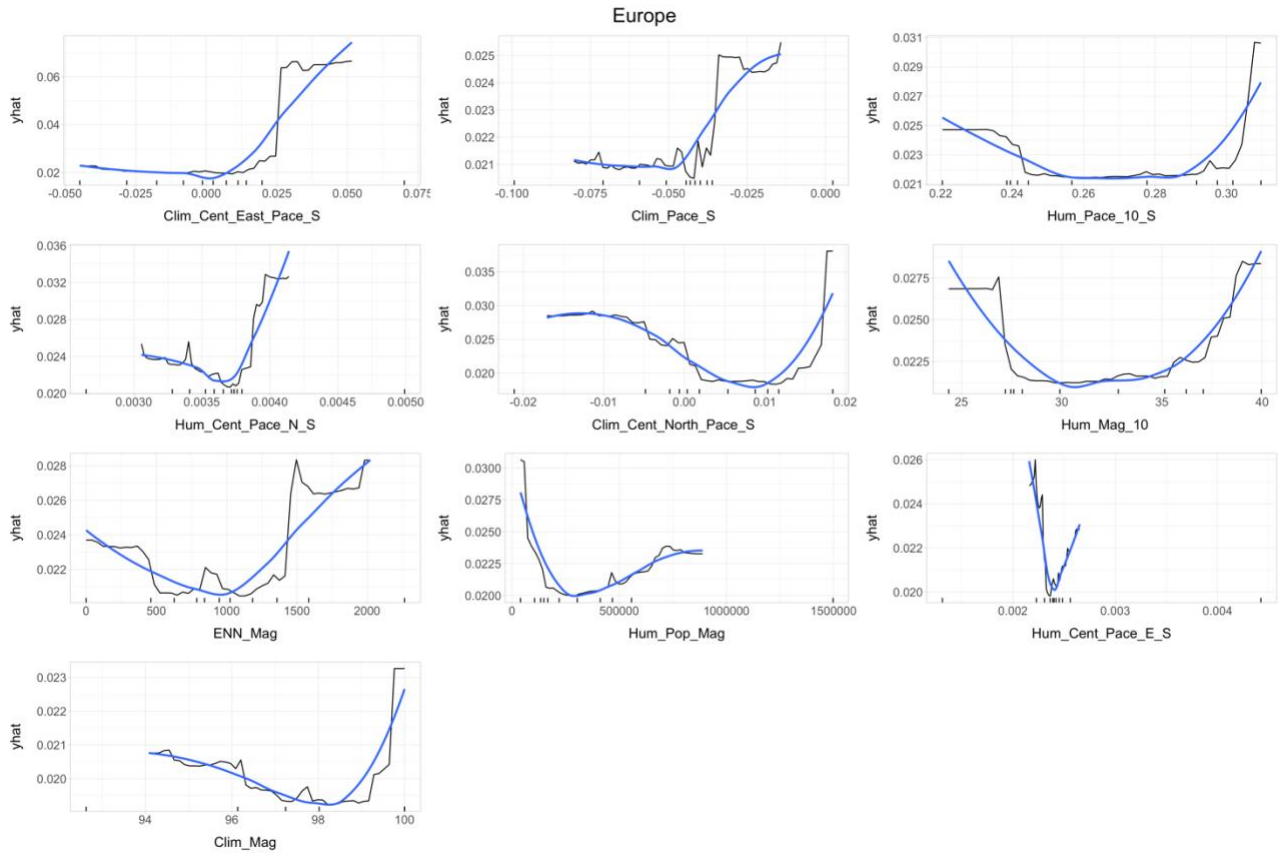

Figure S7. Accumulated Local Effects plots of the predictor variable for expected minimum abundance in Europe during the deglaciation period (19 ka – 11 ka BP).

Tick marks inside the x-axis represent deciles of the distribution of the x-variable. Relationships between the axes below the 10th and above the 90th deciles should be interpreted carefully. The blue lines show a LOESS curve fitted to the data. The variables are described in Appendix 3. For the latitudinal movement (*Clim_Cent_North_Pace_S*), negative values indicate a southern movement. Similarly, for the longitudinal movement (*Clim_Cent_East_Pace_S*), negative values indicate a western movement of the centroid of climate suitability. The same is valid for the centroid movement in human expansion (*Hum_Cent_Pace_N_S*, *Hum_Cent_Pace_E_S*). Other variables include the pace of change in climate suitability (*Clim_Pace_S*), with positive values indicating a rapid increase in suitable areas, magnitude of contraction in climate suitability (*Clim_Mag*), magnitude of fragmentation (*ENN_Mag*), magnitude and pace of human expansion (*Hum_Mag_10*, *Hum_Pace_10_S*, respectively), and magnitude of human population change (*Hum_Pop_Mag*).

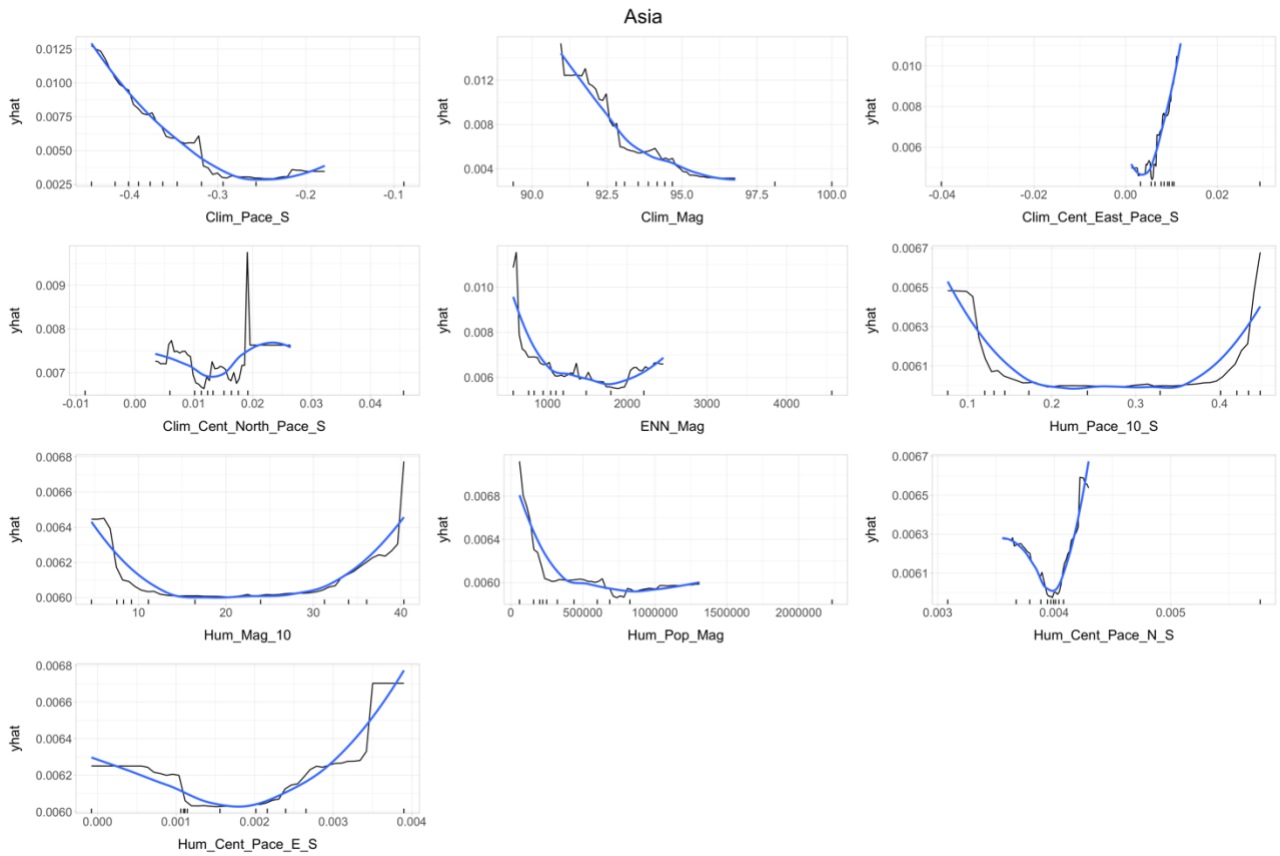

Figure S8. Accumulated Local Effects plots of the predictor variable for expected minimum abundance in Asia during the deglaciation period (19 ka – 11 ka BP).

Tick marks inside the x-axis represent deciles of the distribution of the x-variable. Relationships between the axes below the 10th and above the 90th deciles should be interpreted carefully. The blue lines show a LOESS curve fitted to the data. The variables are described in Appendix 3. For the latitudinal movement (*Clim_Cent_North_Pace_S*), negative values indicate a southern movement. Similarly, for the longitudinal movement (*Clim_Cent_East_Pace_S*), negative values indicate a western movement of the centroid of climate suitability. The same is valid for the centroid movement in human expansion (*Hum_Cent_Pace_N_S*, *Hum_Cent_Pace_E_S*). Other variables include the pace of change in climate suitability (*Clim_Pace_S*), with positive values indicating a rapid increase in suitable areas, magnitude of contraction in climate suitability (*Clim_Mag*), magnitude of fragmentation (*ENN_Mag*), magnitude and pace of human expansion (*Hum_Mag_10*, *Hum_Pace_10_S*, respectively), and magnitude of human population change (*Hum_Pop_Mag*).

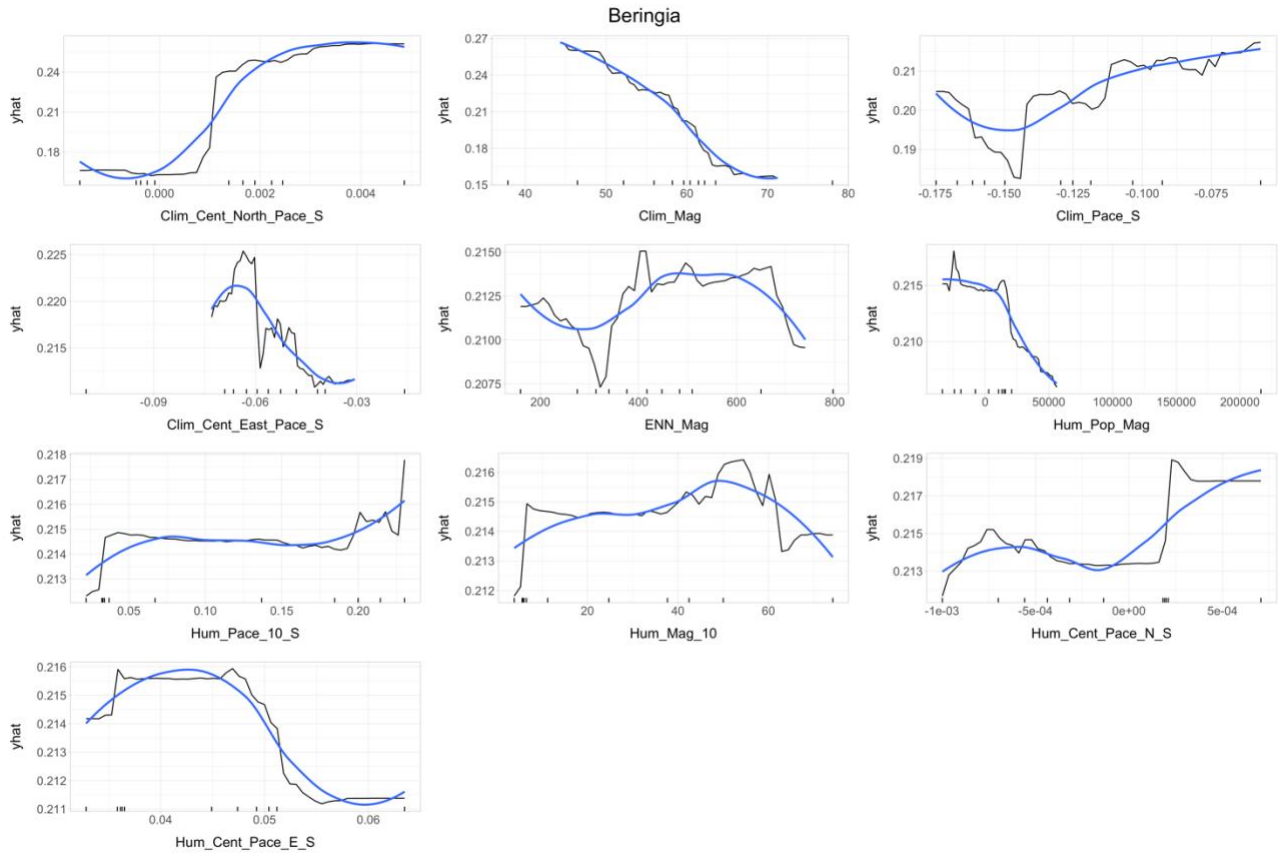

Figure S9. Accumulated Local Effects plots of the predictor variable for expected minimum abundance in Beringia during the deglaciation period (19 ka – 11 ka BP).

Tick marks inside the x-axis represent deciles of the distribution of the x-variable. Relationships between the axes below the 10th and above the 90th deciles should be interpreted carefully. The blue lines show a LOESS curve fitted to the data. The variables are described in Appendix 3. For the latitudinal movement (*Clim_Cent_North_Pace_S*), negative values indicate a southern movement. Similarly, for the longitudinal movement (*Clim_Cent_East_Pace_S*), negative values indicate a western movement of the centroid of climate suitability. The same is valid for the centroid movement in human expansion (*Hum_Cent_Pace_N_S*, *Hum_Cent_Pace_E_S*). Other variables include the pace of change in climate suitability (*Clim_Pace_S*), with positive values indicating a rapid increase in suitable areas, magnitude of contraction in climate suitability (*Clim_Mag*), magnitude of fragmentation (*ENN_Mag*), magnitude and pace of human expansion (*Hum_Mag_10*, *Hum_Pace_10_S*, respectively), and magnitude of human population change (*Hum_Pop_Mag*).

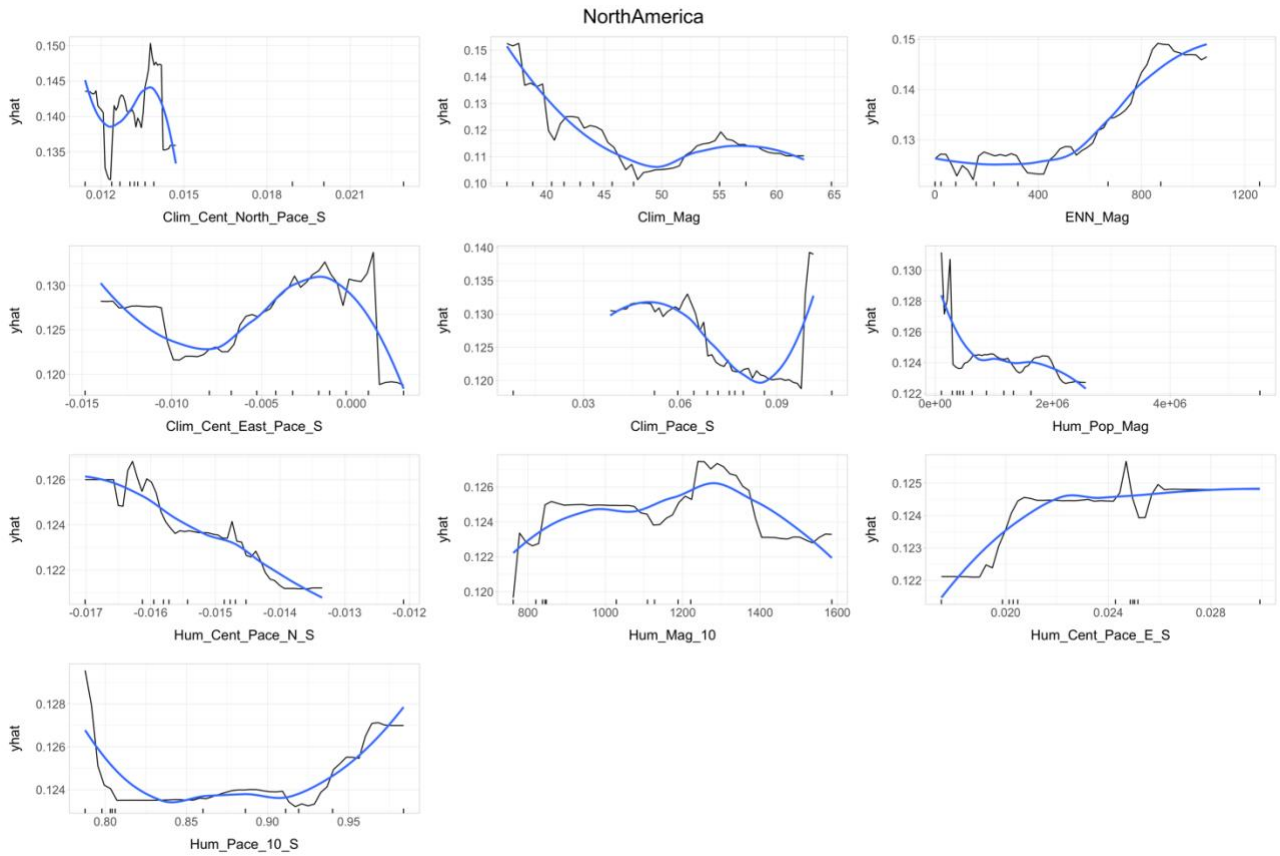

Figure S10. Accumulated Local Effects plots of the predictor variable for expected minimum abundance in North America during the deglaciation period (19 ka – 11 ka BP).

Tick marks inside the x-axis represent deciles of the distribution of the x-variable. Relationships between the axes below the 10th and above the 90th deciles should be interpreted carefully. The blue lines show a LOESS curve fitted to the data. The variables are described in Appendix 3. For the latitudinal movement (*Clim_Cent_North_Pace_S*), negative values indicate a southern movement. Similarly, for the longitudinal movement (*Clim_Cent_East_Pace_S*), negative values indicate a western movement of the centroid of climate suitability. The same is valid for the centroid movement in human expansion (*Hum_Cent_Pace_N_S*, *Hum_Cent_Pace_E_S*). Other variables include the pace of change in climate suitability (*Clim_Pace_S*), with positive values indicating a rapid increase in suitable areas, magnitude of contraction in climate suitability (*Clim_Mag*), magnitude of fragmentation (*ENN_Mag*), magnitude and pace of human expansion (*Hum_Mag_10*, *Hum_Pace_10_S*, respectively), and magnitude of human population change (*Hum_Pop_Mag*).

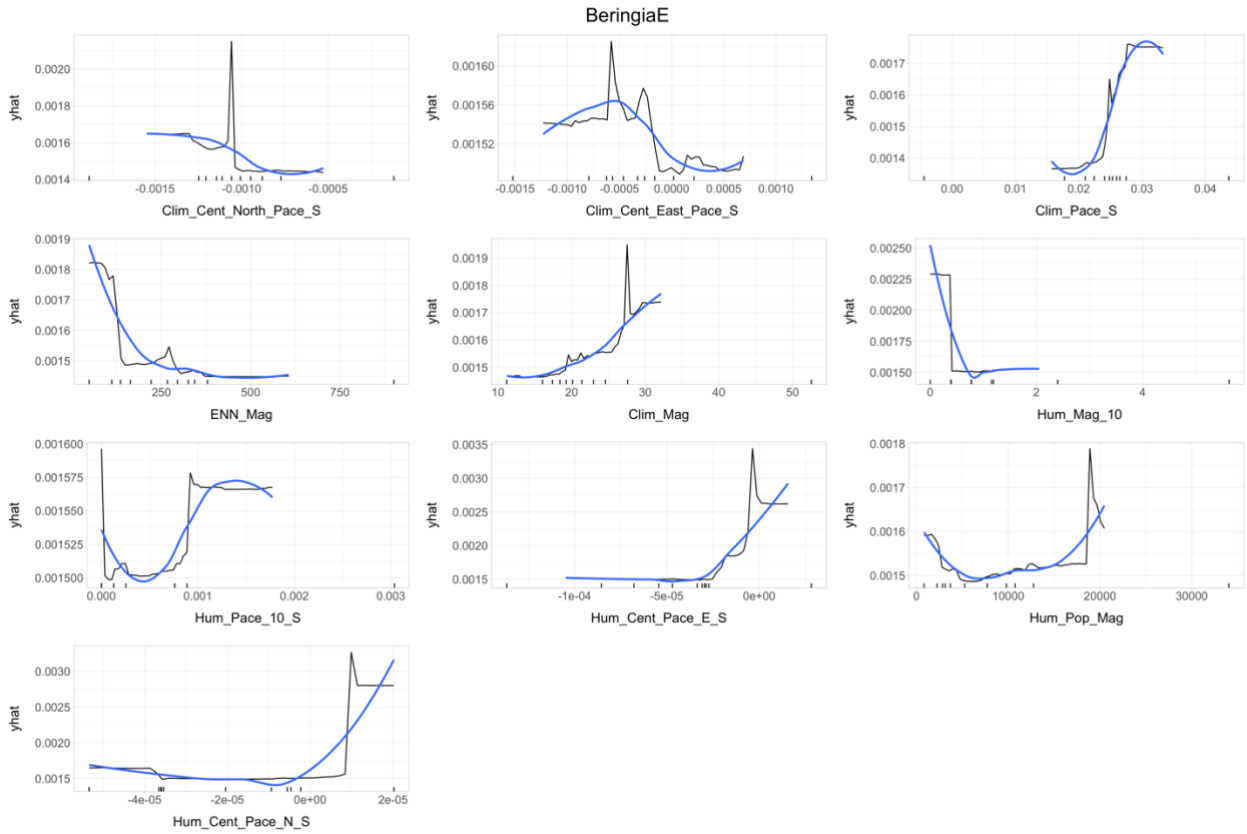

Figure S11. Accumulated Local Effects plots of the predictor variable for final abundance in East Beringia (Alaska, US), during the Holocene period (11 ka BP – 1500 AD).

Tick marks inside the x-axis represent deciles of the distribution of the x-variable. Relationships between the axes below the 10th and above the 90th deciles should be interpreted carefully. The blue lines show a LOESS curve fitted to the data. The variables are described in Appendix 3. For the latitudinal movement (*Clim_Cent_North_Pace_S*), negative values indicate a southern movement. Similarly, for the longitudinal movement (*Clim_Cent_East_Pace_S*), negative values indicate a western movement of the centroid of climate suitability. The same is valid for the centroid movement in human expansion (*Hum_Cent_Pace_N_S*, *Hum_Cent_Pace_E_S*). Other variables include the pace of change in climate suitability (*Clim_Pace_S*), with positive values indicating a rapid increase in suitable areas, magnitude of contraction in climate suitability (*Clim_Mag*), magnitude of fragmentation (*ENN_Mag*), magnitude and pace of human expansion (*Hum_Mag_10*, *Hum_Pace_10_S*, respectively), and magnitude of human population change (*Hum_Pop_Mag*).

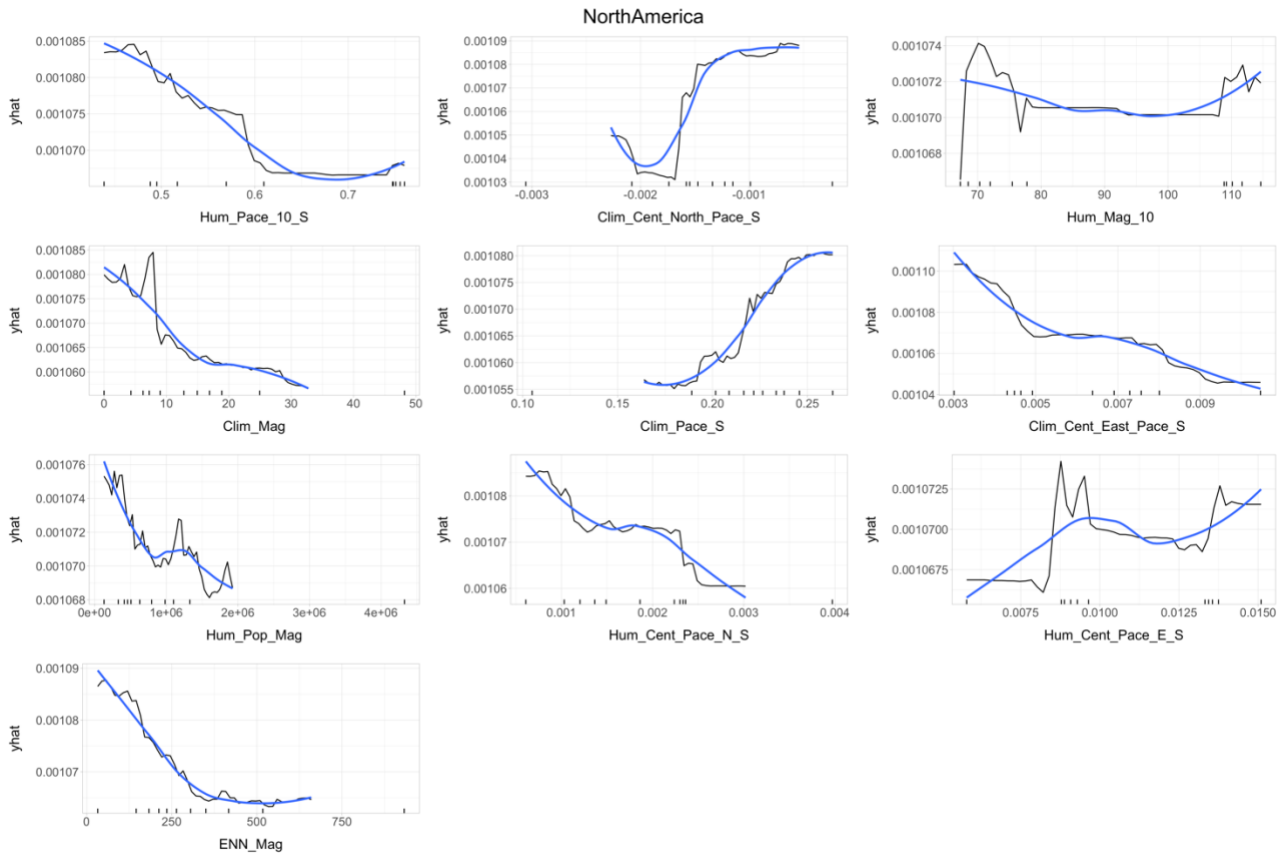

Figure S12. Accumulated Local Effects plots of the predictor variable for final abundance in North America, during the Holocene period (11 ka BP – 1500 AD).

Tick marks inside the x-axis represent deciles of the distribution of the x-variable. Relationships between the axes below the 10th and above the 90th deciles should be interpreted carefully. The blue lines show a LOESS curve fitted to the data. The variables are described in Appendix 3. For the latitudinal movement (*Clim_Cent_North_Pace_S*), negative values indicate a southern movement. Similarly, for the longitudinal movement (*Clim_Cent_East_Pace_S*), negative values indicate a western movement of the centroid of climate suitability. The same is valid for the centroid movement in human expansion (*Hum_Cent_Pace_N_S*, *Hum_Cent_Pace_E_S*). Other variables include the pace of change in climate suitability (*Clim_Pace_S*), with positive values indicating a rapid increase in suitable areas, magnitude of contraction in climate suitability (*Clim_Mag*), magnitude of fragmentation (*ENN_Mag*), magnitude and pace of human expansion (*Hum_Mag_10*, *Hum_Pace_10_S*, respectively), and magnitude of human population change (*Hum_Pop_Mag*).

Movie S1. Spatiotemporal abundances of muskox since the Last Glacial Maximum.

https://universityofadelaide.box.com/s/x6gxrwup3u0we7ou1le84e82ld1e7065

Left panel shows simulated relative abundance of muskox (ensemble mean of the 'best' models) across space and time, since 21 ka BP. Blue diamonds represent fossil locations at fossil age ± 1SD. Right panel shows trend in total simulated abundance across the study region through time.

Movie S2. Relative harvest of muskox populations over the last 21,000 years.

https://universityofadelaide.box.com/s/wqkwu23y00v90hxh3g1zyewpzjykf0vb

Total number of harvested individuals in each grid cell at each time step, scaled between 0 and 1. Bars in inset panel show total relative number of harvested individuals in each sub-region at each time step.

Table S1. Fixed and variable parameters for the spatially explicit population models.

Parameters used in the demographic and harvest components of the models, with information on whether variables had fixed or variable ranges (Type) and their initial (or prior) values (Value/range). References for demographic and harvest parameter values are provided below the table.

Parameter	Description	Type	Value/range	Posterior range
Demographic parameters				
Time steps	Simulation years	fixed	2570 (21 ka BP – 1500 AD)	NA
Generation length	Years per time step (Hansen et al., 2018; Pacifici et al., 2013)	fixed	8	NA
Lattice	Number of grid cells	fixed	6160	NA
Transition rate	Population stages	fixed	1 (adults only)	NA
Growth rate	Maximum growth rate per time step (Cuyler et al., 2020)	variable	0.43 – 2.18	0.59 – 2.11
Environmental stochasticity	Environmental stochasticity per time step (Cuyler et al., 2020)	variable	0.00 – 0.30	0.01 – 0.28
Upper Abundance	Maximum density per grid cell (Cuyler et al., 2020)	variable	100 – 7000	1432 – 6864

Dispersal rate	Maximum dispersal distance per time step (Kafle et al., 2020; Reynolds, 1998)	variable	0 – 500	167 – 477
Proportion of dispersers	Percentage of the population that disperses at each time step (cell-based) (Fordham, Brown, et al., 2021)	variable	0% - 25%	6% - 24%
Dispersal target K	Dispersal rate negatively affected by target population abundance (N)	fixed	10	NA
Allee effect	Region-wide Allee effect (Fordham, Brown, et al., 2021)	variable	0 - 500	1 – 171
Occupancy threshold	Number of populations on the landscape that determines region-wide extinction	fixed	1	NA
Human parameters				
Harvest G	Prey density at which exploitation is half-maximal	fixed	0.4	NA
Harvest Max.	Maximum proportion of the population harvested at each time step (cell-based)	variable	5% - 25%	6% - 24%
Harvest z	Departure from maximal exploitation, determining the type of response of the populations	variable	1 - 2	1.05 – 1.95
Humans SD multiplier	Multiplier to the standard deviation in human abundance	variable	0 - 1	0.05 – 0.95
Humans p-value	p-value at which human density values are chosen from the lognormal distribution	variable	0 – 1	0.04 – 0.94

Table S2. Observed statistics (targets) for pattern-oriented modelling and Approximate Bayesian Computation (ABC) validation.

Targets used in the ABC analysis and validation step include an occupancy pattern, identified by positive abundance at fossil sites at fossil calibrated age ± SD, Root Mean Square Error (RMSE) of the difference between simulated and observed times of extinction in Eurasia across three sub-regions, distance from the extinction location in Eurasia (Taimyr) and arrival time in Greenland. To calculate occupancy pattern, fossil records that overlapped in space and time have been merged to count as one.

Target	Description	Value	97.5% CI: Lower	2.5% CI: Upper
Occupancy pattern	Agreement between simulated and inferred occupancy at fossil sites.	119 [1] (fossils)	NA	NA
Extirpation pattern	Time of extinction in 3 sub-regions of Eurasia based on the fossil record.	12,254 BP [1] (Europe)	12,345 BP [1] (Europe)	12,160 BP [1] (Europe)
		2,738 BP [1] (Asia)	2,856 BP [1] (Asia)	2,569 BP [1] (Asia)
		3,157 BP [1] (Beringia)	3,437 BP [1] (Beringia)	2,633 BP [1] (Beringia)
Extinction location	Centroid coordinates of extinction location in Eurasia (Taimyr).	94.32 (Longitude) 72.94 (Latitude)	NA	NA
Arrival time	Time of arrival in Greenland based on the fossil record.	5,607 BP [1]	5,752 BP [1]	5,4601 BP [1]

[1]All estimates were calculated using the fossil record, which is available in Appendix 1. The estimates for extinction time and time of arrival were calculated using the GRIWM method (Bradshaw et al. 2012).

Chapter IV: Ecological resilience of reindeers to past and future climatic change

Statement of Authorship

Title of Paper	Ecological resilience of reindeers to past and future climatic change
Publication Status	☐ Published ☐ Accepted for Publication ☐ Submitted for Publication ☑ Unpublished and Unsubmitted work written in manuscript style
Publication Details	Title: Ecological resilience of reindeers to past and future climatic change Author(s): Elisabetta Canteri, Stuart C. Brown, Niels Martin Schmidt, Eric Post, David Nogués-Bravo, Damien A. Fordham Journal: Science Advances

Principal Author

Name of Principal Author (Candidate)	Elisabetta Canteri		
Contribution to the Paper	The candidate conceived the idea, together with their advisors. The candidate collected and processed the data, ran the analyses, produced the results, and led the writing of the manuscript, with contribution from all the co-authors.		
Overall percentage (%)	60%		
Signature		Date	26 April 2022

Co-Author Contributions

By signing the Statement of Authorship, each author certifies that:

vii. the candidate's stated contribution to the publication is accurate (as detailed above);

viii. permission is granted for the candidate in include the publication in the thesis; and

ix. the sum of all co-author contributions is equal to 100% less the candidate's stated contribution.

Name of Co-Author	Stuart C. Brown

Contribution to the Paper	Helped running the analyses and contributed with results interpretation and the writing of the manuscript.		
Signature		Date	28 April 2022

Name of Co-Author	Niels Martin Schmidt		
Contribution to the Paper	Contributed with expert knowledge of the species under study, results interpretation, and with the writing of the manuscript.		
Signature		Date	2022-04-26

Name of Co-Author	Eric Post		
Contribution to the Paper	Contributed with expert knowledge of the species under study, results interpretation, and with the writing of the manuscript.		
Signature		Date	2022-04-26

Name of Co-Author	David Nogués-Bravo		
Contribution to the Paper	Contributed with the conceptualization of the research idea, with supervision, writing of the manuscript and funding acquisition.		
Signature		Date	02/05/2022

Name of Co-Author	Damien A. Fordham		
Contribution to the Paper	Contributed with the conceptualization of the research idea, with supervision, writing of the manuscript and funding acquisition.		
Signature		Date	02/05/2022

Title

Ecological resilience of reindeers to past and future climatic change.

Authors

Elisabetta Canteri[1,2], Stuart C. Brown[1,3], Niels Martin Schmidt[4], Eric Post[5], David Nogues-Bravo[2] and Damien A. Fordham[1,2].

[1] The Environment Institute and School of Biological Sciences, University of Adelaide, Adelaide, Australia

[2] Centre for Macroecology, Evolution and Climate, GLOBE Institute, Faculty of Health and Medical Sciences, University of Copenhagen, Copenhagen, Denmark

[3] Section for Evolutionary Genomics, GLOBE Institute, University of Copenhagen, Copenhagen, Denmark

[4] Department of Ecoscience, Aarhus University, Roskilde, Denmark

[5] Department of Wildlife, Fish, and Conservation Biology, University of California Davis, Davis (CA), USA.

Abstract

Understanding how different rates and magnitudes of past climatic changes and anthropic pressures shaped species range and population dynamics could improve forecasts of species responses to future global change. Using spatially explicit population models and pattern-oriented validation methods, we disentangle the ecological mechanisms and threats that drove 21,000 years of reindeer (*Rangifer tarandus*) range dynamics across its Holarctic distribution, allowing us to predict the effects of future climatic variability with improved confidence. We show that reconciling inferences of past demographic change from fossils and ancient DNA requires an interaction between high dispersal ability and spatiotemporal differences in the effects of human and non-human factors. Macroecological models, built and validated on the past, show that humans and climatic warming have regulated the range and abundance of reindeers for 21,000 years, causing population declines and range contractions that are as large as what is being predicted for the future. Our results highlight the importance of disentangling demographic and biogeographic responses to past abiotic and biotic stressors when assessing species survival under future climate change.

Introduction

The reindeer (*Rangifer tarandus*), also known as caribou, is the most abundant large terrestrial herbivore in the Arctic (*1*). However, its populations have experienced a 40% decline over the last 30 years, due to human-driven habitat change and fragmentation (*2*). While climatic change is expected to negatively interact with these current threats, and further amplify population declines (*3*), the direct threat that Arctic warming poses to reindeer persistence remains unclear (*4*). This is partly because reindeers survived severe and abrupt warming events in the past (*5*) that caused other Arctic megafaunal species to go extinct (*6*).

Drivers of late Pleistocene and early Holocene megafaunal extinctions remain uncertain, with an ongoing debate on the relative roles of climate change and human hunting (*7-10*). In the Arctic, overkill by Palaeolithic hunters is thought to have hastened the extinction of many species during the last deglaciation, whose populations were already depleted by extreme and rapid climatic shifts (*7, 11*). It has been suggested that the survival of some (but not all) megafaunal species, could reflect ecological lifestyles and/or biological traits that made them more resilient to past climatic changes (*12*). These include attributes such as larger

climatic tolerances (*13*), higher rates of population increase (*12*), and better dispersal capabilities (*14*). In addition to these ecological mechanisms, evolutionary responses could have also aided persistence during periods of adverse climatic change (*15, 16*). Nevertheless, ecological and evolutionary resilience to past climate and environmental changes in the Arctic is likely to reflect not only intrinsic factors (e.g., the biology of the species), but also extrinsic factors (e.g., the rate and magnitude of the stressors) and their interaction in space and time (*17*).

Climatic conditions in the Arctic have rarely been stable, with temperatures fluctuating enormously during glacial-interglacial cycles (*5*), leading to evolutionary adaptations in Arctic mammals that include the reorganization of the cardiovascular system (*15, 16, 18*) and the development of mechanisms for temperature regulation (*16*). These allowed for important adjustments to new environmental conditions. Large magnitude fluctuations in climatic conditions, operating over centuries, as well as millennia, caused Arctic mammals to shift, contract, and expand their ranges (*19-21*). For species with limited dispersal capabilities or slow reproductive rates, abrupt climatic changes in the past caused regional and range-wide extirpations (*12, 22*). Given the large magnitude and pace of the current warming of the Arctic, with temperatures forecast to increase by up to 12 ˚C above 2010 conditions by the end of the 21st century (*23*), it is more likely that survival will be determined by these sorts of ecological responses to centennial climatic changes, rather than evolutionary responses.

Phenological shifts (a mode of plasticity) have already been documented in the Arctic, across many taxa (*24-27*). Today, Arctic warming is causing tundra vegetation growth to begin earlier in the year (*28*), moving forward the breeding and parturition season for Arctic mammals (*29-31*). This ecological response to warming has caused shifts in foraging, predator-prey dynamics (*26, 32*), and changes in the timing of species migrations (*29*). Movement to track shifting habitats has been the most common ecological response of Arctic mammals to warming (*20, 33*), and it will be paramount for the future survival of Arctic mammals and many other species (*34*).

Reindeers persisted through periods of the Pleistocene when the Arctic warmed by as much as 10 °C in a matter of decades (*35*). They did this by contracting their distribution to climatic refugia (*19, 36, 37*), from which they expanded their range and increased their abundance in response to more favourable rates of climate warming during the Holocene (*37, 38*). It is likely that reindeers were able to persist through these abrupt warming events in the

past, because of a wide climatic tolerance, relatively fast growth rates, and a high dispersal capacity (*19*) — traits possibly associated with ecological resilience (*39*). However, exactly how these ecological preferences and biological traits interacted spatiotemporally with extrinsic factors to enable reindeer to survive periods of extreme climate disruption has not been resolved. Addressing this knowledge gap is important, not only for understanding the ecology and biogeography of reindeer in the Arctic, but also for predicting its resilience to future environmental change.

Process-explicit models integrated with evidence of demographic change from paleo-archives, museum collections, and genomics can now be used to empirically reconstruct past biological events, so as to identify processes that regulate biodiversity dynamics (*40*). While these approaches have been used to reveal how ecological lifestyles and biological traits interact dynamically with human- and non-human factors to cause population declines and extinctions (*11*), they have not been used to establish ecological characteristics associated with resilience to climate and environmental change. Likewise, they have never been used to project future extinction risk, despite potentially providing a more complete understanding of the ecological processes that regulate species responses to climate and environmental change.

Here we use process-explicit macroecological models to reconstruct 21,000 years of range dynamics of reindeer, a cold-adapted Arctic herbivore that regulates the structure and function of the tundra ecosystem (*41, 42*), and that also provides important socio-economic value for many circumpolar indigenous cultures (*3*). To establish the ecological processes that enabled reindeer to survive periods of gradual and extreme climate warming, whilst also being exploited for food, bones, and skins (*43*), we built thousands of plausible spatially explicit population models (SEPMs) that explicitly simulated demographic processes responding to different levels of climate-driven resource availability and human exploitation. Models that could reconcile inferences of demographic change from fossils and aDNA were used to determine the chains of causality responsible for the contemporary distribution of reindeer, and to disentangle the ecological processes and drivers responsible for its range contraction in Eurasia and expansion in North America. They were also used to inform projections of future extinction risk.

We reveal that humans and climatic warming have regulated the range and abundance of reindeers for 21,000 years, causing population declines and range contractions that are as large as what is being predicted for the future. Our results also show that reindeer resilience to

past climatic change and exploitation is likely to have been aided by an interaction between high dispersal ability and important spatiotemporal differences in threatening processes.

Results

Process-explicit macroecological models successfully simulated vital aspects of the range and population dynamics of reindeers as inferred from fossils and aDNA. The 'best models', top 0.5% of all models, selected and validated using pattern-oriented modelling (POM) methods (*44*), implemented using Approximate Bayesian Computation (ABC) (*45*), closely reconciled inferences of spatiotemporal occurrence, arrival time in Greenland, regional extirpation, and trend in population size (Figure 1A). They also correctly projected eDNA evidence of spatiotemporal occurrence with 93% agreement in site-based occurrence.

Accurately reconstructing inferences of past demographic changes from fossils and aDNA required a highly constrained set of demographic parameters, human hunting pressures and climatic requirements. A high dispersal capacity (a high proportion of dispersing individuals and long dispersal distances), small Allee effect, high density, and wide ecological niche (large volume and low specialisation) were all needed to simulate past shifts in the range and abundance of reindeers (Figure 1B). A medium to high rate of exploitation by humans was also needed to reconstruct inferences of past demographic changes.

The 'best models' (models that most closely matched the POM validation targets) reconstructed a large range contraction across the Holarctic, in response to abrupt climatic warming in the Late Pleistocene (Figure 2A). In Europe, reindeers went extinct in our simulations in the Iberian Peninsula at 14.43 ± 2.98 ka BP, in South Central Europe at 13.83 ± 2.75 ka BP, except for some isolated populations in the Austrian and Swiss Alps which persisted until 7 ka BP, where patches of tundra and conifer forest are likely to have persisted for longer (*46, 47*). They went extinct in the British Isles at 10.04 ± 2.26 ka BP, and in North Central Europe at 4.34 ± 4.3 ka BP (Figure 2A), which coincide with the advancement of temperate deciduous forests in the two sub-regions (*46, 47*). In North America, populations were simulated to persist during the Last Glacial Maximum south of the Laurentide ice sheet (Movie S1). Following the melting of the glacial ice, the range moved in a north-easterly direction (Movie S1), causing a northward contraction of the southern boundary between 15 – 7 ka BP (Figure 2A). We show that reindeer populations in Alaska and south of the glacial ice remained unconnected until 11 ka BP, when a first contact was made in central Canada (Movie

S1). They remained partly unconnected for another 3,000 years until they reached full connectivity ~8 ka BP (Movie S1). These observations are supported by phylogenetic analyses and genetic models (*48*, *49*).

The simulated distribution of the reindeer at 1500 C.E. (the end of the simulation; Figure 2B) aligns closely with the current endemic distribution of the species (Figure 2C), with persistence today being in areas of higher simulated densities. These areas also coincide with regions where present-day reindeer populations have high levels of genetic diversity (*38*), in the core of their geographic range.

Climate-human-reindeer interactions

Reindeer abundance declined substantially during the last deglaciation (19 – 11 ka BP) and increased during the Holocene (Figure 3). The steepest declines and increases in population abundance occurred during abrupt warming and cooling events, respectively. However, the magnitude and timing of these declines differed regionally (Figure 3A). The largest relative decline in abundance during the last deglaciation was in Asia, with population declines beginning as early as 19 ka BP. In Europe and Beringia population abundance declined by as much as 62% in 60 generations following the 14.7 ka BP warming event. In Europe, this was followed by an increase in population size above pre-14.7 ka BP levels for ~1,000 years (in response to a cooling event at 13.9 ka BP). In North America, declines in reindeer population abundance during the last deglaciation were much more gradual (Figure 3A). In the Holocene, abrupt population increases occurred in Beringia and North America at ~3 ka BP and ~7 ka BP respectively, in response to increased regional habitat suitability (Figure 3A). These sharp increases coincide with the Neoglacial cooling of the Arctic (*50*), which occurred immediately after the Holocene Thermal Maximum (between 4 ka and 9 ka BP, depending on locality) (*51*). The population size of reindeers then stabilised for the remainder of the Holocene (Figure 3).

Generalised additive models (GAM), indicate that large decreases in population abundance in Asia until the Holocene (11.7 ka BP) were the result of climatic warming impacting habitat suitability, with no negative role of humans (Figure 3A, 4). Similarly, in Beringia and North America, reindeer abundances were negatively affected by warming, without a noticeable effect of human density (Figure 4). The positive relationship between human and reindeer density in Asia during the deglaciation reflects a geographic separation in areas of high reindeer and human relative densities (Movie S1 and Movie S2), resulting in human harvesting mostly affecting populations at the southern range limits (Movie S3).

Reindeer numbers increased rapidly in the northernmost parts of Asia during the last deglaciation (Movie S1), while humans experienced their largest increases in population size in the south (Movie S2).

Conversely, humans in combination with climate warming in Europe are likely to have driven regional declines in reindeer population numbers during the last deglaciation (Figure 4). During this period, human densities in Europe were much higher than elsewhere (Figure 3A, Movie S2), and archaeological evidence suggests that regional exploitation rates were high (*52*), with reindeer bones and antlers frequently found at archaeological sites (*53*). The negative role of humans on reindeer abundance in Europe continued into the Holocene, becoming an even more important regulatory pressure than temperature (Figure 4).

Humans are also likely to have had negative effects on reindeer abundance in Asia during the Holocene (Figure 4), when human densities increased and expanded north (Movie S2). Population fluctuations in Beringia and North America during the Holocene are the result of temperature increases, with no negative effect of humans (Figure 4). In North America, the relationship between reindeer and human abundance was positive, due to high human population growth occurring in southern marginal areas of the reindeer range (Movie S2).

Tests of counterfactual hypothesis of reindeer range dynamics confirmed the regulatory roles that climate and humans have had on the demography and range dynamics of reindeers over the last 21,000 years. They show that reindeers could have persisted in climate refugia in Europe for many millennia in the absence of harvesting by humans (Figure 5, Figure S6). They also reveal much longer persistence times in North America and Asia, in the southern parts of the range (Figure 5, Figure S6). Furthermore, these tests show that climate warming was needed for animals to colonise Greenland and some areas of North America, and to correctly reconstruct inferences of colonisation and extinction dynamics from the fossil record (Figure 5).

Extinction risk from future climate change

Reindeers are projected to decrease in abundance over the 21st century (Figure 6), contracting their distributions in Asia and North America (Figure 6C), persisting in core contemporary habitat (Movie S4). Based on models that account for ecological responses to past warming events, we project that the expected minimum abundance (EMA) of reindeers will decline by 15% (± 11%) and its range area will shrink by 13% (± 8%) by 2100 under a business-as-usual

greenhouse gas emission scenario (RCP8.5). However, reductions could be as high as 70% and 57%, for EMA and range area respectively (Figure 6).

Our simulations reveal that these future rates of decline in EMA and range area occurred in the past during periods of rapid climatic warming. Reductions of EMA ≥ 15% over 12 generations (equivalent to the period between 2016 and 2100, upon which future forecasts were calculated) happened at the beginning of the deglacial period, as the Holarctic range of reindeers began to warm, occurring repeatedly during or immediately following the 14.7 ka BP warming event (Figure S9). Likewise, reductions in range area ≥ 13% happened immediately after the 14.7 ka BP event (Figure S9). The climatic conditions occupiable by reindeers in 2100 (RCP 8.5) will be similar to those that were found at the southern limit of their range at the Last Glacial Maximum (21 ka BP) i.e., south of 50˚N (Figure S10). During the Holocene Thermal Maximum, when temperatures were similar or even warmer than today (*54*), there is likely to have been a much greater overlap in future occupiable climatic conditions (Figure S10).

Discussion

Macroecological models that explicitly simulate biotic responses to climatic change and human hunting show that these extrinsic factors, and their interactions with ecological processes, have shaped the range and abundance of reindeers over the last 21,000 years, causing population declines and range contractions that were as large as what is being predicted for the future. We show that the impacts of climate and human threats on reindeer persistence were heterogeneous in space and time, and that a high dispersal capacity is likely to have aided reindeer resilience to abrupt warming events and human exploitation in the past. Reconciling inferences of past demographic changes from fossils and aDNA also required reindeer to have a broad climatic tolerance, to attain high densities, and to experience only a weak Allee effect. These are biological traits likely associated with ecological resilience to climate and environmental change.

Our macroecological models — built and validated on the past — project a 13-15% reduction of reindeer range and population size by 2100, respectively, as a consequence of human-induced Arctic warming. However, we also show that in the past reindeers have persisted through similar magnitudes of decline, surviving in climatic refugia. For example, reindeer total abundance decreased by 35% and its range shrunk by 10% over 60 generations

in response to the 14.7 ka BP Dansgaard-Oeschger event, when temperatures increased by up to 10 ˚C in less than 50 years (*5*). While these past warming events caused major demographic changes, reindeers were able to bounce back and quickly expand their ranges in response to more favourable climatic conditions, which resulted in the opening up of new available habitats with the melting of the ice sheets in Fennoscandia and North America (*55*).

We show that demographic responses to hunting by humans, as well as climate warming, is needed to reconstruct inferences of past demographic change for reindeers. Harvesting, at medium to high levels, was needed to correctly simulate the past range dynamics of reindeer at the continental scale. However, the importance of human exploitation on regulating reindeer abundance varied spatiotemporally. Hunting during the last deglaciation into the Holocene had pronounced negative effects on reindeer abundance in Europe, likely hastening climate-driven declines of reindeer populations in this region by up to 7,000 years. The effects of humans on reindeers in Asia, Beringia, and North America were more nuanced, particularly at the regional level. Hunting by humans had its strongest impact on reindeer abundance in Asia and in North America at the southern range limit, where relative human densities were higher (*56*). It is likely that the effects of humans on reindeer abundance were not only direct, but also indirect via habitat change and alteration (*57*). Although a synergy between climate and humans in regulating the range dynamics of reindeer had been previously advocated (*19*), we have revealed spatiotemporal differences in the impacts of these two threatening forces.

Despite a long history of climatic disturbance and exploitation, the reindeer is today the most abundant large terrestrial herbivore in the Arctic (*1*), with a global population size numbering in the millions (*2*). Its survival during periods of abrupt climatic change is likely to have been facilitated by its high dispersal capacity, a demographic trait that when lacking has resulted in the extinction of other Arctic mammals (*22*). A high dispersal capacity enabled reindeer to reach important refugial populations during adverse climatic and environmental conditions, and to enhance persistence through population connectivity, which is corroborated by genetic inferences of low levels of isolation-by-distance for reindeer (*19*). A high capacity to track suitable habitats, enabled reindeers to move to areas with lower relative human densities and, thus, to indirectly avoid overhunting. A low Allee effect (as shown by our models) could have allowed reindeers to persist in low numbers, promoting stability through metapopulation processes (*58*).

Reindeers have high ecological plasticity, with current populations living in a wide variety of landscapes, ranging from tundra to boreal forests (*59*). Our models show that reindeers have a wide climatic tolerance, suggesting less sensitivity to climate and environmental changes (*60*). Conversely, Arctic mammals that went extinct during the Pleistocene/Holocene transition likely had reduced climatic tolerances, as evidence suggests they had smaller climatic and geographic envelopes compared to the survivors (*13*). These smaller niches were likely associated with a specialisation for cold and arid environments (*55, 61*), which disappeared during the Holocene as the moisture gradient in the tundra shifted to wetter conditions, favouring mesic specialists like muskox and reindeer (*55*).

We show that reindeers can occupy areas with climatic conditions similar to those forecast for the future, and that they were able to rebound after abrupt warming events. Nevertheless, our future projections suggest a reduction in population size, with extirpations in some areas of Russia and North America, where populations are currently declining (*62*). Our results concord with correlative projections for reindeer, which forecast poleward range shifts (*34*, *38*), extirpations in southern regions, and high fragmentation of the range, being most severe in North America than Eurasia (*38*). Although future Arctic warming is forecast to be similar in magnitude and pace to past events (*63*), absolute temperatures will be higher than experienced since the Last Interglacial (~ 120 ka BP) (*64*), affecting the entire Arctic ecosystem (*4*). With subarctic species expanding poleward, bringing diseases, and increasing the competition for resources (*65*), it is likely that climate change will have impacts on reindeers that have not been explicitly considered in our macroecological models.

Our findings are dependent on currently available projections of past climatic change, human expansion, and inferences of demographic changes from fossils and aDNA. Therefore, the uncertainty around estimates of past range and population dynamics of reindeer is likely to be reduced with new fossil discoveries and more accurate projections of growth and migration of anatomically modern humans. Simulations could also be potentially improved by accounting for the effect of topography operating on the demography of the species at finer spatial scales than the resolution of our models. These include, but are not limited to, elevation and bodies of open water in the Canadian Arctic Archipelago, which are likely to have limited dispersal and connectivity among populations (*66*).

Here, we opened a window into late Quaternary biodiversity dynamics using process-explicit macroecological models to synthesise inferences of past demographic change from

fossils and aDNA, revealing the ecological processes and threats that have shaped the range and abundance of reindeers over the last 21,000 years. This new historic perspective has shown the importance of identifying ecological responses to varying biotic and abiotic stressors for metapopulations, and for using this information in simulation models to assess the future survival of species under climate change.

Materials and Methods

We built process-explicit macroecological models for reindeer that simulate interactions between metapopulation dynamics, climate variability, and human harvesting (Figure S1). We used these models to continuously reconstruct 21,000 years of range contraction and expansion across Eurasia and North America. Simulations of spatiotemporal abundance were optimised with inferences of demographic change from hundreds of fossils and aDNA sequences using pattern-oriented methods (*67*). The R code for the models can be found at Appendix 2. The approach is described in detail in the Supplementary Methods. Appendix 1 and Appendix 2 in support of this manuscript can be accessed at:
https://github.com/ecanteri/Ecological_resilience_reindeer.git

Reindeer niche

Radiocarbon dated and georeferenced fossils for reindeers from the Late Pleistocene and Holocene were sourced from publicly available databases and published literature (see Supplementary Methods for details and sources). The reliability of radiocarbon ages was assessed (*68*) and calibrated using OxCal and the IntCal20 calibration curve (*69*, *70*). This resulted in 939 reliable fossils with ages younger than 21 ka BP (Appendix 1; Figure S2). Fossil data was supplemented with modern occurrence observations retrieved from GBIF (https://doi.org/10.15468/DL.QW3LPI) (*71*) for the period 1700 C.E. – 2019 C.E. (Figure S2; Appendix 1). We discarded fossil material before 21 ka BP, due to constraints in the temporal extent of the paleoclimatic data (*72*).

Fossil and observation locations and time periods (calibrated age ± 1 SD for fossils) were intersected with paleoclimate simulations of average minimum daily temperature in January, annual daily average precipitation, and total evapotranspiration in spring and summer, using the TraCE-21 ka simulation of the transient climate of the last 21,000 years (*73*), accessed through PaleoView (*72*). These climatic variables affect the population dynamics of large

herbivores in polar regions (Supplementary Methods). Because TraCE-21 data is not available after 1989 C.E., we harmonised recent climatic observations from CRU TS v4 (*74*) with the TraCE-21 simulation using the change factor method (*75*). All climate data were resampled to a 1° × 1° resolution.

The paired climate-occurrence data was used to generate a biologically relevant representation of the climatic conditions over which reindeers occurred at fossil and modern occurrence sites (*76*). The resulting 3-dimensional hypervolume (Figure S3), which approximates the fundamental niche of the reindeer (*76*), was exhaustively subsampled to generate thousands of potential realized niches (*11*). This allowed the realised niche of the reindeer to be identified using process-explicit macroecological modelling (see below). Subsampling of the niche was done using Outlier Mean Index (OMI) analysis (*77*), using plausible bounds of climatic specialisation and niche breadth (*11*).

Spatial projections of climate suitability from 21 ka BP to 1500 C.E. (pre-industrialisation) for each niche subsample (n = 2500) were generated at 7-years generational time steps (*78*), accounting for latitudinal variation in grid-cell size and temporal variation in the proportion of a cell that is covered by land or sea ice. Methods used to model the ecological niche of the reindeer are described in detail in the Supplementary Methods.

Human relative abundance

The relative abundance and expansion of palaeolithic humans in Eurasia and North America were modelled using a Climate Informed Spatial Genetics Model (CISGeM) (*79*). Pattern-oriented modelling has shown that CISGeM can accurately reconstruct arrival times of anatomically modern humans and current-day distributions of global and regional genetic diversity (*79, 80*). This is done in CISGeM by modelling local effective population size (N_e) as a function of genetic history, local demography, paleoclimate, sea level and net primary productivity over the last 125k years (*79, 80*). Arrival time, occupancy, and density (here N_e) of humans are forced in CISGeM by spatiotemporal estimates of climate, sea level changes and ice sheet dynamics, operating at 25-year time steps for the past 125 k years. To do this, climate data from the HadCM3 global circulation model prior to the last glacial maximum was harmonized with TraCE-21 data (*81*). To account for parameter uncertainty in spatiotemporal projections of N_e, we used published upper and lower confidence bounds for CISGeM parameters (*79*) to generate 4,950 plausible models of human migration, each with a unique combination of parameters.

We rejected CISGeM model simulations that were unable to successfully replicate human arrival times in North America (*81*). We then calculated the ensemble mean and standard deviation for each grid-cell at each time step in the model from 21 ka BP to 1500 C.E. and used this information to generate 100,000 potential human migration and population growth scenarios (*11*). All N_e values were scaled between 0 and 1 (using the 95th percentile of the values from the multi-model mean) and used as a measure of human relative abundance in the process-explicit macroecological model (see below). CISGeM and its application are described in detail in the Supplementary Methods.

Climate-human-reindeer interactions

Process-explicit macroecological models of the range dynamics of reindeer were generated using spatially explicit population models (*82*). Demographic processes (population growth, dispersal, source-sink dynamics and Allee effect) were simulated as dynamically responding to changing climatic conditions, human harvesting, and their interactions, from 21 ka BP until 1500 C.E. (Figure S1) at a generational time step of 7 years (*78*). Model parameters centred on best estimates for demographic processes (population growth rate and variance, dispersal, Allee effect), environmental attributes (niche breadth and marginality), and threats (human abundance and exploitation rate), were varied across biologically plausible ranges (Table S1), using Latin Hypercube sampling of uniform probability distributions (*82*). This produced 100,000 possible model parametrizations, each with different demographic processes and rates of climatic change and exploitation by humans. Each model was run for a single replicate (*83*). SEPMs were built using the 'poems' and 'paleopop' R packages (*84*, *85*). Their structure and parameters are described in detail in the Supplementary Methods.

We used pattern-oriented modelling (POM) to evaluate different combinations of model parameters (*44*), by cross-matching model simulations with inferences of demographic change from fossils and aDNA, using Approximate Bayesian Computation (ABC) (*86*). We did this using a multivariate validation target, consisting of occupancy at fossil sites (age ± 1 SD), arrival time in Greenland and timing of regional extirpation in Europe (both corrected for the Signor-Lipps effect) (*87*), and slope of trend in effective population size (N_e) estimated from aDNA (*11*). Estimates for these targets are in Table S2.

POM methods and ABC were used to identify the top 0.5% of model simulations (n = 500) that most closely reconcile with the validation targets. In ABC analysis, we used the rejection method (*88*), modified so that the Euclidean distances are scaled by the standard

deviation of the data and not the median absolute deviation (*89*). The parameter distributions of selected models (i.e., posterior distribution) were compared with their prior ranges (*89*) using Bayes Factor analysis (*90*). To improve model fit, we used informed priors derived from the posterior distribution of the selected models and ran additional 10,000 simulations. We repeated this optimisation procedure three times, each time selecting the best 50 models. Model fit was tested using posterior predictive checks (Figure S5, see Supplementary Methods for details).

Reindeer abundance, human density, and number of harvested individuals were mapped in space and time using an ensemble average of the best selected models (weighted by the Euclidean distance from the multivariate target) (*82*). The ensemble average of reindeer abundance was then used to calculate time of extirpation and change in range-wide and regional population size (*11*). We validated our abundance maps using environmental DNA (eDNA) evidence of reindeer occurrence during the Late Pleistocene and Holocene (56 occurrences) (*91*). This secondary test, using independent validation data, was done to confirm whether the selected models did indeed adequately capture the past distribution and range dynamics of the species (*67*).

Impacts of climate change and harvest on reindeer abundance

To disentangle regional and temporal effects of climatic change and human hunting on reindeer population abundance, we used Gaussian generalised additive models to analyse projections of abundance from the ensemble average of the best-performing simulations (*92*). We analysed the abundance response in four separate subregions (Europe, Asia, Beringia, and North America) and for two periods of time (Deglaciation: 21 – 11.7 ka BP; Holocene: 11.7 ka BP – 1500 C.E.). We used mean abundance over 100-year time bins as our response variable, with average temperature (°C) and human density (scaled N_e) as predictors. Time and regions were used as random effects.

The effects of climatic changes and hunting by humans on reindeer abundance and distribution were further tested by examining the biological consequences of two possible alternatives to past events: 1) 'No Harvest', in which models include climatic change but no hunting by humans, and 2) 'Stable Climate', in which human hunting is modelled but climatic conditions at 21 ka BP are kept constant until the end of the simulation. Counterfactual scenarios were parameterised using informed priors, from the posterior distribution of the selected models. We ran 10,000 simulations for each scenario. We compared the ability of the

models to reconcile the POM validation targets and calculated the difference in time of extirpation between the baseline (Harvest and Variable Climate) and the two alternative scenarios.

Future impacts of climate change

To assess future responses of reindeer to human-induced climatic change, we used the parameterization of validated simulations of the past to simulate spatiotemporal abundances from 2016 C.E. to 2100 C.E., under two Representative Concentration Pathways: a mitigation policy scenario (RCP4.5.) and a "business-as-usual" scenario (RCP8.5) (*93*). We accessed future projections of climate change using StableClim (*94*), which have been harmonized to the TraCE-21 data (Figure S7). We ran 10,000 simulations for each scenario using informed priors derived from the posterior distribution of the process-explicit macroecological models that did best at replicating the POM targets. Initial abundances were restricted to the current range of the species (*2*). Simulations accounted for the effect of future land-use change (*95*) on carrying capacity (See Supporting Methods).

For each simulation of future reindeer abundance, we calculated Expected Minimum Abundance (EMA) and range area. We measured extinction risk by estimating the percentage of change in EMA and range area between 2016 and 2100 C.E. We repeated the process for the past simulations over windows of 12 generations, to identify whether magnitudes of reductions similar to future predictions have happened in the past (see Supplementary Methods for details). Finally, we quantified the location of analogues of future climate change at the Last Glacial Maximum (21 ka BP) and the Holocene Thermal Maximum (6.5 ka BP): climatic conditions of occupied cells that range within the minimum and maximum of the climatic conditions of occupied cells in 2100 C.E.

References

1. C. D. Mallory, M. S. Boyce, Observed and predicted effects of climate change on Arctic caribou and reindeer. *Environ Rev* **26**, 13-25 (2018).
2. A. Gunn, "Rangifer tarandus. The IUCN Red List of Threatened Species." (IUCN, 2016; http://dx.doi.org/10.2305/IUCN.UK.2016-1.RLTS.T29742A22167140.en).
3. L. S. Vors, M. S. Boyce, Global declines of caribou and reindeer. *Glob Chang Biol* **15**, 2626-2633 (2009).

4. E. Post, R. B. Alley, T. R. Christensen, M. Macias-Fauria, B. C. Forbes, M. N. Gooseff, A. Iler, J. T. Kerby, K. L. Laidre, M. E. Mann, J. Olofsson, J. C. Stroeve, F. Ulmer, R. A. Virginia, M. Wang, The polar regions in a 2 degrees C warmer world. *Sci Adv* **5**, eaaw9883 (2019).
5. W. Dansgaard, S. J. Johnsen, H. B. Clausen, D. Dahl-Jensen, N. S. Gundestrup, C. U. Hammer, C. S. Hvidberg, J. P. Steffensen, A. E. Sveinbjörnsdottir, J. Jouzel, G. Bond, Evidence for general instability of past climate from a 250-kyr ice-core record. *Nature* **364**, 218-220 (1993).
6. A. Cooper, C. Turney, K. A. Hughen, B. W. Brook, H. G. McDonald, C. J. Bradshaw, Abrupt warming events drove Late Pleistocene Holarctic megafaunal turnover. *Science* **349**, 602-606 (2015).
7. P. L. Koch, A. D. Barnosky, Late Quaternary Extinctions: State of the Debate. *Annu Rev Ecol Evol Syst* **37**, 215-250 (2006).
8. C. Sandom, S. Faurby, B. Sandel, J. C. Svenning, Global late Quaternary megafauna extinctions linked to humans, not climate change. *Proc R Soc B* **281**, 20133254 (2014).
9. B. B. A. Araujo, L. G. R. Oliveira-Santos, M. S. Lima-Ribeiro, J. A. F. Diniz-Filho, F. A. S. Fernandez, Bigger kill than chill: The uneven roles of humans and climate on late Quaternary megafaunal extinctions. *Quat Int* **431**, 216-222 (2017).
10. D. H. Mann, P. Groves, B. V. Gaglioti, B. A. Shapiro, Climate-driven ecological stability as a globally shared cause of Late Quaternary megafaunal extinctions: the Plaids and Stripes Hypothesis. *Biol Rev Camb Philos Soc*, (2018).
11. D. A. Fordham, S. C. Brown, H. R. Akcakaya, B. W. Brook, S. Haythorne, A. Manica, K. T. Shoemaker, J. J. Austin, B. Blonder, J. Pilowsky, C. Rahbek, D. Nogues-Bravo, Process-explicit models reveal pathway to extinction for woolly mammoth using pattern-oriented validation. *Ecol Lett* **25**, 125-137 (2021).
12. C. N. Johnson, Determinants of loss of mammal species during the Late Quaternary 'megafauna' extinctions: life history and ecology, but not body size. *Proc R Soc B* **269**, 2221-2227 (2002).
13. A. B. Toth, S. K. Lyons, W. A. Barr, A. K. Behrensmeyer, J. L. Blois, R. Bobe, M. Davis, A. Du, J. T. Eronen, J. T. Faith, D. Fraser, N. J. Gotelli, G. R. Graves, A. M. Jukar, J. H. Miller, S. Pineda-Munoz, L. C. Soul, A. Villasenor, J. Alroy,

Reorganization of surviving mammal communities after the end-Pleistocene megafaunal extinction. *Science* **365**, 1305-1308 (2019).

14. D. H. Mann, P. Groves, R. E. Reanier, B. V. Gaglioti, M. L. Kunz, B. Shapiro, Life and extinction of megafauna in the ice-age Arctic. *Proc Natl Acad Sci U S A* **112**, 14301-14306 (2015).
15. K. L. Campbell, J. E. Roberts, L. N. Watson, J. Stetefeld, A. M. Sloan, A. V. Signore, J. W. Howatt, J. R. Tame, N. Rohland, T. J. Shen, J. J. Austin, M. Hofreiter, C. Ho, R. E. Weber, A. Cooper, Substitutions in woolly mammoth hemoglobin confer biochemical properties adaptive for cold tolerance. *Nat Genet* **42**, 536-540 (2010).
16. P. Librado, C. Der Sarkissian, L. Ermini, M. Schubert, H. Jonsson, A. Albrechtsen, M. Fumagalli, M. A. Yang, C. Gamba, A. Seguin-Orlando, C. D. Mortensen, B. Petersen, C. A. Hoover, B. Lorente-Galdos, A. Nedoluzhko, E. Boulygina, S. Tsygankova, M. Neuditschko, V. Jagannathan, C. Theves, A. H. Alfarhan, S. A. Alquraishi, K. A. Al-Rasheid, T. Sicheritz-Ponten, R. Popov, S. Grigoriev, A. N. Alekseev, E. M. Rubin, M. McCue, S. Rieder, T. Leeb, A. Tikhonov, E. Crubezy, M. Slatkin, T. Marques-Bonet, R. Nielsen, E. Willerslev, J. Kantanen, E. Prokhortchouk, L. Orlando, Tracking the origins of Yakutian horses and the genetic basis for their fast adaptation to subarctic environments. *Proc Natl Acad Sci U S A* **112**, E6889-6897 (2015).
17. T. P. Dawson, S. T. Jackson, J. I. House, I. C. Prentice, G. M. Mace, Beyond Predictions: Biodiversity Conservation in a Changing Climate. *Science* **332**, 53-58 (2011).
18. S. Liu, E. D. Lorenzen, M. Fumagalli, B. Li, K. Harris, Z. Xiong, L. Zhou, T. S. Korneliussen, M. Somel, C. Babbitt, G. Wray, J. Li, W. He, Z. Wang, W. Fu, X. Xiang, C. C. Morgan, A. Doherty, M. J. O'Connell, J. O. McInerney, E. W. Born, L. Dalen, R. Dietz, L. Orlando, C. Sonne, G. Zhang, R. Nielsen, E. Willerslev, J. Wang, Population genomics reveal recent speciation and rapid evolutionary adaptation in polar bears. *Cell* **157**, 785-794 (2014).
19. E. D. Lorenzen, D. Nogues-Bravo, L. Orlando, J. Weinstock, J. Binladen, K. A. Marske, A. Ugan, M. K. Borregaard, M. T. Gilbert, R. Nielsen, S. Y. Ho, T. Goebel, K. E. Graf, D. Byers, J. T. Stenderup, M. Rasmussen, P. F. Campos, J. A. Leonard, K. P. Koepfli, D. Froese, G. Zazula, T. W. Stafford, Jr., K. Aaris-Sorensen, P. Batra, A. M. Haywood, J. S. Singarayer, P. J. Valdes, G. Boeskorov, J. A. Burns, S. P. Davydov, J.

Haile, D. L. Jenkins, P. Kosintsev, T. Kuznetsova, X. Lai, L. D. Martin, H. G. McDonald, D. Mol, M. Meldgaard, K. Munch, E. Stephan, M. Sablin, R. S. Sommer, T. Sipko, E. Scott, M. A. Suchard, A. Tikhonov, R. Willerslev, R. K. Wayne, A. Cooper, M. Hofreiter, A. Sher, B. Shapiro, C. Rahbek, E. Willerslev, Species-specific responses of Late Quaternary megafauna to climate and humans. *Nature* **479**, 359-364 (2011).

20. A. D. Foote, K. Kaschner, S. E. Schultze, C. Garilao, S. Y. Ho, K. Post, T. F. Higham, C. Stokowska, H. van der Es, C. B. Embling, K. Gregersen, F. Johansson, E. Willerslev, M. T. Gilbert, Ancient DNA reveals that bowhead whale lineages survived Late Pleistocene climate change and habitat shifts. *Nat Commun* **4**, 1677 (2013).
21. A. M. Lister, A. J. Stuart, The impact of climate change on large mammal distribution and extinction: Evidence from the last glacial/interglacial transition. *Collect C R Geosci* **340**, 615-620 (2008).
22. L. Dalen, V. Nystrom, C. Valdiosera, M. Germonpre, M. Sablin, E. Turner, A. Angerbjorn, J. L. Arsuaga, A. Gotherstrom, Ancient DNA reveals lack of postglacial habitat tracking in the arctic fox. *Proc Natl Acad Sci U S A* **104**, 6726-6729 (2007).
23. J.-Y. Lee, J. Marotzke, G. Bala, L. Cao, S. Corti, J. P. Dunne, F. Engelbrecht, E. Fischer, J. C. Fyfe, C. Jones, A. Maycock, J. Mutemi, O. Ndiaye, S. Panickal, T. Zhou, "Future global climate: scenario-based projections and near-term information" in *Climate Change 2021: The Physical Science Basis. Contribution of Working Group I to the Sixth Assessment Report of the Intergovernmental Panel on Climate Change,* V. Masson-Delmotte, P. Zhai, A. Pirani, S. L. Connors, C. Péan, S. Berger, N. Caud, Y. Chen, L. Goldfarb, M. I. Gomis, M. Huang, K. Leitzell, E. Lonnoy, J. B. R. Matthews, T. K. Maycock, T. Waterfield, O. Yelekçi, R. Yu, B. Zhou, Eds. (Cambridge University Press, Cambridge, UK, 2021), chap. 4.
24. O. Gilg, K. M. Kovacs, J. Aars, J. Fort, G. Gauthier, D. Grémillet, R. A. Ims, H. Meltofte, J. Moreau, E. Post, N. M. Schmidt, G. Yannic, L. Bollache, Climate change and the ecology and evolution of Arctic vertebrates. *Ann N Y Acad Sci* **1249**, 166-190 (2012).
25. T. T. Hoye, E. Post, H. Meltofte, N. M. Schmidt, M. C. Forchhammer, Rapid advancement of spring in the High Arctic. *Curr Biol* **17**, R449-451 (2007).
26. L. J. Gormezano, R. F. Rockwell, What to eat now? Shifts in polar bear diet during the ice-free season in western Hudson Bay. *Ecol Evol* **3**, 3509-3523 (2013).

27. J. M. Grebmeier, J. E. Overland, S. E. Moore, E. V. Farley, E. C. Carmack, L. W. Cooper, K. E. Frey, J. H. Helle, F. A. McLaughlin, S. L. McNutt, A major ecosystem shift in the northern Bering Sea. *Science* **311**, 1461-1464 (2006).

28. L. T. Berner, R. Massey, P. Jantz, B. C. Forbes, M. Macias-Fauria, I. Myers-Smith, T. Kumpula, G. Gauthier, L. Andreu-Hayles, B. V. Gaglioti, P. Burns, P. Zetterberg, R. D'Arrigo, S. J. Goetz, Summer warming explains widespread but not uniform greening in the Arctic tundra biome. *Nat Commun* **11**, 4621 (2020).

29. S. C. Davidson, G. Bohrer, E. Gurarie, S. LaPoint, P. J. Mahoney, N. T. Boelman, J. U. H. Eitel, L. R. Prugh, L. A. Vierling, J. Jennewein, E. Grier, O. Couriot, A. P. Kelly, A. J. H. Meddens, R. Y. Oliver, R. Kays, M. Wikelski, T. Aarvak, J. T. Ackerman, J. A. Alves, E. Bayne, B. Bedrosian, J. L. Belant, A. M. Berdahl, A. M. Berlin, D. Berteaux, J. Bety, D. Boiko, T. L. Booms, B. L. Borg, S. Boutin, W. S. Boyd, K. Brides, S. Brown, V. N. Bulyuk, K. K. Burnham, D. Cabot, M. Casazza, K. Christie, E. H. Craig, S. E. Davis, T. Davison, D. Demma, C. R. DeSorbo, A. Dixon, R. Domenech, G. Eichhorn, K. Elliott, J. R. Evenson, K. M. Exo, S. H. Ferguson, W. Fiedler, A. Fisk, J. Fort, A. Franke, M. R. Fuller, S. Garthe, G. Gauthier, G. Gilchrist, P. Glazov, C. E. Gray, D. Gremillet, L. Griffin, M. T. Hallworth, A. L. Harrison, H. L. Hennin, J. M. Hipfner, J. Hodson, J. A. Johnson, K. Joly, K. Jones, T. E. Katzner, J. W. Kidd, E. C. Knight, M. N. Kochert, A. Kolzsch, H. Kruckenberg, B. J. Lagasse, S. Lai, J. F. Lamarre, R. B. Lanctot, N. C. Larter, A. D. M. Latham, C. J. Latty, J. P. Lawler, D. J. Leandri-Breton, H. Lee, S. B. Lewis, O. P. Love, J. Madsen, M. Maftei, M. L. Mallory, B. Mangipane, M. Y. Markovets, P. P. Marra, R. McGuire, C. L. McIntyre, E. A. McKinnon, T. A. Miller, S. Moonen, T. Mu, G. Muskens, J. Ng, K. L. Nicholson, I. J. Oien, C. Overton, P. A. Owen, A. Patterson, A. Petersen, I. Pokrovsky, L. L. Powell, R. Prieto, P. Quillfeldt, J. Rausch, K. Russell, S. T. Saalfeld, H. Schekkerman, J. A. Schmutz, P. Schwemmer, D. R. Seip, A. Shreading, M. A. Silva, B. W. Smith, F. Smith, J. P. Smith, K. R. S. Snell, A. Sokolov, V. Sokolov, D. V. Solovyeva, M. S. Sorum, G. Tertitski, J. F. Therrien, K. Thorup, T. L. Tibbitts, I. Tulp, B. D. Uher-Koch, R. S. A. van Bemmelen, S. Van Wilgenburg, A. L. Von Duyke, J. L. Watson, B. D. Watts, J. A. Williams, M. T. Wilson, J. R. Wright, M. A. Yates, D. J. Yurkowski, R. Zydelis, M. Hebblewhite, Ecological insights from three decades of animal movement tracking across a changing Arctic. *Science* **370**, 712-715 (2020).

30. M. J. Sheriff, M. M. Richter, C. L. Buck, B. M. Barnes, Changing seasonality and phenological responses of free-living male arctic ground squirrels: the importance of sex. *Philos Trans R Soc Lond B Biol Sci* **368**, 20120480 (2013).
31. M. J. Sheriff, C. L. Buck, B. M. Barnes, Autumn conditions as a driver of spring phenology in a free-living arctic mammal. *Climate Change Responses* **2**, (2015).
32. S. E. Moore, H. P. Huntington, Arctic marine mammals and climate change: impacts and resilience. *Ecol Appl* **18**, S157-S165 (2008).
33. K. L. Laidre, I. Stirling, L. F. Lowry, Ø. Wiig, M. P. Heide-Jørgensen, S. H. Ferguson, Quantifying the sensitivity of arctic marine mammals to climate-induced habitat change. *Ecol Appl* **18**, S97-S125 (2008).
34. F. M. van Beest, L. T. Beumer, A. S. Andersen, S. V. Hansson, N. M. Schmidt, Z. Zhang, Rapid shifts in Arctic tundra species' distributions and inter-specific range overlap under future climate change. *Divers Distrib* **27**, 1706-1718 (2021).
35. P. U. Clark, J. D. Shakun, P. A. Baker, P. J. Bartlein, S. Brewer, E. Brook, A. E. Carlson, H. Cheng, D. S. Kaufman, Z. Liu, T. M. Marchitto, A. C. Mix, C. Morrill, B. L. Otto-Bliesner, K. Pahnke, J. M. Russell, C. Whitlock, J. F. Adkins, J. L. Blois, J. Clark, S. M. Colman, W. B. Curry, B. P. Flower, F. He, T. C. Johnson, J. Lynch-Stieglitz, V. Markgraf, J. McManus, J. X. Mitrovica, P. I. Moreno, J. W. Williams, Global climate evolution during the last deglaciation. *Proc Natl Acad Sci U S A* **109**, E1134-1142 (2012).
36. R. S. Sommer, J. Kalbe, J. Ekström, N. Benecke, R. Liljegren, J.-C. Svenning, Range dynamics of the reindeer in Europe during the last 25,000 years. *J Biogeogr* **41**, 298-306 (2014).
37. O. Flagstad, K. H. Roed, Refugial origins of reindeer (Rangifer tarandus L.) inferred from mitochondrial DNA sequences. *Evolution* **57**, 658-670 (2003).
38. G. Yannic, L. Pellissier, J. Ortego, N. Lecomte, S. Couturier, C. Cuyler, C. Dussault, K. J. Hundertmark, R. J. Irvine, D. A. Jenkins, L. Kolpashikov, K. Mager, M. Musiani, K. L. Parker, K. H. Roed, T. Sipko, S. G. Porisson, B. V. Weckworth, A. Guisan, L. Bernatchez, S. D. Cote, Genetic diversity in caribou linked to past and future climate change. *Nat Clim Chang* **4**, 132-137 (2014).
39. C. Moritz, R. Agudo, The future of species under climate change: resilience or decline? *Science* **341**, 504-508 (2013).

40. D. Nogues-Bravo, F. Rodriguez-Sanchez, L. Orsini, E. de Boer, R. Jansson, H. Morlon, D. A. Fordham, S. T. Jackson, Cracking the Code of Biodiversity Responses to Past Climate Change. *Trends Ecol Evol* **33**, 765-776 (2018).
41. E. Post, C. Pedersen, Opposing plant community responses to warming with and without herbivores. *Proc Natl Acad Sci U S A* **105**, 12353-12358 (2008).
42. E. Post, Erosion of community diversity and stability by herbivore removal under warming. *Proc R Soc B* **280**, 20122722 (2013).
43. E. S. Burch, The Caribou/Wild Reindeer as a Human Resource. *Am Antiq* **37**, 339-368 (1972).
44. V. Grimm, E. Revilla, U. Berger, F. Jeltsch, W. M. Mooij, S. F. Railsback, H. H. Thulke, J. Weiner, T. Wiegand, D. L. DeAngelis, Pattern-oriented modeling of agent-based complex systems: lessons from ecology. *Science* **310**, 987-991 (2005).
45. K. Csilléry, M. G. Blum, O. E. Gaggiotti, O. Francois, Approximate Bayesian Computation (ABC) in practice. *Trends Ecol Evol* **25**, 410-418 (2010).
46. H. Binney, M. Edwards, M. Macias-Fauria, A. Lozhkin, P. Anderson, J. O. Kaplan, A. Andreev, E. Bezrukova, T. Blyakharchuk, V. Jankovska, I. Khazina, S. Krivonogov, K. Kremenetski, J. Nield, E. Novenko, N. Ryabogina, N. Solovieva, K. Willis, V. Zernitskaya, Vegetation of Eurasia from the last glacial maximum to present: Key biogeographic patterns. *Quat Sci Rev* **157**, 80-97 (2017).
47. J. R. M. Allen, T. Hickler, J. S. Singarayer, M. T. Sykes, P. J. Valdes, B. Huntley, Last glacial vegetation of northern Eurasia. *Quat Sci Rev* **29**, 2604-2618 (2010).
48. G. Yannic, O. Hagen, F. Leugger, D. N. Karger, L. Pellissier, Harnessing paleo-environmental modeling and genetic data to predict intraspecific genetic structure. *Evol Appl* **13**, 1526-1542 (2020).
49. G. Yannic, L. Pellissier, M. Le Corre, C. Dussault, L. Bernatchez, S. D. Cote, Temporally dynamic habitat suitability predicts genetic relatedness among caribou. *Proc R Soc B* **281**, (2014).
50. N. P. McKay, D. S. Kaufman, C. C. Routson, M. P. Erb, P. D. Zander, The Onset and Rate of Holocene Neoglacial Cooling in the Arctic. *Geophys Res Lett* **45**, 12,487-412,496 (2018).
51. D. Kaufman, Holocene thermal maximum in the western Arctic (0–180°W). *Quat Sci Rev* **23**, 529-560 (2004).

52. P. C. Lent, *Muskoxen and their hunters: A history* (University of Oklahoma Press, 1999), vol. 5, pp. 362-362.
53. R. S. Sommer, A. Nadachowski, Glacial refugia of mammals in Europe: evidence from fossil records. *Mamm Rev* **36**, 251-265 (2006).
54. H. Renssen, H. Seppä, X. Crosta, H. Goosse, D. M. Roche, Global characterization of the Holocene Thermal Maximum. *Quat Sci Rev* **48**, 7-19 (2012).
55. D. H. Mann, P. Groves, M. L. Kunz, R. E. Reanier, B. V. Gaglioti, Ice-age megafauna in Arctic Alaska: extinction, invasion, survival. *Quat Sci Rev* **70**, 91-108 (2013).
56. A. Timmermann, T. Friedrich, Late Pleistocene climate drivers of early human migration. *Nature* **538**, 92-95 (2016).
57. L. Stephens, D. Fuller, N. Boivin, T. Rick, N. Gauthier, A. Kay, B. Marwick, C. G. Armstrong, C. M. Barton, T. Denham, K. Douglass, J. Driver, L. Janz, P. Roberts, J. D. Rogers, H. Thakar, M. Altaweel, A. L. Johnson, M. M. Sampietro Vattuone, M. Aldenderfer, S. Archila, G. Artioli, M. T. Bale, T. Beach, F. Borrell, T. Braje, P. I. Buckland, N. G. Jiménez Cano, J. M. Capriles, A. Diez Castillo, Ç. Çilingiroğlu, M. Negus Cleary, J. Conolly, P. R. Coutros, R. A. Covey, M. Cremaschi, A. Crowther, L. Der, S. Di Lernia, J. F. Doershuk, W. E. Doolittle, K. J. Edwards, J. M. Erlandson, D. Evans, A. Fairbairn, P. Faulkner, G. Feinman, R. Fernandes, S. M. Fitzpatrick, R. Fyfe, E. Garcea, S. Goldstein, R. C. Goodman, J. Dalpoim Guedes, J. Herrmann, P. Hiscock, P. Hommel, K. A. Horsburgh, C. Hritz, J. W. Ives, A. Junno, J. G. Kahn, B. Kaufman, C. Kearns, T. R. Kidder, F. Lanoë, D. Lawrence, G.-A. Lee, M. J. Levin, H. B. Lindskoug, J. A. López-Sáez, S. Macrae, R. Marchant, J. M. Marston, S. McClure, M. D. McCoy, A. V. Miller, M. Morrison, G. Motuzaite Matuzeviciute, J. Müller, A. Nayak, S. Noerwidi, T. M. Peres, C. E. Peterson, L. Proctor, A. R. Randall, S. Renette, G. Robbins Schug, K. Ryzewski, R. Saini, V. Scheinsohn, P. Schmidt, P. Sebillaud, O. Seitsonen, I. A. Simpson, A. Sołtysiak, R. J. Speakman, R. N. Spengler, M. L. Steffen, M. J. Storozum, K. M. Strickland, J. Thompson, T. L. Thurston, S. Ulm, M. C. Ustunkaya, M. H. Welker, C. West, P. R. Williams, D. K. Wright, N. Wright, M. Zahir, A. Zerboni, E. Beaudoin, S. Munevar Garcia, J. Powell, A. Thornton, J. O. Kaplan, M.-J. Gaillard, K. Klein Goldewijk, E. Ellis, Archaeological assessment reveals Earth's early transformation through land use. *Science* **365**, 897-902 (2019).

58. R. Lande, S. Engen, B.-E. Sæther, B.-E. Saether, Extinction Times in Finite Metapopulation Models with Stochastic Local Dynamics. *Oikos* **83**, 383 (1998).
59. F. F. Mallory, T. L. Hillis, Demographic characteristics of circumpolar caribou populations: ecotypes, ecological constraints, releases, and population dynamics. *Rangifer* **18**, 49 (1998).
60. R. G. Pearson, J. C. Stanton, K. T. Shoemaker, M. E. Aiello-Lammens, P. J. Ersts, N. Horning, D. A. Fordham, C. J. Raxworthy, H. Y. Ryu, J. McNees, H. R. Akçakaya, Life history and spatial traits predict extinction risk due to climate change. *Nat Clim Chang* **4**, 217-221 (2014).
61. M. Di Febbraro, F. Carotenuto, S. Castiglione, D. Russo, A. Loy, L. Maiorano, P. Raia, Does the jack of all trades fare best? Survival and niche width in Late Pleistocene megafauna. *J Biogeogr* **44**, 2828-2838 (2017).
62. M. Aronsson, S. Heiðmarsson, H. Jóhannesdóttir, T. Barry, J. Braa, C. T. Burns, S. J. Coulson, C. Cuyler, K. Falk, H. Helgason, K. F. Lárusson, J. P. Lawler, P. Kulmala, D. MacNearney, E. Oberndorfer, V. Ravolainen, N. M. Schmidt, M. Soloviev, C. Coon, T. T. Christensen, *State of the Arctic Terrestrial Biodiversity Report* M. Aronsson, T. Barry, S. Heiðmarsson, H. Jóhannesdóttir, T. Hayes, Eds. (Conservation of Arctic Flora and Fauna International Secretariat, Akureyri, Iceland., 2021).
63. D. A. Fordham, S. T. Jackson, S. C. Brown, B. Huntley, B. W. Brook, D. Dahl-Jensen, M. T. P. Gilbert, B. L. Otto-Bliesner, A. Svensson, S. Theodoridis, J. M. Wilmshurst, J. C. Buettel, E. Canteri, M. McDowell, L. Orlando, J. Pilowsky, C. Rahbek, D. Nogues-Bravo, Using paleo-archives to safeguard biodiversity under climate change. *Science* **369**, 10-10 (2020).
64. IPCC, *Climate Change 2007: The Physical Science Basis. Contribution of Working Group I to the Fourth Assessment Report of the Intergovernmental Panel on Climate Change* S. Solomon, D. Qin, M. Manning, Z. Chen, M. Marquis, K. B. Averyt, M. Tignor, H. L. Miller Eds, (Working group I contribution to the fourth assessment report of the IPCC, Cambridge University Press, Cambridge, United Kingdom; New York, NY, USA, 2007).
65. E. Post, M. C. Forchhammer, M. S. Bret-Harte, T. V. Callaghan, T. R. Christensen, B. Elberling, A. D. Fox, O. Gilg, D. S. Hik, T. T. Hoye, R. A. Ims, E. Jeppesen, D. R. Klein, J. Madsen, A. D. McGuire, S. Rysgaard, D. E. Schindler, I. Stirling, M. P.

Tamstorf, N. J. Tyler, R. van der Wal, J. Welker, P. A. Wookey, N. M. Schmidt, P. Aastrup, Ecological dynamics across the Arctic associated with recent climate change. *Science* **325**, 1355-1358 (2009).

66. G. Yannic, J. Ortego, L. Pellissier, N. Lecomte, L. Bernatchez, S. D. Cote, Linking genetic and ecological differentiation in an ungulate with a circumpolar distribution. *Ecography* **41**, 922-937 (2018).
67. V. Grimm, S. F. Railsback, Pattern-oriented modelling: a 'multi-scope' for predictive systems ecology. *Philos Trans R Soc Lond B Biol Sci* **367**, 298-310 (2012).
68. A. D. Barnosky, E. L. Lindsey, Timing of Quaternary megafaunal extinction in South America in relation to human arrival and climate change. *Quat Int* **217**, 10-29 (2010).
69. P. J. Reimer, W. E. N. Austin, E. Bard, A. Bayliss, P. G. Blackwell, C. Bronk Ramsey, M. Butzin, H. Cheng, R. L. Edwards, M. Friedrich, P. M. Grootes, T. P. Guilderson, I. Hajdas, T. J. Heaton, A. G. Hogg, K. A. Hughen, B. Kromer, S. W. Manning, R. Muscheler, J. G. Palmer, C. Pearson, J. Van Der Plicht, R. W. Reimer, D. A. Richards, E. M. Scott, J. R. Southon, C. S. M. Turney, L. Wacker, F. Adolphi, U. Büntgen, M. Capano, S. M. Fahrni, A. Fogtmann-Schulz, R. Friedrich, P. Köhler, S. Kudsk, F. Miyake, J. Olsen, F. Reinig, M. Sakamoto, A. Sookdeo, S. Talamo, The IntCal20 Northern Hemisphere radiocarbon age calibration curve (0–55 cal kBP). *Radiocarbon* **62**, 725-757 (2020).
70. C. Bronk Ramsey, Bayesian analysis of radiocarbon dates. *Radiocarbon* **51**, 337-360 (2009).
71. GBIF.org. Occurrence download. (The Global Biodiversity Information Facility, 2019). https://doi.org/10.15468/dl.cl2hdw. Accessed 11 April 2019.
72. D. A. Fordham, F. Saltre, S. Haythorne, T. M. L. Wigley, B. L. Otto-Bliesner, K. C. Chan, B. W. Brook, PaleoView: a tool for generating continuous climate projections spanning the last 21 000 years at regional and global scales. *Ecography* **40**, 1348-1358 (2017).
73. A. Z. Liu, A. B. L. Otto-Bliesner, A. F. He, A. E. C. Brady, A. R. Tomas, A. P. U. Clark, A. A. E. Carlson, A. J. Lynch-Stieglitz, A. W. Curry, A. E. Brook, A. D. Erickson, A. R. Jacob, A. J. Kutzbach, A. J. Cheng, Transient simulation of last deglaciation with a new mechanism for Bølling-Allerød warming. *Science* **325**, 310-314 (2009).

74. I. Harris, T. J. Osborn, P. Jones, D. Lister, Version 4 of the CRU TS monthly high-resolution gridded multivariate climate dataset. *Sci Data* **7**, 109 (2020).
75. R. Beyer, M. Krapp, A. Manica, An empirical evaluation of bias correction methods for palaeoclimate simulations. *Clim Past* **16**, 1493-1508 (2020).
76. D. Nogués-Bravo, Predicting the past distribution of species climatic niches. *Glob Ecol Biogeogr* **18**, 521-531 (2009).
77. S. Dolédec, D. Chessel, C. Gimaret-Carpentier, Niche Separation in Community Analysis: A New Method. *Ecology* **81**, 2914-2927 (2000).
78. M. Pacifici, L. Santini, M. Di Marco, D. Baisero, L. Francucci, G. G. Marasini, P. Visconti, C. Rondinini, Generation length for mammals. *Nat Conserv* **5**, 87-94 (2013).
79. A. Eriksson, L. Betti, A. D. Friend, S. J. Lycett, J. S. Singarayer, N. von Cramon-Taubadel, P. J. Valdes, F. Balloux, A. Manica, Late Pleistocene climate change and the global expansion of anatomically modern humans. *Proc Natl Acad Sci U S A* **109**, 16089-16094 (2012).
80. M. Raghavan, M. Steinrücken, K. Harris, S. Schiffels, S. Rasmussen, M. Degiorgio, A. Albrechtsen, C. Valdiosera, M. C. Ávila-Arcos, A.-S. Malaspinas, A. Eriksson, I. Moltke, M. Metspalu, J. R. Homburger, J. Wall, O. E. Cornejo, J. V. Moreno-Mayar, T. S. Korneliussen, T. Pierre, M. Rasmussen, P. F. Campos, P. D. B. Damgaard, M. E. Allentoft, J. Lindo, E. Metspalu, R. Rodríguez-Varela, J. Mansilla, C. Henrickson, A. Seguin-Orlando, H. Malmström, T. Stafford, S. S. Shringarpure, A. Moreno-Estrada, M. Karmin, K. Tambets, A. Bergström, Y. Xue, V. Warmuth, A. D. Friend, J. Singarayer, P. Valdes, F. Balloux, I. Leboreiro, J. L. Vera, H. Rangel-Villalobos, D. Pettener, D. Luiselli, L. G. Davis, E. Heyer, C. P. E. Zollikofer, M. S. Ponce De León, C. I. Smith, V. Grimes, K.-A. Pike, M. Deal, B. T. Fuller, B. Arriaza, V. Standen, M. F. Luz, F. Ricaut, N. Guidon, L. Osipova, M. I. Voevoda, O. L. Posukh, O. Balanovsky, M. Lavryashina, Y. Bogunov, E. Khusnutdinova, M. Gubina, E. Balanovska, S. Fedorova, S. Litvinov, B. Malyarchuk, M. Derenko, M. J. Mosher, D. Archer, J. Cybulski, B. Petzelt, J. Mitchell, R. Worl, P. J. Norman, P. Parham, B. M. Kemp, T. Kivisild, C. Tyler-Smith, M. S. Sandhu, M. Crawford, R. Villems, D. G. Smith, M. R. Waters, T. Goebel, J. R. Johnson, R. S. Malhi, M. Jakobsson, D. J. Meltzer, A. Manica, R. Durbin, C. D. Bustamante, Y. S. Song, R. Nielsen, E. Willerslev, Genomic evidence

for the Pleistocene and recent population history of Native Americans. *Science* **349**, aab3884-aab3884 (2015).

81. E. Canteri, S. C. Brown, N. M. Schmidt, R. Heller, D. Nogues-Bravo, D. A. Fordham. "Spatiotemporal influences of climate and humans on muskox range dynamics over multiple millennia". (University of Adelaide, Submitted manuscript, 2022).
82. D. A. Fordham, S. Haythorne, S. C. Brown, J. C. Buettel, B. W. Brook, poems: R package for simulating species' range dynamics using pattern-oriented validation. *Methods Ecol Evol* **12**, 2364-2371 (2021).
83. T. A. A. Prowse, C. J. A. Bradshaw, S. Delean, P. Cassey, R. C. Lacy, K. Wells, M. E. Aiello-Lammens, H. R. Akçakaya, B. W. Brook, An efficient protocol for the global sensitivity analysis of stochastic ecological models. *Ecosphere* **7**, e01238 (2016).
84. S. Haythorne, D. Fordham, S. Brown, J. Buettel, B. Brook. (R, CRAN, 2021), pp. poems: Pattern-Oriented Ensemble Modeling System.
85. S. Haythorne, J. Pilowsky, S. Brown, D. Fordham. (R, CRAN, 2021), pp. paleopop: Pattern-Oriented Modeling Framework for Coupled Niche-Population Paleo-Climatic Models.
86. S. A. Sisson, Y. Fan, M. Beaumont, *Handbook of approximate Bayesian computation* (CRC Press, 2018).
87. P. W. Signor, J. H. Lipps, "Sampling bias, gradual extinction patterns and catastrophes in the fossil record" in *Geological Implications of Impacts of Large Asteroids and Comets on the Earth* (Geological Society of America Special Papers, Geological Society of America, 1982), vol. 190, pp. 291-296.
88. K. Csilléry, O. François, M. G. B. Blum, abc: an R package for approximate Bayesian computation (ABC). *Methods Ecol Evol* **3**, 475-479 (2012).
89. E. van der Vaart, M. A. Beaumont, A. S. A. Johnston, R. M. Sibly, Calibration and evaluation of individual-based models using Approximate Bayesian Computation. *Ecol Modell* **312**, 182-190 (2015).
90. H. Jeffreys, *The theory of probability* (OUP Oxford, 1998).
91. Y. Wang, M. W. Pedersen, I. G. Alsos, B. De Sanctis, F. Racimo, A. Prohaska, E. Coissac, H. L. Owens, M. K. F. Merkel, A. Fernandez-Guerra, A. Rouillard, Y. Lammers, A. Alberti, F. Denoeud, D. Money, A. H. Ruter, H. Mccoll, N. K. Larsen, A. A. Cherezova, M. E. Edwards, G. B. Fedorov, J. Haile, L. Orlando, L. Vinner, T. S.

Korneliussen, D. W. Beilman, A. A. Bjørk, J. Cao, C. Dockter, J. Esdale, G. Gusarova, K. K. Kjeldsen, J. Mangerud, J. T. Rasic, B. Skadhauge, J. I. Svendsen, A. Tikhonov, P. Wincker, Y. Xing, Y. Zhang, D. G. Froese, C. Rahbek, D. B. Nogues, P. B. Holden, N. R. Edwards, R. Durbin, D. J. Meltzer, K. H. Kjær, P. Möller, E. Willerslev, Late Quaternary dynamics of Arctic biota from ancient environmental genomics. *Nature*, (2021).

92. E. J. Pedersen, D. L. Miller, G. L. Simpson, N. Ross, Hierarchical generalized additive models in ecology: an introduction with mgcv. *PeerJ* **7**, e6876 (2019).
93. D. P. van Vuuren, J. Edmonds, M. Kainuma, K. Riahi, A. Thomson, K. Hibbard, G. C. Hurtt, T. Kram, V. Krey, J.-F. Lamarque, T. Masui, M. Meinshausen, N. Nakicenovic, S. J. Smith, S. K. Rose, The representative concentration pathways: an overview. *Clim Change* **109**, 5-31 (2011).
94. S. C. Brown, T. M. L. Wigley, B. L. Otto-Bliesner, D. A. Fordham, StableClim, continuous projections of climate stability from 21000 BP to 2100 CE at multiple spatial scales. *Sci Data* **7**, 335 (2020).
95. G. C. Hurtt, L. P. Chini, S. Frolking, R. A. Betts, J. Feddema, G. Fischer, J. P. Fisk, K. Hibbard, R. A. Houghton, A. Janetos, C. D. Jones, G. Kindermann, T. Kinoshita, K. Klein Goldewijk, K. Riahi, E. Shevliakova, S. Smith, E. Stehfest, A. Thomson, P. Thornton, D. P. van Vuuren, Y. P. Wang, Harmonization of land-use scenarios for the period 1500–2100: 600 years of global gridded annual land-use transitions, wood harvest, and resulting secondary lands. *Clim Change* **109**, 117-161 (2011).
96. T. H. van Andel, The Climate and Landscape of the Middle Part of the Weichselian Glaciation in Europe: The Stage 3 Project. *Quat Res* **57**, 2-8 (2002).
97. J. W. Williams, E. C. Grimm, J. L. Blois, D. F. Charles, E. B. Davis, S. J. Goring, R. W. Graham, A. J. Smith, M. Anderson, J. Arroyo-Cabrales, A. C. Ashworth, J. L. Betancourt, B. W. Bills, R. K. Booth, P. I. Buckland, B. B. Curry, T. Giesecke, S. T. Jackson, C. Latorre, J. Nichols, T. Purdum, R. E. Roth, M. Stryker, H. Takahara, The Neotoma Paleoecology Database, a multiproxy, international, community-curated data resource. *Quat Res* **89**, 156-177 (2018).
98. A. Martindale, R. Morlan, R. Betts, M. Blake, K. Gajewski, M. Chaput, C. E. Mason, P. V. Richards. Canadian Archaeological Radiocarbon Database (CARD 2.1) (2016). Accessed 04 October 2019.

99. D. G. Anderson, D. S. Miller, S. J. Yerka, J. C. Gillam, E. N. Johanson, D. T. Anderson, A. C. Goodyear, A. M. Smallwood, PIDBA (Paleoindian Database of the Americas) 2010: current status and findings. *Archaeol East N Am* **38**, 63-89 (2010).
100. E. J. Asbjornsen, B. E. Saether, J. D. C. Linnell, S. Engen, R. Andersen, T. Bretten, Predicting the growth of a small introduced muskox population using population prediction intervals. *J Anim Ecol* **74**, 612-618 (2005).
101. J. B. Mosbacher, "Ecology of a high arctic key species: Muskoxen in Northeast Greenland", thesis, Aarhus University, Denmark (2017).
102. P. Droogers, R. G. Allen, Estimating reference evapotranspiration under inaccurate data conditions. *Irrig Drain Syst* **16**, 33–45 (2002).
103. D. Nogues-Bravo, R. Ohlemuller, P. Batra, M. B. Araujo, Climate predictors of late quaternary extinctions. *Evolution* **64**, 2442-2449 (2010).
104. J. P. Desforges, G. M. Marques, L. T. Beumer, M. Chimienti, L. H. Hansen, S. H. Pedersen, N. M. Schmidt, F. M. van Beest, Environment and physiology shape Arctic ungulate population dynamics. *Glob Chang Biol* **27**, 1755-1771 (2021).
105. J. Foster, G. Liston, R. Koster, R. Essery, H. Behr, L. Dumenil, D. Verseghy, S. Thompson, D. Pollard, J. Cohen, Snow cover and snow mass intercomparisons of general circulation models and remotely sensed datasets. *J Clim* **9**, 409-426 (1996).
106. B. Blonder, C. Lamanna, C. Violle, B. J. Enquist, The n-dimensional hypervolume. *Glob Ecol Biogeogr* **23**, 595-609 (2014).
107. C. F. Dormann, J. Elith, S. Bacher, C. Buchmann, G. Carl, G. Carré, J. R. G. Marquéz, B. Gruber, B. Lafourcade, P. J. Leitão, T. Münkemüller, C. McClean, P. E. Osborne, B. Reineking, B. Schröder, A. K. Skidmore, D. Zurell, S. Lautenbach, Collinearity: a review of methods to deal with it and a simulation study evaluating their performance. *Ecography* **36**, 27-46 (2013).
108. J. Thioulouse, S. Dray, A.-B. Dufour, A. Siberchicot, T. Jombart, S. Pavoine, *Multivariate Analysis of Ecological Data with ade4* (Springer, New York, NY, ed. 1st, 2018), pp. 1 online resource (334 pages).
109. G. W. Luck, The relationships between net primary productivity, human population density and species conservation. *J Biogeogr* **34**, 201-212 (2007).

110. H. Lieth, "Modeling the primary productivity of the world" in *Primary productivity of the biosphere*, H. Lieth, R. J. Whittaker, Eds. (Springer-Verlag, New York, USA, 1975).
111. V. Grimm, E. Revilla, U. Berger, F. Jeltsch, W. M. Mooij, S. F. Railsback, H.-H. Thulke, J. Weiner, T. Wiegand, D. L. DeAngelis, Pattern-Oriented Modeling of Agent-Based Complex Systems: Lessons from Ecology. *Science* **310**, 987 (2005).
112. L. R. Binford, *Constructing frames of reference: an analytical method for archaeological theory building using ethnographic and environmental data sets* (University of California Press, 2019).
113. R. S. C. Cooke, T. C. Gilbert, P. Riordan, D. Mallon, Improving generation length estimates for the IUCN Red List. *PLoS One* **13**, e0191770 (2018).
114. IUCN, "Guidelines for Using the IUCN Red List Categories and Criteria" (International Union for the Conservation of Nature, 2019; http://www.iucnredlist.org/documents/RedListGuidelines.pdf).
115. J. VanDerWal, L. P. Shoo, C. N. Johnson, S. E. Williams, Abundance and the environmental niche: environmental suitability estimated from niche models predicts the upper limit of local abundance. *Am Nat* **174**, 282-291 (2009).
116. D. A. Fordham, H. R. Akçakaya, B. W. Brook, A. Rodríguez, P. C. Alves, E. Civantos, M. Triviño, M. J. Watts, M. B. Araújo, Adapted conservation measures are required to save the Iberian lynx in a changing climate. *Nat Clim Chang* **3**, 899-903 (2013).
117. M. A. D. Ferguson, F. Messier, Mass Emigration of Arctic Tundra Caribou from a Traditional Winter Range: Population Dynamics and Physical Condition. *J Wildl Manage* **64**, 168-178 (2000).
118. S. Couturier, D. Jean, R. D. Otto, S. p. Rivard, *Demography of the migratory tundra caribou (Rangifer tarandus) of the Nord-du-Québec region and Labrador* (Ministère des Ressources naturelles, de la Faune et des Parcs, Direction de l'aménagement de la faune du Nord-du-Québec and Direction de la recherche sur la faune, Québec, 2004).
119. B. W. Brook, C. J. Bradshaw, Strength of evidence for density dependence in abundance time series of 1198 species. *Ecology* **87**, 1445-1451 (2006).
120. NERC Centre for Population Biology. The Global Population Dynamic Database. (NERC Centre for Population Biology, Ascot, Berkshire (UK), 1999).

121. A. Uboni, T. Horstkotte, E. Kaarlejarvi, A. Seveque, F. Stammler, J. Olofsson, B. C. Forbes, J. Moen, Long-Term Trends and Role of Climate in the Population Dynamics of Eurasian Reindeer. *PLoS One* **11**, e0158359 (2016).
122. B. Peeters, V. Veiberg, A. O. Pedersen, A. Stien, R. J. Irvine, R. Aanes, B. E. S'Ther, O. Strand, B. B. Hansen, Climate and density dependence cause changes in adult sex ratio in a large Arctic herbivore. *Ecosphere* **8**, e01699-e01699 (2017).
123. T. Petzoldt. (R, CRAN, 2020), pp. Estimation of Growth Rates with Package growthrates.
124. W. E. Ricker, Stock and recruitment. *J Fish Res Board Can* **11**, 559-623 (1954).
125. K. Joly, E. Gurarie, M. S. Sorum, P. Kaczensky, M. D. Cameron, A. F. Jakes, B. L. Borg, D. Nandintsetseg, J. G. C. Hopcraft, B. Buuveibaatar, P. F. Jones, T. Mueller, C. Walzer, K. A. Olson, J. C. Payne, A. Yadamsuren, M. Hebblewhite, Longest terrestrial migrations and movements around the world. *Sci Rep* **9**, 15333 (2019).
126. F. Messier, J. Huot, D. Le Henaff, S. Luttich, Demography of the George River Caribou Herd: Evidence of Population Regulation by Forage Exploitation and Range Expansion. *Arctic* **41**, (1988).
127. J. Alroy, A multispecies overkill simulation of the end-Pleistocene megafaunal mass extinction. *Science* **292**, 1893-1896 (2001).
128. B. W. Brook, D. M. J. S. Bowman, The uncertain blitzkrieg of Pleistocene megafauna. *J Biogeogr* **31**, 517-523 (2004).
129. B. W. Brook, C. N. Johnson, Selective hunting of juveniles as a cause of the imperceptible overkill of the Australian Pleistocene megafauna. *Alcheringa* **30**, 39-48 (2006).
130. D. A. Fordham, S. Haythorne, B. W. Brook, Sensitivity Analysis of Range Dynamics Models (SARDM): Quantifying the influence of parameter uncertainty on forecasts of extinction risk from global change. *Environ Model Softw* **83**, 193-197 (2016).
131. O. Bennike, Colonisation of Greenland by plants and animals after the last ice age: a review. *Polar Rec* **35**, 323-336 (1999).
132. C. J. A. Bradshaw, A. Cooper, C. S. M. Turney, B. W. Brook, Robust estimates of extinction time in the geological record. *Quat Sci Rev* **33**, 14-19 (2012).
133. K. Clark, I. Karsch-Mizrachi, D. J. Lipman, J. Ostell, E. W. Sayers, GenBank. *Nucleic Acids Res* **44**, D67-D72 (2016).

134. M. Kearse, R. Moir, A. Wilson, S. Stones-Havas, M. Cheung, S. Sturrock, S. Buxton, A. Cooper, S. Markowitz, C. Duran, T. Thierer, B. Ashton, P. Meintjes, A. Drummond, Geneious Basic: An integrated and extendable desktop software platform for the organization and analysis of sequence data. *Bioinformatics* **28**, 1647-1649 (2012).
135. R. C. Edgar, MUSCLE: multiple sequence alignment with high accuracy and high throughput. *Nucleic Acids Res* **32**, 1792-1797 (2004).
136. P. J. Reimer, E. Bard, A. Bayliss, J. W. Beck, P. G. Blackwell, C. B. Ramsey, C. E. Buck, H. Cheng, R. L. Edwards, M. Friedrich, P. M. Grootes, T. P. Guilderson, H. Haflidason, I. Hajdas, C. Hatté, T. J. Heaton, D. L. Hoffmann, A. G. Hogg, K. A. Hughen, K. F. Kaiser, B. Kromer, S. W. Manning, M. Niu, R. W. Reimer, D. A. Richards, E. M. Scott, J. R. Southon, R. A. Staff, C. S. M. Turney, J. van der Plicht, IntCal13 and Marine13 Radiocarbon Age Calibration Curves 0–50,000 Years cal BP. *Radiocarbon* **55**, 1869-1887 (2016).
137. M. A. Suchard, P. Lemey, G. Baele, D. L. Ayres, A. J. Drummond, A. Rambaut, Bayesian phylogenetic and phylodynamic data integration using BEAST 1.10. *Virus Evol* **4**, vey016 (2018).
138. D. Posada, jModelTest: phylogenetic model averaging. *Mol Biol Evol* **25**, 1253-1256 (2008).
139. A. Rambaut, A. J. Drummond, D. Xie, G. Baele, M. A. Suchard, Posterior Summarization in Bayesian Phylogenetics Using Tracer 1.7. *Syst Biol* **67**, 901-904 (2018).
140. C. M. Crespi, W. J. Boscardin, Bayesian Model Checking for Multivariate Outcome Data. *Comput Stat Data Anal* **53**, 3765-3772 (2009).
141. J. L. Chen, S. C. Kang, X. H. Meng, Q. L. You, Assessments of the Arctic amplification and the changes in the Arctic sea surface. *Adv Clim Change Res* **10**, 193-202 (2019).
142. M. C. Serreze, R. G. Barry, Processes and impacts of Arctic amplification: A research synthesis. *Glob Planet Change* **77**, 85-96 (2011).
143. B. Blonder, C. B. Morrow, B. Maitner, D. J. Harris, C. Lamanna, C. Violle, B. J. Enquist, A. J. Kerkhoff, S. McMahon, New approaches for delineating n-dimensional hypervolumes. *Methods Ecol Evol* **9**, 305-319 (2017).

144. GBIF.org. Occurrence download. (The Global Biodiversity Information Facility, 2022). https://doi.org/10.15468/dl.bqyj3b. Accessed 01 March 20122.
145. C. Merow, M. J. Smith, J. A. Silander, A practical guide to MaxEnt for modeling species' distributions: what it does, and why inputs and settings matter. *Ecography* **36**, 1058-1069 (2013).

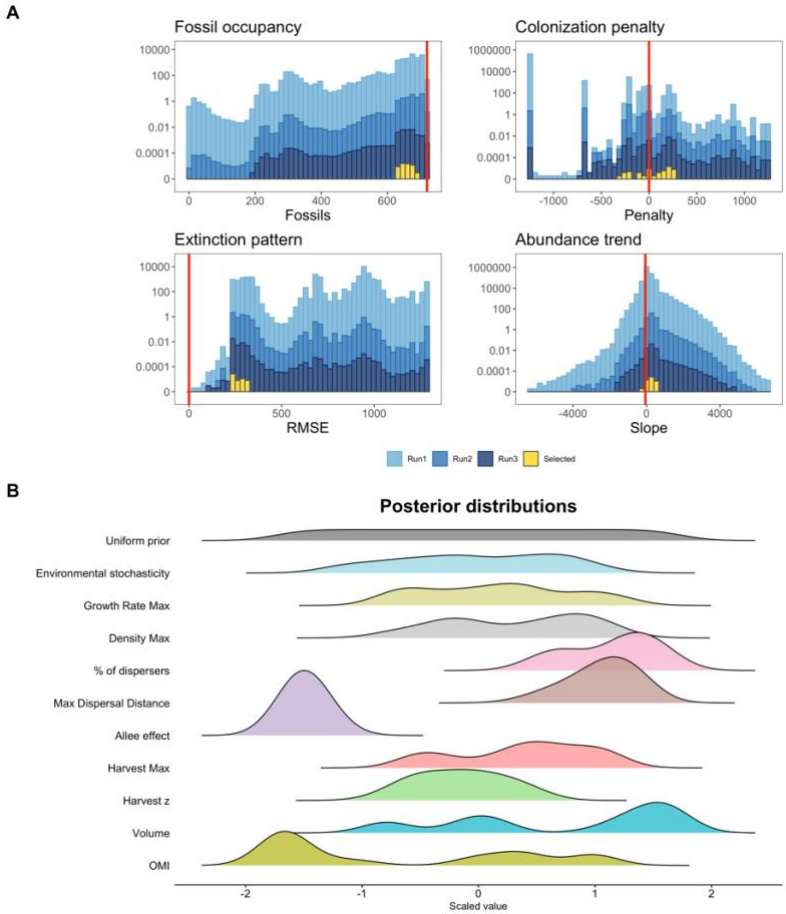

Figure 1. Model performance and posterior distributions for modelled parameters.

A, Histograms show the distribution of summary statistics for simulations of the final run of simulations and the previous two (blue bars). Yellow bars show the summary statistics for simulations of Run 3 selected using POM and ABC. Red vertical lines show the values used as validation targets in ABC. Y-axes are on the log scale (1e06). **B**, Density of the posterior distribution compared to a uniformly distributed prior (values are scaled). Variable demographic parameters in the SEPM are: variation in population growth rate (Environmental stochasticity); maximum population growth rate (Growth Rate Max); proportion of individuals dispersing at each time step (% of dispersers); maximum dispersal distance (Max Dispersal Distance); Alle effect; and maximum abundance (Density Max). Variable harvest parameters are: percentage of the population that is harvested (Harvest Max); extent to which harvest follows a Type II to Type III functional response (Harvest z). Variable parameters describing ecological niche requirements are: distance between the climatic conditions of the occupied and potential fundamental niche (OMI), and breadth of climatic conditions the species can occupy (niche volume).

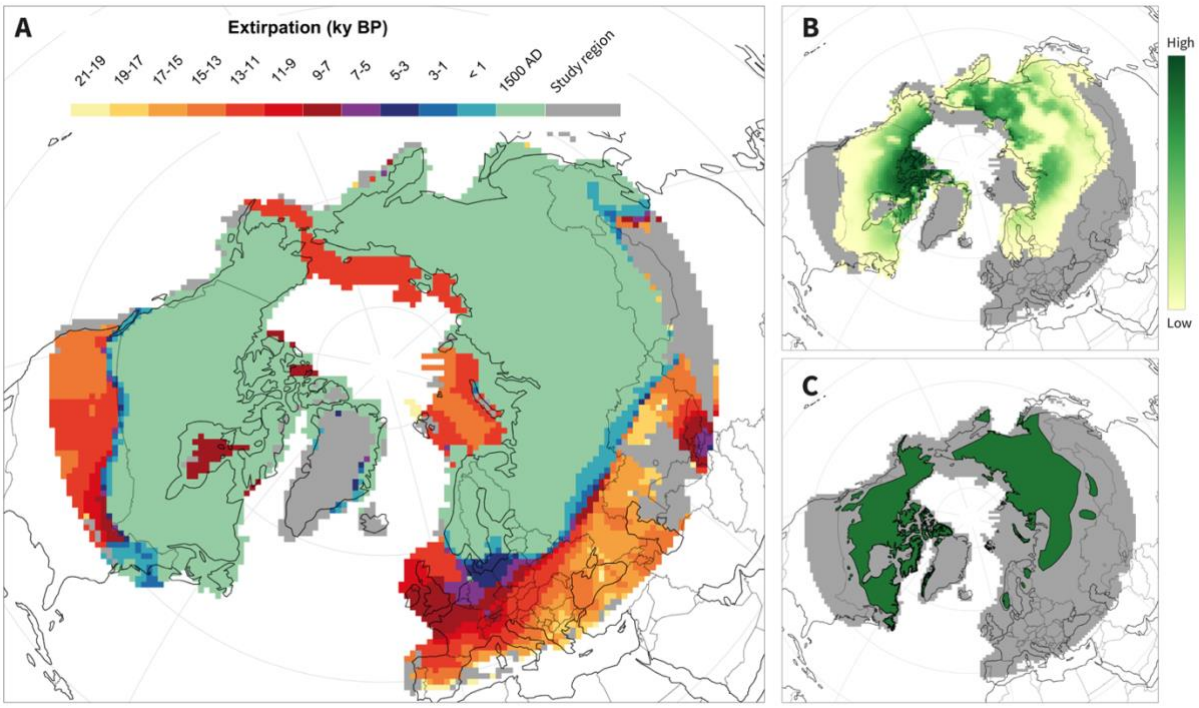

Figure 2. Change in the distribution of reindeer over the last 21,000 years.

A, Projected time of extirpation of reindeer. **B**, Areas simulated to be occupied in 1500 C.E., with their relative densities. **C**, the current natural distribution of reindeer (*2*).

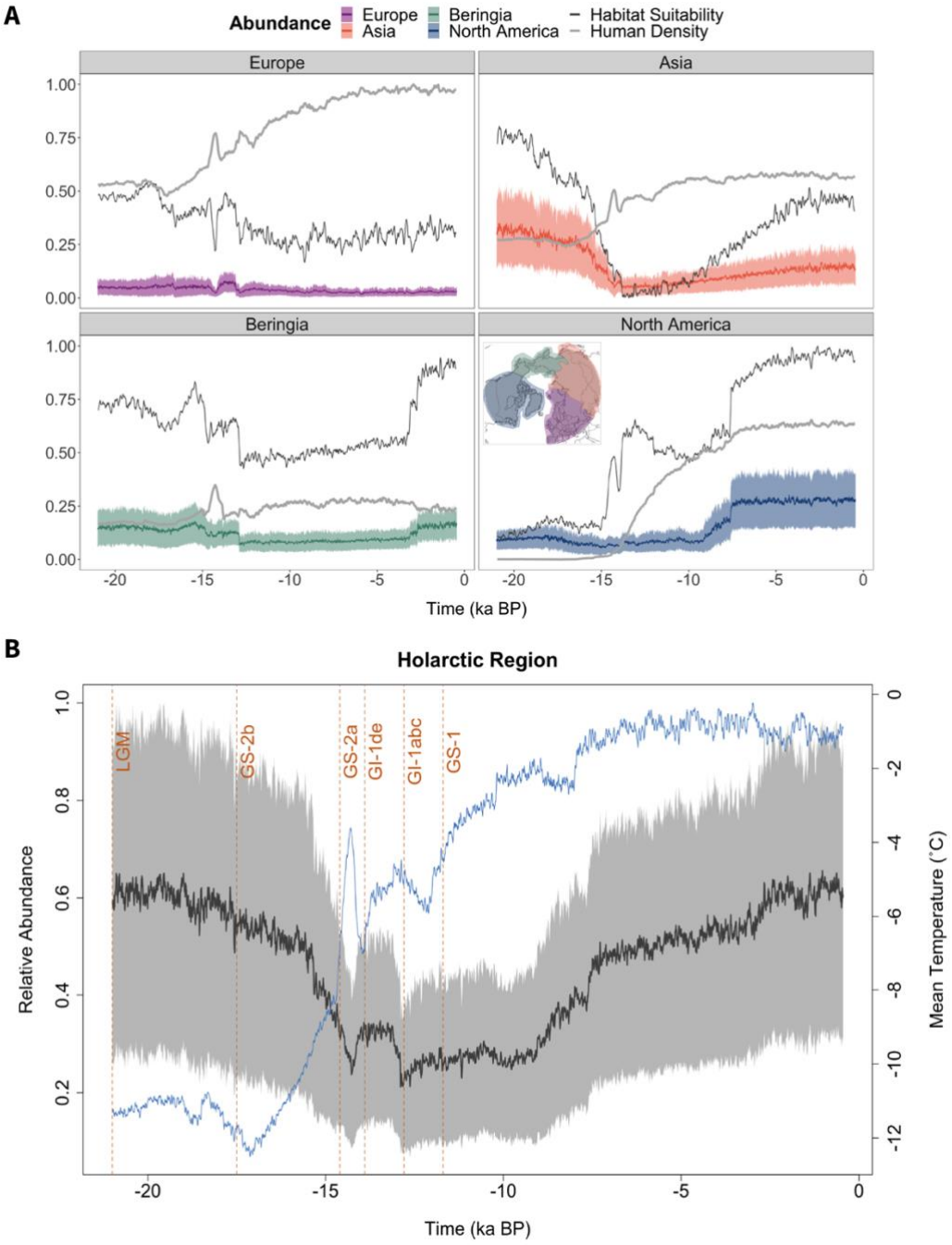

Figure 3. Trends in simulated total abundance.

A, Reindeer relative abundance (mean simulated abundance ± 1 SD), habitat suitability (dark grey thin line), and human density (light grey thick line) in Europe, Asia, Beringia, and North America. Region subdivision is represented as an inset in the North American panel. **B** shows multi-model average relative abundance (mean ± 1 SD) on the left y-axis and mean temperature on the right y-axis (blue line), over the full Holarctic region. Orange vertical lines show the time of major climatic events since 21 ka BP.

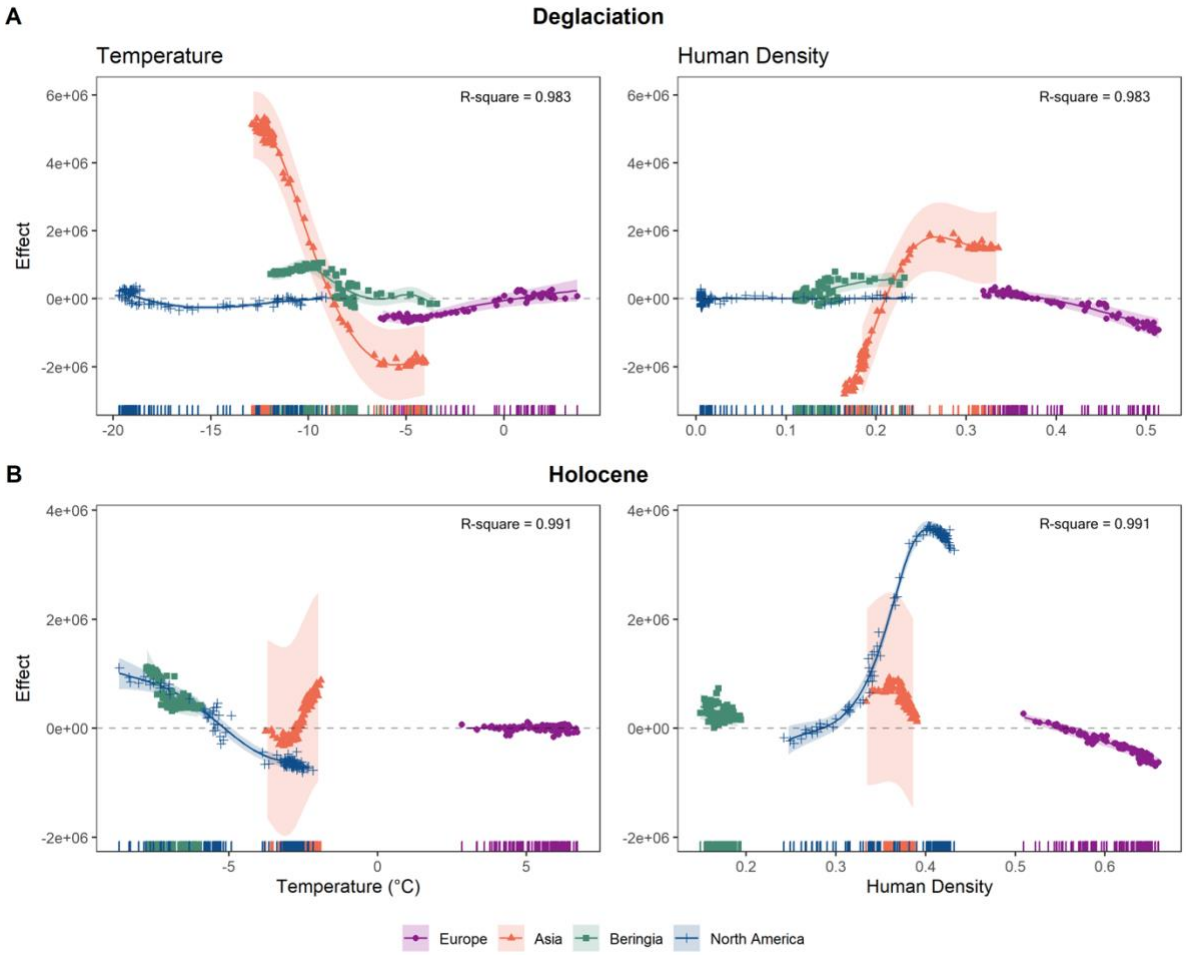

Figure 4. Effect of temperature and human density on reindeer abundance.

Relationship between trends in reindeer abundance and average temperature and human density for Europe, Asia, Beringia, and North America. Coloured lines represent the effect (y-axis) of average temperature and human density (x-axes) on reindeer abundance over the last deglaciation (21 – 11.7 ka BP) (**A**) and over the Holocene (11.7 ka BP – 1500 C.E.) (**B**) according to generalised additive models. The shading represents the 90% CI around the effects. Coloured points represent the partial residuals. Rugs on the x-axis show the distribution of the predictors for each region.

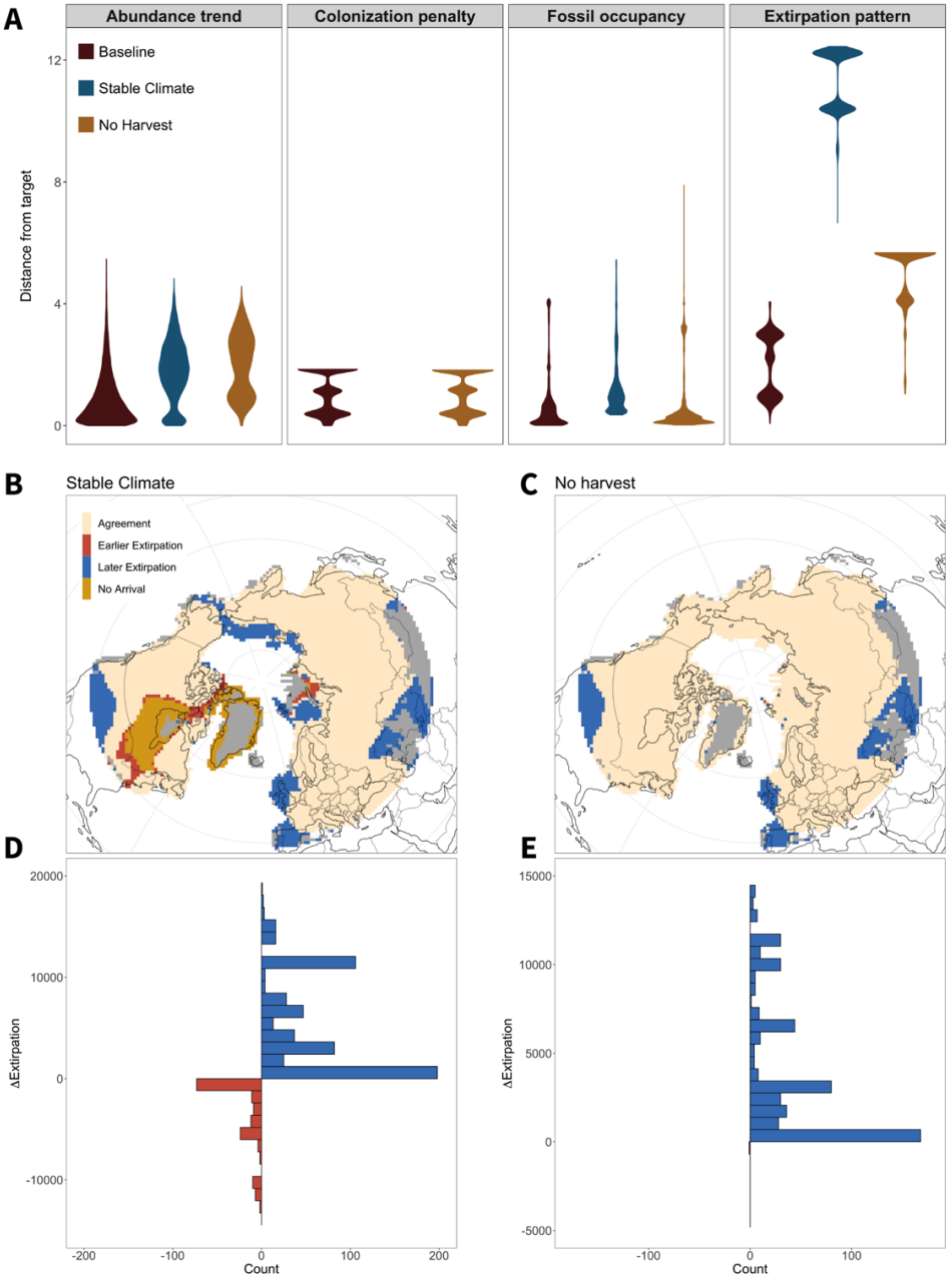

Figure 5. Footprint of humans and climates on the range dynamics of reindeers. **A**, Violin plots showing the Euclidean distance between summary statistics and validation target for the baseline (human harvesting and climate change) and two counterfactual scenarios: no climate change from 21 ka BP (Stable Climate) and no harvest through the simulation (No Harvest). Violin of colonization penalty for the "Stable Climate" scenario is missing, as no model simulated arrival in Greenland. Maps show the difference in extirpation times between the baseline and the "Stable Climate" scenario (**B**) and between the baseline and the "No Harvest" scenario (**C**). Histograms show the years of difference in extirpation times between the baseline and each scenario (**D**: Stable Climate; **E**: No Harvest).

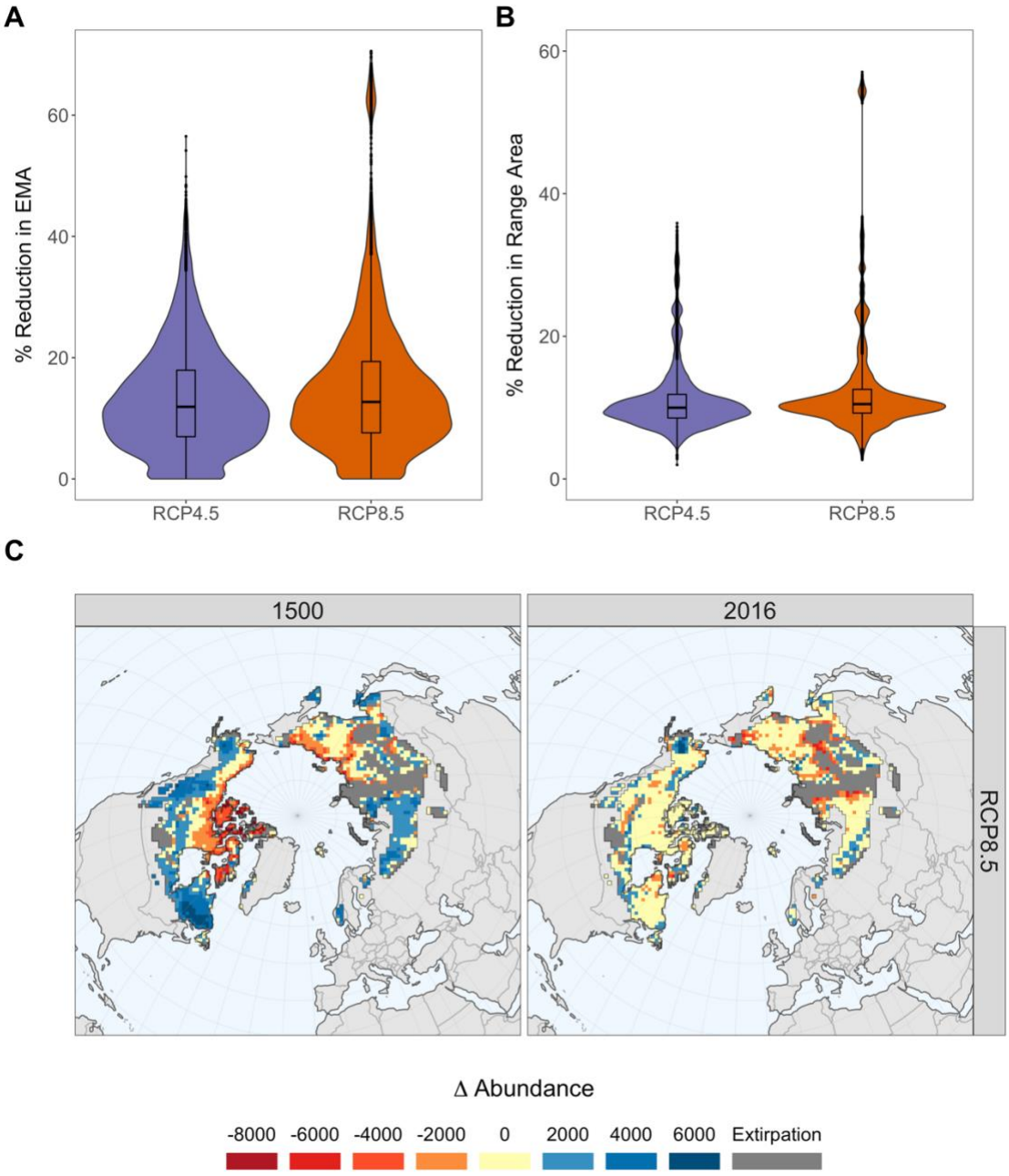

Figure 6. Reduction in future abundance and range area.

Violin plots show reduction in Expected Minimum Abundance (EMA) (**A**) and in range area (**B**) for the period 2016 – 2100 under two RCP trajectories (RCP4.5: blue; RCP8.5: red). **C**, Difference in absolute abundance between 2100 and 1500 and between 2100 and 2016. Warm colours indicate higher abundances in 1500 or 2016 compared to the future, while cool colours indicate higher abundances in 2100. Pale yellow indicates no change and dark grey indicates areas of future extirpation. Projections are based on outputs from 10,000 optimised models.

Supplementary Methods

Data

Fossil records and modern occurrences

We compiled dated georeferenced fossil records and modern observations of reindeers (*Rangifer tarandus*) to model the ecological niche of the species over the last 21,000 years, and to estimate regional extinction and colonisation events.

Fossil records provide geolocations of individual animals that roamed in Eurasia and North America during the Late Pleistocene and Holocene. All records were obtained from the literature and publicly available databases, including Stage3, Neotoma, CARD, and PIDBA (*96-99*). For each fossil record, we obtained information about its location, age, dating method, and association with human remains. We calibrated the radiocarbon dates using the OxCal online tool and the IntCal20 calibration curve (*69, 70*). To assess the quality of the fossil records, we followed the criteria defined by Barnosky & Lindsey (*68*). We discarded unreliable records (i.e., score ≤ 10; n = 297), records with no date (n = 5), and records with calibrated dates older than 21,000 years BP (n = 449). We obtained a final number of 939 fossil records, that we used to calibrate the climatic niche (Appendix 1; Figure S2).

Modern records of reindeers (n = 16,564) were retrieved from GBIF (https://doi.org/10.15468/dl.cl2hdw) (*71*). We removed records with missing or incorrect coordinates, missing date information, and records from re-introduction or translocation areas, fossils, and zoo specimens. The remaining records come from museum specimens, and human (citizen science projects) or machine (camera-traps) observations. We filtered out unreliable records, by constraining records to the known range limits of the species. This filtering resulted in 5,239 modern observations of reindeers to be used for the calibration of the climatic niche (Appendix 1; Figure S2).

Paleoclimate data

We used PaleoView (*72*) to generate gridded paleoclimate reconstructions for the Northern Hemisphere and for the period 21,000 BP to 0 BP. Climatic variables were chosen by considering the potential direct and indirect effects on population dynamics of the species. Temperature in spring-summer and mean annual precipitation are important distant predictors for grazing arctic species because they drive primary productivity and therefore food availability and quality, which in turn

indirectly determines the breeding success and the viability of offspring (*100*). Extreme winter and snow conditions limit access to food and cause increased energy costs reducing fecundity and increasing mortality of arctic ungulates (*100, 101*). The temperature of the coldest month can therefore be used as proximal predictor for physiological constraints.

We generated continuous 30-year average projections for average minimum daily temperature in January, average maximum daily temperature in January, average maximum daily temperature in July, precipitation seasonality, annual precipitation, and temperature seasonality at generational time steps (7 years; see below). We also generated monthly, seasonal, and annual reference evapotranspiration (ET) using mean minimum temperature, mean maximum temperature, monthly precipitation (all extracted from PaleoView) and solar radiation estimated from latitude, using a modified Hargreaves equation [Equation 5 in Droogers and Allen (*102*)]. Combinations of mean annual temperature, mean temperature of the warmest month, mean temperature of the coldest month, mean winter temperature, mean summer temperature, annual precipitation, precipitation seasonality and ET have been previously used to model range dynamics of large vertebrates in Eurasia (*19, 38, 48, 103*). These climatic variables are also important distal predictors for arctic grazers, as they influence plant community composition and primary productivity, and thus forage availability and quality, which ultimately affect vital demographic rates and reindeer population dynamics (*104*). While important proximal predictors, such as snow depth and snow conditions (*100, 104*) were considered, they are difficult to simulate at a Holarctic scale (*105*), particularly over paleo time scales.

The spatial resolution of the paleoclimatic data was resampled from 2.5 x 2.5˚ to 1 x 1˚ resolution, using bilinear interpolation. All fossils were paired to the paleoclimate projections by intersecting climatic values in each specific georeferenced fossil location for the period ± 1SD around the age of the fossil (*11*). Values for precipitation and ET were then rounded to 2 decimal places, with temperature rounded to one decimal place. Fossil records that had identical climate values in space and time were then merged to keep unique records only. For example, in a location with records: fossil A = 10,800 – 7,500 cal BP; fossil B = 11,500 – 10,000 cal BP; fossil C = 11,200 – 9,400 cal BP, the resulting set of climatic conditions will belong only to fossil A (10,800 – 7,500) and fossil B (11,500 – 10,800).

To better capture the climatic niche of the species, we decided to randomly sample points from the Eurasian part of the range of the species, as defined by the IUCN Red List (*2*), because most of the modern records were North American observations. We downloaded from the IUCN Red List website (*2*) the shapefile of the range of the species and constrained it to Eurasia. We calculated the

point density (individuals/m^2) in North America, using the GBIF data we already had, and we calculated the number of points that we would have to sample in Eurasia to obtain the same point density. Because we already had some observations (mainly in Scandinavia), we calculated the number of GBIF points already covering the Eurasian range and we subtracted them from the total number of points to be sampled. This resulted in an additional 127 points for minimum temperature in January, annual precipitation and reference evapotranspiration in spring and summer for the year 0 BP (1950 C.E.) to be randomly sampled from the Eurasian range.

Modern climate data

As PaleoView projections do not go beyond 1989 C.E. (*72*), we used the CRU TS v. 4.03 (*74*) to pair the modern climate with the modern occurrences of the species. The CRU climate data contains temperature and precipitation data from 1901 to 2018 at a 0.5 x 0.5° resolution. We resampled the resolution to a 1 x 1˚ grid cell resolution using bilinear interpolation. To align the CRU data with PaleoView, we used a change factor bias correction (*75*), allowing us to align the modern climate data to PaleoView at 1974 C.E. This resulted in continuous projections of our climate variables from 21,000 BP to 2018 C.E.

We paired the historical (GBIF) records with the modern climate by assuming that the individuals were present on the same location for one generation. We extracted all the climatic values associated to half a generation before and after the year of the observation, in a specific location. As an example, a reindeer record dated 2001 will be associated to climatic values that span the interval 1998-2004, with a generation length of 7 years. We excluded records that did not have matching years. As for the paleoclimate, we removed duplicated sets of values.

Climatic niche

We used the climatic values associated with fossil and modern occurrence records to derive a multi-temporal n-dimensional hypervolume of the climatic niche requirements of the reindeer, representing the climatic space where the species can persist and thrive (*76, 106*). We did this using the 'hypervolume' package in R (*106*).

Before building the niche models we tested for collinearity among climatic variables, defining as threshold $|r| > 0.7$ (*107*). We used the three least correlated variables ($|r| < 0.7$) to generate the niche hypervolume: 1) average minimum daily temperature in January; 2) annual precipitation; 3) total ET in spring and summer. We built gaussian hypervolumes, tuning the kernel density estimation (KDE)

bandwidth using cross-validation (*106*). The final hypervolume contains 30,426 set of climatic conditions (data points, Figure S3), and approximates the fundamental niche of the reindeer (*76*).

We exhaustively subsampled the full multi-temporal niche hypervolume by setting cutting 'boxes' with different widths (from 0.5 to 1, every 0.05), and moving throughout the 3-dimensional space. These subsamples are representative of the potential realised niche used by the reindeer and allowed the actual realised niche of the reindeer to be identified in a later step using process-explicit macroecological modelling (see below). This process generated 7,405 unique niche subsamples. We calculated marginality (OMI) of each unique niche subsample using the 'ade4' R package (*108*), based on the method described in (*77*). The breadth of each niche subsample was calculated based on the volume of the resulting 3-dimensional hypervolume. To do this, each subsample hypervolume was generated, using the KDE bandwidth of the full niche hypervolume. To relate each subsample to the full niche, the data was scaled and centred based on the mean and SD of the full niche. We used measures of breadth and marginality to select 2,500 potential realised niches for reindeer, ensuring that the distributions of marginality and breadth for the 7,405 niche samples were maintained.

We used the 2,500 potential realised niches and the full niche for the reindeer to project climate suitability through space and time (every 7 years), using the 'hypervolume_project' function in the 'hypervolume' R package (*106*), for the period 21,000 BP to 1500 C.E. Projections using this kernel density approach at its default settings produce similar results to the standard maximum entropy method (Blonder et al., 2018). Ecological niche models of climate suitability were then reprojected using bilinear interpolation to a Lambert Azimuthal Equal Area projection centred on -15° east and 57° north, with a resolution of 100 km x 100 km.

Human densities

We modelled the peopling of Eurasia and North America by Paleolithic humans using the Climate Informed Spatial Genetics Model (CISGeM), where genetic history and local demography is informed by paleoclimatic and paleo-vegetation reconstructions of net primary productivity (NPP) (*79*), which has been shown to be a primary determinant of global human population densities (*109*). The model has previously been shown to reconstruct arrival times of anatomically modern humans and current-day distributions of global and regional genetic diversity (*79, 80*). Like other numerical models of early human migration (*56*), arrival, occupancy, and density (here N_e) are forced by spatiotemporal estimates of climate and sea level changes over the past 125 thousand years.

In CISGeM, the world is represented by a hexagonal grid, each cell 100 km wide. The potential number of people who can live in each cell (carrying capacity) is determined by

reconstructions of NPP done by coupling the HadCM3 paleoclimate model to the Miami vegetation model (*110*). Every 25 years (approximately the generation time of humans), the carrying capacity is updated to allow for changes in climate, as well as sea level and ice sheet extent. At each generation, any cell that is inhabited will grow with a rate *r* (until it reaches the local carrying capacity), sending out migrants to other inhabited cells at rate *m*, or colonists to previously uninhabited cells at rate *c*. The relationship between carrying capacity and NPP, as well as the values of other demographic parameters, were fitted using pattern-oriented methods (*111*) using an Approximate Bayesian Computation framework (*86*). Targets for model calibration were pairwise genetic differentiation among a large panel of modern-day human populations. In other words, the demography was calibrated to produce realistic genetic differentiation patterns across the globe. Eriksson *et al.* provide a detailed description of CISGeM parameters and procedures (*79*).

Based on the ABC fit (*79*), we took the best 4,950 parameter combinations and reconstructed population sizes through time. Effective population size in 21,000 BP was initialised (for each parameter combination) with values based on the HadCM3 climate model. A burn-in period of approximately 80 generations (where climatic conditions were held constant at 21,000 BP conditions) was used to ensure equilibrium effective population size at the beginning of the simulation. An upper plausible threshold for N_e was set at 500 individuals per grid-cell based on estimates of true abundance in modern-day hunter-gatherer societies (*112*). We filtered for runs in which humans colonize North America and Greenland, and we calculated average $N_e \pm$ SD. The final average and SD in human populations was projected to match the climate suitability projections. Finally human densities based on N_e were scaled between 0 and 1, using the 95^{th} percentile of the ensemble mean as threshold.

Process-explicit models

Ecological niche models of climate suitability and CISGeM estimates of human population size were coupled with stochastic demographic models to simulate extinction and colonization dynamics and other metapopulation processes at the landscape level (Figure S1). The resulting process-explicit macroecological model was coded in R using the 'poems' and 'paleopop' packages (*84, 85*). The models were run at generational time steps (7 years) from 21,000 BP to 1,500 C.E.

Generation length

We used a generation length of 7 years following the calculations from Pacifici *et al.* (*78*), according to the following equation:

$$GL = R\_span * 0.29 + AFR$$

Where *R_span* is the species reproductive life span, defined as the difference between the age at last reproduction and the age at first reproduction (*AFR*) (*113, 114*). A generation length of 7 years for the reindeer has also been approved by expert knowledge.

Upper abundance

The upper abundance (carrying capacity) of each cell was based on climate suitability (*115*). To convert climate suitability to upper abundance, we assumed that the maximum area of suitable habitat in any given cell was ≤ 2,500 km^2 not 10,000 km^2. This approach appropriately addresses the mismatch between the spatial scale of the model and how reindeers are likely to have used the landscape (*11, 116*). We set upper abundance at 3.3 reindeers/km^2 and allowed it to vary between 0.4 and 6.2 individuals/km^2. These values are based on density estimates for populations that have been monitored during winter (*117*). Reindeers tend to aggregate in very high numbers to forage during summer, resulting in biased estimate of population densities (*118*). We specifically looked for estimates resulting from monitoring schemes occurring during other seasons.

Population growth

We used time series data of population abundance (Figure S4) to calculate finite rates of population increase and their variance, and maximum population growth rate (*119*). Specifically, we fitted linear models to time series data from Finland (n = 4), Norway (Svalbard) (n = 3) and Norway (mainland) (n = 3) (*120-122*), using the 'fit_easylinear' function of the 'growthrates' package in R (*123*). These time-series are either density or count data, contain no gaps and have more than 5 years of sampling. We used only the increasing subsets of the time-series to calculate maximum growth rate. To better understand model fit and its sensitivity to the number of data points in the time series, we repeatedly fitted models to 3, 4, 5, 6 and 7 data points for each time-series. We then selected, for each time series, the estimate of maximum growth rate resulting from the model with the highest R^2. The upper range of the estimates comes from Brøggerhalvøya (Svalbard) time-series, with a model fit to 3 data points. The lower range of the estimates comes from the Rakkonjarga (Norway) time-series, with a model fit to 5 data points. This resulted in a parameter range for Rmax of 1.087 – 1.347. We scaled Rmax to the generation level by taking the exponent (1.347^7) and treated this as an upper estimate of Rmax in the model, with a parameter range of maximum R0 = 1.75 – 7.94.

We used time series data for 4 populations around carrying capacity to calculate the standard deviation (SD) in population growth rate (*120-122*). We used the years 1998-2013 of the Reindalen (Svalbard) time-series, the years 2005 – 2013 of the Rakkonjarga (Norway) time-series, and the full time-series for Palojarvi (Finland) and Snøhetta (Norway). For each time series, we modelled a fictional population already at carrying capacity, fluctuating for 700 years (100 generations). We set an initial abundance of 1000 individuals, with carrying capacity at 1000 individuals. Doing this resulted in a mean estimate of SD_{R0} of 0.35, which we treated as an upper estimate based on model simulations. The upper and lower bounds for SD_{R0} were set at 0 to 0.35 (Table S1).

Density dependence was modelled in the process-explicit simulations using a Ricker-logistic function (*124*). A Ricker-logistic function was chosen because it assumes an almost exponential growth rate when populations abundances are small and predicts a decrease in population growth rate when populations approach carrying capacity, reflecting competition for resources at carrying capacity.

Dispersal

Studies indicate that the reindeer is a highly mobile species, being the species with the longest terrestrial migrations (*125*). The round-trip Euclidean migration distance within a year was calculated to be 1350 km (*125*), making the one-way distance 675 km. We treat the latter as the maximum distance the species can disperse in one generation, assuming that individuals are able to move that far. We use an average maximum distance of 385 km, which agrees with the range shift and expansion monitored during one generation for populations in Alaska (*117*, *126*). We set upper and lower bounds on the percentage of population dispersing per generation of 5 – 30% (*119*) and on maximum dispersal distance of 100 – 675 km.

Dispersal was modelled using the following equation:

$$m_{ij} = \begin{cases} a^{\left(\frac{-D_{ij}}{b}\right)}, & D < D_{max} \\ 0, & D \geq D_{max} \end{cases} \quad (2)$$

Where movement (m) between cell *i* and *j* is a function of the parameters *a*, *b*, and *Dmax*; and *Dij* is the distance between the two populations. The parameter *a* is 0.5 × the total proportion of dispersers that leave a cell at each time step and *b* and *Dmax* are modelled as one of 9 combinations depending on the estimate of D (Appendix 3 [Table 2] in Fordham *et al.* (*11*)). This approach prevents large dispersal rates to closely neighbouring cells (i.e., the drainage effect) by pre-calculating a fixed proportion of individuals that should move to a given cell based on *a*, *Dmax* and *Dij*.

Dispersal was limited depending on the habitat suitability within source and target cells, and on the proportion of glacial ice present in target cells. Dispersal was completely blocked to cells covered by the sea and fractionally reduced to cells containing glacial ice. We did this using a friction map and distance-equivalence multipliers, calculated using a cost-surface generator (*82*). For example, if two patches of highly suitable habitat are separated by a strait, following the land towards the second patch is less costly than directly crossing the strait.

Allee effect

We set a local quasi-extinction threshold (*116*) which made cell abundance zero if abundance fell below the Allee threshold. Due to lack of information on Alle effect for reindeer, we followed the methodology used for the woolly mammoth in Fordham *et al.* (*11*). The range of values for the Allee effect were 0 (i.e., no Allee effect) to 500 individuals per grid cell (Table S1).

Environmental correlation

This was a fixed parameter in our models that was set to b = 850 km (*60*), where b is the decay constant of an exponential decline model. This parameter accounts for similarity in environmental fluctuations for populations located close together versus further apart.

Human hunting

Human hunting of reindeers was modelled as a function of the timing of arrival and relative density of humans at a given cell. Using Latin Hypercube sampling (see below) we generated 100,000 plausible reconstructions of human population abundance, by sampling within ± 1 SD of N_e using a lognormal distribution (*11*). Because reindeers were among the favourite preys of anatomically modern humans, we let the maximum exploitation vary between 5% and 50% of the population abundance, under a Type II to a Type III functional response. Harvesting is modelled as a function of density of prey population (P; current population size divided by maximum population size), maximal predation rate (F), prey density at which predation is half-maximal (G), and a measure of departure from maximal predation (z). The equations used to model harvest can be found in Fordham *et al.* (*11*). In our models, the parameter z is a variable parameter, which takes values between 1 and 2 (*127*). A value of z = 1 results in a Type II functional response, where predation is modulated only by prey density and predator satiation, implying complete naivety of prey. At z > 1.5 hunting success takes on an increasingly sigmoidal Type III functional response, under which prey become harder to hunt at low densities. This might result from prey adaptation (evolved or learned behaviour), prey

switching by hunters, or prey being located in refugia (*128, 129*). Parameter G was set constant to 0.4 (*127, 129*), and F varied from 0.05 to 0.50. The harvesting pressure was set globally – i.e., there were no regional differences in harvesting pressure.

Latin Hypercube Sampling

We generated process-explicit macroecological models using combinations of values for demographic parameters and environmental attributes that varied across plausible ranges (*82*). Sampling of these values was done using Latin Hypercube sampling from uniform distributions, providing a robust coverage of the multi-dimensional parameter space (*130*). We produced 100,000 conceivable models with different combinations of demographic parameters values using mean (± 1SD) estimates of human abundance. We produced another estimate of 100,000 conceivable models with demographic parameters identical to the first set but using the median (± 1 MAD) estimate of human abundance. This resulted in 200,000 plausible demographic models, each of which we ran as a single replicate (*83*).

Models were initialised at carrying capacity in all areas except Greenland, where abundance was set to zero in any cells with carrying capacity greater than zero. Following initialisation (i.e., burn in) cells in Greenland were allowed to be colonised. We did this because although ice-free areas were present in Greenland during the Last Glacial Maximum, these were unlikely to have sustained vegetation and animals (*131*).

Pattern-oriented modelling

We used pattern-oriented modelling (POM) techniques (*44*) to evaluate the adequacy of the process-explicit macroecological models to simulate mechanistic responses to climate change and human exploitation, and to reconstruct known range dynamics and the current distribution of the reindeer. Model simulations of changes in abundance through time and space were assessed using a multivariate target based on inferences from the fossil record and historical observations.

Observed and modelled summary statistics

We extracted summary statistics for each simulation and calculated the deviation from the simulated and inferred pattern. We did this for:

- Occupancy pattern: agreement between simulated and inferred occupancy. Occupancy at a fossil site was correctly simulated if there was positive abundance in that grid cell (or the 8

surrounding cells) during the calibrated age ± 1SD. We summed the number of records where there was agreement between simulated and inferred occupancy.

- Local extirpation pattern: based on the fossil record, we calculated times of extirpation across four sub-regions in Europe: Iberia (Iberian Peninsula at its maximum extent of land), British Isles (including UK and Ireland), South Central Europe (Europe below 50˚N), North Central Europe (Europe between 50˚N and southern Sweden) (Table S2). We used the 'GRIWM' method (*132*) to calculate regional extinction time, which accounts for the Signor-Lipps effect (*87*). The resulting extinction times were: 12,727 BP (95% CI: 12,995 BP – 12,418 BP) for Iberia, 9,120 BP (95% CI: 9,385 BP – 8,880 BP) for British Isles, 9,677 BP (95% CI: 10,182 BP – 8,956 BP) for South Central Europe, and 3,443 BP (95% CI: 3,665 BP – 3,232 BP) for North Central Europe. We calculated the Root Mean Square Error (RMSE) of the difference between the simulated and inferred regional extinction times, from the fossil records, and from each simulation (*82*).
- Arrival time in Greenland. We used 'GRIWM' to calculate an arrival time in Greenland of 9,294 BP (95% CI: from 9,643 BP to 8,938 BP) based on the fossil records. Simulated time of arrival was calculated as the first positive abundance in Greenland and the number of generations away from the inferred arrival window was noted. If the arrival time in our simulations fell within the mean ± 1SD arrival time based on the fossil records, the penalty was 0.
- Slope of the total abundance trend. For each simulation we calculated total abundance over the full period and fitted a linear regression. We did the same with the Bayesian Skyline Plot of effective population size (N_e) for the reindeer. We then used the slope of the N_e as target for validating the simulations, meaning that simulations whose slope in total abundance trend approximate the slope in N_e were selected.

Effective population size

Trends in effective population size (N_e), as Bayesian Skyline plots, can be used as validation target of the change in total population size. The Bayesian Skyline plot of effective population size for the reindeer was calculated using a previously compiled dataset, containing 853 radiocarbon-dated fossils of reindeer, out of which 162 have associated aDNA sequences, which are available in GenBank (*133*). Sequences were aligned in Geneious v1.9.8 (*134*) using default settings of the MUSCLE algorithm (*135*). Radiocarbon dates were calibrated using OxCal and the IntCal13 calibration curve

(*136*). We reconstructed the genealogy using BEAUti v.1.10.4 and BEAST v1.10.4 (*137*). We used the average calibrated date of each fossil record as prior information for the tip-dates, and the standard deviation to derive uncertainty in the tip-dates. We used jModelTest v2.1.10 (*138*) to find the best substitution model and, based on Akaike's Information Criterion (AIC), we selected the HKY + Gamma + Invariant Sites substitution model. We used a strict molecular clock, a Coalescent Bayesian Skyline Tree Prior, a constant Skyline Model and the UPGMA starting tree. The Markov Chain Monte Carlo run was set with a chain length of 10^8 and to log parameters every 10^4 simulations to avoid possible autocorrelation during the MCMC analysis. We then analysed the output using Tracer v1.7.1 (*139*). Our approach resembles the approach used by (*20*) to investigate changes in mammal N_e based on aDNA and contemporary sequences.

Approximate Bayesian Computation analysis

We used Approximate Bayesian Computation (ABC) (*86*) to validate our 200,000 process-explicit simulations using the 'abc' package in R (*88*). Specifically, we used ABC to fit the simulation models to data and estimate (and narrow down) the posterior distribution of model parameters. There were 12 variable parameters in the process-explicit models, covering demographic, harvest, and niche parameters (Table S1). We used the 'rejection' method and a modified version of the 'abc' function in the 'abc' R package. With the rejection method, Euclidian distances are calculated between each summary statistic and the target. In the modified function, we scaled the Euclidean distances using the SD of the data, and not the median absolute deviation (MAD, the default), following Equation 5 in van der Vaart *et al.* (*89*). The SD was chosen as scaling factor because the MAD of one summary statistic (colonization penalty) was zero, leading to an undefined distance. Simulations were accepted if the sum of the distances fell below the threshold defined by a tolerance value of 0.0025 (*88*). ABC modelling is therefore selecting simulations that can simultaneously replicate multiple key biogeographical patterns.

After the first run of simulations, the "best" models did well at hitting inferences of spatiotemporal occurrence and change in total population size but found it more difficult to replicate the extirpation patterns in Europe and timing of colonisation in Greenland. To improve the ability of the models to hit the validation targets, we decided to run additional sets of 10,000 simulations using informed priors. For each parameter, we generated new values under different distribution types (uniform, normal, lognormal, Poisson, gamma, beta, negative binomial) constrained within the 90^{th} percentile of the posterior parameter distributions (ranges of posterior values in Table S1). We compared each distribution to the original posterior parameter distribution by calculating minimum

AIC values and the delta AIC (ΔAIC). Based on the distribution with the lowest ΔAIC, we sampled 10,000 values for each parameter, which we used to run additional process-explicit simulations. Niches for the following runs were selected based on the range of OMI and volume of the niches selected from the ABC. Niches whose values of OMI and volumes were within the range of minimum and maximum OMI and volume of the niches used in the best model were retained. After each run of simulations, we repeated the ABC validation to extract the best models. We used Bayes Factors to estimate parameter convergence after each run. If the prior and posterior distribution of each parameter did not converge, we repeated the process of sampling new informed priors, running the simulations and validating the simulations with ABC. We repeated this process a total of seven times.

Model fit

We calculated model fit with the 'gfit' function of the 'abc' package, and with posterior predictive checks. We calculated summary metrics for each model and then calculated the distance between the summary metrics for each model and the target, and the distance among summary metrics across the models. The models are expected to be a good fit of the observed data if the distances 'between' and 'among' are congruent (*140*). However, at the end of the optimisation process the model was not a good fit for two targets out of four (fossil occupancy and extirpation pattern; p-value < 0.001) (Figure S5), resulting in a poor model fit. This was confirmed by the Goodness-Of-Fit (GOF) analysis from the 'abc' package, resulting in a p-value of 0.01. Therefore, we decided to calculate model fit for each of the previous runs. The run with the best model fit was the third run, with a GOF p-value = 0.274 and posterior predictive checks resulting in p-value = 1 for three out of four targets (Figure S5). The poor model fit for runs following the third run indicate model overfit. Therefore, the results presented in the manuscript are for the third run.

Timing of extirpation

The selected models were used to generate an ensemble average of total population abundance, human density, and number of harvested individuals, all weighted by the inverse of the Euclidean distance of the model from the idealized targets. Based on the ensemble average of population abundance, we generated an extirpation map showing the timing of extirpation in each grid cell up to 1500 C.E.

Effects of climate change and human harvest on reindeer abundance

To determine the magnitude of impacts of climatic changes and hunting by humans on reindeer abundance and distribution, we performed two counterfactual scenarios: no harvest, in which there is climatic change but no modelled hunting by humans, and stable climate, in which human harvesting is present but climate suitability at 21,000 BP has been held constant until the end of the simulation (1500 C.E.). The counterfactual scenarios were run using informed priors, deriving from the posterior parameter distribution of the selected models, as determined by the ABC. We ran 10,000 simulations per scenario and compared them to the baseline (non-counterfactual) posterior draws of the selected models. We calculated the ensemble average from the 10,000 simulations for the baseline model and the two counterfactual scenarios to calculate extirpation maps, one for each scenario. We then calculated the difference between the baseline extirpation map and each of the two scenarios.

To disentangle regional and temporal effects of climate change and human hunting on reindeer total abundance, we analysed the abundance trend of the ensemble average of the selected simulations using gaussian generalised additive models (*92*). We analysed the abundance response in four separate sub-regions (Europe, Asia, Beringia, and North America) and for two periods of time (Deglaciation: 21 – 11.7 ka BP; Holocene: 11.7 ka BP – 1500 C.E.). We used mean abundance over 100-year time bins as our response variable, with combinations of average temperature (°C), and average human density (scaled N_e). Time and regions were used as random effects. The model can be expressed as:

$$Abundance \sim s(Temperature, by = Region) + s(Human\ Density, by = Region) + s(Time) + s(Region)$$

Future impacts of climate change

To predict reindeer responses to future climate change, we ran process-explicit macroecological models at generational time steps for the period 2016 – 2100, parameterised using the posterior parameter distributions of the paleo-models selected by ABC. Carrying capacities were constrained using land-use change projections for the same period, and abundances were initialised based on the current range of the species.

Climate data

We accessed future projections of climate change using StableClim, which includes paleoclimate simulations from the TraCE-21ka experiment for the period 21,000 BP – 100 BP (1850 C.E.),

historical simulations (1850 – 2005) for 19 Atmosphere-Ocean General Circulation Models (AOGCMs) from the Coupled Model Inter-comparison Project phase 5 (CMIP5), and the Representative Concentration Pathway (RCP) 2.6, 4.5, 6.0, and 8.5 trajectories for the same 19 AOGCM used for the historical simulations (*94*). We used RCP 4.5 and RCP 8.5 to run simulations under an intermediate scenario and a worst-case scenario, respectively. StableClim projections were aligned to the paleoclimate data used to build the multi-temporal climatic niche of the reindeer using the change factor bias correction (*75*) and anomalies for the year 1974 C.E. (Figure S7). We checked that the newly aligned dataset projects future anomalies for the Arctic (above 66°N) that are congruent with the literature. We used the average of the years 1980 – 1999 as baseline and calculated the difference between the baseline and each year between 2000 and 2100, for minimum temperature in January, maximum temperature in July and annual precipitation. Maximum and mean anomalies for the years 2000 – 2100 are shown in Figure S8 and agree with other estimates of anomalies for the Arctic by 2100 (*141, 142*). Niches selected from the ABC analysis on the paleo-models were used to project climate suitability across space and time, at generational time steps (7 years) and for the years between 1953 – 2100, using the 'hypervolume_project' function in the 'hypervolume' package in R (*143*). Ecological niche models of climate suitability were then reprojected using bilinear interpolation to a Lambert Azimuthal Equal Area projection centred on -15° east and 57° north, with a resolution of 100 km x 100 km.

Land-use change

We applied a land-use change multiplier to the carrying capacities in the models, in order to constrain the population models to areas with levels of disturbance suitable for the species. Land-use change projections for the years 2016 – 2100 were accessed using the Land Use Harmonization Project version 1 (LUH1) (*95*). The dataset contains History Database of the Global Environment (HYDE) v3.1 land-use change projections for the years 1500 – 2005, and simulations of land-use change for RCP 2.6, 4.5, 6.0, and 8.5 from CMIP5 (*95*). The database reports the proportion of grid cell that is occupied by cropland, primary land, pasture, secondary land, and urban land. We used the GBIF records to extract the values for each type of land in grid cells occupied by reindeers and calculated the 90% CI of the distributions. We found that the proportion of grid cell occupied by cropland, pasture and urban land was < 0.004, while it was < 0.35 for secondary land and > 0.36 for primary land. Therefore, reindeers are present in primary land and partly in secondary land, while being absent in croplands, pastures, and urban lands. We combined primary and secondary land to set a threshold below which reindeers cannot be found. We extracted the values in occupied grid cells and calculated

the 90% CI (0.42 - 1.00, for both RCP 4.5 and RCP 8.5). Values < 0.42 were converted to 0. The values were then used as multipliers to the carrying capacity in the models.

Process-explicit models

We ran 10,000 models for each climate change scenario (RCP 4.5 and RCP 8.5) parameterised using informed priors, deriving from the posterior parameter distribution of the models selected from ABC (Table S1). Populations were simulated to respond only to changes in habitat suitability, without harvesting. We scaled the carrying capacities based on the proportion of 'undisturbed' land, as defined by the land-use change projections. Abundances were initialised in grid cells within the current range of the reindeer, as reported in the IUCN Red List of Threatened Species (*2*). Models were run at generational time steps (7 years) from 2016 to 2100, with a burn-in period of 50 generations.

Extinction risk and climate analogues

We generated an ensemble average of the 10,000 future simulations, accounting for probability of occurrence (*11*). To determine a minimum threshold for occurrence, we calculated the probability of occurrence that maximized the area under the receiving operating curve for occurrence record based on predictions from a binomial GLM. Occurrence records were downloaded from GBIF, spanning the period 2012 – 2022 (https://doi.org/10.15468/dl.bqyj3b) (*144*). We extracted the mean probability of occurrence for each record and for 25 randomly sampled background points (*145*) for the year 2016. Using 10 repeats of 10-fold cross validation, we built 100 binomial GLMs using different thresholds between 0 and 1 at 0.01 intervals. AUC was calculated for each of the models with the smallest threshold (RCP 4.5: 0.07; RCP 8.5: 0.07) being chosen to maximise AUC (RCP 4.5: AUC = 0.951; RCP 8.5: AUC = 0.949). Probability of occurrences below the threshold were set to 0 and those above the threshold to 1. The binary map was then used as a mask to population abundances of the ensemble average and of each model.

We calculated Expected Minimum Abundance (EMA) and range area (number of occupied cells * area of the cell), for each model after accounting for probability of occurrence. We calculated percentage of reduction in EMA and range area between the year 2016 and 2100 using the equation:

$$\%Reduction = \left(\frac{t_1 - t_2}{t_1}\right) * 100$$

Where t_2 is the value of EMA or range area at 2100 and t_1 is the value of EMA or range area at 2016. Finally, we used the same formula to calculate the percentage of reduction in EMA and range area within millennial bins from 21,000 BP to 1500 C.E., using a rolling window spanning 84 years (12 generations). For each selected simulation, we calculated the percentage of time steps (generations) within each millennial bin that showed a reduction ≥ 15% in EMA and ≥ 13% in range area (same magnitude to what is predicted for the future).

To check for climate analogues between past, present, and future, we first extracted climatic values in grid cells simulated to be occupied by reindeers at 2100. For each time step between 21,000 BP and 1500 C.E. we then extracted the grid cells occupied by reindeers with climatic conditions within the minimum and maximum of the climatic conditions at 2100. We repeated the approach for areas simulated to be occupied by reindeers in 2016. Finally, we calculated the overlap between the present and the Last Glacial Maximum (21,000 BP), and between the present and the Holocene Thermal Maximum (6,503 BP).

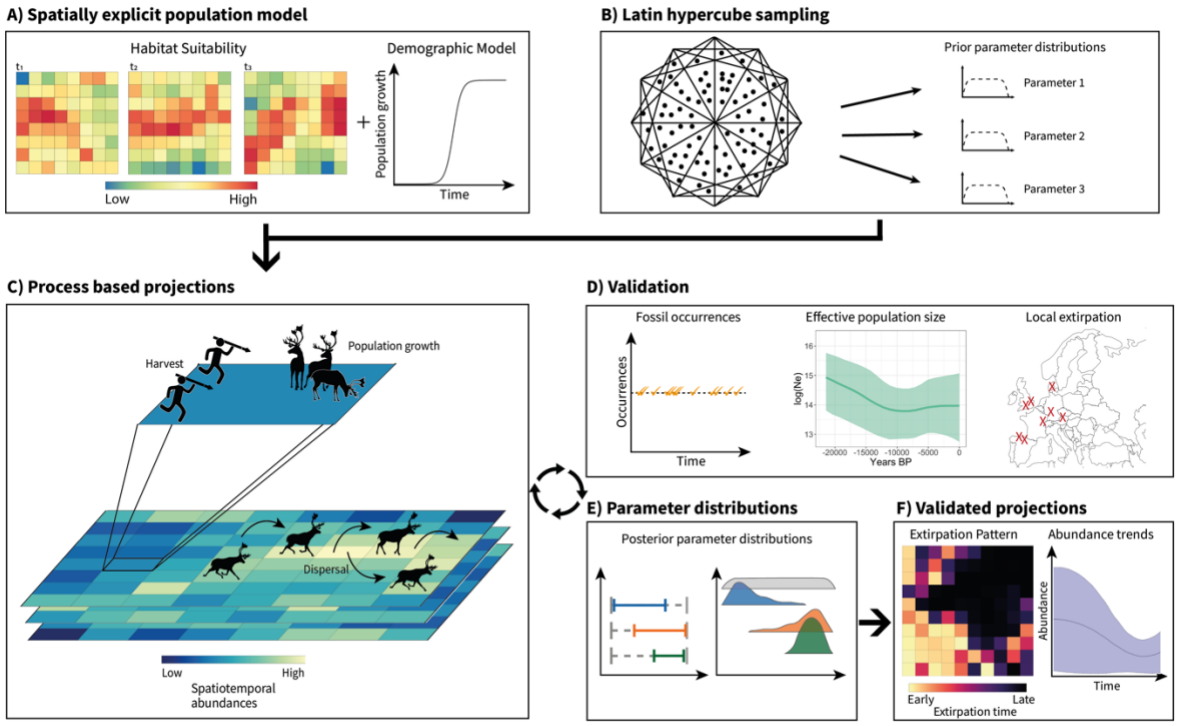

Figure S1. Modelling the range dynamics of reindeer using spatially explicit population models.

A) Spatially explicit population models (SEPMs) account for spatiotemporal change in habitat suitability and demography. **B)** Uncertainty in climate-human-reindeer interactions is modelled by generating thousands of models with unique combinations of parameter values sampled from wide but plausible ranges, using Latin Hypercube sampling. **C)** Each model simulates changes in spatiotemporal abundance in response to climatic change and hunting by humans. **D)** Model projections are validated using Approximate Bayesian Computation and pattern-oriented methods, which compare observed or inferred patterns (targets) to simulated patterns. **E)** Prior and posterior distributions can be visualized to identify important model parameters, which can be used to optimize the models. **F)** After the optimization process, a subset of 'best' models can be used to generate validated projections of abundance and extinction dynamics.

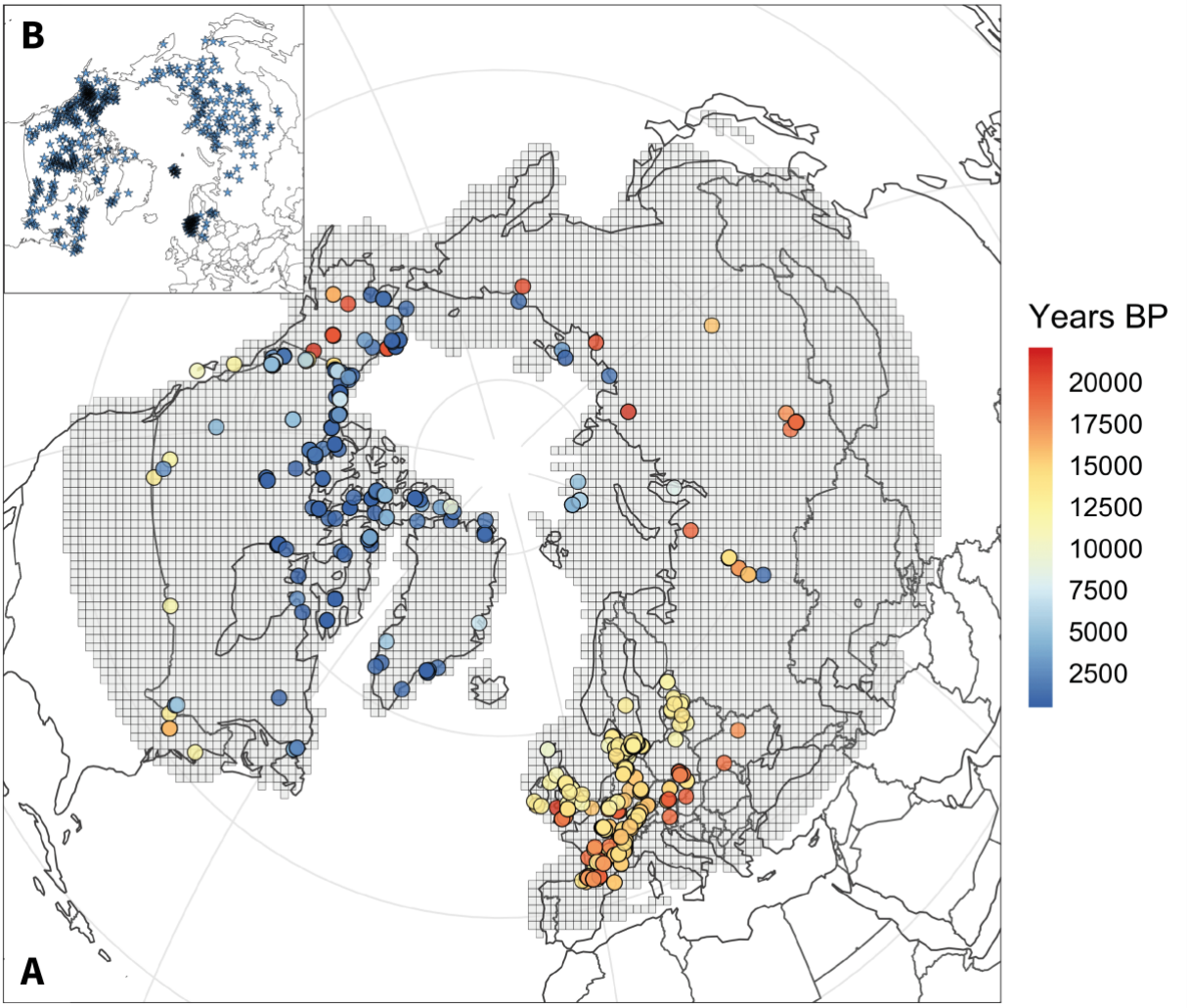

Figure S2. Distribution of fossil records and modern occurrences of reindeer over the study region.

A, the distribution of fossil records over the study region, with red circles representing older fossils and blue circles representing more recent records. **B**, the distribution of modern occurrences obtained from GBIF, representing sightings of individuals occurring only in areas where the reindeer is endemic.

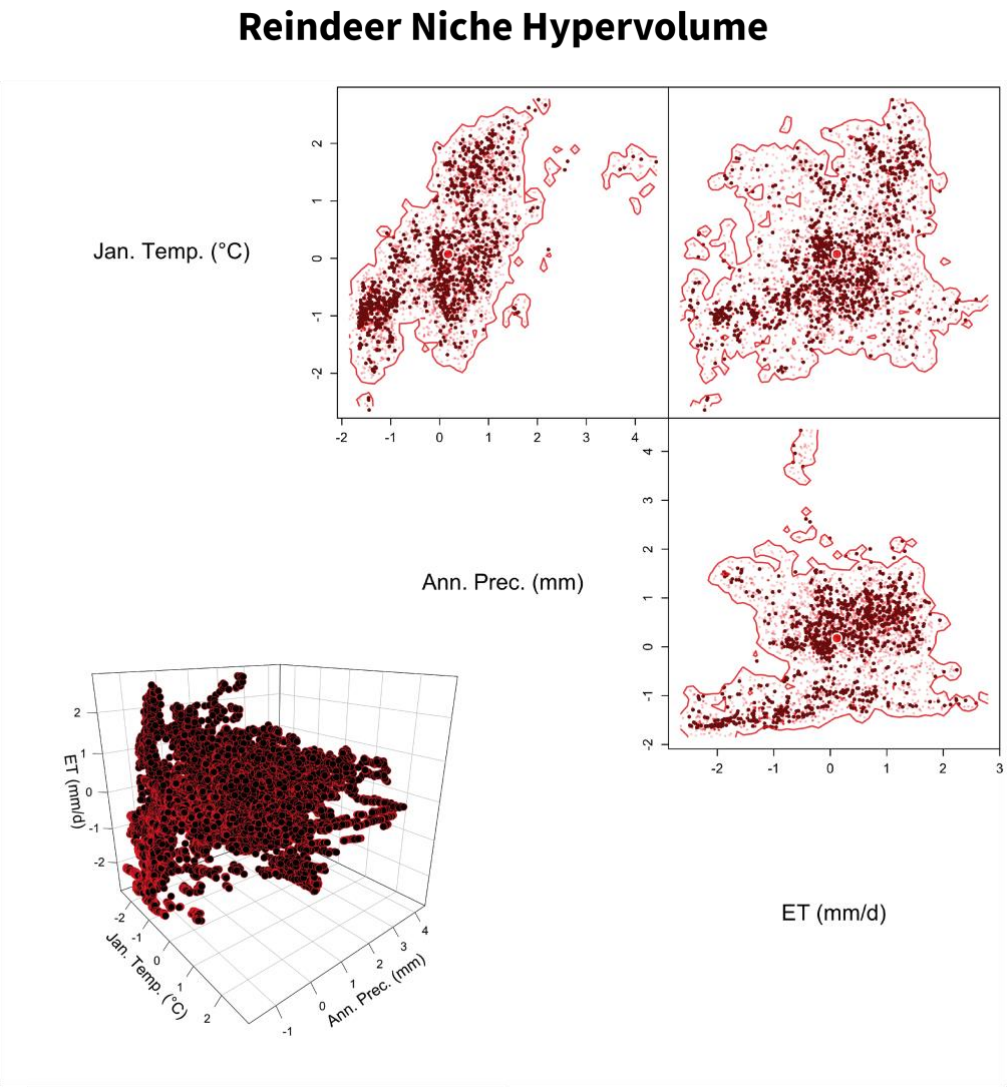

Figure S3. Reindeer Niche Hypervolume.

Here is represented the multi-temporal niche hypervolume of the reindeer in 2-dimensions and 3-dimensions. The hypervolume was built based on 3 climate variables: average minimum daily temperature in January, annual daily average precipitation and reference evapotranspiration in spring and summer. These variables were chosen because they indirectly affect the survival of the species and because they were the least correlated variables. The hypervolume gives a representation of the climatic space where the species can persist and thrive.

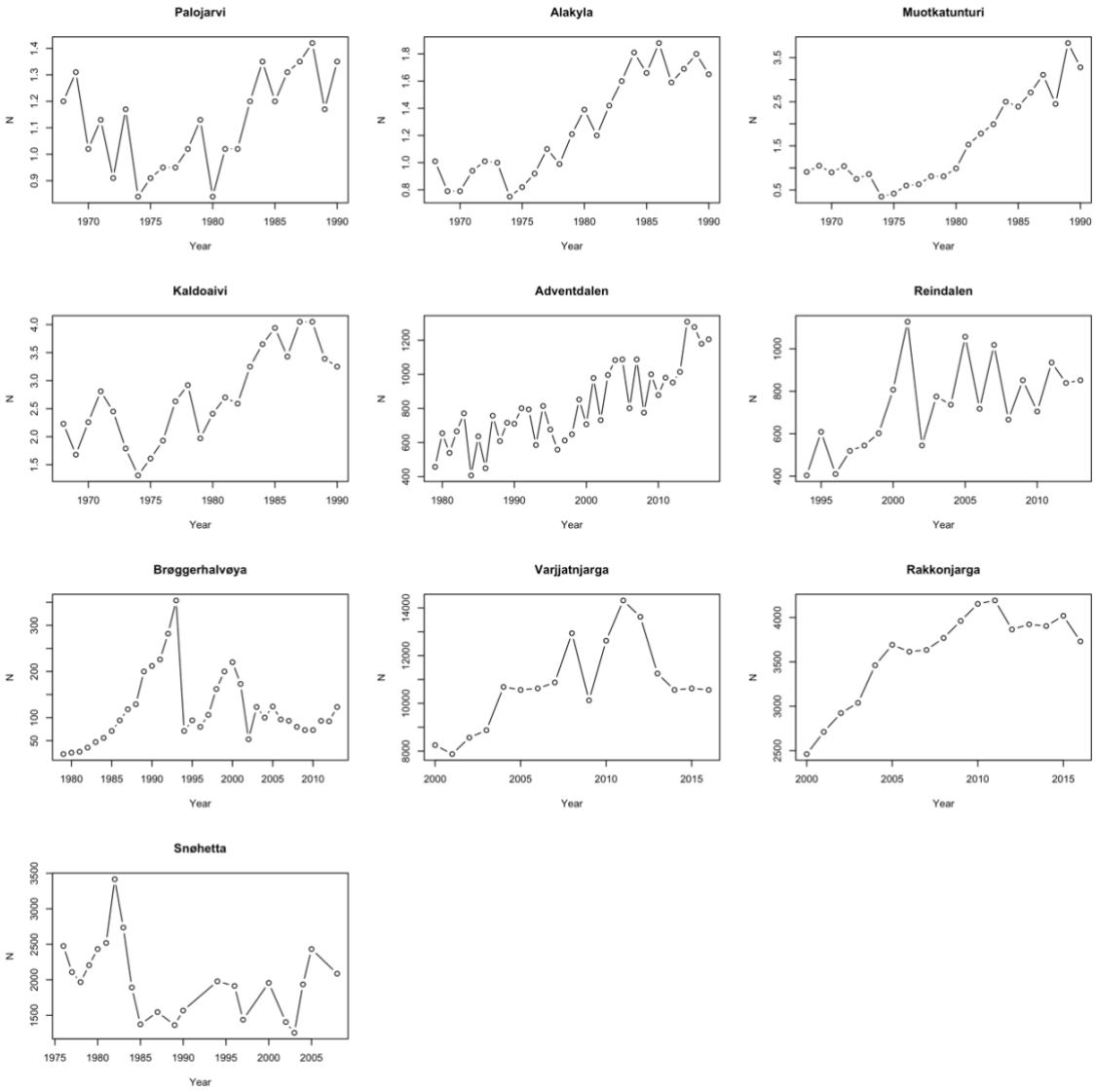

Figure S4. Time-series data of reindeer populations.

The plots show the time-series data on population abundance used to calculate finite rates of population increase and their variance, and maximum population growth rate. The time-series data come for populations from Finland (n = 4), Norway (Svalbard) (n = 3) and Norway (mainland) (n = 3). We repeatedly fitted linear models to 3,4,5,6 and 7 data points of the time-series. We then selected, for each time series, the estimate of maximum growth rate resulting from the model with the highest r^2. This gave the range of annual maximum growth rate for reindeer, which we scaled to generation length by taking the exponent. We used the years 1998-2013 of the Reindalen (Svalbard) time-series, the years 2005 – 2013 of the Rakkonjarga (Norway) time-series, and the full time-series for Palojarvi (Finland) and Snøhetta (Norway) to calculate the standard deviation (SD) in population growth rate.

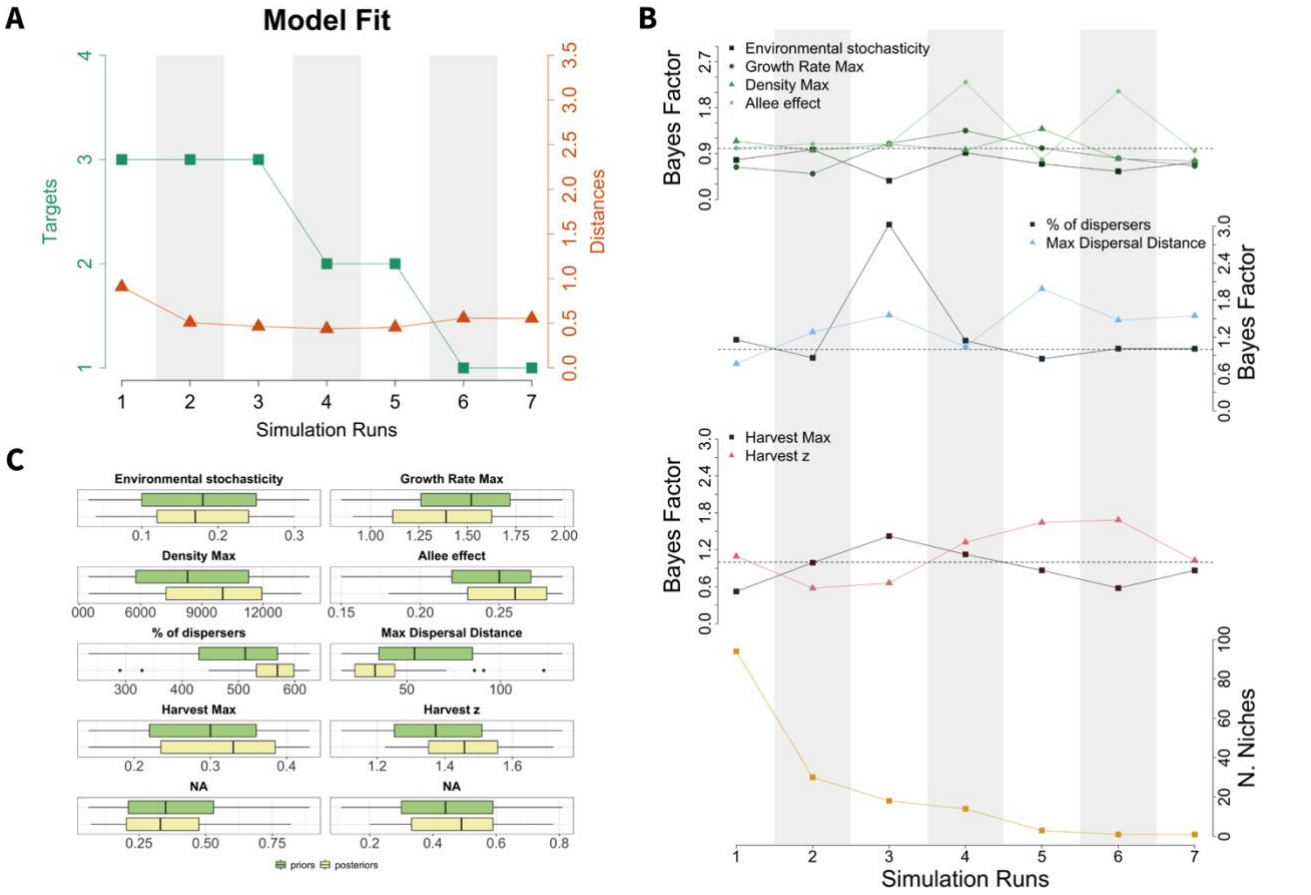

Figure S5. Model Selection.

A shows the results of the posterior predictive checks and model goodness of fit, for each model run (x-axis). The left y-axis and the green squares show the number of targets for which the posterior predictive checks result in p-values > 0.05. The right y-axis and the orange triangles show the distances from the targets calculated from the permutation tests on the summary statistics of the models (based on the 'gfit' function of the 'abc' package in R). The smallest the distance from the target, the better are the models at replicating the observed patterns. **B** shows values of Bayes Factors for demographic, dispersal, and harvest parameters in the models, and the number of selected niches after ABC, for each model run. Bayes Factors were calculated between the distribution of parameter values for the best 50 models and the prior distribution of the same parameters, to estimate parameter convergence. **C**, Boxplots show the difference in distribution between priors and posteriors in model run 3.

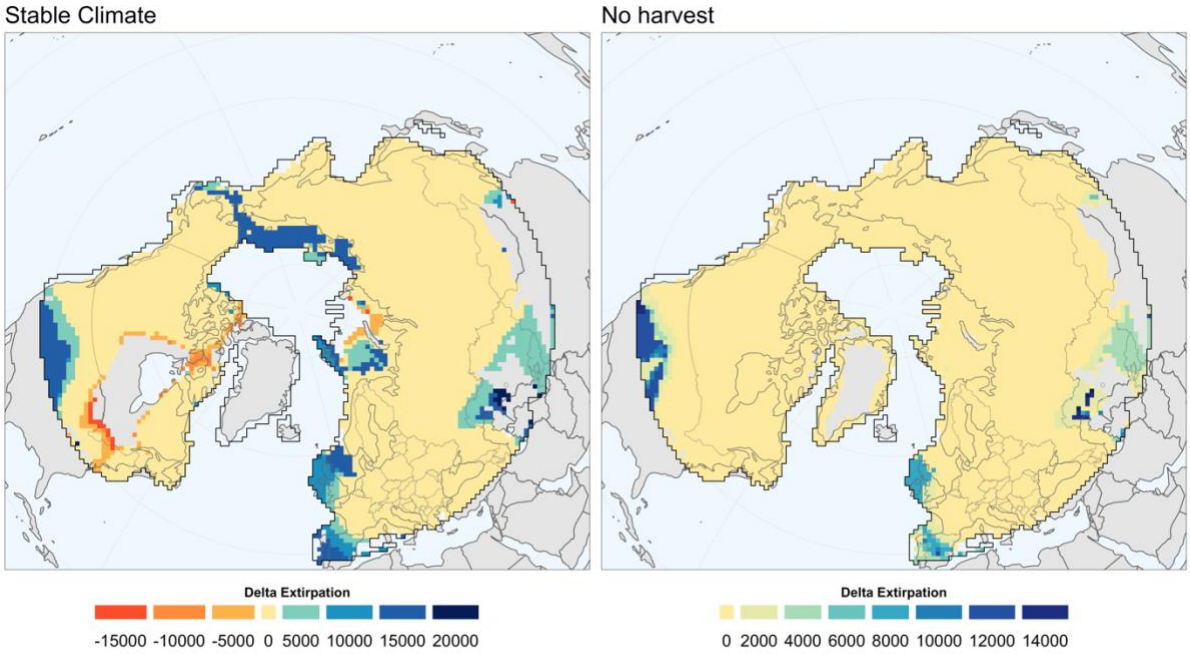

Figure S6. Difference in time of extirpation of reindeer populations between the baseline and each counterfactual scenario.

Absolute difference in projected time of extirpation of reindeer between the baseline (human harvesting and climate change) and two counterfactual scenarios: no climate change from 21 ka BP (Stable Climate), and no harvest through the simulation (No Harvest). Cooler colours indicate later extirpation in the counterfactual scenario, while warmer colours indicate earlier extirpation compared to the baseline. Pale yellow indicates no difference. The black line shows the extent of the study region.

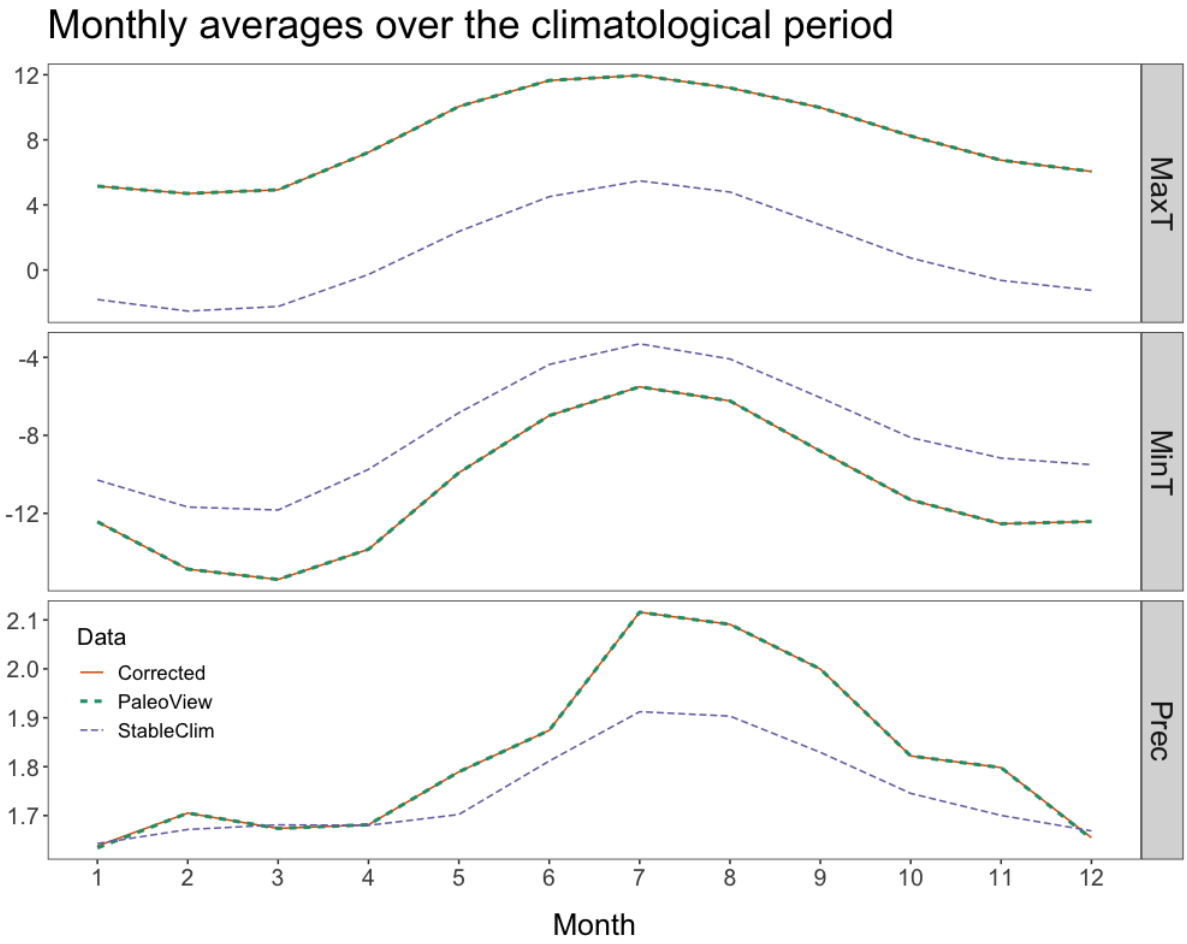

Figure S7. Climate data alignment.

Future climate change projections accessed using StableClim were aligned to paleoclimate reconstructions accessed using PaleoView. The alignment of the two climate datasets was done based on anomalies for the year 1974 C.E. The plots show the monthly averages for the year 1974 for StableClim (blue), PaleoView (green) and the StableClim-corrected data (red). PaleoView and the corrected StableClim align perfectly.

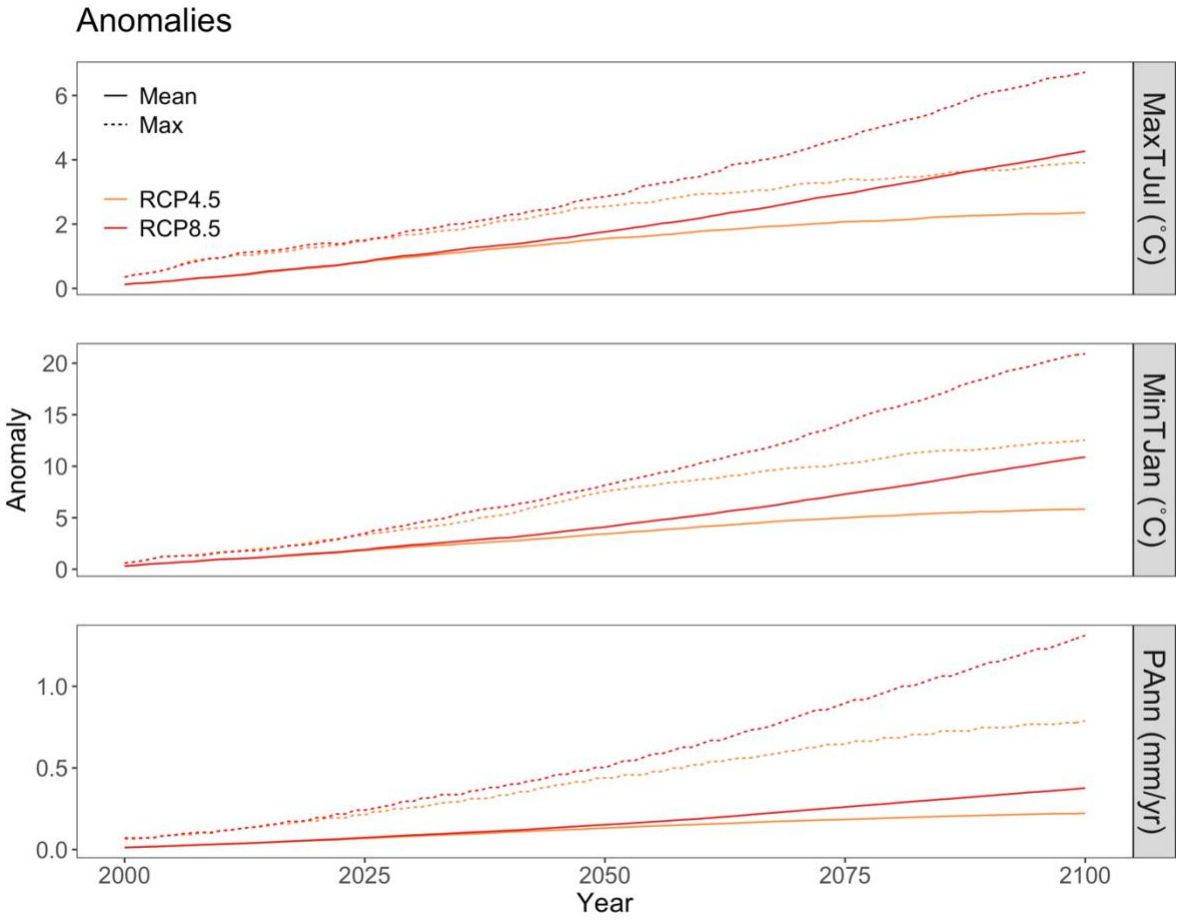

Figure S8. Anomalies in projected climate forecast.

The plots show the mean (red) and maximum (blue) anomaly for the years 2000 – 2100, calculated as the difference in climate compared to the average of the years 1980 – 1999 (baseline). Climatic variables considered are maximum daily temperature in July, minimum daily temperature in January and annual precipitation.

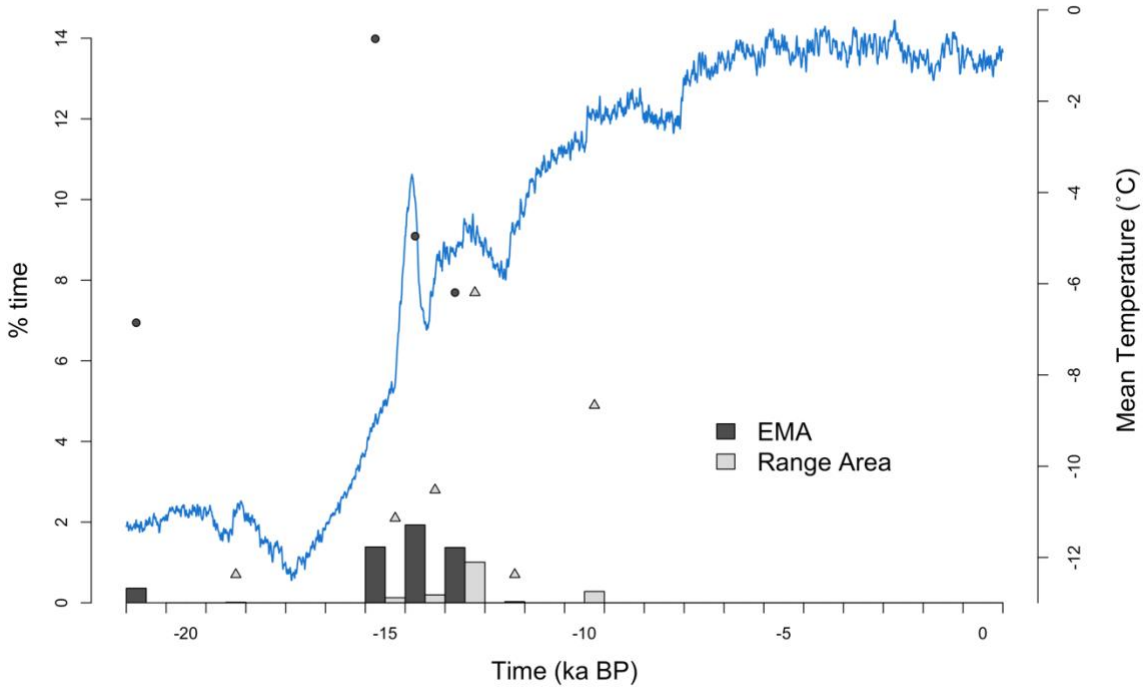

Figure S9. Past events of reduction in Expected Minimum Abundance (EMA) and range area with magnitudes similar to future predictions.

The bars show the percentage of time steps (generations) within each millennial bin that experienced reductions ≥ 15% in EMA (dark grey) and ≥ 13% in range area (light grey) over 84 years (12 generations). The bars show the average across the 'best' models, while points and triangles show the maximum for EMA and range area, respectively. The blue line represents the average temperature across the study region.

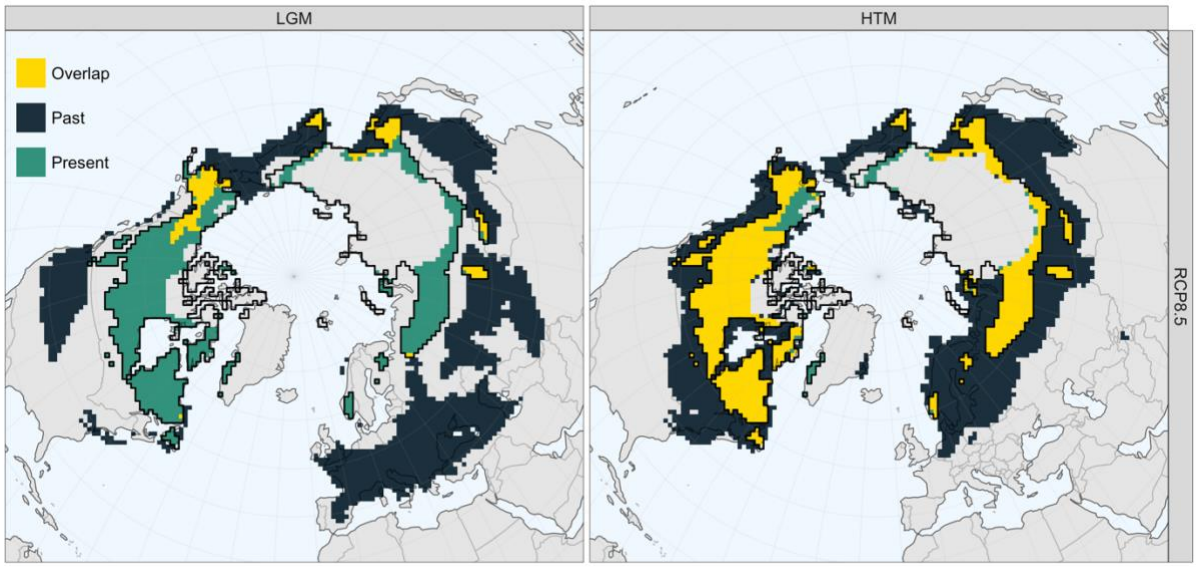

Figure S10. Analogues of future climate at the Last Glacial Maximum and the Holocene Thermal Maximum.

Areas with climatic conditions in 2100 that are occupiable by reindeers today and during the Last Glacial Maximum (LGM; 21 ka BP) and the Holocene Thermal Maximum (HTM, ~6.5 ka BP). Green shows areas where analogues of future conditions are in the current distribution of reindeers; dark blue shows areas where analogues are in past (LGM and HTM) distributions; yellow shows areas of overlap (analogues in the current and past distributions). The black line shows the extent of the present-day range of the reindeer, as defined by Gunn (*2*).

Movie S1. Spatiotemporal abundance over the last 21000 years.

https://universityofadelaide.box.com/s/t81g4x7pehehgibekucbh3y0gplipwk8

Relative abundance of reindeer (ensemble mean of the 'best' models) from 21 ka BP to 1500 C.E. Blue diamonds show fossil locations at fossil age ± 1 SD. The blue line shows the extent of the study region and the division into sub-regions.

Movie S2. Relative density of anatomically modern humans since 21 ka BP.

https://universityofadelaide.box.com/s/hcca4hb70nmxj93ipdmvhnaew0fkqr68

Relative human density (ensemble mean of the 'best' models) from 21 ka BP to 1500 C.E. Red lines show the division of the study region into sub-region.

Movie S3. Reindeer harvest since 21 ka BP.

https://universityofadelaide.box.com/s/3ybceb2uqzlvhb9em57hmeceea3gmz6r

Total number of harvested individuals in each grid cell at each time step, scaled between 0 and 1. The purple line shows the extent of the study region and the division in sub-regions. Bars in inset panel show total relative number of harvested individuals in each sub-region at each time step.

Movie S4. Spatiotemporal abundance simulated for the future, from 2016 to 2100.

https://universityofadelaide.box.com/s/s9d02cnqdkaoe9jcydx6gw3fhzxyy8q9

Predicted relative abundance of reindeer from 2016 to 2100 C.E. The blue line shows the extent of the study region.

Table S1. Fixed and variable parameters for the spatially explicit population models.

Parameters used in the demographic and harvest components of the models, with information on whether variables had fixed or variable ranges (Type) and their initial (or prior) values (Value/range). References for demographic and harvest parameter values are provided below the table.

Parameter	***Description***	***Type***	***Value/range***	***Posterior range***
Demographic parameters				
Growth rate	Maximum growth rate per time step	variable	1.75 – 7.94	0.91 – 1.94
Environmental stochasticity	Environmental stochasticity per time step	variable	0.00 – 0.35	0.04 – 0.30
Upper Abundance	Maximum density per grid cell	variable	1000 – 15500	3464 – 13875
Dispersal rate	Maximum dispersal distance per time step	variable	100 – 675	290 – 626
Proportion of dispersers	Percentage of the population that disperses at each time step (cell-based)	variable	5% – 30%	18% – 29%
Dispersal target K	Dispersal rate negatively affected by target population abundance (N)	fixed	10	NA
Allee effect	Region-wide Allee effect	variable	0 – 500	15 – 123

Occupancy threshold	Number of populations on the landscape that determines region-wide extinction	fixed	1	NA
Human parameters				
Harvest G	Prey density at which exploitation is half-maximal	fixed	0.4	NA
Harvest Max.	Maximum proportion of the population harvested at each time step (cell-based)	variable	5% – 50%	14% – 43%
Harvest z	Departure from maximal exploitation, determining the type of response of the populations	variable	1 – 2	1.2 – 1.7
Humans SD multiplier	Multiplier to the standard deviation in human abundance	variable	0 – 1	0.07 – 0.82
Humans p-value	p-value at which human density values are chosen from the lognormal distribution	variable	0 – 1	0.20 – 0.78

Table S2. Observed statistics (targets) for pattern-oriented modelling and Approximate Bayesian Computation (ABC) validation.

Targets used in the ABC analysis and validation step include an occupancy pattern, identified by positive abundance at fossil sites at fossil calibrated age ± SD, Root Mean Square Error (RMSE) of the difference between simulated and observed times of extinction in Europe across four sub-regions, arrival time in Greenland, and slope of the N_e trend. To calculate occupancy pattern, fossil records that overlapped in space and time have been merged to count as one.

Target	**Description**	**Value**	**97.5% CI: Lower**	**2.5% CI: Upper**
Occupancy pattern	Agreement between simulated and inferred occupancy at fossil sites.	720 [1] (fossils)	NA	NA
Extirpation pattern	Time of extinction in 4 subregions of Europe based on the fossil record.	12,727 BP [1] (Iberia)	12,995 BP [1] (Iberia)	12,418 BP [1] (Iberia)
		9,121 BP [1] (British Isles)	9,385 BP [1] (British Isles)	8,880 BP [1] (British Isles)
		9,677 BP [1] (South Central Europe)	10,182 BP [1] (South Central Europe)	8,956 BP [1] (South Central Europe)
		3,444 BP [1] (North Central Europe)	3,437 BP [1] (North Central Europe)	2,633 BP [1] (North Central Europe)
Arrival time	Time of arrival in Greenland based on the fossil record.	9,294 BP [1]	9,643 BP [1]	8,939 BP [2]
N_e Trend	Slope of the trend in effective population size (N_e)	-65.43	NA	NA

[1]All estimates were calculated using the fossil record, which is available in Appendix 1. The estimates for extinction time and time of arrival were calculated using the GRIWM method (Bradshaw et al. 2012).

Table S3. Detailed results of the gaussian generalised additive model on reindeer abundance trend during the last deglaciation.

Effect sizes and significance of smoothed terms (temperature and human density) for each subregion and for the deglaciation period (21 – 11.7 ka BP). We used mean abundance over 100-year time bins as our response variable, with combinations of average temperature (°C), and average human density (scaled N_e). Time and regions were used as random effects. Formula:

Abundance ~ s(Temperature, by = Region) + s(Human Density, by = Region) + s(Time) + s(Region)

	Estimate	**Std. Error**	**t value**	**Pr(>|t|)**
(Intercept)	1114841	67423	16.54	< 2e-16 ***
	edf	**Ref.df**	**F**	**p-value**
Asia	5.880 Temperature	9 Temperature	40.746 Temperature	< 2e-16 *** Temperature
	5.528 Human Density	7 Human Density	23.005 Human Density	< 2e-16 *** Human Density
Beringia	6.0363459 Temperature	9 Temperature	17.091 Temperature	< 2e-16 *** Temperature
	1.639 Human Density	8 Human Density	1.318 Human Density	0.000848 *** Human Density
Europe	3.4290632 Temperature	6 Temperature	3.917 Temperature	2.29e-06 *** Temperature
	1.580 Human Density	5 Human Density	2.355 Human Density	0.000439 *** Human Density

North America	3.192 Temperature	7 Temperature	13.205 Temperature	< 2e-16 *** Temperature
	0.003 Human Density	8 Human Density	0.000 Human Density	0.321145 Human Density
Time	0.040	93	0.000	0.610361
Region	0.0001	3	0.000	1.85e-06 ***

Signif. codes: 0 ‘***’ 0.001 ‘**’ 0.01 ‘*’ 0.05 ‘.’ 0.1 ‘ ’ 1

Table S4. Detailed results of the gaussian generalised additive model on reindeer abundance trend during the Holocene.

Effect sizes and significance of smoothed terms (temperature and human density) for each subregion and for the Holocene (11.7 ka BP – 1500 C.E.). We used mean abundance over 100-year time bins as our response variable, with combinations of average temperature (°C), and average human density (scaled N_e). Time and regions were used as random effects. Formula:

Abundance ~ s(Temperature, by = Region) + s(Human Density, by = Region) + s(Time) + s(Region)

	Estimate	**Std. Error**	**t value**	**Pr(>|t|)**
(Intercept)	728608	119212	6.112	2.81e-09 ***
	edf	**Ref.df**	**F**	**p-value**
Asia	3.853 Temperature	7 Temperature	60.951 Temperature	< 2e-16 *** Temperature
	2.727 Human Density	7 Human Density	22.556 Human Density	< 2e-16 *** Human Density
Beringia	3.292 Temperature	5 Temperature	49.862 Temperature	< 2e-16 *** Temperature
	8.637 Human Density	5 Human Density	1.805 Human Density	0.0613 . Human Density
Europe	1.740 Temperature	6 Temperature	0.000 Temperature	0.4433 Temperature

	2.026 Human Density	5 Human Density	123.551 Human Density	< 2e-16 *** Human Density
North America	3.345 Temperature	8 Temperature	15.544 Temperature	< 2e-16 *** Temperature
	5.441 Human Density	8 Human Density	155.201 Human Density	< 2e-16 *** Human Density
Time	1.031	112	4.759	< 2e-16 ***
Region	7.137	3	0.000	0.0241 *

Signif. codes: 0 ‘***’ 0.001 ‘**’ 0.01 ‘*’ 0.05 ‘.’ 0.1 ‘ ’ 1

Chapter V: Discussion

In this PhD dissertation, I have used different types of data and techniques to explore the effects of global change drivers on different levels of biodiversity to gain a better understanding of extinction dynamics and extinction risk. In **Chapter II**, I analysed mitochondrial DNA (mtDNA) sequences of ~1000 bird species to identify a relationship between intra-specific genetic diversity and conservation status. In **Chapter III** and **Chapter IV**, I used fossil records, modern occurrence records, paleoclimate reconstructions, ancient DNA sequences (aDNA), and process-explicit macroecological models to disentangle the spatiotemporal effects of natural and human factors on species' population and range dynamics. This allowed me to identify the ecological processes that determine how species respond to threatening forces.

The results presented in this PhD dissertation show that genetic diversity in birds reflects their conservation status and is therefore connected to changes in population and range size that happened either in the recent or ancient past (**Chapter II**). By reconstructing the range dynamics of muskox and reindeer over the last 21,000 years, I was able to show that their range and population sizes have been deeply affected by Pleistocene climatic fluctuations, with more gradual rates of warming and more stable climatic conditions during the Holocene favouring the expansion and recovery of the two species (**Chapter III** and **Chapter IV**). The most severe population declines, range contractions and extirpations for muskox and reindeer were simulated to have happened during or immediately following abrupt warming events, indicating a strong role of magnitude and pace of climatic change in species range and population dynamics. I show, for both species, that humans amplified the effects of climate change and regulated population abundances. However, there were strong spatiotemporal differences in the timing and magnitude of the influence of humans.

Results from **Chapter III** and **Chapter IV** also revealed that these extinction drivers interacted with key ecological processes. The ability to tolerate broader climatic conditions and to disperse long distances provided a degree of ecological resilience to the negative effects of climatic change, and indirectly allowed movements away from areas densely occupied by humans. Local extirpations were simulated to occur in areas with declines in habitat suitability, fast growing human populations, and limited refugia (e.g., Europe). Finally, I was able to show that projections validated on the past can improve future predictions of extinction risk. This revealed that reindeers will likely be able to cope with the accelerating warming of the Arctic (**Chapter IV**).

The results presented in this PhD dissertation suggest that the vulnerability of species to environmental changes is tightly linked to demographic responses to different magnitudes and rates of threatening processes, which in turn can affect intra-specific genetic diversity. When climate fluctuations are abrupt, or when they work in synergy with other stressors, population and range sizes decline rapidly, eroding genetic variability and increasing extinction risk. Species resilience seems to be favoured by high mobility, larger climatic tolerances, and higher levels of genetic diversity, which increase the potential of species to track suitable habitats and to evolve adaptations to environmental changes.

Impacts of global change on extinction risk

Results from **Chapter III** and **Chapter IV** suggest that climatic variability, and its influence on habitat suitability, is the main driver of the range dynamics of both muskox and reindeer over the last

21,000 years. The strong role of climate in driving demographic changes of the two species had been previously inferred from analyses of fossils and aDNA (Campos et al., 2010; Lorenzen et al., 2011; Markova et al., 2015; Sommer et al., 2014). However, I found that human hunting likely hastened regional extirpations of muskox and reindeer in Europe, establishing new information on the impacts of human and non-human forces on the two species. A synergy between climate change and human hunting has also been advocated as the cause of the extinction of the woolly mammoth (Fordham et al., 2021), and regional extirpations of horse and bison (Lorenzen et al., 2011; Metcalf et al., 2014). Declines in the ranges and population sizes of Pleistocene megafauna likely had an effect at the genetic level. The study of fossils and aDNA has revealed evidence of isolation-by-distance and reduced genetic diversity before regional and range-wide extinctions for many megafaunal species (Lorenzen et al., 2011; Palkopoulou et al., 2015), suggesting contributions of genetic drift and inbreeding in small and isolated populations (Spielman et al., 2004). Analyses of bird genomes have shown that increases and decreases in effective population sizes correspond to the climatic fluctuations of the Pleistocene (Nadachowska-Brzyska et al., 2015), and to the extent of suitable habitat availability over time (Bruniche-Olsen et al., 2021). Moreover, species currently considered "threatened" to extinction are the ones that suffered the most severe genetic depletions in the past (Nadachowska-Brzyska et al., 2015), and are now harbouring low genomic diversity (Bruniche-Olsen et al., 2021). This aligns with the results presented in **Chapter II**, where I show that threatened bird species have lower levels of mtDNA intra-specific genetic diversity than non-threatened species, and that a relationship exists between genetic variability and extinction risk.

Results in **Chapter III** of this thesis suggest a high vulnerability of muskox to future climate change, owing to the high sensitivity of the species to abrupt warming events and by its low genetic diversity (Hansen et al., 2018; MacPhee et al., 2005). The relationship between genetic diversity and extinction risk identified in **Chapter II** has been also established in mammals (Li et al., 2016; Spielman et al., 2004; Willoughby et al., 2015), suggesting that the low genetic variability in muskox could make the species more vulnerable to environmental changes. For reindeer, results from **Chapter IV** show that range contractions and population declines in the past were as large and even greater than what is being predicted for the future, occurring during periods of past abrupt warming. Analogues between past and future climatic conditions, pinpointed in **Chapter IV**, indicate that reindeers have already occupied areas with climatic conditions similar to future forecasts. At the genetic level, reindeers have shown little isolation-by-distance over time (Lorenzen et al., 2011), and high genetic structure across populations. This implies that populations have been connected by

metapopulation processes, but that this connectivity was not high enough to allow genetic homogenisation by gene flow (Yannic et al., 2020; Yannic et al., 2018). These results suggest that reindeers are likely to survive 21st century climatic changes in the Arctic, albeit in reduced numbers and in climate refugia.

Ecological processes that aid species resilience

By focusing on megafaunal species that survived the last deglaciation, I was able to identify ecological processes of key importance for species resilience. Long-distance dispersal and a high proportion of dispersers are ecological processes that were important for both muskox and reindeer models (**Chapter III** and **Chapter IV**). High dispersal ability is a key mechanism for species to track changes in habitat suitability, promoting survival and resilience against environmental change (Moritz & Agudo, 2013). Indeed, an enhanced dispersal ability is possibly among the reasons why muskox and reindeer survived the Pleistocene/Holocene transition, while other megafaunal species went extinct. Dispersal capacity was likely to be less important for the woolly mammoth, potentially increasing extinction risk (Fordham et al., 2021), and analysis of aDNA sequences of Arctic fox have shown that a lack of ability to track suitable habitats has resulted in the extirpation of the species in Europe (Dalen et al., 2007). Results from **Chapter IV** also suggest that the high dispersal ability of reindeers positively interacted with climatic variability and human expansion, as it allowed reindeers to track changes in habitat suitability and to access areas with lower relative human densities (Eriksson et al., 2012). This interaction between extinction drivers and dispersal processes likely contributed to reindeer resilience and survival in the past.

Both muskox and reindeer also showed a selection for relatively high maximum densities and for niches with large volumes and low marginality – niches that approximated their multi-temporal niches (**Chapter III** and **Chapter IV**). As the multi-temporal niche contains a broader range of climatic conditions than the realised niche of a species (Nogués-Bravo, 2009), a selection for niches with large volumes and low marginality suggests a higher tolerance to environmental changes, which likely aided their survival. Indeed, a comparison of niches between the "winners" and "losers" of Late Quaternary extinctions showed that species that went extinct had smaller climatic and geographic envelopes compared to the ones that survived (Blois et al., 2013). These support predictions that species that are unable to move and have narrow climatic niches might be at a greater risk of extinction (Pereira et al., 2012).

Lastly, the relationship between genetic diversity and extinction risk found in **Chapter II** implies that higher levels of genetic diversity could enhance species resilience to environmental change. Genetic diversity reflects the potential of species to adapt and evolve in response to environmental changes and determines the fitness of individuals and the viability of populations (Banks et al., 2013). At the ecosystem level, higher levels of genetic diversity have already been associated with resistance to disturbance (Hughes & Stachowicz, 2004), enhanced energy and nutrient fluxes (Schweitzer et al., 2005), and increases in aboveground primary productivity (Cook-Patton et al., 2011; Crutsinger et al., 2006). However, the roles of genetic diversity and other genetic mechanisms in long-term species survival remain poorly understood. It is likely that advances in genomic techniques might soon unravel the roles of genes in determining species resilience and extinction risk.

Conclusions and future directions

The results presented in this PhD dissertation demonstrate that genes, fossils, and process-explicit models can be integrated, providing valuable tools to explain past, current, and future patterns of species distributions and abundances, and to determine extinction risk. Over the last few decades, paleontological evidence has been increasingly used to understand and describe current biodiversity patterns. Information from fossil remains has been implemented in cladistics, phylogenetics and phylogeography (Benton & Emerson, 2007; Bray et al., 2013; Jackson & Blois, 2015; Raghavan et al., 2015; Weinstock et al., 2005), to improve our understanding on the evolutionary history of species and populations. Paleo-records have also been implemented in species distribution models to test biogeographic and evolutionary scenarios, and for quantifying past climate change impacts on current-day distributions (Nogués-Bravo, 2009; Svenning et al., 2011; Varela et al., 2011). Recently, paleoecology has increasingly gained recognition for the conservation of species under future climate change (Barnosky et al., 2017; Chevalier et al., 2020; Dietl et al., 2015; Fordham et al., 2020; Nogues-Bravo et al., 2018; Turvey & Saupe, 2019; Willis et al., 2007), with research analysing past dynamics that might have analogues in the future (Burke et al., 2018; Jackson et al., 2009; Jackson & Williams, 2004; Nolan et al., 2018; Williams & Blois, 2018). In this context, the idea presented in this PhD dissertation of using information from the past to better understand the present and predict the future is not novel. However, the novelty of the work presented in this thesis resides in the use of paleo-archives together with process-explicit models. Although process-explicit models have been used to model vegetation (Prentice et al., 2007) and physiologic (Desforges et al., 2019; Desforges et al.,

2021) responses to environmental drivers, and eco-evolutionary dynamics shaping biodiversity patterns (Hagen et al., 2021; Rangel et al., 2018), this approach is new for the modelling of species distributions, which have relied on correlative approaches (Franklin, 2010). Moreover, the integration of process-explicit models with paleo-archives has only recently been advocated as a promising approach for safeguarding biodiversity under global change (Fordham et al., 2020).

The models used in this thesis have proved that explicitly simulating the processes and drivers that shape species distributions is important for disentangling species responses to global change. Still, they are not exempt from limitations. For example, the choice of climatic variables used to build the climatic niche of the species is likely to be critical for the outcome of the models and requires careful consideration. Although climatic variables could be used as a proxy for primary productivity, models could benefit from their integration with vegetation models, by creating a direct link between plant-herbivore trophic interactions. The process-explicit models used in this thesis also lack some important processes that shape the distribution of species: biotic interactions. Although human exploitation is a form of biotic interaction captured in the models, other predator-prey dynamics are not included, as well as interspecific competition with other herbivores, which could amplify the effects of climate change and human hunting on the range and population dynamics of species. Moreover, simulations of future reindeer abundances do not include extinction drivers other than climate change, which could underestimate the effects of future global change. Although future projections of land-use change are used to modify the carrying capacity of the species, habitat degradation was not directly modelled and did not function as a barrier to dispersal. To help disentangle the relative impacts of different global change drivers on species and to improve future predictions of extinction risk, global change drivers could be analysed using counterfactual scenarios (i.e., no land-use, but climate change), where each driver is sequentially turned off in the models, similar to what has been done in reindeer simulations of the past (**Chapter IV**).

In **Chapter III** and **Chapter IV**, I used trends in effective population size, reconstructed from genetic sequences, to evaluate the performance of the models. Other forms of genetic information could be used as targets in the validation phase, such as the genetic structure of populations (F_{ST}). To better understand the effects of global change drivers at the genetic level, future research could use the process-explicit modelling approach used in this thesis to explicitly simulate the mechanisms that generate genetic diversity and genetic structure of populations, as they include demographic and metapopulation processes.

The models developed in this thesis have important applications for species conservation. For example, they revealed that both muskox and reindeer experienced a northward range shift, with contraction at the southern range edge, and that reindeer is forecast to persist in areas of higher current densities, in accordance with the centre-margin hypothesis (Brown et al., 1996). A comparison of process-explicit models across different species, both extant and extinct, could help determine if a general pattern exists on how ranges contract. This would be beneficial for conservation management decisions, as it would establish the populations, within a species range, that are important for range expansion and persistence during periods of climatic and environmental change, and that should thus be prioritized for management. These models can also be used to predict the success of translocations and reintroductions, or to guide decisions for the establishment of protected areas. By integrating genes, fossils, and process-explicit models, I showed how research at the intersection of genetics, paleoecology, and macroecology can improve our understanding of biodiversity responses to global change drivers and, ultimately, help avert future biodiversity loss.

References

Andersen, K. K., Azuma, N., Barnola, J. M., Bigler, M., Biscaye, P., Caillon, N., Chappellaz, J., Clausen, H. B., Dahl-Jensen, D., Fischer, H., Fluckiger, J., Fritzsche, D., Fujii, Y., Goto-Azuma, K., Gronvold, K., Gundestrup, N. S., Hansson, M., Huber, C., Hvidberg, C. S., . . . North Greenland Ice Core Project, m. (2004). High-resolution record of Northern Hemisphere climate extending into the last interglacial period. *Nature*, *431*(7005), 147-151. https://doi.org/10.1038/nature02805

Ardelean, C. F., Becerra-Valdivia, L., Pedersen, M. W., Schwenninger, J. L., Oviatt, C. G., Macias-Quintero, J. I., Arroyo-Cabrales, J., Sikora, M., Ocampo-Diaz, Y. Z. E., Rubio, C., II, Watling, J. G., de Medeiros, V. B., De Oliveira, P. E., Barba-Pingaron, L., Ortiz-Butron, A., Blancas-Vazquez, J., Rivera-Gonzalez, I., Solis-Rosales, C., Rodriguez-Ceja, M., . . . Willerslev, E. (2020). Evidence of human occupation in Mexico around the Last Glacial Maximum. *Nature*, *584*(7819), 87-92. https://doi.org/10.1038/s41586-020-2509-0

Austin, M. P. (1987). Models for the Analysis of Species Respones to Environmental gradients. *Vegetatio*, *69*, 35-45.

Banks, S. C., Cary, G. J., Smith, A. L., Davies, I. D., Driscoll, D. A., Gill, A. M., Lindenmayer, D. B., & Peakall, R. (2013). How does ecological disturbance influence genetic diversity? *Trends Ecol Evol*, *28*(11), 670-679. https://doi.org/10.1016/j.tree.2013.08.005

Barnosky, A. D., Hadly, E. A., Gonzalez, P., Head, J., Polly, P. D., Lawing, A. M., Eronen, J. T., Ackerly, D. D., Alex, K., Biber, E., Blois, J., Brashares, J., Ceballos, G., Davis, E., Dietl, G. P., Dirzo, R., Doremus, H., Fortelius, M., Greene, H. W., . . . Zhang, Z. (2017). Merging paleobiology with conservation biology to guide the future of terrestrial ecosystems. *Science*, *355*(6325), eaah4787. https://doi.org/doi:10.1126/science.aah4787

Barnosky, A. D., & Lindsey, E. L. (2010). Timing of Quaternary megafaunal extinction in South America in relation to human arrival and climate change. *Quat Int*, *217*(1-2), 10-29. https://doi.org/10.1016/j.quaint.2009.11.017

Barnosky, A. D., Matzke, N., Tomiya, S., Wogan, G. O., Swartz, B., Quental, T. B., Marshall, C., McGuire, J. L., Lindsey, E. L., Maguire, K. C., Mersey, B., & Ferrer, E. A. (2011). Has the Earth's sixth mass extinction already arrived? *Nature*, *471*(7336), 51-57. https://doi.org/10.1038/nature09678

Behrensmeyer, A. K., Kidwell, S. M., & Gastaldo, R. A. (2000). Taphonomy and paleobiology. *Paleobiology*, *26*(sp4), 103-147. https://doi.org/10.1666/0094-8373(2000)26[103:TAP]2.0.CO;2

Benton, M. J., & Emerson, B. C. (2007). How Did Life Become So Diverse? The Dynamics of Diversification According to the Fossil Record and Molecular Phylogenetics. *Palaeontology*, *50*(1), 23-40. https://doi.org/10.1111/j.1475-4983.2006.00612.x

Berger, J., Hartway, C., Gruzdev, A., & Johnson, M. (2018). Climate Degradation and Extreme Icing Events Constrain Life in Cold-Adapted Mammals. *Sci Rep*, *8*(1), 1156. https://doi.org/10.1038/s41598-018-19416-9

Blois, J. L., Zarnetske, P. L., Fitzpatrick, M. C., & Finnegan, S. (2013). Climate change and the past, present, and future of biotic interactions. *Science*, *341*(6145), 499-504. https://doi.org/10.1126/science.1237184

Botta, F., Dahl-Jensen, D., Rahbek, C., Svensson, A., & Nogues-Bravo, D. (2019). Abrupt Change in Climate and Biotic Systems. *Curr Biol*, *29*(19), R1045-R1054. https://doi.org/10.1016/j.cub.2019.08.066

Braconnot, P., Harrison, S. P., Kageyama, M., Bartlein, P. J., Masson-Delmotte, V., Abe-Ouchi, A., Otto-Bliesner, B., & Zhao, Y. (2012). Evaluation of climate models using palaeoclimatic data. *Nat Clim Chang*, *2*(6), 417-424. https://doi.org/10.1038/nclimate1456

Bray, S. C. E., Austin, J. J., Metcalf, J. L., Østbye, K., Østbye, E., Lauritzen, S.-E., Aaris-Sørensen, K., Valdiosera, C., Adler, C. J., & Cooper, A. (2013). Ancient DNA identifies post-glacial recolonisation, not recent bottlenecks, as the primary driver of contemporary mtDNA phylogeography and diversity in Scandinavian brown bears. *Divers Distrib*, *19*(3), 245-256. https://doi.org/10.1111/j.1472-4642.2012.00923.x

Brook, B. W., & Barnosky, A. D. (2012). Quaternary Extinctions and Their Link to Climate Change. In L. Hannah (Ed.), *Saving a Million Species: Extinction Risk from Climate Change* (pp. 179-198). Island Press/Center for Resource Economics. https://doi.org/10.5822/978-1-61091-182-5_11

Brook, B. W., Sodhi, N. S., & Bradshaw, C. J. (2008). Synergies among extinction drivers under global change. *Trends Ecol Evol*, *23*(8), 453-460. https://doi.org/10.1016/j.tree.2008.03.011

Brown, J. H., Stevens, G. C., & Kaufman, D. M. (1996). THE GEOGRAPHIC RANGE: Size, Shape, Boundaries, and Internal Structure. *Annu Rev Ecol Syst*, *27*(1), 597-623. https://doi.org/10.1146/annurev.ecolsys.27.1.597

Brown, S. C., Wigley, T. M. L., Otto-Bliesner, B. L., Rahbek, C., & Fordham, D. A. (2020). Persistent Quaternary climate refugia are hospices for biodiversity in the Anthropocene. *Nat Clim Chang*, *10*(3), 244-248. https://doi.org/10.1038/s41558-019-0682-7

Bruniche-Olsen, A., Kellner, K. F., Belant, J. L., & DeWoody, J. A. (2021). Life-history traits and habitat availability shape genomic diversity in birds: implications for conservation. *Proc R Soc B*, *288*(1961), 20211441. https://doi.org/10.1098/rspb.2021.1441

Burke, K. D., Williams, J. W., Chandler, M. A., Haywood, A. M., Lunt, D. J., & Otto-Bliesner, B. L. (2018). Pliocene and Eocene provide best analogs for near-future climates. *Proc Natl Acad Sci U S A*, *115*(52), 13288-13293. https://doi.org/10.1073/pnas.1809600115

Campos, P. F., Willerslev, E., Sher, A., Orlando, L., Axelsson, E., Tikhonov, A., Aaris-Sorensen, K., Greenwood, A. D., Kahlke, R. D., Kosintsev, P., Krakhmalnaya, T., Kuznetsova, T., Lemey, P., MacPhee, R., Norris, C. A., Shepherd, K., Suchard, M. A., Zazula, G. D., Shapiro, B., & Gilbert, M. T. (2010). Ancient DNA analyses exclude humans as the driving force behind late Pleistocene musk ox (*Ovibos moschatus*) population dynamics. *Proc Natl Acad Sci U S A*, *107*(12), 5675-5680. https://doi.org/10.1073/pnas.0907189107

Caughley, G. (1994). Directions in Conservation Biology. *J Anim Ecol*, *63*(2), 215-244. https://doi.org/10.2307/5542

Ceballos, G., & Ehrlich, P. R. (2002). Mammal population losses and the extinction crisis. *Science*, *296*(5569), 904-907. https://doi.org/10.1126/science.1069349

Ceballos, G., Ehrlich, P. R., Barnosky, A. D., Garcia, A., Pringle, R. M., & Palmer, T. M. (2015). Accelerated modern human-induced species losses: Entering the sixth mass extinction. *Sci Adv*, *1*(5), e1400253. https://doi.org/10.1126/sciadv.1400253

Channell, R., & Lomolino, M. V. (2000). Dynamic biogeography and conservation of endangered species. *Nature*, *403*(6765), 84-86. https://doi.org/10.1038/47487

Channell, R., & Lomolino, M. V. (2000). Trajectories to extinction: spatial dynamics of the contraction of geographical ranges. *J Biogeogr*, *27*(1), 169-179. https://doi.org/10.1046/j.1365-2699.2000.00382.x

Chevalier, M., Davis, B. A. S., Heiri, O., Seppä, H., Chase, B. M., Gajewski, K., Lacourse, T., Telford, R. J., Finsinger, W., Guiot, J., Kühl, N., Maezumi, S. Y., Tipton, J. R., Carter, V. A., Brussel, T., Phelps, L. N., Dawson, A., Zanon, M., Vallé, F., . . . Kupriyanov, D. (2020). Pollen-based climate reconstruction techniques for late Quaternary studies. *Earth Sci Rev*, *210*, 103384. https://doi.org/10.1016/j.earscirev.2020.103384

Collins, W. D., Bitz, C. M., Blackmon, M. L., Bonan, G. B., Bretherton, C. S., Carton, J. A., Chang, P., Doney, S. C., Hack, J. J., Henderson, T. B., Kiehl, J. T., Large, W. G., Mckenna, D. S., Santer, B. D., & Smith, R. D. (2006). The Community Climate System Model Version 3 (CCSM3). *J Clim*, *19*(11), 2122-2143. https://doi.org/10.1175/jcli3761.1

Connolly, S. R., Keith, S. A., Colwell, R. K., & Rahbek, C. (2017). Process, Mechanism, and Modeling in Macroecology. *Trends Ecol Evol*, *32*(11), 835-844. https://doi.org/10.1016/j.tree.2017.08.011

Cook-Patton, S. C., Mcart, S. H., Parachnowitsch, A. L., Thaler, J. S., & Agrawal, A. A. (2011). A direct comparison of the consequences of plant genotypic and species diversity on communities and ecosystem function. *Ecology*, *92*, 915-923. https://doi.org/10.1890/10-0999.1

Cooper, A., Turney, C., Hughen, K. A., Brook, B. W., McDonald, H. G., & Bradshaw, C. J. (2015). Abrupt warming events drove Late Pleistocene Holarctic megafaunal turnover. *Science*, *349*(6248), 602-606. https://doi.org/10.1126/science.aac4315

Crutsinger, G. M., Collins, M. D., Fordyce, J. A., Gompert, Z., Nice, C. C., & Sanders, N. J. (2006). Plant genotypic diversity predicts community structure and governs an ecosystem process. *Science*, *313*, 966-968. https://doi.org/10.1126/science.1128326

Dalen, L., Nystrom, V., Valdiosera, C., Germonpre, M., Sablin, M., Turner, E., Angerbjorn, A., Arsuaga, J. L., & Gotherstrom, A. (2007). Ancient DNA reveals lack of postglacial habitat tracking in the arctic fox. *Proc Natl Acad Sci U S A*, *104*(16), 6726-6729. https://doi.org/10.1073/pnas.0701341104

Dansgaard, W., Johnsen, S. J., Clausen, H. B., Dahl-Jensen, D., Gundestrup, N. S., Hammer, C. U., Hvidberg, C. S., Steffensen, J. P., Sveinbjörnsdottir, A. E., Jouzel, J., & Bond, G. (1993). Evidence for general instability of past climate from a 250-kyr ice-core record. *Nature*, *364*(6434), 218-220. https://doi.org/10.1038/364218a0

Desforges, J.-P., Marques, G. M., Beumer, L. T., Chimienti, M., Blake, J., Rowell, J. E., Adamczewski, J., Schmidt, N. M., & van Beest, F. M. (2019). Quantification of the full lifecycle bioenergetics of a large mammal in the high Arctic. *Ecol Modell*, *401*, 27-39. https://doi.org/10.1016/j.ecolmodel.2019.03.013

Desforges, J. P., Marques, G. M., Beumer, L. T., Chimienti, M., Hansen, L. H., Pedersen, S. H., Schmidt, N. M., & van Beest, F. M. (2021). Environment and physiology shape Arctic

ungulate population dynamics. *Glob Chang Biol*, *27*(9), 1755-1771. https://doi.org/10.1111/gcb.15484

Dietl, G. P., Kidwell, S. M., Brenner, M., Burney, D. A., Flessa, K. W., Jackson, S. T., & Koch, P. L. (2015). Conservation Paleobiology: Leveraging Knowledge of the Past to Inform Conservation and Restoration. *Annu Rev Earth Planet Sci*, *43*(1), 79-103. https://doi.org/10.1146/annurev-earth-040610-133349

Dirzo, R., Young, H. S., Galetti, M., Ceballos, G., Isaac, N. J., & Collen, B. (2014). Defaunation in the Anthropocene. *Science*, *345*(6195), 401-406. https://doi.org/10.1126/science.1251817

Eiserhardt, W. L., Borchsenius, F., Plum, C. M., Ordonez, A., & Svenning, J.-C. (2015). Climate-driven extinctions shape the phylogenetic structure of temperate tree floras. *Ecol Lett*, *18*(3), 263-272. https://doi.org/10.1111/ele.12409

Elith, J., & Leathwick, J. R. (2009). Species Distribution Models: Ecological Explanation and Prediction Across Space and Time. *Annu Rev Ecol Evol Syst*, *40*(1), 677-697. https://doi.org/10.1146/annurev.ecolsys.110308.120159

Eriksson, A., Betti, L., Friend, A. D., Lycett, S. J., Singarayer, J. S., von Cramon-Taubadel, N., Valdes, P. J., Balloux, F., & Manica, A. (2012). Late Pleistocene climate change and the global expansion of anatomically modern humans. *Proc Natl Acad Sci U S A*, *109*(40), 16089-16094. https://doi.org/10.1073/pnas.1209494109

Flato, G., Marotzke, J., Abiodun, B., Braconnot, P., Chou, S. C., Collins, W., Cox, P., Driouech, F., Emori, S., Eyring, V., Forest, C., Gleckler, P., Guilyardi, E., Jakob, C., Kattsov, V., C., R., & Rummukainen, M. (2013). Evaluation of Climate Models. In I. Held, A. Pitman, S. Planton, & Z.-C. Zhao (Eds.), *Climate Change 2013: The Physical Science Basis* (pp. 749-824). Cambridge University Press.

Fois, M., Cuena-Lombraña, A., Fenu, G., & Bacchetta, G. (2018). Using species distribution models at local scale to guide the search of poorly known species: Review, methodological issues and future directions. *Ecol Modell*, *385*, 124-132. https://doi.org/10.1016/j.ecolmodel.2018.07.018

Fordham, D. A., Akçakaya, H. R., Alroy, J., Saltré, F., Wigley, T. M. L., & Brook, B. W. (2016). Predicting and mitigating future biodiversity loss using long-term ecological proxies. *Nat Clim Chang*, *6*(10), 909-916. https://doi.org/10.1038/nclimate3086

Fordham, D. A., Bertelsmeier, C., Brook, B. W., Early, R., Neto, D., Brown, S. C., Ollier, S., & Araujo, M. B. (2018). How complex should models be? Comparing correlative and

mechanistic range dynamics models. *Glob Chang Biol*, *24*(3), 1357-1370. https://doi.org/10.1111/gcb.13935

Fordham, D. A., Brook, B. W., Moritz, C., & Nogues-Bravo, D. (2014). Better forecasts of range dynamics using genetic data. *Trends Ecol Evol*, *29*(8), 436-443. https://doi.org/10.1016/j.tree.2014.05.007

Fordham, D. A., Brown, S. C., Akcakaya, H. R., Brook, B. W., Haythorne, S., Manica, A., Shoemaker, K. T., Austin, J. J., Blonder, B., Pilowsky, J., Rahbek, C., & Nogues-Bravo, D. (2021). Process-explicit models reveal pathway to extinction for woolly mammoth using pattern-oriented validation. *Ecol Lett*, *25*(1), 125-137. https://doi.org/10.1111/ele.13911

Fordham, D. A., Jackson, S. T., Brown, S. C., Huntley, B., Brook, B. W., Dahl-Jensen, D., Gilbert, M. T. P., Otto-Bliesner, B. L., Svensson, A., Theodoridis, S., Wilmshurst, J. M., Buettel, J. C., Canteri, E., McDowell, M., Orlando, L., Pilowsky, J., Rahbek, C., & Nogues-Bravo, D. (2020). Using paleo-archives to safeguard biodiversity under climate change. *Science*, *369*(6507), 10-10. https://doi.org/10.1126/science.abc5654

Fordham, D. A., Saltre, F., Brown, S. C., Mellin, C., & Wigley, T. M. L. (2018). Why decadal to century timescale palaeoclimate data are needed to explain present-day patterns of biological diversity and change. *Glob Chang Biol*, *24*(3), 1371-1381. https://doi.org/10.1111/gcb.13932

Fordham, D. A., Saltre, F., Haythorne, S., Wigley, T. M. L., Otto-Bliesner, B. L., Chan, K. C., & Brook, B. W. (2017). PaleoView: a tool for generating continuous climate projections spanning the last 21 000 years at regional and global scales. *Ecography*, *40*(11), 1348-1358. https://doi.org/10.1111/ecog.03031

Frankham, R. (2005). Genetics and extinction. *Biol Conserv*, *126*(2), 131-140. https://doi.org/10.1016/j.biocon.2005.05.002

Franklin, J. (2010). *Mapping Species Distributions: spatial inference and prediction*. Cambridge University Press. https://doi.org/10.1017/CBO9780511810602

Gaston, K. J. (2003). *The Structure and Dynamics of Geographic Ranges*. Oxford University Press. https://books.google.com.au/books?id=zBqpX1ajLFMC

Gordon, C., Cooper, C., Senior, C. A., Banks, H., Gregory, J. M., Johns, T. C., Mitchell, J. F. B., & Wood, R. A. (2000). The simulation of SST, sea ice extents and ocean heat transports in a version of the Hadley Centre coupled model without flux adjustments. *Clim Dyn*, *16*(2-3), 147-168. https://doi.org/10.1007/s003820050010

Grootes, P. M., Stuiver, M., White, J. W. C., Johnsen, S., & Jouzel, J. (1993). Comparison of oxygen isotope records from the GISP2 and GRIP Greenland ice cores. *Nature*, *366*(6455), 552-554. https://doi.org/10.1038/366552a0

Guisan, A., Tingley, R., Baumgartner, J. B., Naujokaitis-Lewis, I., Sutcliffe, P. R., Tulloch, A. I., Regan, T. J., Brotons, L., McDonald-Madden, E., Mantyka-Pringle, C., Martin, T. G., Rhodes, J. R., Maggini, R., Setterfield, S. A., Elith, J., Schwartz, M. W., Wintle, B. A., Broennimann, O., Austin, M., . . . Buckley, Y. M. (2013). Predicting species distributions for conservation decisions. *Ecol Lett*, *16*(12), 1424-1435. https://doi.org/10.1111/ele.12189

Guisan, A., & Zimmermann, N. E. (2000). Predictive habitat distribution models in ecology. *Ecol Modell*, *135*(2-3), 147-186. https://doi.org/10.1016/s0304-3800(00)00354-9

Hagen, O., Fluck, B., Fopp, F., Cabral, J. S., Hartig, F., Pontarp, M., Rangel, T. F., & Pellissier, L. (2021). gen3sis: A general engine for eco-evolutionary simulations of the processes that shape Earth's biodiversity. *PLoS Biol*, *19*(7), e3001340. https://doi.org/10.1371/journal.pbio.3001340

Hansen, C. C. R., Hvilsom, C., Schmidt, N. M., Aastrup, P., Van Coeverden de Groot, P. J., Siegismund, H. R., & Heller, R. (2018). The muskox lost a substantial part of Its genetic diversity on its long road to Greenland. *Curr Biol*, *28*(24), 4022-4028 e4025. https://doi.org/10.1016/j.cub.2018.10.054

Hickler, T., Smith, B., Sykes, M. T., Davis, M. B., Sugita, S., & Walker, K. (2004). Using a Generalized Vegetation Model to Simulate Vegetation Dynamics in Northeastern USA. *Ecology*, *85*(2), 519-530. https://doi.org/10.1890/02-0344

Holt, R. D., & Keitt, T. H. (2005). Species' borders: a unifying theme in ecology. *Oikos*, *108*(1), 3-6. https://doi.org/DOI 10.1111/j.0030-1299.2005.13145.x

Hughes, A. R., & Stachowicz, J. J. (2004). Genetic diversity enhances the resistance of a seagrass ecosystem to disturbance. *Proc Natl Acad Sci U S A*, *101*(24), 8998-9002. https://doi.org/10.1073/pnas.0402642101

IPBES. (2019). *Summary for policymakers of the global assessment report on biodiversity and ecosystem services of the Intergovernmental Science-Policy Platform on Biodiversity and Ecosystem Services.* IPBES. https://doi.org/10.5281/zenodo.3553579

IPCC. (2014). *Climate Change 2014: Synthesis Report. Contribution of Working Groups I, II and III to the Fifth Assessment Report of the Intergovernmental Panel on Climate Change*.

IUCN. (2019). *Guidelines for Using the IUCN Red List Categories and Criteria*. http://www.iucnredlist.org/documents/RedListGuidelines.pdf

IUCN. (2021). *The IUCN Red List of Threatened Species. Version 2021-1*. IUCN. Retrieved 29 April from https://www.iucnredlist.org

Jackson, S. T., Betancourt, J. L., Booth, R. K., & Gray, S. T. (2009). Ecology and the ratchet of events: climate variability, niche dimensions, and species distributions. *Proc Natl Acad Sci U S A, 106 Suppl 2*, 19685-19692. https://doi.org/10.1073/pnas.0901644106

Jackson, S. T., & Blois, J. L. (2015). Community ecology in a changing environment: Perspectives from the Quaternary. *Proc Natl Acad Sci U S A, 112*(16), 4915-4921. https://doi.org/10.1073/pnas.1403664111

Jackson, S. T., & Hobbs, R. J. (2009). Ecological restoration in the light of ecological history. *Science, 325*(5940), 567-569. https://doi.org/10.1126/science.1172977

Jackson, S. T., & Williams, J. W. (2004). MODERN ANALOGS IN QUATERNARY PALEOECOLOGY: Here Today, Gone Yesterday, Gone Tomorrow? *Annu Rev Earth Planet Sci*, *32*(1), 495-537. https://doi.org/10.1146/annurev.earth.32.101802.120435

Kafle, P., Peller, P., Massolo, A., Hoberg, E., Leclerc, L. M., Tomaselli, M., & Kutz, S. (2020). Range expansion of muskox lungworms track rapid arctic warming: implications for geographic colonization under climate forcing. *Sci Rep*, *10*(1), 17323. https://doi.org/10.1038/s41598-020-74358-5

Kearney, M., & Porter, W. (2009). Mechanistic niche modelling: combining physiological and spatial data to predict species' ranges. *Ecol Lett*, *12*(4), 334-350. https://doi.org/10.1111/j.1461-0248.2008.01277.x

Keller, L. (2002). Inbreeding effects in wild populations. *Trends Ecol Evol*, *17*(5), 230-241. https://doi.org/10.1016/s0169-5347(02)02489-8

Koch, P. L., & Barnosky, A. D. (2006). Late Quaternary Extinctions: State of the Debate. *Annu Rev Ecol Evol Syst*, *37*(1), 215-250. https://doi.org/10.1146/annurev.ecolsys.34.011802.132415

Kristensen, D. K., Kristensen, E., Forchhammer, M. C., Michelsen, A., & Schmidt, N. M. (2011). Arctic herbivore diet can be inferred from stable carbon and nitrogen isotopes in C3 plants, faeces, and wool. *Can J Zool*, *89*(10), 892-899. https://doi.org/10.1139/z11-073

Lavergne, S., Mouquet, N., Thuiller, W., & Ronce, O. (2010). Biodiversity and Climate Change: Integrating Evolutionary and Ecological Responses of Species and Communities. *Annu Rev Ecol Evol Syst*, *41*(1), 321-350. https://doi.org/10.1146/annurev-ecolsys-102209-144628

Lee, J.-Y., Marotzke, J., Bala, G., Cao, L., Corti, S., Dunne, J. P., Engelbrecht, F., Fischer, E., Fyfe, J. C., Jones, C., Maycock, A., Mutemi, J., Ndiaye, O., Panickal, S., & Zhou, T. (2021). Future global climate: scenario-based projections and near-term information. In V. Masson-Delmotte, P. Zhai, A. Pirani, S. L. Connors, C. Péan, S. Berger, N. Caud, Y. Chen, L. Goldfarb, M. I. Gomis, M. Huang, K. Leitzell, E. Lonnoy, J. B. R. Matthews, T. K. Maycock, T. Waterfield, O. Yelekçi, R. Yu, & B. Zhou (Eds.), *Climate Change 2021: The Physical Science Basis. Contribution of Working Group I to the Sixth Assessment Report of the Intergovernmental Panel on Climate Change*. Cambridge University Press.

Li, H., Xiang-Yu, J., Dai, G., Gu, Z., Ming, C., Yang, Z., Ryder, O. A., Li, W. H., Fu, Y. X., & Zhang, Y. P. (2016). Large numbers of vertebrates began rapid population decline in the late 19th century. *Proc Natl Acad Sci U S A*, *113*(49), 14079-14084. https://doi.org/10.1073/pnas.1616804113

Lomolino, M. V., & Channell, R. (1995). Splendid Isolation: Patterns of Geographic Range Collapse in Endangered Mammals. *J Mammal*, *76*(2), 335-347. https://doi.org/10.2307/1382345

Lomolino, M. V., & Channell, R. (1998). Range Collapse, Re-Introductions, and Biogeographic Guidelines for Conservation. *Conserv Biol*, *12*(2), 481-484. https://doi.org/10.1046/j.1523-1739.1998.97201.x

Lorenzen, E. D., Nogues-Bravo, D., Orlando, L., Weinstock, J., Binladen, J., Marske, K. A., Ugan, A., Borregaard, M. K., Gilbert, M. T., Nielsen, R., Ho, S. Y., Goebel, T., Graf, K. E., Byers, D., Stenderup, J. T., Rasmussen, M., Campos, P. F., Leonard, J. A., Koepfli, K. P., . . . Willerslev, E. (2011). Species-specific responses of Late Quaternary megafauna to climate and humans. *Nature*, *479*(7373), 359-364. https://doi.org/10.1038/nature10574

Lucas, P. M., Gonzalez-Suarez, M., & Revilla, E. (2016). Toward multifactorial null models of range contraction in terrestrial vertebrates. *Ecography*, *39*(11), 1100-1108. https://doi.org/10.1111/ecog.01819

Lynch, M., Conery, J., & Burger, R. (1995). Mutation Accumulation and the Extinction of Small Populations. *Am Nat*, *146*(4), 489-518. http://www.jstor.org.proxy.library.adelaide.edu.au/stable/2462976

MacArthur, R. H. (1958). Population Ecology of Some Warblers of Northeastern Coniferous Forests. *Ecology*, *39*, 599-619.

MacPhee, R. D., Tikhonov, A. N., Mol, D., & Greenwood, A. D. (2005). Late Quaternary loss of genetic diversity in muskox (Ovibos). *BMC Evol Biol*, *5*, 49. https://doi.org/10.1186/1471-2148-5-49

Malhi, Y., Doughty, C. E., Galetti, M., Smith, F. A., Svenning, J. C., & Terborgh, J. W. (2016). Megafauna and ecosystem function from the Pleistocene to the Anthropocene. *Proc Natl Acad Sci U S A*, *113*(4), 838-846. https://doi.org/10.1073/pnas.1502540113

Markova, A. K., Puzachenko, A. Y., van Kolfschoten, T., Kosintsev, P. A., Kuznetsova, T. V., Tikhonov, A. N., Bachura, O. P., Ponomarev, D. V., van der Plicht, J., & Kuitems, M. (2015). Changes in the Eurasian distribution of the musk ox (Ovibos moschatus) and the extinct bison (Bison priscus) during the last 50 ka BP. *Quat Int*, *378*, 99-110. https://doi.org/10.1016/j.quaint.2015.01.020

Mayewski, P. A., Rohling, E. E., Curt Stager, J., Karlén, W., Maasch, K. A., Meeker, L. D., Meyerson, E. A., Gasse, F., van Kreveld, S., Holmgren, K., Lee-Thorp, J., Rosqvist, G., Rack, F., Staubwasser, M., Schneider, R. R., & Steig, E. J. (2004). Holocene climate variability. *Quat Res*, *62*(3), 243-255. https://doi.org/10.1016/j.yqres.2004.07.001

Meredith, M., Sommerkorn, M., Cassotta, S., Derksen, C., Ekaykin, A., Hollowed, A., Kofinas, G., Mackintosh, A., Melbourne-Thomas, J., Muelbert, M. M. C., Ottersen, G., Pritchard, H., & Schuur, E. A. G. (2019). Polar Regions. In H.-O. Pörtner, D. C. Roberts, V. Masson-Delmotte, P. Zhai, M. Tignor, E. Poloczanska, & N. Weyer (Eds.), *IPCC Special Report on the Ocean and Cryosphere in a Changing Climate*. Intergovernmental Panel on Climate Change.

Metcalf, J. L., Prost, S., Nogues-Bravo, D., DeChaine, E. G., Anderson, C., Batra, P., Araujo, M. B., Cooper, A., & Guralnick, R. P. (2014). Integrating multiple lines of evidence into historical biogeography hypothesis testing: a Bison bison case study. *Proc R Soc B*, *281*(1777), 20132782. https://doi.org/10.1098/rspb.2013.2782

Monjeau, J. A., Araujo, B., Abramson, G., Kuperman, M. N., Laguna, M. F., & Lanata, J. L. (2017). The controversy space on Quaternary megafaunal extinctions. *Quat Int*, *431*, 194-204. https://doi.org/10.1016/j.quaint.2015.10.022

Moreno-Amat, E., Rubiales, J. M., Morales-Molino, C., & García-Amorena, I. (2017). Incorporating plant fossil data into species distribution models is not straightforward: Pitfalls and possible solutions. *Quat Sci Rev*, *170*, 56-68. https://doi.org/10.1016/j.quascirev.2017.06.022

Moritz, C., & Agudo, R. (2013). The future of species under climate change: resilience or decline? *Science*, *341*(6145), 504-508. https://doi.org/10.1126/science.1237190

Nadachowska-Brzyska, K., Li, C., Smeds, L., Zhang, G., & Ellegren, H. (2015). Temporal Dynamics of Avian Populations during Pleistocene Revealed by Whole-Genome Sequences. *Curr Biol*, *25*(10), 1375-1380. https://doi.org/10.1016/j.cub.2015.03.047

Newbold, T., Hudson, L. N., Arnell, A. P., Contu, S., De Palma, A., Ferrier, S., Hill, S. L., Hoskins, A. J., Lysenko, I., Phillips, H. R., Burton, V. J., Chng, C. W., Emerson, S., Gao, D., Pask-Hale, G., Hutton, J., Jung, M., Sanchez-Ortiz, K., Simmons, B. I., . . . Purvis, A. (2016). Has land use pushed terrestrial biodiversity beyond the planetary boundary? A global assessment. *Science*, *353*(6296), 288-291. https://doi.org/10.1126/science.aaf2201

Nogués-Bravo, D. (2009). Predicting the past distribution of species climatic niches. *Glob Ecol Biogeogr*, *18*(5), 521-531. https://doi.org/10.1111/j.1466-8238.2009.00476.x

Nogues-Bravo, D., Rodriguez-Sanchez, F., Orsini, L., de Boer, E., Jansson, R., Morlon, H., Fordham, D. A., & Jackson, S. T. (2018). Cracking the Code of Biodiversity Responses to Past Climate Change. *Trends Ecol Evol*, *33*(10), 765-776. https://doi.org/10.1016/j.tree.2018.07.005

Nolan, C., Overpeck, J. T., Allen, J. R. M., Anderson, P. M., Betancourt, J. L., Binney, H. A., Brewer, S., Bush, M. B., Chase, B. M., Cheddadi, R., Djamali, M., Dodson, J., Edwards, M. E., Gosling, W. D., Haberle, S., Hotchkiss, S. C., Huntley, B., Ivory, S. J., Kershaw, A. P., . . . Jackson, S. T. (2018). Past and future global transformation of terrestrial ecosystems under climate change. *Science*, *361*(6405), 920-923. https://doi.org/10.1126/science.aan5360

Olofsson, J., Oksanen, L., Callaghan, T., Hulme, P. E., Oksanen, T., & Suominen, O. (2009). Herbivores inhibit climate-driven shrub expansion on the tundra. *Glob Chang Biol*, *15*(11), 2681-2693. https://doi.org/10.1111/j.1365-2486.2009.01935.x

Ordonez, A., & Svenning, J. C. (2017). Consistent role of Quaternary climate change in shaping current plant functional diversity patterns across European plant orders. *Sci Rep*, *7*(1), 42988. https://doi.org/10.1038/srep42988

Ordonez, A., & Williams, J. W. (2013). Climatic and biotic velocities for woody taxa distributions over the last 16 000 years in eastern North America. *Ecol Lett*, *16*(6), 773-781. https://doi.org/10.1111/ele.12110

Ordonez, A., Williams, J. W., & Svenning, J.-C. (2016). Mapping climatic mechanisms likely to favour the emergence of novel communities. *Nat Clim Chang*, *6*(12), 1104-1109. https://doi.org/10.1038/nclimate3127

Orlando, L., & Cooper, A. (2014). Using Ancient DNA to Understand Evolutionary and Ecological Processes. *Annu Rev Ecol Evol Syst*, *45*(1), 573-598. https://doi.org/10.1146/annurev-ecolsys-120213-091712

Palkopoulou, E., Mallick, S., Skoglund, P., Enk, J., Rohland, N., Li, H., Omrak, A., Vartanyan, S., Poinar, H., Gotherstrom, A., Reich, D., & Dalen, L. (2015). Complete genomes reveal signatures of demographic and genetic declines in the woolly mammoth. *Curr Biol*, *25*(10), 1395-1400. https://doi.org/10.1016/j.cub.2015.04.007

Pearson, R. G., & Dawson, T. P. (2003). Predicting the impacts of climate change on the distribution of species: are bioclimate envelope models useful? *Glob Ecol Biogeogr*, *12*(5), 361-371. https://doi.org/10.1046/j.1466-822X.2003.00042.x

Pereira, H. M., Leadley, P. W., Proenca, V., Alkemade, R., Scharlemann, J. P., Fernandez-Manjarres, J. F., Araujo, M. B., Balvanera, P., Biggs, R., Cheung, W. W., Chini, L., Cooper, H. D., Gilman, E. L., Guenette, S., Hurtt, G. C., Huntington, H. P., Mace, G. M., Oberdorff, T., Revenga, C., . . . Walpole, M. (2010). Scenarios for global biodiversity in the 21st century. *Science*, *330*(6010), 1496-1501. https://doi.org/10.1126/science.1196624

Pereira, H. M., Navarro, L. M., & Martins, I. S. (2012). Global Biodiversity Change: The Bad, the Good, and the Unknown. *Annu Rev Environ Resour*, *37*(1), 25-50. https://doi.org/10.1146/annurev-environ-042911-093511

Peterson, A. (2003). Predicting the Geography of Species' Invasions via Ecological Niche Modeling. *Q Rev Biol*, *78*(4), 419-433. https://doi.org/10.1086/378926

Post, E. (2013). Erosion of community diversity and stability by herbivore removal under warming. *Proc R Soc B*, *280*(1757), 20122722. https://doi.org/10.1098/rspb.2012.2722

Post, E., Alley, R. B., Christensen, T. R., Macias-Fauria, M., Forbes, B. C., Gooseff, M. N., Iler, A., Kerby, J. T., Laidre, K. L., Mann, M. E., Olofsson, J., Stroeve, J. C., Ulmer, F., Virginia, R. A., & Wang, M. (2019). The polar regions in a 2 degrees C warmer world. *Sci Adv*, *5*(12), eaaw9883. https://doi.org/10.1126/sciadv.aaw9883

Post, E., & Pedersen, C. (2008). Opposing plant community responses to warming with and without herbivores. *Proc Natl Acad Sci U S A*, *105*(34), 12353-12358. https://doi.org/10.1073/pnas.0802421105

Prentice, I. C., Bondeau, A., Cramer, W., Harrison, S. P., Hickler, T., Lucht, W., Sitch, S., Smith, B., & Sykes, M. T. (2007). Dynamic Global Vegetation Modeling: Quantifying Terrestrial Ecosystem Responses to Large-Scale Environmental Change. In *Terrestrial Ecosystems in a Changing World* (pp. 175-192). Springer Berlin Heidelberg. https://doi.org/10.1007/978-3-540-32730-1_15

Raghavan, M., Steinrücken, M., Harris, K., Schiffels, S., Rasmussen, S., Degiorgio, M., Albrechtsen, A., Valdiosera, C., Ávila-Arcos, M. C., Malaspinas, A.-S., Eriksson, A., Moltke, I., Metspalu, M., Homburger, J. R., Wall, J., Cornejo, O. E., Moreno-Mayar, J. V., Korneliussen, T. S., Pierre, T., . . . Willerslev, E. (2015). Genomic evidence for the Pleistocene and recent population history of Native Americans. *Science*, *349*(6250), aab3884-aab3884. https://doi.org/10.1126/science.aab3884

Rangel, T. F., Edwards, N. R., Holden, P. B., Diniz-Filho, J. A. F., Gosling, W. D., Coelho, M. T. P., Cassemiro, F. A. S., Rahbek, C., & Colwell, R. K. (2018). Modeling the ecology and evolution of biodiversity: Biogeographical cradles, museums, and graves. *Science*, *361*(6399). https://doi.org/10.1126/science.aar5452

Reed, D. H., & Frankham, R. (2003). Correlation between Fitness and Genetic Diversity. *Conserv Biol*, *17*(1), 230-237. http://www.jstor.org.proxy.library.adelaide.edu.au/stable/3095289

Ripple, W. J., Chapron, G., Lopez-Bao, J. V., Durant, S. M., Macdonald, D. W., Lindsey, P. A., Bennett, E. L., Beschta, R. L., Bruskotter, J. T., Campos-Arceiz, A., Corlett, R. T., Darimont, C. T., Dickman, A. J., Dirzo, R., Dublin, H. T., Estes, J. A., Everatt, K. T., Galetti, M., Goswami, V. R., . . . Zhang, L. (2016). Saving the World's Terrestrial Megafauna. *BioScience*, *66*(10), 807-812. https://doi.org/10.1093/biosci/biw092

Rodríguez-Rey, M., Herrando-Pérez, S., Gillespie, R., Jacobs, Z., Saltré, F., Brook, B. W., Prideaux, G. J., Roberts, R. G., Cooper, A., Alroy, J., Miller, G. H., Bird, M. I., Johnson, C. N., Beeton, N., Turney, C. S. M., & Bradshaw, C. J. A. (2015). Criteria for assessing the quality of Middle Pleistocene to Holocene vertebrate fossil ages. *Quat Geochronol*, *30*, 69-79. https://doi.org/10.1016/j.quageo.2015.08.002

Schmidt, N. M., Mosbacher, J. B., Vesterinen, E. J., Roslin, T., & Michelsen, A. (2018). Limited dietary overlap amongst resident Arctic herbivores in winter: complementary insights from complementary methods. *Oecologia*, *187*(3), 689-699. https://doi.org/10.1007/s00442-018-4147-x

Schweitzer, J. A., Bailey, J. K., Hart, S. C., & Whitham, T. G. (2005). Nonadditive effects of mixing cottonwood genotypes on litter decomposition and nutrient dynamics. *Ecology*, *86*, 2834-2840. https://doi.org/10.1890/04-1955

Screen, J. A., & Simmonds, I. (2010). The central role of diminishing sea ice in recent Arctic temperature amplification. *Nature*, *464*(7293), 1334-1337. https://doi.org/10.1038/nature09051

Simberloff, D. (1986). The Proximate Causes of Extinction. In D. M. Raup & D. Jablonski, *Patterns and Processes in the History of Life* Berlin, Heidelberg.

Smith, C. I., Chamberlain, A. T., Riley, M. S., Stringer, C., & Collins, M. J. (2003). The thermal history of human fossils and the likelihood of successful DNA amplification. *J Hum Evol*, *45*(3), 203-217. https://doi.org/10.1016/s0047-2484(03)00106-4

Sommer, R. S., Kalbe, J., Ekström, J., Benecke, N., Liljegren, R., & Svenning, J.-C. (2014). Range dynamics of the reindeer in Europe during the last 25,000 years. *J Biogeogr*, *41*(2), 298-306. https://doi.org/10.1111/jbi.12193

Spielman, D., Brook, B. W., & Frankham, R. (2004). Most species are not driven to extinction before genetic factors impact them. *Proc Natl Acad Sci U S A*, *101*(42), 15261-15264. https://doi.org/10.1073/pnas.0403809101

Steffensen, J. P., Andersen, K. K., Bigler, M., Clausen, H. B., Dahl-Jensen, D., Fischer, H., Goto-Azuma, K., Hansson, M., Johnsen, S. J., Jouzel, J., Masson-Delmotte, V., Popp, T., Rasmussen, S. O., Rothlisberger, R., Ruth, U., Stauffer, B., Siggaard-Andersen, M.-L., Sveinbjornsdottir, A. E., Svensson, A., & White, J. W. C. (2008). High-resolution Greenland ice core data show abrupt climate change happens in few years. *Science*, *321*(5889), 680-684. https://doi.org/10.1126/science.1157707

Stuart, A. J. (2015). Late Quaternary megafaunal extinctions on the continents: a short review. *Geol J*, *50*(3), 338-363. https://doi.org/10.1002/gj.2633

Stuart, A. J., Kosintsev, P. A., Higham, T. F., & Lister, A. M. (2004). Pleistocene to Holocene extinction dynamics in giant deer and woolly mammoth. *Nature*, *431*(7009), 684-689. https://doi.org/10.1038/nature02890

Stuart, A. J., & Lister, A. M. (2012). Extinction chronology of the woolly rhinoceros Coelodonta antiquitatis in the context of late Quaternary megafaunal extinctions in northern Eurasia. *Quat Sci Rev*, *51*, 1-17. https://doi.org/10.1016/j.quascirev.2012.06.007

Svenning, J.-C., Fløjgaard, C., Marske, K. A., Nógues-Bravo, D., & Normand, S. (2011). Applications of species distribution modeling to paleobiology. *Quat Sci Rev*, *30*(21-22), 2930-2947. https://doi.org/10.1016/j.quascirev.2011.06.012

Thomas, C. D., Cameron, A., Green, R. E., Bakkenes, M., Beaumont, L. J., Collingham, Y. C., Erasmus, B. F. N., de Siqueira, M. F., Grainger, A., Hannah, L., Hughes, L., Huntley, B., van Jaarsveld, A. S., Midgley, G. F., Miles, L., Ortega-Huerta, M. A., Townsend Peterson, A., Phillips, O. L., & Williams, S. E. (2004). Extinction risk from climate change. *Nature*, *427*(6970), 145-148. https://doi.org/10.1038/nature02121

Timmermann, A., & Friedrich, T. (2016). Late Pleistocene climate drivers of early human migration. *Nature*, *538*(7623), 92-95. https://doi.org/10.1038/nature19365

Turvey, S. T., & Saupe, E. E. (2019). Insights from the past: unique opportunity or foreign country? *Philos Trans R Soc Lond B Biol Sci*, *374*(1788), 20190208. https://doi.org/10.1098/rstb.2019.0208

Van Der Wal, R. (2006). Do herbivores cause habitat degradation or vegetation state transition? Evidence from the tundra. *Oikos*, *114*(1), 177-186. https://doi.org/10.1111/j.2006.0030-1299.14264.x

Varela, S., Lobo, J. M., & Hortal, J. (2011). Using species distribution models in paleobiogeography: A matter of data, predictors and concepts. *Palaeogeogr Palaeoclimatol Palaeoecol*, *310*(3-4), 451-463. https://doi.org/10.1016/j.palaeo.2011.07.021

Vors, L. S., & Boyce, M. S. (2009). Global declines of caribou and reindeer. *Glob Chang Biol*, *15*(11), 2626-2633. https://doi.org/10.1111/j.1365-2486.2009.01974.x

Wang, Y., Pedersen, M. W., Alsos, I. G., De Sanctis, B., Racimo, F., Prohaska, A., Coissac, E., Owens, H. L., Merkel, M. K. F., Fernandez-Guerra, A., Rouillard, A., Lammers, Y., Alberti, A., Denoeud, F., Money, D., Ruter, A. H., Mccoll, H., Larsen, N. K., Cherezova, A. A., . . . Willerslev, E. (2021). Late Quaternary dynamics of Arctic biota from ancient environmental genomics. *Nature*. https://doi.org/10.1038/s41586-021-04016-x

Weinstock, J., Willerslev, E., Sher, A., Tong, W., Ho, S. Y., Rubenstein, D., Storer, J., Burns, J., Martin, L., Bravi, C., Prieto, A., Froese, D., Scott, E., Xulong, L., & Cooper, A. (2005). Evolution, systematics, and phylogeography of pleistocene horses in the new world: a molecular perspective. *PLoS Biol*, *3*(8), e241. https://doi.org/10.1371/journal.pbio.0030241

Whittaker, R. H. (1956). Vegetation of the Great Smoky Mountains. *Ecol Monogr*, *26*(1), 2-80. https://doi.org/10.2307/1943577

Whittaker, R. J., Araújo, M. B., Jepson, P., Ladle, R. J., Watson, J. E. M., & Willis, K. J. (2005). Conservation Biogeography: assessment and prospect. *Divers Distrib*, *11*(1), 3-23. https://doi.org/10.1111/j.1366-9516.2005.00143.x

Willerslev, E., Hansen, A. J., Binladen, J., Brand, T. B., Gilbert, M. T. P., Shapiro, B., Bunce, M., Wiuf, C., Gilichinsky, D. A., & Cooper, A. (2003). Diverse plant and animal genetic records from Holocene and Pleistocene sediments. *Science*, *300*(5620), 791-795. https://doi.org/10.1126/science.1084114

Williams, J. E., & Blois, J. L. (2018). Range shifts in response to past and future climate change: Can climate velocities and species' dispersal capabilities explain variation in mammalian range shifts? *J Biogeogr*, *45*(9), 2175-2189. https://doi.org/10.1111/jbi.13395

Williams, J. W., Kharouba, H. M., Veloz, S., Vellend, M., McLachlan, J., Liu, Z., Otto-Bliesner, B., & He, F. (2013). The ice age ecologist: testing methods for reserve prioritization during the last global warming. *Glob Ecol Biogeogr*, *22*(3), 289-301. https://doi.org/10.1111/j.1466-8238.2012.00760.x

Willis, K. J., Araujo, M. B., Bennett, K. D., Figueroa-Rangel, B., Froyd, C. A., & Myers, N. (2007). How can a knowledge of the past help to conserve the future? Biodiversity conservation and the relevance of long-term ecological studies. *Philos Trans R Soc Lond B Biol Sci*, *362*(1478), 175-186. https://doi.org/10.1098/rstb.2006.1977

Willoughby, J. R., Sundaram, M., Wijayawardena, B. K., Kimble, S. J. A., Ji, Y., Fernandez, N. B., Antonides, J. D., Lamb, M. C., Marra, N. J., & DeWoody, J. A. (2015). The reduction of genetic diversity in threatened vertebrates and new recommendations regarding IUCN conservation rankings. *Biol Conserv*, *191*, 495-503. https://doi.org/10.1016/j.biocon.2015.07.025

Wisz, M. S., Pottier, J., Kissling, W. D., Pellissier, L., Lenoir, J., Damgaard, C. F., Dormann, C. F., Forchhammer, M. C., Grytnes, J. A., Guisan, A., Heikkinen, R. K., Hoye, T. T., Kuhn, I., Luoto, M., Maiorano, L., Nilsson, M. C., Normand, S., Ockinger, E., Schmidt, N. M., . . . Svenning, J. C. (2013). The role of biotic interactions in shaping distributions and realised assemblages of species: implications for species distribution modelling. *Biol Rev Camb Philos Soc*, *88*(1), 15-30. https://doi.org/10.1111/j.1469-185X.2012.00235.x

Yannic, G., Hagen, O., Leugger, F., Karger, D. N., & Pellissier, L. (2020). Harnessing paleo-environmental modeling and genetic data to predict intraspecific genetic structure. *Evol Appl*, *13*(6), 1526-1542. https://doi.org/10.1111/eva.12986

Yannic, G., Ortego, J., Pellissier, L., Lecomte, N., Bernatchez, L., & Cote, S. D. (2018). Linking genetic and ecological differentiation in an ungulate with a circumpolar distribution. *Ecography*, *41*(6), 922-937. https://doi.org/10.1111/ecog.02995

Young, H. S., McCauley, D. J., Galetti, M., & Dirzo, R. (2016). Patterns, Causes, and Consequences of Anthropocene Defaunation. *Annu Rev Ecol Evol Syst*, *47*(1), 333-358. https://doi.org/10.1146/annurev-ecolsys-112414-054142

Zimov, S. A., Chuprynin, V. I., Oreshko, A. P., Chapin, F. S., Reynolds, J. F., & Chapin, M. C. (1995). Steppe-Tundra Transition: A Herbivore-Driven Biome Shift at the End of the Pleistocene. *Am Nat*, *146*(5), 765-794. https://doi.org/10.1086/285824

Appendix

IUCN Red List protects avian genetic diversity (published version)

ECOGRAPHY

Brevia

IUCN Red List protects avian genetic diversity

Elisabetta Canteri, Damien A. Fordham, Sen Li, Peter A. Hosner, Carsten Rahbek and David Nogués-Bravo

E. Canteri (https://orcid.org/0000-0001-9867-8247) ✉ (elisabetta.canteri@adelaide.edu.au) and D. A. Fordham (https://orcid.org/0000-0003-2137-7010-5592), The Environment Inst. and School of Biological Sciences, Univ. of Adelaide, SA, Australia. – EC, DAF, P. A. Hosner, C. Rahbek and D. Nogués-Bravo, Center for Macroecology, Evolution and Climate, GLOBE Inst., Univ. of Copenhagen, Copenhagen, Denmark. PAH and CR also at: Center for Global Mountain Biodiversity, GLOBE Institute, Univ. of Copenhagen, Copenhagen, Denmark. PAH also at: Natural History Museum of Denmark, Univ. of Copenhagen, Copenhagen, Denmark. CR also at: Inst. of Ecology, Peking Univ., Beijing, China and Danish Inst. for Advanced Study, Univ. of Southern Denmark, Odense, Denmark. – S. Li, Section for Evolutionary Genomics, GLOBE Inst., Univ. of Copenhagen, Copenhagen, Denmark.

Ecography
44: 1–4, 2021
doi: 10.1111/ecog.05895

Subject Editor: Tim Newbold
Editor-in-Chief: Miguel Araújo
Accepted 30 September 2021

Low genetic diversity may be associated with an increase in species' extinction risk (Spielman et al. 2004, Frankham 2005). Still, global conservation assessments do not consider relevant genetic-based estimates for evaluating species threat status. Rather, they rely primarily on changes in population abundance and range size, with the inherent assumption that intra-specific genetic variability is tightly correlated with population size and range area (Frankham 1996). If this assumption was universally true, species considered to be at high risk, because of small range sizes and/or low abundances, should have lower levels of genetic diversity than low-risk species and vice-versa. However, contradictory evidence, for birds and mammals (Reed 2010), suggests that omitting genetic diversity from threat classification criteria could potentially lead to under- or over-estimating the actual extinction risk of species.

Here, we investigate whether bird species considered at risk of extinction, by widely used threat assessment criteria (IUCN 2021), have less intra-specific nucleotide diversity than non-threatened bird species (Supporting information). To accomplish this aim, we established differences in intra-specific nucleotide diversity for threatened (Vulnerable – VU, Endangered – EN and Critically Endangered – CR) vs non-threatened bird species (Least Concern – LC and Near Threatened – NT) by compiling 28 403 publicly available avian mitochondrial DNA (mtDNA) sequences from GenBank. We calculated cytochrome-b (cyt-b) nucleotide diversity for 1036 species (approximately 10% of all bird species), with an average number of sequences per species being 27 ± 44 (Supporting information). The average sequence length (base-pairs) across species was 887 ± 201. Using phylANOVAs, to control for phylogenetic signal (Freckleton et al. 2002), corrected for varying sample sizes between groups, we show that threatened species have significantly lower cyt-b nucleotide diversity ($p < 0.05$, in 953 out of the 1000 phylANOVA repetitions; mean $p = 0.010 \pm 0.025$) than non-threatened species (Fig. 1a; Supporting information), with medium to large effect size in 97.2% of repetitions ($\omega^2 > 0.06$). The mean effect size was 0.16 ± 0.05 (Supporting information).

Our results reveal that current threat assessment criteria indirectly prioritize species with low levels of cyt-b nucleotide diversity, which can be at greater risk of extinction by virtue of low genetic diversity (Frankham 2005) (Fig. 1c). For example, the African houbara (*Chlamydotis undulata*, VU) is among the birds with the lowest

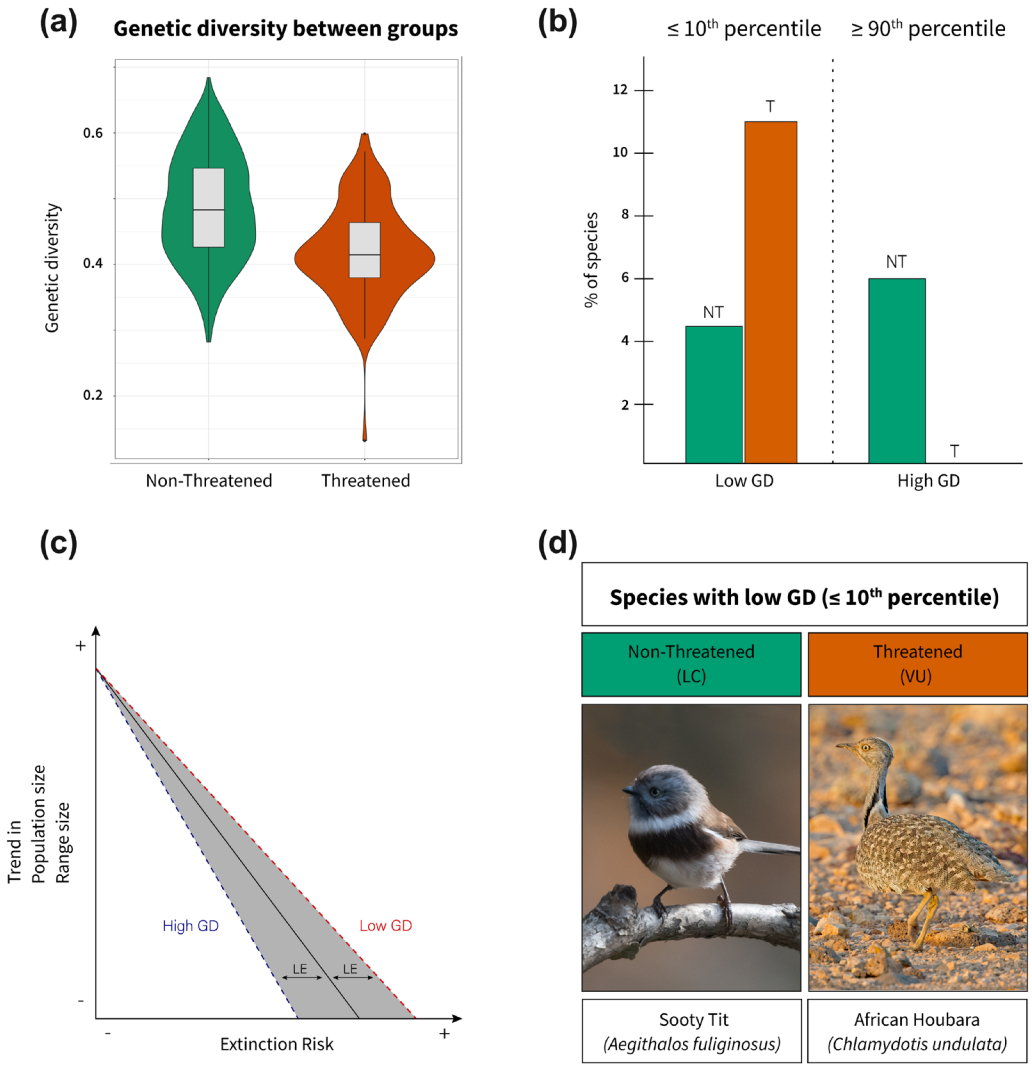

Figure 1. Genetic diversity in threatened and non-threatened bird species. (a) Threatened species have significantly lower intra-specific cyt-b nucleotide diversity than non-threatened species. (b) Percentage of threatened (T) and non-threatened (NT) species with the lowest (≤10th percentile) and highest (≥ 90th percentile) values of cyt-b nucleotide diversity. (c) Conceptual figure showing a species experiencing declines (negative trend) in range size and/or population abundance through time, enhancing its extinction risk. Due to low or high genetic diversity (GD; low or high GD), the same species might be of greater (red dashed line) or lesser (blue dashed line) extinction risk, respectively, potentially producing a mismatch between the evaluated extinction risk (black solid line) and the actual extinction risk (latent extinction risk, LE). (d) Examples of a non-threatened (sooty tit: *Aegithalos fuliginosus*; photo credits: Tim Melling) and a threatened bird species (African houbara: *Chlamydotis undulata*) with some of the lowest levels of cyt-b nucleotide diversity (≤10th percentile).

cyt-b nucleotide diversity in our data set (≤10th percentile: GD ≤ 0.0015; Fig. 1d), and its persistence is affected by inbreeding and/or genetic drift (Korrida et al. 2012). Moreover, the millerbird (*Acrocephalus familiaris*, CR) and the inaccessible finch (*Nesospiza acunhae*, VU) are both range-restricted small-island endemics with limited cyt-b nucleotide diversity (≤ 10th percentile; Supporting information), making them particularly vulnerable to rapid environmental changes from introduced predators and extreme climatic events (Vincenzi et al. 2017). Although mtDNA has been shown, under some circumstances, to be of limited use for inferring population size (Bazin et al. 2006, Nabholz et al. 2009), the low levels of nucleotide diversity in threatened species of birds suggest a correlation, direct or indirect, between cyt-b nucleotide diversity and small population or range size. For species that have not experienced large range contractions and population declines in recent times (non-threatened species), we found that cyt-b nucleotide diversity was generally high (≥90th percentile: GD ≥ 0.0302). Higher levels of genetic diversity might, through the process of local adaptation, aid species' resilience to rapid environmental changes (DeWoody et al. 2021) and reverse or slow species' decline (Fig. 1c). However, in some instances, non-threatened species can harbour low genetic

diversity, most probably due to recent or past bottlenecks (Weber et al. 2000).

Four per cent of all non-threatened birds analysed had low levels of cyt-b nucleotide diversity (≤ 10th percentile; Fig. 1b). For example, the sooty tit (*Aegithalos fuliginosus*, LC; Fig. 1d) is the non-threatened species with the lowest cyt-b nucleotide diversity in our data set (Supporting information). Despite having a restricted range, the sooty tit is considered as 'Least Concern', due to a population that is suspected to be stable (IUCN 2021). Low nucleotide diversity for the sooty tit signals that extinction risk for the species might be higher than its IUCN threat status indicates, encouraging further assessments of its conservation status using census and genomic techniques. Low genetic diversity in non-threatened species can result from recent or past dramatic demographic events, after which levels of intra-specific genetic diversity remain temporally low, while the overall population size increases (Weber et al. 2000). For these species, whole-genome studies will help reveal the role of genetic diversity in long-term species survival.

While our results could be contingent on the length of sequences, sample size, and geographic and taxonomic biases associated with genetic sequences in public repositories such as GenBank, we found no correlation between nucleotide diversity and average sequence length or number of sequences (Supporting information). Furthermore, we found a low phylogenetic signal ($\lambda = 0.56$, $p < 0.001$), and the phylANOVAs confirm the independence of the data in relation to the evolutionary history of the species (Supporting information). Indeed, there is a significant difference between the F-statistics calculated on the actual data and the F-statistics calculated with simulated data (null hypothesis; Supporting information). Lastly, our results do not reflect geographic biases in our dataset, which covers ~57% of all avian families and all zoogeographic realms (Supporting information). Despite existing challenges with using mitochondrial data and single genetic markers (Carling and Brumfield 2007), including the real possibility that genetic diversity calculated using mtDNA might not reflect genome-wide diversity or the diversity of specific functionally relevant parts of the genome, the relationship between conservation status and genetic diversity, explored in this paper, concords with long-standing expectations from the literature (DeWoody et al. 2021), including findings from meta-analyses across smaller subsets of taxa (Spielman et al. 2004, Willoughby et al. 2015) using nuclear DNA (allozymes, microsatellites, minisatellites), and other mtDNA genes (Petit-Marty et al. 2021).

Species-level conservation criteria capture low levels of intra-specific nucleotide variability in species of greatest concern. Nonetheless, low levels of nucleotide diversity are present in a small proportion of non-threatened birds, causing them, in theory, to be more vulnerable to rapidly changing environmental conditions than their conservation status, alone, indicates (Frankham 2005). As genomic techniques get cheaper, the inclusion of whole-genome data in relevant measures of genetic diversity is a likely near-term prospect for conservation. Future research should aim to integrate large-scale field-work campaigns with strategic sequencing of contemporary and historical specimens from biological collections, in order to unravel eco-evolutionary determinants of increased extinction risk.

Acknowledgements – We thank Jonathan Kennedy for technical support and guidance. We thank Tim Melling for allowing us to use his photo of the sooty tit.
Funding – This research was funded by Australian Research Council funding (grant no. FT140101192, DP180102392), awarded to DAF, the VILLUM FONDEN (grant no. 25925) awarded to CR, and the DFF project DEMOCHANGE (grant no. 8021-00282B) awarded to DNB.

Author contributions

Elisabetta Canteri: conceptualization (equal); data curation (equal); formal analysis (lead); writing - original draft (equal); writing – review and edit (equal). **Damien A. Fordham**: conceptualization (equal); funding acquisition (equal); supervision (equal); writing – review and edit (equal). **Sen Li**: investigation (lead); software (lead); writing – review and edit (equal). **Peter A. Hosner**: data curation (equal); writing – review and edit (equal). **Carsten Rahbek**: funding acquisition (equal); writing – review and edit (equal). **David Nogues-Bravo**: funding acquisition (equal); conceptualization (equal); supervision (lead); writing – original draft (equal); writing – review and edit (equal).

Transparent Peer Review

The peer review history for this article is available at <https://publons.com/publon/10.1111/ecog.05895>.

Data availability statement

Data are available from the Dryad Digital Repository: <https://doi.org/10.5061/dryad.pzgmsbcn6> (Canteri et al. 2021).

References

Bazin, E. et al. 2006. Population size does not influence mitochondrial genetic diversity in animals. – Science 312: 570–572.
Canteri, E. et al. 2021. Data from: IUCN Red List protects avian genetic diversity. – Dryad Digital Repository, <https://doi.org/10.5061/dryad.pzgmsbcn6>.
Carling, M. D. and Brumfield, R. T. 2007. Gene sampling strategies for multi-locus population estimates of genetic diversity (θ). – PLoS One 2: e160.
DeWoody, J. A. et al. 2021. The long-standing significance of genetic diversity in conservation. – Mol. Ecol. 30: 4147–4154.
Frankham, R. 1996. Relationship of genetic variation to population size in wildlife. – Conserv. Biol. 10: 1500–1508.
Frankham, R. 2005. Genetics and extinction. – Biol. Conserv. 126: 131–140.

Freckleton, R. et al. 2002. Phylogenetic analysis and comparative data: a test and review of evidence. – Am. Nat. 160: 712–726.
IUCN 2021. The IUCN Red List of threatened species. Ver. 2021-1. – <www.iucnredlist.org>.
Korrida, A. et al. 2012. Patterns of genetic diversity and population structure of the threatened houbara and macqueen's bustards as revealed by microsatellite markers. – Genet. Mol. Res. 11: 3207–3221.
Nabholz, B. et al. 2009. The erratic mitochondrial clock: variations of mutation rate, not population size, affect mtDNA diversity across birds and mammals. – BMC Evol. Biol. 9: 1–13.
Petit-Marty, N. et al. 2021. Use of the nucleotide diversity in COI mitochondrial gene as an early diagnostic of conservation status of animal species. – Conserv. Lett. 14: e12756.
Reed, D. H. 2010. Albatrosses, eagles and newts, Oh My!: exceptions to the prevailing paradigm concerning genetic diversity and population viability? – Anim. Conserv. 13: 448–457.
Spielman, D. et al. 2004. Most species are not driven to extinction before genetic factors impact them. – Proc. Natl Acad. Sci. USA 101: 15261–15264.
Vincenzi, S. et al. 2017. Genetic and life-history consequences of extreme climate events. – Proc. R. Soc. B 284: 2016–2118.
Weber, D. S. et al. 2000. An empirical genetic assessment of the severity of the northern elephant seal population bottleneck. – Curr. Biol. 10: 1287–1290.
Willoughby, J. R. et al. 2015. The reduction of genetic diversity in threatened vertebrates and new recommendations regarding IUCN conservation rankings. – Biol. Conserv. 191: 495–503.